Thesis for the degree of Doctor of Philosophy in
Natural Science, specializing in Chemistry

Quantum dynamical effects in complex chemical systems

S. Karl-Mikael Svensson

UNIVERSITY OF GOTHENBURG
Department of Chemistry and Molecular Biology
Gothenburg, Sweden, 2020

Front cover: Artistic representation of an imaginary time path
integral open polymer attached to a dividing surface on the top of a
potential energy barrier.

Typeset with LaTeX.

---

*https://creativecommons.org/licenses/by/4.0/

To my grandparents.

Abstract

When using mathematical models to computationally investigate a chemical system it is important that the methods used are accurate enough to account for the relevant properties of the system and at the same time simple enough to be computationally affordable. This thesis presents research that so far has resulted in three published papers and one unpublished manuscript. It concerns the application and development of computational methods for chemistry, with some extra emphasis on the calculation of reaction rate constants.

In astrochemistry radiative association is a relevant reaction mechanism for the formation of molecules. The rate constants for such reactions are often difficult to obtain though experiments. In the first published paper of the thesis a rate constant for the formation of the hydroxyl radical, through the radiative association of atomic oxygen and hydrogen, is presented. This rate constant was calculated by a combination of different methods and should be an improvement over previously available rate constants.

In the the second published paper of this thesis two kinds of basis functions, for use with a variational principle for the dynamics of quantum distributions in phase space, i.e. Wigner functions, is presented. These are tested on model systems and found to have some appealing properties.

The classical Wigner method is an approximate method of simulation, where an initial quantum distribution is propagated in time with classical mechanics. In the third published paper of this thesis a new method of sampling the initial quantum distribution, with an imaginary time Feynman path integral, is derived and tested on model systems. In the unpublished manuscript, this new method is applied to reaction rate constants and tested on two model sys-

tems. The new sampling method shows some promise for future applications.

Preface

> You have guessed right; I have lately been so deeply engaged in one occupation that I have not allowed myself sufficient rest, as you see: but I hope, I sincerely hope, that all these employments are now at an end, and that I am at length free.
>
> Victor Frankenstein (Mary Shelley)[1]

This thesis is a compilation thesis consisting of two main parts. To start from the back, the second part is a collection of papers that have been coauthored by the author of the thesis and represent the research that the thesis is based upon.

The first part of this thesis is the frame, which is an introduction to and discussion of the papers in the second part. The frame is itself divided into three parts. First is an introduction where the general subject of the thesis is presented and put on the scientific map, with the aim of being accessible to a broader audience than the rest of this book. Second is a chapter with the theory on which the work is based. Third, and last in the frame, there is a chapter describing and discussing the new developments that has come out of the research. The contents of the third chapter overlaps with the content of the papers, but the aim is for it to be more pedagogical than the papers themselves are.

Contents

Nomenclature

Come, let us go down and confuse their language so they will not understand each other.

Genesis 11:7

Abbreviations

C^3SE Chalmers Centre for Computational Science and Engineering

CMD Centroid molecular dynamics

DVR Discrete variable representation

FK-LPI Feynman-Kleinert linearized path integral

KIDA Kinetic Database for Astrochemistry

LPI Linearized path integral

LSC-IVR Linearized semi-classical initial value representation

OPCW Open polymer classical Wigner

PIMC Path integral Monte Carlo

PIMD Path integral molecular dynamics

RPMD Ring polymer molecular dynamics

SC-IVR Semi-classical initial value representation

SNIC Swedish National Infrastructure for Computing

UDfA UMIST Database for Astrochemistry

WKB Wentzel–Kramers–Brillouin

Physical and mathematical constants

$\hbar$ Reduced Planck's constant $1.054571800 \times 10^{-34}\,\mathrm{Js}$

k_{B} Boltzmann's constant $1.38064852 \times 10^{-23}\,\mathrm{JK^{-1}}$

i Imaginary unit $\sqrt{-1}$

Variables, operators, functions, and transforms

β $\dfrac{1}{k_{\mathrm{B}}T}$

$\boldsymbol{\alpha}$ Vector of parameters

$\boldsymbol{\eta}$ Position vector

$\boldsymbol{\lambda}$ Momentum vector

mod   Modulus operator

$\boldsymbol{\Omega}$ Arbitrary physical quantity

$\boldsymbol{p}$ Momentum vector

$\boldsymbol{x}$ Position vector

$\delta\left(\boldsymbol{\zeta}\right)$ Dirac delta function

$[f(t)]_{\mathrm{F}}\left(\omega\right)$ Fourier transform of function $f(t)$ as a function of angular frequency ω.

$|\boldsymbol{p}\rangle$ Momentum eigenket

$|\boldsymbol{x}\rangle$ Position eigenket

$|\Psi\rangle$ Ket describing the state of the system described by the wavefunction Ψ

$\mathcal{O}$ Big O

H_n n^{th} order Hermite polynomial $\mathsf{H}_n(x) = (-1)^n \, \mathrm{e}^{x^2} \, \dfrac{\mathrm{d}^n}{\mathrm{d}x^n} \, \mathrm{e}^{-x^2}$

$\widehat{\boldsymbol{\Omega}}$ Arbitrary quantum mechanical operator

$\widehat{\boldsymbol{p}}$ Momentum operator

$\widehat{\boldsymbol{x}}$ Position operator

$\widehat{F}(\widehat{x} - s)$ Probability flux operator $\dfrac{1}{2} m^{-1} \left(\delta(\widehat{x} - s) \widehat{p} + \widehat{p} \delta(\widehat{x} - s) \right)$

$\widehat{H}$ Hamiltonian operator $\widehat{T} + \widehat{V}$

$\widehat{L}$ Liouvillian operator

$\widehat{T}$ Kinetic energy operator

$\widehat{V}$ Potential energy operator

Φ_{W} Parametrized Wigner function

Ψ Wavefunction

ρ Classical probability distribution function

θ Heaviside step function

$\text{Tr}\left\{ \widehat{\boldsymbol{\Omega}} \right\}$ Trace of operator $\widehat{\boldsymbol{\Omega}}$.

$\left[\widehat{\boldsymbol{\Omega}} \right]_{\text{W}}(\boldsymbol{x}, \boldsymbol{p})$ Wigner transform of operator $\widehat{\boldsymbol{\Omega}}$

* Complex conjugate

^{T} Transpose of vector or matrix

D Number of degrees of freedom in the system

E Energy

H Classical Hamiltonian function

k_{r} Reaction rate constant

Q_{R} Canonical reactant partition function

s A dividing surface

T Absolute temperature

t Time

V Potential energy

x_{r} Reaction coordinate

Z Canonical partition function

$\frac{1}{(2\pi\hbar)^D} \lvert\Psi\rangle \langle\Psi\rvert$ Probability density operator

List of Figures

List of Tables

List of Papers

The included papers are reproduced with permission from the journals when needed.

Paper I   *Formation of the Hydroxyl Radical by Radiative Association*
S. Karl-Mikael Svensson, Magnus Gustafsson, and Gunnar Nyman
The Journal of Physical Chemistry A, 2015, 119 (50), pp 12263–12269, DOI: 10.1021/acs.jpca.5b06300

Paper II   *Dynamics of Gaussian Wigner functions derived from a time-dependent variational principle*
Jens Aage Poulsen, S. Karl-Mikael Svensson, and Gunnar Nyman
AIP Advances, 2017, 7 (11), pp 115018-1–115018-12, DOI: 10.1063/1.5004757

Paper III   *Classical Wigner Model Based on a Feynman Path Integral Open Polymer*
S. Karl-Mikael Svensson, Jens Aage Poulsen, and Gunnar Nyman
The Journal of Chemical Physics, 2020, 152 (9), pp 094111-1–094111-20, DOI: 10.1063/1.5126183

Paper IV   *Calculation of Reaction Rate Constants From a Classical Wigner Model Based on a Feynman Path Integral Open Polymer*
S. Karl-Mikael Svensson, Jens Aage Poulsen, and Gunnar Nyman
Manuscript

Contributions from the Author

Paper I   The author performed the computations, did the analysis of the result, and wrote most of the paper.

Paper II The author ran some of the calculations and did a few minor derivations.

Paper III The author checked the derivations and did some on his own, rewrote and extended the code of the computer program, performed the computations using the new method, did the analysis of the results, and wrote most of the paper.

Paper IV The author did all of the derivations, performed most of the computations, did the analysis of the results, and wrote most of the manuscript.

Acknowledgments

This thesis would not have come to fruition without the assistance of multiple people, the most obvious of which are my supervisor and co-supervisor, *Gunnar Nyman* and *Jens Poulsen*. Also, *Magnus Gustafsson* was supervising the work behind paper I. Furthermore, I would like to thank *Johan Bergenholtz* for being my examiner.

The supportive environment of the physical chemistry group is also gratefully acknowledged.

A significant fraction of the computations that this thesis refers to were run on clusters, Glenn, Hebbe, and Vera, belonging to Chalmers Centre for Computational Science and Engineering (C^3SE) that is a part of the Swedish National Infrastructure for Computing (SNIC).

Finally, many thanks to my family for their support during my studies.

Frame

Chapter 1

Introduction

> The underlying physical laws necessary for the mathematical theory of a large part of physics and the whole of chemistry are thus completely known, and the difficulty is only that the exact application of these laws leads to equations much too complicated to be soluble. It therefore becomes desirable that approximate practical methods of applying quantum mechanics should be developed, which can lead to an explanation of the main features of complex atomic systems without too much computation.
>
> Paul A. M. Dirac[2]

Computational chemistry is the craft of calculating, preferably on a computer, the answers to chemical questions from mathematical models of how entities in chemistry such as atoms, molecules, fluids, or even more fundamental entities such as electrons and atomic nuclei behave. Running calculations on a computer instead of doing experiments in a laboratory may have the advantage of being faster and cheaper, and allowing many more things to be tried simultaneously. However, the practical experiment in the laboratory has direct access to the physical reality of the universe and the chemistry within it, thus potentially giving the "truth", while the mathematical

models used in calculations are inevitably approximations of reality, thus giving potentially good but nevertheless approximate results.

There is another difference between computational and experimental chemistry, and that is the type of questions that can be answered. In a simulation the movement of individual atoms, that are experimentally untrackable, in a chemical reaction can be followed over time, scales of time and volume impossible in practical experimentation can be accessible, and environments, species and processes of exotic or even alchemical nature can be handled.

When choosing a computational method to answer a given question there are many choices to make. One of the common ones is the choice between quantum mechanics and classical mechanics. Quantum mechanics is correct but computationally expensive with its delocalization, tunnelling, zero point energy, and interference while classical mechanics may be wrong but computationally cheap with simple trajectories for the motion of a body, just as we as humans experience things in our daily macroscopic lives. In many cases classical mechanics is good enough. However, when light atoms such as hydrogen are involved, temperatures are low such as often in astrochemistry, or there is significant quantum interference, then quantum mechanics may be essential to describe chemistry in a meaningful way. This leads back to Dirac's quote[2] in the beginning of this chapter:

> It therefore becomes desirable that approximate practical methods of applying quantum mechanics should be developed, which can lead to an explanation of the main features of complex atomic systems without too much computation.

This statement from 1929 is still as valid as it was back then, even as the limits of what is considered too much computation have changed, and is a concise description of the mission of the work in this thesis.

Generally, chemistry deals with atomic nuclei, electrons, and aggregates of such particles. On the lowest level of chemistry, with electrons and atomic nuclei as separate entities, it is almost always clearly so that the electrons behave quantum mechanically, but the question is if the nuclei should be handled with classical or quantum

mechanics. Often the Born-Oppenheimer approximation[3] is utilized, meaning that it is assumed that the movement of the electrons and the movement of the nuclei can be handled separately. Entities significantly heavier than atomic nuclei, such as colloidal particles, for all practical purposes move according to classical mechanics even if the forces between them may be of a quantum mechanical nature. Some specific examples of when nuclear quantum effects can make an important difference in computations include:

- The volume of light atoms may become large due to thermal quantum fluctuations.[4]

- Resonances in quasi-bound states may make a significant contribution to a reaction rate constant.[5]

- The delocalization of hydrogen can have a significant impact on the acidity of an active site in an enzyme.[6]

The work presented in this thesis concerns methods used to handle the movements of atomic nuclei, when some measure of quantum mechanics is desirable. Of course the methods can be used for any type of particle, not only atomic nuclei, but atomic nuclei tend to be what chemists in this field of study focus on. A particular focus for parts of the thesis is the calculation of reaction rate constants.

Chapter 2

Background

> A man would make but a very sorry chemist if he attended to that department of human knowledge alone. If your wish is to become really a man of science, and not merely a petty experimentalist, I should advise you to apply to every branch of natural philosophy, including mathematics.

> Fellow-professor M. Waldman (Mary Shelley)[1]

Quantum mechanics can be formulated in many ways. The one that most people are familiar with is probably the wavefunction formulation, which was published in 1926 by Schrödinger[7–12]*. This formulation uses the Schrödinger equation

$$i\hbar\frac{\partial}{\partial t}\Psi\left(\boldsymbol{x},t\right) = \widehat{H}\Psi\left(\boldsymbol{x},t\right) \tag{2.1}$$

or in bra-ket notation

$$i\hbar\frac{\partial}{\partial t}\left|\Psi\left(t\right)\right\rangle = \widehat{H}\left|\Psi\left(t\right)\right\rangle, \tag{2.2}$$

where i is the imaginary unit $(\sqrt{-1})$, $\hbar$ is the reduced Planck's constant, t is time, $\boldsymbol{x}$ is a position vector, $\Psi\left(\boldsymbol{x},t\right)$ is the wavefunction

---

*The original papers are in German. Schrödinger published a summary in English in the same year.[13]

of the system at time t and position $\boldsymbol{x}$, $\widehat{H}$ is the Hamiltonian operator, and $|\Psi(t)\rangle$ is the ket representing the state of the system described by the wavefunction Ψ at time t. This is, however, not always the most practical formulation to start with when trying to simplify quantum mechanics.

In this chapter of this thesis two other formulations of quantum mechanics are presented in sections 2.1 and 2.2, calculations of reaction rate constants are introduced in section 2.3, and common methods to use for approximate quantum dynamics can be found in section 2.4.

2.1 Wigner transform and the Wigner phase space

> Of the many approaches to the semiclassical limit from the quantum domain, the Wigner method is one of the most immediately appealing.

<div align="right">Eric J. Heller[14]</div>

A formulation of quantum mechanics ascribed to Wigner[15] and Moyal[16] is the phase space formulation. In this formulation one works with functions that depend on both position and momentum simultaneously, something that may seem very strange from the wavefunction point of view, but that allows the equations to look more like classical mechanics.

The Wigner transform of an arbitrary operator $\widehat{\boldsymbol{\Omega}}$ is

$$
\begin{aligned}
\left[\widehat{\boldsymbol{\Omega}}\right]_{\mathrm{W}}(\boldsymbol{x}, \boldsymbol{p}) &= \int \mathrm{d}^D \boldsymbol{\eta}\ \mathrm{e}^{-i\boldsymbol{\eta}\bullet\boldsymbol{p}/\hbar} \left\langle \boldsymbol{x} + \frac{\boldsymbol{\eta}}{2} \middle| \widehat{\boldsymbol{\Omega}} \middle| \boldsymbol{x} - \frac{\boldsymbol{\eta}}{2} \right\rangle \\
&= \int \mathrm{d}^D \boldsymbol{\lambda}\ \mathrm{e}^{i\boldsymbol{x}\bullet\boldsymbol{\lambda}/\hbar} \left\langle \boldsymbol{p} + \frac{\boldsymbol{\lambda}}{2} \middle| \widehat{\boldsymbol{\Omega}} \middle| \boldsymbol{p} - \frac{\boldsymbol{\lambda}}{2} \right\rangle
\end{aligned}
\tag{2.3}
$$

where $\boldsymbol{p}$ is a momentum vector, $\boldsymbol{\eta}$ is a vector where the elements have the dimension of length, D is the number of degrees of freedom in the system, $\boldsymbol{\lambda}$ is a vector where the elements have the dimension of momentum, and the integrals are over all space. $\left|\boldsymbol{x} \pm \dfrac{\boldsymbol{\eta}}{2}\right\rangle$ and $\left|\boldsymbol{p} \pm \dfrac{\boldsymbol{\lambda}}{2}\right\rangle$ are eigenkets of position and momentum respectively, meaning that $\langle \boldsymbol{x}|\Psi\rangle = \Psi(\boldsymbol{x})$ and $\langle \boldsymbol{p}|\Psi\rangle = \Psi(\boldsymbol{p})$.

The Wigner transform of a product of two operators is

$$
\begin{aligned}
&\left[\widehat{\boldsymbol{\Omega}}_1 \widehat{\boldsymbol{\Omega}}_2\right]_{\mathrm{W}}(\boldsymbol{x}, \boldsymbol{p}) \\
&= \left[\widehat{\boldsymbol{\Omega}}_1\right]_{\mathrm{W}}(\boldsymbol{x}, \boldsymbol{p})\, \mathrm{e}^{-\frac{i\hbar}{2}\left(\overleftarrow{\frac{\partial}{\partial \boldsymbol{p}}}\bullet\overrightarrow{\frac{\partial}{\partial \boldsymbol{x}}} - \overleftarrow{\frac{\partial}{\partial \boldsymbol{x}}}\bullet\overrightarrow{\frac{\partial}{\partial \boldsymbol{p}}}\right)} \left[\widehat{\boldsymbol{\Omega}}_2\right]_{\mathrm{W}}(\boldsymbol{x}, \boldsymbol{p})
\end{aligned}
\tag{2.4}
$$

where the arrows above the partial derivatives show in which direction they act.

If taking the Wigner transform of the probability density operator, $\frac{1}{(2\pi\hbar)^D}\left|\Psi\right\rangle\left\langle\Psi\right|$, the so called Wigner function is obtained. This function is a quasi probability distribution in phase space that has the property that it can be used to obtain the expectation value of a physical quantity $\boldsymbol{\Omega}$ trough

$$\left\langle\widehat{\boldsymbol{\Omega}}\right\rangle = \iint \mathrm{d}^D\boldsymbol{x}\,\mathrm{d}^D\boldsymbol{p}\,\left[\tfrac{1}{(2\pi\hbar)^D}\left|\Psi\right\rangle\left\langle\Psi\right|\right]_{\mathrm{W}}(\boldsymbol{x},\boldsymbol{p})\left[\widehat{\boldsymbol{\Omega}}\right]_{\mathrm{W}}(\boldsymbol{x},\boldsymbol{p})$$

(2.5)

which looks very similar to classical mechanics

$$\left\langle\boldsymbol{\Omega}\right\rangle = \iint \mathrm{d}^D\boldsymbol{x}\,\mathrm{d}^D\boldsymbol{p}\,\rho\left(\boldsymbol{x},\boldsymbol{p}\right)\boldsymbol{\Omega}\left(\boldsymbol{x},\boldsymbol{p}\right)$$

(2.6)

where $\rho\left(\boldsymbol{x},\boldsymbol{p}\right)$ is the classical probability distribution function in phase space.

For the interested reader the following section shows how to derive equation 2.3 and 2.5 from the more common formulation of quantum mechanics.

Derivation of the phase space formulation from the wavefunction formulation

To obtain equation 2.5, start with the standard equation

$$\left\langle\widehat{\boldsymbol{\Omega}}\right\rangle = \int \mathrm{d}^D\boldsymbol{x}\,\Psi^*\left(\boldsymbol{x}\right)\widehat{\boldsymbol{\Omega}}\Psi\left(\boldsymbol{x}\right) = \left\langle\Psi\left|\widehat{\boldsymbol{\Omega}}\right|\Psi\right\rangle.$$

(2.7)

Introduce two unity operators, $\widehat{1} = \int \mathrm{d}^D\boldsymbol{x}\,\left|\boldsymbol{x}\right\rangle\left\langle\boldsymbol{x}\right|$,

$$\left\langle\widehat{\boldsymbol{\Omega}}\right\rangle = \iint \mathrm{d}^D\boldsymbol{x}_1\,\mathrm{d}^D\boldsymbol{x}_2\,\left\langle\Psi|\boldsymbol{x}_1\right\rangle\left\langle\boldsymbol{x}_1\left|\widehat{\boldsymbol{\Omega}}\right|\boldsymbol{x}_2\right\rangle\left\langle\boldsymbol{x}_2|\Psi\right\rangle$$

$$= \iint \mathrm{d}^D\boldsymbol{x}_1\,\mathrm{d}^D\boldsymbol{x}_2\,\left\langle\boldsymbol{x}_2|\Psi\right\rangle\left\langle\Psi|\boldsymbol{x}_1\right\rangle\left\langle\boldsymbol{x}_1\left|\widehat{\boldsymbol{\Omega}}\right|\boldsymbol{x}_2\right\rangle$$

(2.8)

and then introduce two more unity operators, $\widehat{1} = \int \mathrm{d}^D\boldsymbol{p}\,\left|\boldsymbol{p}\right\rangle\left\langle\boldsymbol{p}\right|$,

$$\left\langle\widehat{\boldsymbol{\Omega}}\right\rangle = \iiiint \mathrm{d}^D\boldsymbol{x}_1\,\mathrm{d}^D\boldsymbol{x}_2\,\mathrm{d}^D\boldsymbol{p}_1\,\mathrm{d}^D\boldsymbol{p}_2$$

$$\times \left\langle\boldsymbol{x}_2|\boldsymbol{p}_1\right\rangle\left\langle\boldsymbol{p}_1|\Psi\right\rangle\left\langle\Psi|\boldsymbol{p}_2\right\rangle\left\langle\boldsymbol{p}_2|\boldsymbol{x}_1\right\rangle\left\langle\boldsymbol{x}_1\left|\widehat{\boldsymbol{\Omega}}\right|\boldsymbol{x}_2\right\rangle.$$

(2.9)

$|\boldsymbol{x}\rangle$ and $|\boldsymbol{p}\rangle$ are just a Fourier transform away from each other,

$$|\boldsymbol{p}\rangle = \frac{1}{(2\pi\hbar)^{\frac{D}{2}}} \int \mathrm{d}^D\boldsymbol{x} \ \mathrm{e}^{i\boldsymbol{x}\bullet\boldsymbol{p}/\hbar} |\boldsymbol{x}\rangle \tag{2.10}$$

$$|\boldsymbol{x}\rangle = \frac{1}{(2\pi\hbar)^{\frac{D}{2}}} \int \mathrm{d}^D\boldsymbol{p} \ \mathrm{e}^{-i\boldsymbol{x}\bullet\boldsymbol{p}/\hbar} |\boldsymbol{p}\rangle \,, \tag{2.11}$$

which means that, since $\langle \boldsymbol{x}'|\boldsymbol{x}\rangle = \delta\left(\boldsymbol{x}' - \boldsymbol{x}\right)$ and $\langle \boldsymbol{p}'|\boldsymbol{p}\rangle = \delta\left(\boldsymbol{p}' - \boldsymbol{p}\right)$, where $\delta\left(\boldsymbol{x}' - \boldsymbol{x}\right)$ is the Dirac delta function,

$$\begin{aligned}
\langle \boldsymbol{p}|\boldsymbol{x}\rangle &= \frac{1}{(2\pi\hbar)^{\frac{D}{2}}} \int \mathrm{d}^D\boldsymbol{x}' \ \mathrm{e}^{-i\boldsymbol{x}'\bullet\boldsymbol{p}/\hbar} \langle \boldsymbol{x}'|\boldsymbol{x}\rangle \\
&= \frac{1}{(2\pi\hbar)^{\frac{D}{2}}} \int \mathrm{d}^D\boldsymbol{x}' \ \mathrm{e}^{-i\boldsymbol{x}'\bullet\boldsymbol{p}/\hbar} \delta\left(\boldsymbol{x}' - \boldsymbol{x}\right) \\
&= \frac{1}{(2\pi\hbar)^{\frac{D}{2}}} \ \mathrm{e}^{-i\boldsymbol{x}\bullet\boldsymbol{p}/\hbar} \,.
\end{aligned} \tag{2.12}$$

This leads to

$$\begin{aligned}
\left\langle \widehat{\boldsymbol{\Omega}} \right\rangle &= \frac{1}{(2\pi\hbar)^D} \iiiint \mathrm{d}^D\boldsymbol{x}_1 \ \mathrm{d}^D\boldsymbol{x}_2 \ \mathrm{d}^D\boldsymbol{p}_1 \ \mathrm{d}^D\boldsymbol{p}_2 \\
&\quad \times \mathrm{e}^{i\boldsymbol{x}_2\bullet\boldsymbol{p}_1/\hbar} \ \mathrm{e}^{-i\boldsymbol{x}_1\bullet\boldsymbol{p}_2/\hbar} \langle \boldsymbol{p}_1|\Psi\rangle \langle \Psi|\boldsymbol{p}_2\rangle \left\langle \boldsymbol{x}_1 \middle| \widehat{\boldsymbol{\Omega}} \middle| \boldsymbol{x}_2 \right\rangle .
\end{aligned} \tag{2.13}$$

The variables of integration can be changed from $\boldsymbol{x}_1$, $\boldsymbol{x}_2$, $\boldsymbol{p}_1$, and $\boldsymbol{p}_2$ to $\boldsymbol{x}=\frac{\boldsymbol{x}_1+\boldsymbol{x}_2}{2}$, $\boldsymbol{\eta} = \boldsymbol{x}_1 - \boldsymbol{x}_2$, $\boldsymbol{p}=\frac{\boldsymbol{p}_1+\boldsymbol{p}_2}{2}$, and $\boldsymbol{\lambda} = \boldsymbol{p}_1 - \boldsymbol{p}_2$. For this change the absolute value of the determinant of the Jacobian matrix,

simplified because the matrix is block diagonal, becomes

$$
\det \begin{vmatrix} \begin{pmatrix} \dfrac{\partial \boldsymbol{x}}{\partial \boldsymbol{x}_1} & \dfrac{\partial \boldsymbol{\eta}}{\partial \boldsymbol{x}_1} & \dfrac{\partial \boldsymbol{p}}{\partial \boldsymbol{x}_1} & \dfrac{\partial \boldsymbol{\lambda}}{\partial \boldsymbol{x}_1} \\[4pt] \dfrac{\partial \boldsymbol{x}}{\partial \boldsymbol{x}_2} & \dfrac{\partial \boldsymbol{\eta}}{\partial \boldsymbol{x}_2} & \dfrac{\partial \boldsymbol{p}}{\partial \boldsymbol{x}_2} & \dfrac{\partial \boldsymbol{\lambda}}{\partial \boldsymbol{x}_2} \\[4pt] \dfrac{\partial \boldsymbol{x}}{\partial \boldsymbol{p}_1} & \dfrac{\partial \boldsymbol{\eta}}{\partial \boldsymbol{p}_1} & \dfrac{\partial \boldsymbol{p}}{\partial \boldsymbol{p}_1} & \dfrac{\partial \boldsymbol{\lambda}}{\partial \boldsymbol{p}_1} \\[4pt] \dfrac{\partial \boldsymbol{x}}{\partial \boldsymbol{p}_2} & \dfrac{\partial \boldsymbol{\eta}}{\partial \boldsymbol{p}_2} & \dfrac{\partial \boldsymbol{p}}{\partial \boldsymbol{p}_2} & \dfrac{\partial \boldsymbol{\lambda}}{\partial \boldsymbol{p}_2} \end{pmatrix} \end{vmatrix} = \det \begin{vmatrix} \begin{pmatrix} \dfrac{1}{2} & 1 & 0 & 0 \\[4pt] \dfrac{1}{2} & -1 & 0 & 0 \\[4pt] 0 & 0 & \dfrac{1}{2} & 1 \\[4pt] 0 & 0 & \dfrac{1}{2} & -1 \end{pmatrix} \end{vmatrix}
$$

$$
= \begin{vmatrix} \det \begin{pmatrix} \dfrac{1}{2} & 1 \\[4pt] \dfrac{1}{2} & -1 \end{pmatrix} \det \begin{pmatrix} \dfrac{1}{2} & 1 \\[4pt] \dfrac{1}{2} & -1 \end{pmatrix} \end{vmatrix}
$$

$$
= \left| \left(\det \begin{pmatrix} \dfrac{1}{2} & 1 \\[4pt] \dfrac{1}{2} & -1 \end{pmatrix} \right)^2 \right| = \left| \left(-\dfrac{1}{2} - \dfrac{1}{2} \right)^2 \right| = 1. \tag{2.14}
$$

Thus, the equation becomes

$$
\begin{aligned}
\left\langle \widehat{\boldsymbol{\Omega}} \right\rangle &= \frac{1}{(2\pi\hbar)^D} \iiiint \mathrm{d}^D\boldsymbol{x}\,\mathrm{d}^D\boldsymbol{\eta}\,\mathrm{d}^D\boldsymbol{p}\,\mathrm{d}^D\boldsymbol{\lambda} \\
&\quad \times \mathrm{e}^{i\left(\boldsymbol{x}-\frac{\boldsymbol{\eta}}{2}\right)\bullet\left(\boldsymbol{p}+\frac{\boldsymbol{\lambda}}{2}\right)/\hbar}\,\mathrm{e}^{-i\left(\boldsymbol{x}+\frac{\boldsymbol{\eta}}{2}\right)\bullet\left(\boldsymbol{p}-\frac{\boldsymbol{\lambda}}{2}\right)/\hbar} \\
&\quad \times \left\langle \boldsymbol{p}+\frac{\boldsymbol{\lambda}}{2}\middle|\Psi\right\rangle\left\langle \Psi\middle|\boldsymbol{p}-\frac{\boldsymbol{\lambda}}{2}\right\rangle\left\langle \boldsymbol{x}+\frac{\boldsymbol{\eta}}{2}\middle|\widehat{\boldsymbol{\Omega}}\middle|\boldsymbol{x}-\frac{\boldsymbol{\eta}}{2}\right\rangle \\
&= \frac{1}{(2\pi\hbar)^D} \iiiint \mathrm{d}^D\boldsymbol{x}\,\mathrm{d}^D\boldsymbol{\eta}\,\mathrm{d}^D\boldsymbol{p}\,\mathrm{d}^D\boldsymbol{\lambda} \\
&\quad \times \mathrm{e}^{i\left(\boldsymbol{x}\bullet\boldsymbol{p}+\frac{1}{2}\boldsymbol{x}\bullet\boldsymbol{\lambda}-\frac{1}{2}\boldsymbol{\eta}\bullet\boldsymbol{p}-\frac{1}{4}\boldsymbol{\eta}\bullet\boldsymbol{\lambda}-\boldsymbol{x}\bullet\boldsymbol{p}+\frac{1}{2}\boldsymbol{x}\bullet\boldsymbol{\lambda}-\frac{1}{2}\boldsymbol{\eta}\bullet\boldsymbol{p}+\frac{1}{4}\boldsymbol{\eta}\bullet\boldsymbol{\lambda}\right)/\hbar} \\
&\quad \times \left\langle \boldsymbol{p}+\frac{\boldsymbol{\lambda}}{2}\middle|\Psi\right\rangle\left\langle \Psi\middle|\boldsymbol{p}-\frac{\boldsymbol{\lambda}}{2}\right\rangle\left\langle \boldsymbol{x}+\frac{\boldsymbol{\eta}}{2}\middle|\widehat{\boldsymbol{\Omega}}\middle|\boldsymbol{x}-\frac{\boldsymbol{\eta}}{2}\right\rangle \\
&= \frac{1}{(2\pi\hbar)^D} \iiiint \mathrm{d}^D\boldsymbol{x}\,\mathrm{d}^D\boldsymbol{\eta}\,\mathrm{d}^D\boldsymbol{p}\,\mathrm{d}^D\boldsymbol{\lambda}\,\mathrm{e}^{i(\boldsymbol{x}\bullet\boldsymbol{\lambda}-\boldsymbol{\eta}\bullet\boldsymbol{p})/\hbar} \\
&\quad \times \left\langle \boldsymbol{p}+\frac{\boldsymbol{\lambda}}{2}\middle|\Psi\right\rangle\left\langle \Psi\middle|\boldsymbol{p}-\frac{\boldsymbol{\lambda}}{2}\right\rangle\left\langle \boldsymbol{x}+\frac{\boldsymbol{\eta}}{2}\middle|\widehat{\boldsymbol{\Omega}}\middle|\boldsymbol{x}-\frac{\boldsymbol{\eta}}{2}\right\rangle,
\end{aligned}
\tag{2.15}
$$

where Wigner transforms can be isolated, giving

$$
\left\langle \widehat{\Omega} \right\rangle = \iint \mathrm{d}^D\boldsymbol{x}\ \mathrm{d}^D\boldsymbol{p}
$$
$$
\times \left(\int \mathrm{d}^D\boldsymbol{\lambda}\ \mathrm{e}^{i\boldsymbol{x}\bullet\boldsymbol{\lambda}/\hbar} \left\langle \boldsymbol{p}+\frac{\boldsymbol{\lambda}}{2} \right| \tfrac{1}{(2\pi\hbar)^D} |\Psi\rangle\langle\Psi| \left| \boldsymbol{p}-\frac{\boldsymbol{\lambda}}{2} \right\rangle \right)
$$
$$
\times \left(\int \mathrm{d}^D\boldsymbol{\eta}\ \mathrm{e}^{-i\boldsymbol{\eta}\bullet\boldsymbol{p}/\hbar} \left\langle \boldsymbol{x}+\frac{\boldsymbol{\eta}}{2} \right| \widehat{\Omega} \left| \boldsymbol{x}-\frac{\boldsymbol{\eta}}{2} \right\rangle \right)
$$
$$
= \iint \mathrm{d}^D\boldsymbol{x}\ \mathrm{d}^D\boldsymbol{p}\ \left[\tfrac{1}{(2\pi\hbar)^D} |\Psi\rangle\langle\Psi| \right]_{\mathrm{W}}(\boldsymbol{x},\boldsymbol{p}) \left[\widehat{\Omega} \right]_{\mathrm{W}}(\boldsymbol{x},\boldsymbol{p}).
$$
$$
(2.16)
$$

This is equation 2.5.

To prove equation 2.3 two unity operators can be inserted

$$
\int \mathrm{d}^D\boldsymbol{\eta}\ \mathrm{e}^{-i\boldsymbol{\eta}\bullet\boldsymbol{p}/\hbar} \left\langle \boldsymbol{x}+\frac{\boldsymbol{\eta}}{2} \right| \widehat{\Omega} \left| \boldsymbol{x}-\frac{\boldsymbol{\eta}}{2} \right\rangle
$$
$$
= \iiint \mathrm{d}^D\boldsymbol{\eta}\ \mathrm{d}^D\boldsymbol{p}_1\ \mathrm{d}^D\boldsymbol{p}_2\ \mathrm{e}^{-i\boldsymbol{\eta}\bullet\boldsymbol{p}/\hbar}
$$
$$
\times \left\langle \boldsymbol{x}+\frac{\boldsymbol{\eta}}{2} \middle| \boldsymbol{p}_1 \right\rangle \left\langle \boldsymbol{p}_1 \middle| \widehat{\Omega} \middle| \boldsymbol{p}_2 \right\rangle \left\langle \boldsymbol{p}_2 \middle| \boldsymbol{x}-\frac{\boldsymbol{\eta}}{2} \right\rangle
$$
$$
= \frac{1}{(2\pi\hbar)^D} \iiint \mathrm{d}^D\boldsymbol{\eta}\ \mathrm{d}^D\boldsymbol{p}_1\ \mathrm{d}^D\boldsymbol{p}_2\ \mathrm{e}^{-i\boldsymbol{\eta}\bullet\boldsymbol{p}/\hbar}
$$
$$
\times \mathrm{e}^{i\left(\boldsymbol{x}+\frac{\boldsymbol{\eta}}{2}\right)\bullet\boldsymbol{p}_1/\hbar} \left\langle \boldsymbol{p}_1 \middle| \widehat{\Omega} \middle| \boldsymbol{p}_2 \right\rangle \mathrm{e}^{-i\left(\boldsymbol{x}-\frac{\boldsymbol{\eta}}{2}\right)\bullet\boldsymbol{p}_2/\hbar}
$$
$$
= \frac{1}{(2\pi\hbar)^D} \iiint \mathrm{d}^D\boldsymbol{\eta}\ \mathrm{d}^D\boldsymbol{p}_1\ \mathrm{d}^D\boldsymbol{p}_2
$$
$$
\times \mathrm{e}^{i\left(-\boldsymbol{\eta}\bullet\boldsymbol{p}+\boldsymbol{x}\bullet\boldsymbol{p}_1+\frac{1}{2}\boldsymbol{\eta}\bullet\boldsymbol{p}_1-\boldsymbol{x}\bullet\boldsymbol{p}_2+\frac{1}{2}\boldsymbol{\eta}\bullet\boldsymbol{p}_2\right)/\hbar} \left\langle \boldsymbol{p}_1 \middle| \widehat{\Omega} \middle| \boldsymbol{p}_2 \right\rangle
$$
$$
= \frac{1}{(2\pi\hbar)^D} \iiint \mathrm{d}^D\boldsymbol{\eta}\ \mathrm{d}^D\boldsymbol{p}_1\ \mathrm{d}^D\boldsymbol{p}_2
$$
$$
\times \mathrm{e}^{i\boldsymbol{\eta}\bullet\left(-\boldsymbol{p}+\frac{\boldsymbol{p}_1+\boldsymbol{p}_2}{2}\right)/\hbar} \mathrm{e}^{i\boldsymbol{x}\bullet(\boldsymbol{p}_1-\boldsymbol{p}_2)/\hbar} \left\langle \boldsymbol{p}_1 \middle| \widehat{\Omega} \middle| \boldsymbol{p}_2 \right\rangle. \quad (2.17)
$$

Changing the variables in the integration from $\boldsymbol{p}_1$, and $\boldsymbol{p}_2$ to $\boldsymbol{p}'=\frac{\boldsymbol{p}_1+\boldsymbol{p}_2}{2}$, and $\boldsymbol{\lambda}=\boldsymbol{p}_1-\boldsymbol{p}_2$, with the absolute value of the determinant of the

Jacobian matrix being

$$
\left| \det \begin{pmatrix} \dfrac{\partial \boldsymbol{p}'}{\partial \boldsymbol{p}_1} & \dfrac{\partial \boldsymbol{\lambda}}{\partial \boldsymbol{p}_1} \\ \dfrac{\partial \boldsymbol{p}'}{\partial \boldsymbol{p}_2} & \dfrac{\partial \boldsymbol{\lambda}}{\partial \boldsymbol{p}_2} \end{pmatrix} \right| = \left| \det \begin{pmatrix} \dfrac{1}{2} & 1 \\ \dfrac{1}{2} & -1 \end{pmatrix} \right| = \left| -\dfrac{1}{2} - \dfrac{1}{2} \right| = 1
$$

$$(2.18)$$

the equation becomes

$$
\int \mathrm{d}^D \boldsymbol{\eta} \, \mathrm{e}^{-i\boldsymbol{\eta}\bullet\boldsymbol{p}/\hbar} \left\langle \boldsymbol{x} + \frac{\boldsymbol{\eta}}{2} \middle| \widehat{\boldsymbol{\Omega}} \middle| \boldsymbol{x} - \frac{\boldsymbol{\eta}}{2} \right\rangle
$$
$$
= \frac{1}{(2\pi\hbar)^D} \iiint \mathrm{d}^D\boldsymbol{\eta} \, \mathrm{d}^D\boldsymbol{p}' \, \mathrm{d}^D\boldsymbol{\lambda}
$$
$$
\times \mathrm{e}^{i\boldsymbol{\eta}\bullet(\boldsymbol{p}'-\boldsymbol{p})/\hbar} \, \mathrm{e}^{i\boldsymbol{x}\bullet\boldsymbol{\lambda}/\hbar} \left\langle \boldsymbol{p}' + \frac{\boldsymbol{\lambda}}{2} \middle| \widehat{\boldsymbol{\Omega}} \middle| \boldsymbol{p}' - \frac{\boldsymbol{\lambda}}{2} \right\rangle. \quad (2.19)
$$

Since the Dirac delta function can be written

$$
\delta\left(\boldsymbol{\zeta}\right) = \frac{1}{(2\pi)^D} \int \mathrm{d}^D\boldsymbol{\xi} \, \mathrm{e}^{i\boldsymbol{\zeta}\bullet\boldsymbol{\xi}}, \tag{2.20}
$$

where $\boldsymbol{\zeta}$ and $\boldsymbol{\xi}$ are just dummy vector variables, and

$$
\delta\left(c\boldsymbol{\zeta}\right) = \frac{1}{|c|^D}\delta\left(\boldsymbol{\zeta}\right), \tag{2.21}
$$

where c is a scalar constant, $\boldsymbol{p}'$ can be integrated out,

$$
\int \mathrm{d}^D\boldsymbol{\eta}\ \mathrm{e}^{-i\boldsymbol{\eta}\bullet\boldsymbol{p}/\hbar} \left\langle \boldsymbol{x} + \frac{\boldsymbol{\eta}}{2} \middle| \widehat{\boldsymbol{\Omega}} \middle| \boldsymbol{x} - \frac{\boldsymbol{\eta}}{2} \right\rangle
$$
$$
= \frac{1}{\hbar^D} \iint \mathrm{d}^D\boldsymbol{p}'\ \mathrm{d}^D\boldsymbol{\lambda} \left(\frac{1}{(2\pi)^D} \int \mathrm{d}^D\boldsymbol{\eta}\ \mathrm{e}^{i\boldsymbol{\eta}\bullet(\boldsymbol{p}'-\boldsymbol{p})/\hbar} \right)
$$
$$
\times \mathrm{e}^{i\boldsymbol{x}\bullet\boldsymbol{\lambda}/\hbar} \left\langle \boldsymbol{p}' + \frac{\boldsymbol{\lambda}}{2} \middle| \widehat{\boldsymbol{\Omega}} \middle| \boldsymbol{p}' - \frac{\boldsymbol{\lambda}}{2} \right\rangle
$$
$$
= \frac{1}{\hbar^D} \iint \mathrm{d}^D\boldsymbol{p}'\ \mathrm{d}^D\boldsymbol{\lambda}\, \delta \left(\frac{\boldsymbol{p}'-\boldsymbol{p}}{\hbar} \right)
$$
$$
\times \mathrm{e}^{i\boldsymbol{x}\bullet\boldsymbol{\lambda}/\hbar} \left\langle \boldsymbol{p}' + \frac{\boldsymbol{\lambda}}{2} \middle| \widehat{\boldsymbol{\Omega}} \middle| \boldsymbol{p}' - \frac{\boldsymbol{\lambda}}{2} \right\rangle
$$
$$
= \iint \mathrm{d}^D\boldsymbol{p}'\ \mathrm{d}^D\boldsymbol{\lambda}\, \delta \left(\boldsymbol{p}' - \boldsymbol{p} \right)
$$
$$
\times \mathrm{e}^{i\boldsymbol{x}\bullet\boldsymbol{\lambda}/\hbar} \left\langle \boldsymbol{p}' + \frac{\boldsymbol{\lambda}}{2} \middle| \widehat{\boldsymbol{\Omega}} \middle| \boldsymbol{p}' - \frac{\boldsymbol{\lambda}}{2} \right\rangle
$$
$$
= \int \mathrm{d}^D\boldsymbol{\lambda}\ \mathrm{e}^{i\boldsymbol{x}\bullet\boldsymbol{\lambda}/\hbar} \left\langle \boldsymbol{p} + \frac{\boldsymbol{\lambda}}{2} \middle| \widehat{\boldsymbol{\Omega}} \middle| \boldsymbol{p} - \frac{\boldsymbol{\lambda}}{2} \right\rangle . \tag{2.22}
$$

As expected, this is equation 2.3.

The relation between the Wigner transform and Fourier transform

An interesting, and sometime useful, property of the Wigner transform is that it is the Fourier transform of a matrix element. If in equation 2.3 $\langle \boldsymbol{x}+\frac{\boldsymbol{\eta}}{2}|\widehat{\boldsymbol{\Omega}}|\boldsymbol{x}-\frac{\boldsymbol{\eta}}{2}\rangle$ is just written as a function of $\boldsymbol{\eta}$, $f(\boldsymbol{\eta})$, then it can be easily seen that

$$
\left[\widehat{\boldsymbol{\Omega}} \right]_{\mathrm{W}} (\boldsymbol{x}, \boldsymbol{p}) = \int \mathrm{d}^D\boldsymbol{\eta}\ \mathrm{e}^{-i\boldsymbol{\eta}\bullet\boldsymbol{p}/\hbar}\, f(\boldsymbol{\eta}) \tag{2.23}
$$

is a Fourier transform. Taking the inverse of this Fourier transform would give back the original function.

$$
\frac{1}{(2\pi)^D} \int \mathrm{d}^D\frac{\boldsymbol{p}}{\hbar}\ \mathrm{e}^{i\boldsymbol{\eta}\bullet\boldsymbol{p}/\hbar} \left[\widehat{\boldsymbol{\Omega}} \right]_{\mathrm{W}} (\boldsymbol{x}, \boldsymbol{p}) = f(\boldsymbol{\eta}) \tag{2.24}
$$

More nicely written as

$$\frac{1}{(2\pi\hbar)^D} \int \mathrm{d}^D \boldsymbol{p} \; \mathrm{e}^{i\boldsymbol{\eta}\bullet\boldsymbol{p}/\hbar} \left[\widehat{\boldsymbol{\Omega}}\right]_{\mathrm{W}} (\boldsymbol{x}, \boldsymbol{p}) = \left\langle \boldsymbol{x} + \frac{\boldsymbol{\eta}}{2} \middle| \widehat{\boldsymbol{\Omega}} \middle| \boldsymbol{x} - \frac{\boldsymbol{\eta}}{2} \right\rangle.$$

$$(2.25)$$

As any pair of positions $\boldsymbol{x}_1$ and $\boldsymbol{x}_2$ can be rewritten as $\boldsymbol{x} + \frac{\boldsymbol{\eta}}{2}$ and $\boldsymbol{x} - \frac{\boldsymbol{\eta}}{2}$ through $\boldsymbol{x} = \frac{\boldsymbol{x}_1 + \boldsymbol{x}_2}{2}$ and $\boldsymbol{\eta} = \boldsymbol{x}_1 - \boldsymbol{x}_2$, this means that any position matrix element can be written as

$$\left\langle \boldsymbol{x}_1 \middle| \widehat{\boldsymbol{\Omega}} \middle| \boldsymbol{x}_2 \right\rangle = \frac{1}{(2\pi\hbar)^D} \int \mathrm{d}^D \boldsymbol{p} \; \mathrm{e}^{i(\boldsymbol{x}_1 - \boldsymbol{x}_2)\bullet\boldsymbol{p}/\hbar}$$
$$\times \left[\widehat{\boldsymbol{\Omega}}\right]_{\mathrm{W}} \left(\frac{\boldsymbol{x}_1 + \boldsymbol{x}_2}{2}, \boldsymbol{p}\right).$$

$$(2.26)$$

The classical Wigner method

Although he did not recommend using the method, Heller[14] in 1976 introduced the first version of the classical Wigner method. It was later, in 1998, introduced in a more general form by Wang, Sun, and Miller.[17] The classical Wigner method approximates quantum mechanics by propagating a Wigner transformed quantity forward in time with classical mechanics, i.e.

$$\left[\mathrm{e}^{\frac{i\widehat{H}t}{\hbar}} \, \widehat{\boldsymbol{\Omega}} \, \mathrm{e}^{-\frac{i\widehat{H}t}{\hbar}}\right]_{\mathrm{W}} (\boldsymbol{x}, \boldsymbol{p}) \simeq \left[\widehat{\boldsymbol{\Omega}}\right]_{\mathrm{W}} (\boldsymbol{x}(t), \boldsymbol{p}(t)).$$

$$(2.27)$$

This gives exact quantum mechanics for a free particle, linear potential, and harmonic potential. For other kinds of potentials it is an approximation.[14]

Wang, Sun, and Miller[17] developed the classical Wigner method as a linearization approximation of the semi-classical initial value representation (SC-IVR) of Miller[18] (well explained by the same author in a later paper[19]). Because of the linearization approximation applied to SC-IVR to obtain the classical Wigner method a common name for the classical Wigner method is linearized semi-classical initial value representation (LSC-IVR). The thing that is linearized is the differences between the positions and momenta in the paths forward and backward in time. When going from SC-IVR to LSC-IVR the quantum coherence in real time, that SC-IVR has, is lost.

Condensed phase and large systems have many degrees of freedom coupled together that typically can result in rapid decoherence, so for these kinds of systems the loss of quantum real time coherence is not necessarily a big problem.[20] With the linearization approximation comes the benefit of less oscillatory integrands which are easier to evaluate numerically than the ones in ordinary SC-IVR.[20]

Another, possibly more straightforward, way of deriving the classical Wigner method is the linearized path integral (LPI) approach.[21,22] The derivation of LPI is shown in the last part of section 2.2. There it is also proven that the classical Wigner method is exact for constant, linear, and harmonic potentials and sums of these.

The classical Wigner method is exact at the initial time, with zero point energy and motion, static tunneling , interference and so on, but the method can not handle such things as dynamic tunneling and dynamic quantum interference.

An example of successful usage of the classical Wigner method is calculation of vibrational energy relaxation rate constants,[23,24] where a few different systems were tested. Another example is the calculation of kinetic energy and density fluctuation spectrum of liquid neon at 27 K.[25] A third example is the calculation of a quantum correction factor for the far IR-spectrum of liquid water at 296 K.[26]

An instance where the limitations of the classical Wigner method have a detrimental effect is the simulation of a graphite surface.[27] In an anisotropic material, such as graphite, there will be more zero point energy in some directions than in others, and during the classical propagation this energy can leak to the directions with less zero point energy. Another example where the leakage of zero point energy causes problems for the classical Wigner method is the calculation of the self diffusion coefficient of liquid water.[28]

2.2   Feynman path integral formulation of quantum mechanics

> Yes, there is goal and meaning in our path -
> but it's the way that is the labour's worth.

Karin M. Boye (transl. David McDuff)[29]

The path integral formulation of quantum mechanics was introduced in 1948 by Feynman.[30] It is also explained in the famous book by Feynman and Hibbs.[31] In this formulation of quantum mechanics one looks at all possible paths from one position to another and makes a weighted "average" over all the paths, with the weights being complex numbers that all are equal in magnitude.

Derivation of the path integral formulation

We can start with the position matrix element of the time propagation operator

$$\left\langle \boldsymbol{x}_{\text{Final}} \left| e^{-\frac{i\widehat{H}t}{\hbar}} \right| \boldsymbol{x}_{\text{Initial}} \right\rangle .$$

Inserting the unit operator $N-1$ times and at the same time dividing the time propagation operator into N parts gives

$$\left\langle \boldsymbol{x}_{\text{Final}} \left| e^{-\frac{i\widehat{H}t}{\hbar}} \right| \boldsymbol{x}_{\text{Initial}} \right\rangle = \left\{ \prod_{j=1}^{N-1} \int \mathrm{d}^D \boldsymbol{x}_j \right\} \left\langle \boldsymbol{x}_{\text{Final}} \left| e^{-\frac{i\widehat{H}t}{N\hbar}} \right| \boldsymbol{x}_{N-1} \right\rangle$$
$$\ldots \left\langle \boldsymbol{x}_2 \left| e^{-\frac{i\widehat{H}t}{N\hbar}} \right| \boldsymbol{x}_1 \right\rangle \left\langle \boldsymbol{x}_1 \left| e^{-\frac{i\widehat{H}t}{N\hbar}} \right| \boldsymbol{x}_{\text{Initial}} \right\rangle . \tag{2.28}$$

For simplicity $\boldsymbol{x}_{\text{Initial}}$ will be called $\boldsymbol{x}_0$ and $\boldsymbol{x}_{\text{Final}}$ will be called $\boldsymbol{x}_N$ in the following.

In the limit $N \to \infty$ the Trotter product[32] can be used, giving

$$\lim_{N\to\infty} e^{-\frac{i\widehat{H}t}{N\hbar}} = \lim_{N\to\infty} e^{-\frac{i\widehat{T}t}{N\hbar}} e^{-\frac{i\widehat{V}t}{N\hbar}}, \tag{2.29}$$

where $\widehat{V}$ is the potential energy operator and $\widehat{T}$ is the kinetic energy operator. If it is also assumed that the potential only depends on position, then

$$
\begin{aligned}
\left\langle \boldsymbol{x}_N \left| \mathrm{e}^{-\frac{i\widehat{H}t}{\hbar}} \right| \boldsymbol{x}_0 \right\rangle &= \lim_{N\to\infty} \left\{ \prod_{j=1}^{N-1} \int \mathrm{d}^D \boldsymbol{x}_j \right\} \\
&\times \left\langle \boldsymbol{x}_N \left| \mathrm{e}^{-\frac{i\widehat{T}t}{N\hbar}} \mathrm{e}^{-\frac{i\widehat{V}t}{N\hbar}} \right| \boldsymbol{x}_{N-1} \right\rangle \\
&\ldots \left\langle \boldsymbol{x}_2 \left| \mathrm{e}^{-\frac{i\widehat{T}t}{N\hbar}} \mathrm{e}^{-\frac{i\widehat{V}t}{N\hbar}} \right| \boldsymbol{x}_1 \right\rangle \\
&\times \left\langle \boldsymbol{x}_1 \left| \mathrm{e}^{-\frac{i\widehat{T}t}{N\hbar}} \mathrm{e}^{-\frac{i\widehat{V}t}{N\hbar}} \right| \boldsymbol{x}_0 \right\rangle \\
&= \lim_{N\to\infty} \left\{ \prod_{j=1}^{N-1} \int \mathrm{d}^D \boldsymbol{x}_j \right\} \\
&\times \left\langle \boldsymbol{x}_N \left| \mathrm{e}^{-\frac{i\widehat{T}t}{N\hbar}} \right| \boldsymbol{x}_{N-1} \right\rangle \mathrm{e}^{-\frac{iV(\boldsymbol{x}_{N-1})t}{N\hbar}} \\
&\ldots \left\langle \boldsymbol{x}_2 \left| \mathrm{e}^{-\frac{i\widehat{T}t}{N\hbar}} \right| \boldsymbol{x}_1 \right\rangle \mathrm{e}^{-\frac{iV(\boldsymbol{x}_1)t}{N\hbar}} \\
&\times \left\langle \boldsymbol{x}_1 \left| \mathrm{e}^{-\frac{i\widehat{T}t}{N\hbar}} \right| \boldsymbol{x}_0 \right\rangle \mathrm{e}^{-\frac{iV(\boldsymbol{x}_0)t}{N\hbar}} \\
&= \lim_{N\to\infty} \left\{ \prod_{j=1}^{N-1} \int \mathrm{d}^D \boldsymbol{x}_j \right\} \left\langle \boldsymbol{x}_N \left| \mathrm{e}^{-\frac{i\widehat{T}t}{N\hbar}} \right| \boldsymbol{x}_{N-1} \right\rangle \\
&\ldots \left\langle \boldsymbol{x}_2 \left| \mathrm{e}^{-\frac{i\widehat{T}t}{N\hbar}} \right| \boldsymbol{x}_1 \right\rangle \left\langle \boldsymbol{x}_1 \left| \mathrm{e}^{-\frac{i\widehat{T}t}{N\hbar}} \right| \boldsymbol{x}_0 \right\rangle \\
&\times \mathrm{e}^{-\frac{it}{N\hbar}\sum_{j=0}^{N-1} V(\boldsymbol{x}_j)}, \tag{2.30}
\end{aligned}
$$

where $V(\boldsymbol{x}_j)$ is the potential energy

The kinetic energy operator is $\widehat{T} = \dfrac{1}{2}\left(\boldsymbol{m}^{-1}\widehat{\boldsymbol{p}}\right) \bullet \widehat{\boldsymbol{p}}$, where $\widehat{\boldsymbol{p}}$ is the momentum operator and $\boldsymbol{m}$ is a square diagonal matrix with the masses for the various degrees of freedom in the diagonal. For each

19

$\left\langle \boldsymbol{x}_j \middle| \mathrm{e}^{-\frac{i\widehat{T}t}{N\hbar}} \middle| \boldsymbol{x}_{j'} \right\rangle$ in the above equation

$$
\begin{aligned}
\left\langle \boldsymbol{x}_j \middle| \mathrm{e}^{-\frac{i\widehat{T}t}{N\hbar}} \middle| \boldsymbol{x}_{j'} \right\rangle &= \left\langle \boldsymbol{x}_j \middle| \mathrm{e}^{-\frac{i\frac{1}{2}\left(\boldsymbol{m}^{-1}\widehat{\boldsymbol{p}}\right)\bullet\widehat{\boldsymbol{p}}t}{N\hbar}} \middle| \boldsymbol{x}_{j'} \right\rangle \\
&= \frac{1}{(2\pi\hbar)^D} \iint \mathrm{d}^D\boldsymbol{p}_j \; \mathrm{d}^D\boldsymbol{p}_{j'} \; \langle \boldsymbol{x}_j | \boldsymbol{p}_j \rangle \\
&\quad \times \left\langle \boldsymbol{p}_j \middle| \mathrm{e}^{-\frac{i\frac{1}{2}\left(\boldsymbol{m}^{-1}\widehat{\boldsymbol{p}}\right)\bullet\widehat{\boldsymbol{p}}t}{N\hbar}} \middle| \boldsymbol{p}_{j'} \right\rangle \langle \boldsymbol{p}_{j'} | \boldsymbol{x}_{j'} \rangle \\
&= \frac{1}{(2\pi\hbar)^D} \iint \mathrm{d}^D\boldsymbol{p}_j \; \mathrm{d}^D\boldsymbol{p}_{j'} \; \mathrm{e}^{\frac{i\boldsymbol{x}_j\bullet\boldsymbol{p}_j}{\hbar}} \; \mathrm{e}^{-\frac{i\boldsymbol{x}_{j'}\bullet\boldsymbol{p}_{j'}}{\hbar}} \\
&\quad \times \left\langle \boldsymbol{p}_j \middle| \mathrm{e}^{-\frac{i\frac{1}{2}\left(\boldsymbol{m}^{-1}\widehat{\boldsymbol{p}}\right)\bullet\widehat{\boldsymbol{p}}t}{N\hbar}} \middle| \boldsymbol{p}_{j'} \right\rangle \\
&= \frac{1}{(2\pi\hbar)^D} \iint \mathrm{d}^D\boldsymbol{p}_j \; \mathrm{d}^D\boldsymbol{p}_{j'} \; \mathrm{e}^{\frac{i\boldsymbol{x}_j\bullet\boldsymbol{p}_j}{\hbar}} \; \mathrm{e}^{-\frac{i\boldsymbol{x}_{j'}\bullet\boldsymbol{p}_{j'}}{\hbar}} \\
&\quad \times \mathrm{e}^{-\frac{i\frac{1}{2}\left(\boldsymbol{m}^{-1}\boldsymbol{p}_j\right)\bullet\boldsymbol{p}_j t}{N\hbar}} \; \langle \boldsymbol{p}_j | \boldsymbol{p}_{j'} \rangle \\
&= \frac{1}{(2\pi\hbar)^D} \iint \mathrm{d}^D\boldsymbol{p}_j \; \mathrm{d}^D\boldsymbol{p}_{j'} \; \mathrm{e}^{\frac{i\boldsymbol{x}_j\bullet\boldsymbol{p}_j}{\hbar}} \; \mathrm{e}^{-\frac{i\boldsymbol{x}_{j'}\bullet\boldsymbol{p}_{j'}}{\hbar}} \\
&\quad \times \mathrm{e}^{-\frac{i\frac{1}{2}\left(\boldsymbol{m}^{-1}\boldsymbol{p}_j\right)\bullet\boldsymbol{p}_j t}{N\hbar}} \; \delta\left(\boldsymbol{p}_j - \boldsymbol{p}_{j'}\right).
\end{aligned} \tag{2.31}
$$

Integrating over $\boldsymbol{p}_{j'}$ one acquires

$$
\begin{aligned}
\left\langle \boldsymbol{x}_j \left| e^{-\frac{i\widehat{T}t}{N\hbar}} \right| \boldsymbol{x}_{j'} \right\rangle &= \frac{1}{(2\pi\hbar)^D} \int \mathrm{d}^D\boldsymbol{p}_j \; e^{\frac{i\left(\boldsymbol{x}_j - \boldsymbol{x}_{j'}\right)\bullet\boldsymbol{p}_j}{\hbar}} \; e^{-\frac{i\frac{1}{2}\left(\boldsymbol{m}^{-1}\boldsymbol{p}_j\right)\bullet\boldsymbol{p}_j t}{N\hbar}} \\
&= \frac{1}{(2\pi\hbar)^D} \int \mathrm{d}^D\boldsymbol{p}_j \; e^{-\frac{it}{2N\hbar}\left(\left(\boldsymbol{m}^{-1}\boldsymbol{p}_j\right)\bullet\boldsymbol{p}_j - \frac{2N}{t}\left(\boldsymbol{x}_j - \boldsymbol{x}_{j'}\right)\bullet\boldsymbol{p}_j\right)} \\
&= \frac{1}{(2\pi\hbar)^D} \int \mathrm{d}^D\boldsymbol{p}_j \; e^{-\frac{it}{2N\hbar}\sum_{j''=1}^D \left(\frac{p^2_{j'',j}}{m_{j''}} - \frac{2N}{t}\left(x_{j'',j} - x_{j'',j'}\right)p_{j'',j}\right)} \\
&= \frac{1}{(2\pi\hbar)^D} \int \mathrm{d}^D\boldsymbol{p}_j \\
&\quad \times e^{-\frac{it}{2N\hbar}\sum_{j''=1}^D \left(\frac{1}{m_{j''}}\left(p^2_{j'',j} - \frac{2Nm_{j''}}{t}\left(x_{j'',j} - x_{j'',j'}\right)p_{j'',j}\right)\right)} \\
&= \frac{1}{(2\pi\hbar)^D} \int \mathrm{d}^D\boldsymbol{p}_j \\
&\quad \times e^{-\frac{it}{2N\hbar}\sum_{j''=1}^D \left(\frac{1}{m_{j''}}\left(p_{j'',j} - \frac{Nm_{j''}}{t}\left(x_{j'',j} - x_{j'',j'}\right)\right)^2\right)} \\
&\quad \times e^{\frac{it}{2N\hbar}\sum_{j''=1}^D \left(\frac{N^2 m^2_{j''}}{m_{j''} t^2}\left(x_{j'',j} - x_{j'',j'}\right)^2\right)} \\
&= \frac{1}{(2\pi\hbar)^D} e^{\frac{i}{\hbar}\sum_{j''=1}^D \left(\frac{Nm_{j''}}{2t}\left(x_{j'',j} - x_{j'',j'}\right)^2\right)} \int \mathrm{d}^D\boldsymbol{p}_j \\
&\quad \times e^{-\frac{it}{2N\hbar}\sum_{j''=1}^D \left(\frac{1}{m_{j''}}\left(p_{j'',j} - \frac{Nm_{j''}}{t}\left(x_{j'',j} - x_{j'',j'}\right)\right)^2\right)}, \quad (2.32)
\end{aligned}
$$

where j'' denotes a component of $\boldsymbol{x}$ or $\boldsymbol{p}$. Changing variables of integration from $p_{j'',j}$ to

$$\zeta_{j''} = \sqrt{\frac{t}{2Nm_{j''}\hbar}} \left(p_{j'',j} - \frac{Nm_{j''}}{t}(x_{j'',j} - x_{j'',j'}) \right) \text{ gives}$$

$$\left\langle \boldsymbol{x}_j \left| e^{-\frac{i\widehat{T}t}{N\hbar}} \right| \boldsymbol{x}_{j'} \right\rangle = \frac{1}{(2\pi\hbar)^D} e^{\frac{i}{\hbar}\sum_{j''=1}^{D}\left(\frac{Nm_{j''}}{2t}(x_{j'',j}-x_{j'',j'})^2\right)}$$

$$\times \left(\frac{2N\hbar}{t}\right)^{\frac{D}{2}} \sqrt{\prod_{j''=1}^{D} m_{j''}} \int d^D\boldsymbol{\zeta} \; e^{-i\sum_{j''=1}^{D}\zeta_{j''}^2}$$

$$= \frac{1}{(2\pi\hbar)^D} e^{\frac{iN}{2t\hbar}(\boldsymbol{m}(\boldsymbol{x}_j-\boldsymbol{x}_{j'}))\bullet(\boldsymbol{x}_j-\boldsymbol{x}_{j'})} \left(\frac{2N\hbar}{t}\right)^{\frac{D}{2}}$$

$$\times \sqrt{\det(\boldsymbol{m})} \int d^D\boldsymbol{\zeta} \prod_{j''=1}^{D} \left(\cos\left(\zeta_{j''}^2\right) - i\sin\left(\zeta_{j''}^2\right)\right)$$

$$= \frac{1}{(2\pi\hbar)^D} e^{\frac{iN}{2t\hbar}(\boldsymbol{m}(\boldsymbol{x}_j-\boldsymbol{x}_{j'}))\bullet(\boldsymbol{x}_j-\boldsymbol{x}_{j'})} \left(\frac{2N\hbar}{t}\right)^{\frac{D}{2}}$$

$$\times \sqrt{\det(\boldsymbol{m})} \prod_{j''=1}^{D} \left(\sqrt{\frac{\pi}{2}} - i\sqrt{\frac{\pi}{2}}\right)$$

$$= \frac{1}{(2\pi\hbar)^D} e^{\frac{iN}{2t\hbar}(\boldsymbol{m}(\boldsymbol{x}_j-\boldsymbol{x}_{j'}))\bullet(\boldsymbol{x}_j-\boldsymbol{x}_{j'})} \left(\frac{2\pi N\hbar}{it}\right)^{\frac{D}{2}}$$

$$\times \sqrt{\det(\boldsymbol{m})}$$

$$= \left(\frac{N}{2\pi it\hbar}\right)^{\frac{D}{2}} \sqrt{\det(\boldsymbol{m})} \; e^{\frac{iN}{2t\hbar}(\boldsymbol{m}(\boldsymbol{x}_j-\boldsymbol{x}_{j'}))\bullet(\boldsymbol{x}_j-\boldsymbol{x}_{j'})}. \quad (2.33)$$

Putting this result into equation 2.30 gives

$$
\left\langle \boldsymbol{x}_N \middle| \mathrm{e}^{-\frac{i\hat{H}t}{\hbar}} \middle| \boldsymbol{x}_0 \right\rangle = \lim_{N\to\infty} \left\{ \prod_{j=1}^{N-1} \int \mathrm{d}^D \boldsymbol{x}_j \right\}
$$

$$
\times \left(\left(\frac{N}{2\pi it\hbar} \right)^{\frac{D}{2}} \sqrt{\det(\boldsymbol{m})} \, \mathrm{e}^{\frac{iN}{2t\hbar}(\boldsymbol{m}(\boldsymbol{x}_N - \boldsymbol{x}_{N-1}))\bullet(\boldsymbol{x}_N - \boldsymbol{x}_{N-1})} \right.
$$

$$
\cdots \left(\frac{N}{2\pi it\hbar} \right)^{\frac{D}{2}} \sqrt{\det(\boldsymbol{m})} \, \mathrm{e}^{\frac{iN}{2t\hbar}(\boldsymbol{m}(\boldsymbol{x}_2 - \boldsymbol{x}_1))\bullet(\boldsymbol{x}_2 - \boldsymbol{x}_1)}
$$

$$
\left. \times \left(\frac{N}{2\pi it\hbar} \right)^{\frac{D}{2}} \sqrt{\det(\boldsymbol{m})} \, \mathrm{e}^{\frac{iN}{2t\hbar}(\boldsymbol{m}(\boldsymbol{x}_1 - \boldsymbol{x}_0))\bullet(\boldsymbol{x}_1 - \boldsymbol{x}_0)} \right)
$$

$$
\times \mathrm{e}^{-\frac{it}{N\hbar}\sum_{j=0}^{N-1} V(\boldsymbol{x}_j)}
$$

$$
= \lim_{N\to\infty} \left(\frac{N}{2\pi it\hbar} \right)^{\frac{ND}{2}} (\det(\boldsymbol{m}))^{\frac{N}{2}} \left\{ \prod_{j=1}^{N-1} \int \mathrm{d}^D \boldsymbol{x}_j \right\}
$$

$$
\times \mathrm{e}^{\frac{iN}{2t\hbar}\sum_{j=0}^{N-1}(\boldsymbol{m}(\boldsymbol{x}_{j+1} - \boldsymbol{x}_j))\bullet(\boldsymbol{x}_{j+1} - \boldsymbol{x}_j)}
$$

$$
\times \mathrm{e}^{-\frac{it}{N\hbar}\sum_{j=0}^{N-1} V(\boldsymbol{x}_j)}
$$

$$
= \lim_{N\to\infty} \left(\frac{N}{2\pi it\hbar} \right)^{\frac{ND}{2}} (\det(\boldsymbol{m}))^{\frac{N}{2}} \left\{ \prod_{j=1}^{N-1} \int \mathrm{d}^D \boldsymbol{x}_j \right\}
$$

$$
\times \mathrm{e}^{\frac{it}{N\hbar}\sum_{j=0}^{N-1}\left(\frac{N^2}{t^2}\frac{1}{2}(\boldsymbol{m}(\boldsymbol{x}_{j+1} - \boldsymbol{x}_j))\bullet(\boldsymbol{x}_{j+1} - \boldsymbol{x}_j) - V(\boldsymbol{x}_j) \right)} . \tag{2.34}
$$

Now, let's introduce $\dfrac{t}{N} = \Delta t$ and rewrite all $\boldsymbol{x}_j$ as $\boldsymbol{x}(t')$, where $t' = j\Delta t$.

$$
\left\langle \boldsymbol{x}_N \middle| \mathrm{e}^{-\frac{i\hat{H}t}{\hbar}} \middle| \boldsymbol{x}_0 \right\rangle = \lim_{N\to\infty} \left(\frac{\det(\boldsymbol{m})}{(2\pi i\Delta t\hbar)^D} \right)^{\frac{N}{2}} \left\{ \prod_{j=1}^{N-1} \int \mathrm{d}^D \boldsymbol{x}(j\Delta t) \right\}
$$

$$
\times \mathrm{e}^{\frac{i}{\hbar}\Delta t \sum_{j=0}^{N-1}\left(\frac{1}{2}\left(\boldsymbol{m}\frac{\boldsymbol{x}((j+1)\Delta t) - \boldsymbol{x}(j\Delta t)}{\Delta t} \right)\bullet \frac{\boldsymbol{x}((j+1)\Delta t) - \boldsymbol{x}(j\Delta t)}{\Delta t} \right)}
$$

$$
\times \mathrm{e}^{\frac{i}{\hbar}\Delta t \sum_{j=0}^{N-1}(-V(\boldsymbol{x}(j\Delta t)))} \tag{2.35}
$$

where it can be recognized that as $N \to \infty$ and $\Delta t \to 0$

$$
\lim_{\Delta t\to 0} \frac{\boldsymbol{x}((j+1)\Delta t) - \boldsymbol{x}(j\Delta t)}{\Delta t} = \frac{\mathrm{d}\boldsymbol{x}(t')}{\mathrm{d}t'} = \dot{\boldsymbol{x}}(t'). \tag{2.36}
$$

This is the very definition of a derivative and the sum in the exponent is the Riemann integral over dt', so

$$\left\langle \boldsymbol{x}_N \left| e^{-\frac{i\hat{H}t}{\hbar}} \right| \boldsymbol{x}_0 \right\rangle = \lim_{N\to\infty} \left(\frac{\det(\boldsymbol{m})}{(2\pi i \Delta t \hbar)^D} \right)^{\frac{N}{2}} \left\{ \prod_{t'} \int d^D \boldsymbol{x}(t') \right\}$$

$$\times e^{\frac{i}{\hbar} \int_0^t dt' \left(\frac{1}{2}(\boldsymbol{m}\dot{\boldsymbol{x}}(t')) \bullet \dot{\boldsymbol{x}}(t') - V(\boldsymbol{x}(t')) \right)}. \tag{2.37}$$

Here the integrand in the exponent is a Langrangian, and integrating a Lagrangian over time gives the classical action, $S_{\text{cl}}(\boldsymbol{x}(t'), \dot{\boldsymbol{x}}(t'), t)$. $\left\{ \prod_{t'} \int d^D \boldsymbol{x}(t') \right\}$ is an integration over all paths from $\boldsymbol{x}(0)$ to $\boldsymbol{x}(t)$. $\left(\frac{\det(\boldsymbol{m})}{(2\pi i \Delta t \hbar)^D} \right)^{\frac{N}{2}}$ is a normalization factor, that can be called A^N. A shorter way to write then is

$$\left\langle \boldsymbol{x}_N \left| e^{-\frac{i\hat{H}t}{\hbar}} \right| \boldsymbol{x}_0 \right\rangle = \lim_{N\to\infty} A^N \left\{ \prod_{t'} \int d^D \boldsymbol{x}(t') \right\}$$

$$\times e^{\frac{i}{\hbar} S_{\text{cl}}(\boldsymbol{x}(t'), \dot{\boldsymbol{x}}(t'), t)}. \tag{2.38}$$

This is the path integral formulation. It uses a weighted average over all paths, with the weights being complex exponentials of the classical action of the path, all of which have equal magnitude.

The matrix element in equation 2.38 is called a kernel,

$$K(\boldsymbol{x}_N, \boldsymbol{x}_0, t) = \left\langle \boldsymbol{x}_N \left| e^{-\frac{i\hat{H}t}{\hbar}} \right| \boldsymbol{x}_0 \right\rangle. \tag{2.39}$$

The kernel can be used to propagate a wave function $\Psi(\boldsymbol{x}, 0)$ a time t forward in time to $\Psi(\boldsymbol{x}, t)$ through

$$\Psi(\boldsymbol{x}, t) = \langle \boldsymbol{x} | \Psi(t) \rangle = \int d^D \boldsymbol{x}' \, K(\boldsymbol{x}, \boldsymbol{x}', t) \langle \boldsymbol{x}' | \Psi(0) \rangle$$

$$= \int d^D \boldsymbol{x}' \left\langle \boldsymbol{x} \left| e^{-\frac{i\hat{H}t}{\hbar}} \right| \boldsymbol{x}' \right\rangle \langle \boldsymbol{x}' | \Psi(0) \rangle$$

$$= \left\langle \boldsymbol{x} \left| e^{-\frac{i\hat{H}t}{\hbar}} \right| \Psi(0) \right\rangle = e^{-\frac{i\hat{H}t}{\hbar}} \langle \boldsymbol{x} | \Psi(0) \rangle$$

$$= e^{-\frac{i\hat{H}t}{\hbar}} \Psi(\boldsymbol{x}, 0). \tag{2.40}$$

In general equations such as 2.38 and 2.40 are not analytically solvable and in a numerical approximation, with finite N, it is very difficult to converge an integral of such a quickly oscillating complex function as is relevant here. Thus, this formulation may not be very useful for directly calculating real time propagation, but is rather, at least from a computational chemist's point of view, of interest as a starting point from which approximate models and methods can be developed.

Imaginary time path integrals

Looking at the Boltzmann operator $\mathrm{e}^{-\beta\widehat{H}}$, or $\mathrm{e}^{-\frac{\widehat{H}}{k_{\mathrm{B}}T}}$, where $\beta = \dfrac{1}{k_{\mathrm{B}}T}$, k_{B} is Boltzmann's constant, and T is absolute temperature, it looks similar to the time propagation operator $\mathrm{e}^{-\frac{i\widehat{H}t}{\hbar}}$. In fact, if an imaginary time, given as $t = -i\beta\hbar$, would be inserted into the time propagation operator then the Boltzmann operator would be obtained.

Using this imaginary time in equation 2.34 gives

$$
\begin{aligned}
\left\langle \boldsymbol{x}_N \middle| \mathrm{e}^{-\beta\widehat{H}} \middle| \boldsymbol{x}_0 \right\rangle &= \lim_{N\to\infty} \left(\frac{N}{2\pi\beta\hbar^2} \right)^{\frac{ND}{2}} \left(\det\left(\boldsymbol{m}\right) \right)^{\frac{N}{2}} \\
&\times \left\{ \prod_{j=1}^{N-1} \int \mathrm{d}^D \boldsymbol{x}_j \right\} \mathrm{e}^{\frac{\beta}{N} \sum_{j=0}^{N-1} \left(\frac{N^2}{-\beta^2\hbar^2} \frac{1}{2} (\boldsymbol{m}(\boldsymbol{x}_{j+1}-\boldsymbol{x}_j)) \bullet (\boldsymbol{x}_{j+1}-\boldsymbol{x}_j) - V(\boldsymbol{x}_j) \right)} \\
&= \lim_{N\to\infty} \left(\frac{N}{2\pi\beta} \right)^{\frac{ND}{2}} \hbar^{ND} \left(\det\left(\boldsymbol{m}\right) \right)^{\frac{N}{2}} \left\{ \prod_{j=1}^{N-1} \int \mathrm{d}^D \boldsymbol{x}_j \right\} \\
&\times \mathrm{e}^{-\frac{\beta}{N} \sum_{j=0}^{N-1} \left(\frac{N^2}{2\beta^2\hbar^2} (\boldsymbol{m}(\boldsymbol{x}_{j+1}-\boldsymbol{x}_j)) \bullet (\boldsymbol{x}_{j+1}-\boldsymbol{x}_j) + V(\boldsymbol{x}_j) \right)} \,.
\end{aligned}
\tag{2.41}
$$

$-\frac{-i\beta\hbar}{N}$ is the new Δt in imaginary time. The kinetic energy terms $\frac{N^2}{2\beta^2\hbar^2} m_{j''} \left(x_{j'',j+1} - x_{j'',j} \right)^2$ are of the same form as the potential energy of harmonic springs with force constant $-\frac{N^2}{\beta^2\hbar^2} m_{j''}$. These are typically called "spring terms". Thus the integrand can be seen as a Boltzmann factor, at the temperature NT, of the potential energy of a number of copies of the system, $\boldsymbol{x}_j$, connected by harmonic springs.

Using this imaginary time kernel to calculate the canonical partition function, Z, one simply has to set $\boldsymbol{x}_0 = \boldsymbol{x}_N$ and integrate over
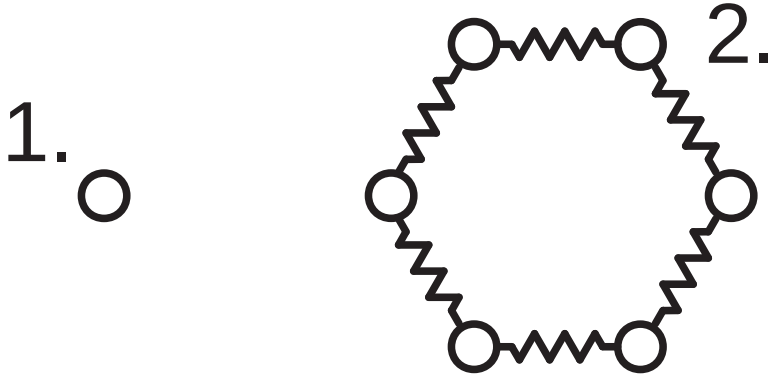
Figure 2.1: Illustration of a classical particle (1.) and its corresponding imaginary time path integral ring polymer (2.). The zigzag lines represent the spring terms.

$$\boldsymbol{x}_N$$

$$Z = \mathrm{Tr}\left\{\mathrm{e}^{-\beta\widehat{H}}\right\} = \int \mathrm{d}^D\boldsymbol{x}_N \left\langle \boldsymbol{x}_N \middle| \mathrm{e}^{-\beta\widehat{H}} \middle| \boldsymbol{x}_N \right\rangle$$

$$= \lim_{N\to\infty} \left(\frac{N}{2\pi\beta}\right)^{\frac{ND}{2}} \hbar^{ND} \left(\det\left(\boldsymbol{m}\right)\right)^{\frac{N}{2}} \left\{\prod_{j=1}^{N} \int \mathrm{d}^D\boldsymbol{x}_j\right\}$$

$$\times \mathrm{e}^{-\frac{\beta}{N}\sum_{j=1}^{N}\left(\frac{N^2}{2\beta^2\hbar^2}\left(\boldsymbol{m}\left(\boldsymbol{x}_{(j\bmod N)+1}-\boldsymbol{x}_j\right)\right)\bullet\left(\boldsymbol{x}_{(j\bmod N)+1}-\boldsymbol{x}_j\right)+V(\boldsymbol{x}_j)\right)},$$

$$(2.42)$$

where Tr denotes a trace and mod is the modulus operator.

The extended phase space of N copies of the system connected by harmonic springs is often seen as turning each single particle into a "polymer" with N monomers. The circular path integral found in equation 2.42 is then called a "ring polymer". This is schematically illustrated in figure 2.1.

Since the imaginary time kernel is real valued it is much easier to handle than the real time kernel, that is complex valued. By simply approximating N to be finite, equations 2.41 and 2.42 become accessible to numerical integration. Indeed two molecular simulation methods based immediately upon this is path integral Monte Carlo (PIMC)[33] and path integral molecular dynamics (PIMD)[34], which respectively use Monte Carlo and molecular dynamics to sample the integrand.

There are also methods for quantum dynamics that use this imaginary time path integral, such as centroid molecular dynamics (CMD)[35] and ring polymer molecular dynamics (RPMD)[36]. These dynamical methods will be explained somewhat in section 2.4.

Linearized path integral

The classical Wigner method can be derived from the real time path integral. This was first published by Shi and Geva[21] and somewhat later by Poulsen, Nyman, and Rossky.[22]

Starting with a matrix element of an operator at time t,

$$\left\langle \boldsymbol{x}_0 \left| \widehat{\boldsymbol{\Omega}}(t) \right| \boldsymbol{x}_0' \right\rangle = \left\langle \boldsymbol{x}_0 \left| e^{\frac{i\widehat{H}t}{\hbar}} \, \widehat{\boldsymbol{\Omega}} \, e^{-\frac{i\widehat{H}t}{\hbar}} \right| \boldsymbol{x}_0' \right\rangle, \tag{2.43}$$

and inserting unity operators,

$$\left\langle \boldsymbol{x}_0 \left| \widehat{\boldsymbol{\Omega}}(t) \right| \boldsymbol{x}_0' \right\rangle = \iint \mathrm{d}^D \boldsymbol{x}_N \, \mathrm{d}^D \boldsymbol{x}_N' \left\langle \boldsymbol{x}_0 \left| e^{\frac{i\widehat{H}t}{\hbar}} \right| \boldsymbol{x}_N \right\rangle$$
$$\times \left\langle \boldsymbol{x}_N \left| \widehat{\boldsymbol{\Omega}} \right| \boldsymbol{x}_N' \right\rangle \left\langle \boldsymbol{x}_N' \left| e^{-\frac{i\widehat{H}t}{\hbar}} \right| \boldsymbol{x}_0' \right\rangle, \tag{2.44}$$

a product of two kernels and a matrix element at time 0 is obtained. The interesting aspect here is the kernels. Drawing on equation 2.34,

the product of the kernels can be written

$$
\left\langle \boldsymbol{x}_0 \middle| e^{\frac{i\widehat{H}t}{\hbar}} \middle| \boldsymbol{x}_N \right\rangle \left\langle \boldsymbol{x}'_N \middle| e^{-\frac{i\widehat{H}t}{\hbar}} \middle| \boldsymbol{x}'_0 \right\rangle
$$

$$
= \lim_{N \to \infty} \left(\frac{N}{2\pi(-i)t\hbar} \right)^{\frac{ND}{2}} (\det(\boldsymbol{m}))^{\frac{N}{2}} \left\{ \prod_{j=1}^{N-1} \int \mathrm{d}^D \boldsymbol{x}_j \right\}
$$

$$
\times e^{-\frac{it}{N\hbar} \sum_{j=0}^{N-1} \left(\frac{N^2}{t^2} \frac{1}{2}(\boldsymbol{m}(\boldsymbol{x}_{j+1}-\boldsymbol{x}_j)) \bullet (\boldsymbol{x}_{j+1}-\boldsymbol{x}_j) - V(\boldsymbol{x}_j) \right)}
$$

$$
\times \left(\frac{N}{2\pi it\hbar} \right)^{\frac{ND}{2}} (\det(\boldsymbol{m}))^{\frac{N}{2}} \left\{ \prod_{j=1}^{N-1} \int \mathrm{d}^D \boldsymbol{x}'_j \right\}
$$

$$
\times e^{\frac{it}{N\hbar} \sum_{j=0}^{N-1} \left(\frac{N^2}{t^2} \frac{1}{2}(\boldsymbol{m}(\boldsymbol{x}'_{j+1}-\boldsymbol{x}'_j)) \bullet (\boldsymbol{x}'_{j+1}-\boldsymbol{x}'_j) - V(\boldsymbol{x}'_j) \right)}
$$

$$
= \lim_{N \to \infty} \left(\frac{\det(\boldsymbol{m})}{(2\pi \Delta t\hbar)^D} \right)^{N} \left\{ \prod_{j=1}^{N-1} \iint \mathrm{d}^D \boldsymbol{x}_j \, \mathrm{d}^D \boldsymbol{x}'_j \right\}
$$

$$
\times e^{-\frac{i}{\hbar} \Delta t \sum_{j=0}^{N-1} \left(\frac{1}{2} \frac{\left(\boldsymbol{m}(\boldsymbol{x}_{j+1}-\boldsymbol{x}_j)\right) \bullet (\boldsymbol{x}_{j+1}-\boldsymbol{x}_j)}{\Delta t^2} - V(\boldsymbol{x}_j) \right)}
$$

$$
\times e^{\frac{i}{\hbar} \Delta t \sum_{j=0}^{N-1} \left(\frac{1}{2} \frac{\left(\boldsymbol{m}(\boldsymbol{x}'_{j+1}-\boldsymbol{x}'_j)\right) \bullet (\boldsymbol{x}'_{j+1}-\boldsymbol{x}'_j)}{\Delta t^2} - V(\boldsymbol{x}'_j) \right)}, \tag{2.45}
$$

where it is assumed that the same N is used for both kernels and $\frac{t}{N} = \Delta t$. The coordinates can be changed to $\bar{\boldsymbol{x}}_j = \dfrac{\boldsymbol{x}_j + \boldsymbol{x}'_j}{2}$ and

$\Delta \boldsymbol{x} = \boldsymbol{x}'_j - \boldsymbol{x}_j$ (The Jacobian can be found in equation 2.14.), giving

$$
\left\langle \boldsymbol{x}_0 \left| \mathrm{e}^{\frac{i\widehat{H}t}{\hbar}} \right| \boldsymbol{x}_N \right\rangle \left\langle \boldsymbol{x}'_N \left| \mathrm{e}^{-\frac{i\widehat{H}t}{\hbar}} \right| \boldsymbol{x}'_0 \right\rangle
$$

$$
= \lim_{N\to\infty} \left(\frac{\det(\boldsymbol{m})}{(2\pi\Delta t\hbar)^D} \right)^N \left\{ \prod_{j=1}^{N-1} \iint \mathrm{d}^D\bar{\boldsymbol{x}}_j \, \mathrm{d}^D\Delta\boldsymbol{x}_j \right\}
$$

$$
\times \mathrm{e}^{-\frac{i}{\hbar}\Delta t \sum_{j=0}^{N-1} \left(\frac{1}{2} \frac{\left(\boldsymbol{m}\left(\bar{\boldsymbol{x}}_{j+1} - \frac{\Delta\boldsymbol{x}_{j+1}}{2} - \bar{\boldsymbol{x}}_j + \frac{\Delta\boldsymbol{x}_j}{2} \right) \right) \bullet \left(\bar{\boldsymbol{x}}_{j+1} - \frac{\Delta\boldsymbol{x}_{j+1}}{2} - \bar{\boldsymbol{x}}_j + \frac{\Delta\boldsymbol{x}_j}{2} \right)}{\Delta t^2} \right)}
$$

$$
\times \mathrm{e}^{-\frac{i}{\hbar}\Delta t \sum_{j=0}^{N-1} \left(-V\left(\bar{\boldsymbol{x}}_j - \frac{\Delta\boldsymbol{x}_j}{2} \right) \right)}
$$

$$
\times \mathrm{e}^{\frac{i}{\hbar}\Delta t \sum_{j=0}^{N-1} \left(\frac{1}{2} \frac{\left(\boldsymbol{m}\left(\bar{\boldsymbol{x}}_{j+1} + \frac{\Delta\boldsymbol{x}_{j+1}}{2} - \bar{\boldsymbol{x}}_j - \frac{\Delta\boldsymbol{x}_j}{2} \right) \right) \bullet \left(\bar{\boldsymbol{x}}_{j+1} + \frac{\Delta\boldsymbol{x}_{j+1}}{2} - \bar{\boldsymbol{x}}_j - \frac{\Delta\boldsymbol{x}_j}{2} \right)}{\Delta t^2} \right)}
$$

$$
\times \mathrm{e}^{\frac{i}{\hbar}\Delta t \sum_{j=0}^{N-1} \left(-V\left(\bar{\boldsymbol{x}}_j + \frac{\Delta\boldsymbol{x}_j}{2} \right) \right)}
$$

$$
= \lim_{N\to\infty} \left(\frac{\det(\boldsymbol{m})}{(2\pi\Delta t\hbar)^D} \right)^N \left\{ \prod_{j=1}^{N-1} \iint \mathrm{d}^D\bar{\boldsymbol{x}}_j \, \mathrm{d}^D\Delta\boldsymbol{x}_j \right\}
$$

$$
\times \mathrm{e}^{-\frac{i}{\hbar}\Delta t \sum_{j=0}^{N-1} \left(\frac{1}{2} \sum_{j''=1}^{D} \frac{m_{j''}\left(\bar{x}_{j'',j+1} - \frac{\Delta x_{j'',j+1}}{2} - \bar{x}_{j'',j} + \frac{\Delta x_{j'',j}}{2} \right)^2}{\Delta t^2} \right)}
$$

$$
\times \mathrm{e}^{-\frac{i}{\hbar}\Delta t \sum_{j=0}^{N-1} \left(-V\left(\bar{\boldsymbol{x}}_j - \frac{\Delta\boldsymbol{x}_j}{2} \right) \right)}
$$

$$
\times \mathrm{e}^{\frac{i}{\hbar}\Delta t \sum_{j=0}^{N-1} \left(\frac{1}{2} \sum_{j''=1}^{D} \frac{m_{j''}\left(\bar{x}_{j'',j+1} + \frac{\Delta x_{j'',j+1}}{2} - \bar{x}_{j'',j} - \frac{\Delta x_{j'',j}}{2} \right)^2}{\Delta t^2} \right)}
$$

$$
\times \mathrm{e}^{\frac{i}{\hbar}\Delta t \sum_{j=0}^{N-1} \left(-V\left(\bar{\boldsymbol{x}}_j + \frac{\Delta\boldsymbol{x}_j}{2} \right) \right)}, \tag{2.46}
$$

where $\bar{x}_{j'',j}$ and $\Delta x_{j'',j}$ are the elements of the vectors $\bar{\boldsymbol{x}}_j$ and $\Delta\boldsymbol{x}_j$.

The kinetic energies can be further expanded and simplified,

$$
\left\langle \boldsymbol{x}_0 \left| \mathrm{e}^{\frac{i\widehat{H}t}{\hbar}} \right| \boldsymbol{x}_N \right\rangle \left\langle \boldsymbol{x}'_N \left| \mathrm{e}^{-\frac{i\widehat{H}t}{\hbar}} \right| \boldsymbol{x}'_0 \right\rangle
$$

$$
= \lim_{N\to\infty} \left(\frac{\det(\boldsymbol{m})}{(2\pi \Delta t \hbar)^D} \right)^N \left\{ \prod_{j=1}^{N-1} \iint \mathrm{d}^D \bar{\boldsymbol{x}}_j \; \mathrm{d}^D \Delta \boldsymbol{x}_j \right\}
$$

$$
\times \exp\left(-\frac{i}{\hbar}\Delta t \sum_{j=0}^{N-1} \frac{1}{2} \sum_{j''=1}^{D} \left(\vphantom{\frac{}{}} \right.\right.
$$

$$
\frac{m_{j''}\left(\bar{x}^2_{j'',j+1} - \bar{x}_{j'',j+1}\Delta x_{j'',j+1} - 2\bar{x}_{j'',j+1}\bar{x}_{j'',j} + \bar{x}_{j'',j+1}\Delta x_{j'',j} \right)}{\Delta t^2}
$$

$$
+ \frac{m_{j''}\left(\frac{\Delta x^2_{j'',j+1}}{4} + \bar{x}_{j'',j}\Delta x_{j'',j+1} - \frac{\Delta x_{j'',j+1}\Delta x_{j'',j}}{2} \right)}{\Delta t^2}
$$

$$
\left. \left. + \frac{m_{j''}\left(\bar{x}^2_{j'',j} - \bar{x}_{j'',j}\Delta x_{j'',j} + \frac{\Delta x^2_{j'',j}}{4} \right)}{\Delta t^2} \right) \right)
$$

$$
\times \exp\left(\frac{i}{\hbar}\Delta t \sum_{j=0}^{N-1} \frac{1}{2} \sum_{j''=1}^{D} \left(\vphantom{\frac{}{}} \right.\right.
$$

$$
\frac{m_{j''}\left(\bar{x}^2_{j'',j+1} + \bar{x}_{j'',j+1}\Delta x_{j'',j+1} - 2\bar{x}_{j'',j+1}\bar{x}_{j'',j} - \bar{x}_{j'',j+1}\Delta x_{j'',j} \right)}{\Delta t^2}
$$

$$
+ \frac{m_{j''}\left(\frac{\Delta x^2_{j'',j+1}}{4} - \bar{x}_{j'',j}\Delta x_{j'',j+1} - \frac{\Delta x_{j'',j+1}\Delta x_{j'',j}}{2} \right)}{\Delta t^2}
$$

$$
\left. \left. + \frac{m_{j''}\left(\bar{x}^2_{j'',j} + \bar{x}_{j'',j}\Delta x_{j'',j} + \frac{\Delta x^2_{j'',j}}{4} \right)}{\Delta t^2} \right) \right)
$$

$$
\times \mathrm{e}^{\frac{i}{\hbar}\Delta t \sum_{j=0}^{N-1}\left(V\left(\bar{\boldsymbol{x}}_j - \frac{\Delta \boldsymbol{x}_j}{2} \right) - V\left(\bar{\boldsymbol{x}}_j + \frac{\Delta \boldsymbol{x}_j}{2} \right) \right)}, \tag{2.47}
$$

$$\left\langle \boldsymbol{x}_0 \left| e^{\frac{i\hat{H}t}{\hbar}} \right| \boldsymbol{x}_N \right\rangle \left\langle \boldsymbol{x}'_N \left| e^{-\frac{i\hat{H}t}{\hbar}} \right| \boldsymbol{x}'_0 \right\rangle$$

$$= \lim_{N \to \infty} \left(\frac{\det(\boldsymbol{m})}{(2\pi \Delta t \hbar)^D} \right)^N \left\{ \prod_{j=1}^{N-1} \iint \mathrm{d}^D \bar{\boldsymbol{x}}_j \; \mathrm{d}^D \Delta \boldsymbol{x}_j \right\}$$

$$\times e^{\frac{i}{\hbar} \Delta t \sum_{j=0}^{N-1} \left(\frac{1}{2} \sum_{j''=1}^{D} \frac{m_{j''} \left(2\bar{x}_{j'',j+1} \Delta x_{j'',j+1} - 2\bar{x}_{j'',j+1} \Delta x_{j'',j} \right)}{\Delta t^2} \right)}$$

$$\times e^{\frac{i}{\hbar} \Delta t \sum_{j=0}^{N-1} \left(\frac{1}{2} \sum_{j''=1}^{D} \frac{m_{j''} \left(-2\bar{x}_{j'',j} \Delta x_{j'',j+1} + 2\bar{x}_{j'',j} \Delta x_{j'',j} \right)}{\Delta t^2} \right)}$$

$$\times e^{\frac{i}{\hbar} \Delta t \sum_{j=0}^{N-1} \left(V\left(\bar{\boldsymbol{x}}_j - \frac{\Delta \boldsymbol{x}_j}{2} \right) - V\left(\bar{\boldsymbol{x}}_j + \frac{\Delta \boldsymbol{x}_j}{2} \right) \right)}$$

$$= \lim_{N \to \infty} \left(\frac{\det(\boldsymbol{m})}{(2\pi \Delta t \hbar)^D} \right)^N \left\{ \prod_{j=1}^{N-1} \iint \mathrm{d}^D \bar{\boldsymbol{x}}_j \; \mathrm{d}^D \Delta \boldsymbol{x}_j \right\}$$

$$\times e^{\frac{i}{\hbar} \Delta t \sum_{j=0}^{N-1} \left(\frac{\left(\boldsymbol{m}\left(\bar{\boldsymbol{x}}_{j+1} - \bar{\boldsymbol{x}}_j \right) \right) \bullet \Delta \boldsymbol{x}_{j+1}}{\Delta t^2} - \frac{\left(\boldsymbol{m}\left(\bar{\boldsymbol{x}}_{j+1} - \bar{\boldsymbol{x}}_j \right) \right) \bullet \Delta \boldsymbol{x}_j}{\Delta t^2} \right)}$$

$$\times e^{\frac{i}{\hbar} \Delta t \sum_{j=0}^{N-1} \left(V\left(\bar{\boldsymbol{x}}_j - \frac{\Delta \boldsymbol{x}_j}{2} \right) - V\left(\bar{\boldsymbol{x}}_j + \frac{\Delta \boldsymbol{x}_j}{2} \right) \right)}$$

$$= \lim_{N \to \infty} \left(\frac{\det(\boldsymbol{m})}{(2\pi \Delta t \hbar)^D} \right)^N \left\{ \prod_{j=1}^{N-1} \iint \mathrm{d}^D \bar{\boldsymbol{x}}_j \; \mathrm{d}^D \Delta \boldsymbol{x}_j \right\}$$

$$\times e^{\frac{i}{\hbar} \Delta t \sum_{j=1}^{N-1} \left(\frac{\left(\boldsymbol{m}\left(\bar{\boldsymbol{x}}_j - \bar{\boldsymbol{x}}_{j-1} \right) \right) \bullet \Delta \boldsymbol{x}_j}{\Delta t^2} - \frac{\left(\boldsymbol{m}\left(\bar{\boldsymbol{x}}_{j+1} - \bar{\boldsymbol{x}}_j \right) \right) \bullet \Delta \boldsymbol{x}_j}{\Delta t^2} \right)}$$

$$\times e^{\frac{i}{\hbar} \Delta t \left(-\frac{(\boldsymbol{m}(\bar{\boldsymbol{x}}_1 - \bar{\boldsymbol{x}}_0)) \bullet \Delta \boldsymbol{x}_0}{\Delta t^2} + \frac{(\boldsymbol{m}(\bar{\boldsymbol{x}}_N - \bar{\boldsymbol{x}}_{N-1})) \bullet \Delta \boldsymbol{x}_N}{\Delta t^2} \right)}$$

$$\times e^{\frac{i}{\hbar} \Delta t \sum_{j=0}^{N-1} \left(V\left(\bar{\boldsymbol{x}}_j - \frac{\Delta \boldsymbol{x}_j}{2} \right) - V\left(\bar{\boldsymbol{x}}_j + \frac{\Delta \boldsymbol{x}_j}{2} \right) \right)} . \tag{2.48}$$

The potential energy can then be Taylor-expanded around $\Delta \boldsymbol{x}_j = \boldsymbol{0}$,

$$V\left(\bar{\boldsymbol{x}}_j - \frac{\Delta \boldsymbol{x}_j}{2} \right) - V\left(\bar{\boldsymbol{x}}_j + \frac{\Delta \boldsymbol{x}_j}{2} \right)$$

$$= -\left(\frac{\mathrm{d}V(\boldsymbol{x})}{\mathrm{d}\boldsymbol{x}} \right)^T_{\boldsymbol{x} = \bar{\boldsymbol{x}}_j} \bullet \Delta \boldsymbol{x}_j$$

$$- \frac{1}{24} \sum_{j''=1}^{D} \left(\frac{\mathrm{d}^3 V(x)}{\mathrm{d}x^3} \right)_{x = \bar{x}_{j'',j}} (\Delta x_{j'',j})^3 - \dots . \tag{2.49}$$

^{T} denote the transpose of a vector. $\Delta\boldsymbol{x}_j$ is the separation between the path the system will take going forward in time from 0 to t and when going backward in time from t to 0. In the limit of classical mechanics the path forward in time and the path backward in time will be the same, so we are going to approximate $\Delta\boldsymbol{x}_j$ as being small and truncate the Taylor expansion after the linear term, i.e.

$$
\left\langle \boldsymbol{x}_0 \left| e^{\frac{i\hat{H}t}{\hbar}} \right| \boldsymbol{x}_N \right\rangle \left\langle \boldsymbol{x}_N' \left| e^{-\frac{i\hat{H}t}{\hbar}} \right| \boldsymbol{x}_0' \right\rangle
$$

$$
\approx \lim_{N\to\infty} \left(\frac{\det(\boldsymbol{m})}{(2\pi\Delta t\hbar)^D} \right)^N \left\{ \prod_{j=1}^{N-1} \iint d^D\bar{\boldsymbol{x}}_j \; d^D\Delta\boldsymbol{x}_j \right\}
$$

$$
\times e^{\frac{i}{\hbar}\Delta t \sum_{j=1}^{N-1} \left(\frac{\left(\boldsymbol{m}\left(\bar{\boldsymbol{x}}_j - \bar{\boldsymbol{x}}_{j-1}\right)\right)\bullet\Delta\boldsymbol{x}_j}{\Delta t^2} - \frac{\left(\boldsymbol{m}\left(\bar{\boldsymbol{x}}_{j+1}-\bar{\boldsymbol{x}}_j\right)\right)\bullet\Delta\boldsymbol{x}_j}{\Delta t^2} \right)}
$$

$$
\times e^{\frac{i}{\hbar}\Delta t \left(-\frac{(\boldsymbol{m}(\bar{\boldsymbol{x}}_1 - \bar{\boldsymbol{x}}_0))\bullet\Delta\boldsymbol{x}_0}{\Delta t^2} + \frac{(\boldsymbol{m}(\bar{\boldsymbol{x}}_N - \bar{\boldsymbol{x}}_{N-1}))\bullet\Delta\boldsymbol{x}_N}{\Delta t^2} \right)}
$$

$$
\times e^{\frac{i}{\hbar}\Delta t \sum_{j=0}^{N-1} \left(-\left(\frac{dV(\boldsymbol{x})}{d\boldsymbol{x}}\right)^T_{\boldsymbol{x}=\bar{\boldsymbol{x}}_j} \bullet\Delta\boldsymbol{x}_j \right)} . \tag{2.50}
$$

The time-derivative $\ddot{\bar{\boldsymbol{x}}}_j = \frac{\bar{\boldsymbol{x}}_{j+1} - 2\bar{\boldsymbol{x}}_j + \bar{\boldsymbol{x}}_{j-1}}{(\Delta t)^2}$ can be used to simplify the expression,

$$
\left\langle \boldsymbol{x}_0 \left| e^{\frac{i\hat{H}t}{\hbar}} \right| \boldsymbol{x}_N \right\rangle \left\langle \boldsymbol{x}_N' \left| e^{-\frac{i\hat{H}t}{\hbar}} \right| \boldsymbol{x}_0' \right\rangle
$$

$$
\approx \lim_{N\to\infty} \left(\frac{\det(\boldsymbol{m})}{(2\pi\Delta t\hbar)^D} \right)^N \left\{ \prod_{j=1}^{N-1} \iint d^D\bar{\boldsymbol{x}}_j \; d^D\Delta\boldsymbol{x}_j \right\}
$$

$$
\times e^{\frac{i}{\hbar}\Delta t \sum_{j=1}^{N-1} \left(-\left(\boldsymbol{m}\ddot{\bar{\boldsymbol{x}}}_j\right)\bullet\Delta\boldsymbol{x}_j \right)}
$$

$$
\times e^{\frac{i}{\hbar}\Delta t \left(-\frac{(\boldsymbol{m}(\bar{\boldsymbol{x}}_1 - \bar{\boldsymbol{x}}_0))\bullet\Delta\boldsymbol{x}_0}{(\Delta t)^2} + \frac{(\boldsymbol{m}(\bar{\boldsymbol{x}}_N - \bar{\boldsymbol{x}}_{N-1}))\bullet\Delta\boldsymbol{x}_N}{(\Delta t)^2} \right)}
$$

$$
\times e^{\frac{i}{\hbar}\Delta t \sum_{j=0}^{N-1} \left(-\left(\frac{dV(\boldsymbol{x})}{d\boldsymbol{x}}\right)^T_{\boldsymbol{x}=\bar{\boldsymbol{x}}_j} \bullet\Delta\boldsymbol{x}_j \right)}
$$

$$
= \lim_{N\to\infty} \left(\frac{\det(\boldsymbol{m})}{(2\pi\Delta t\hbar)^D} \right)^N \left\{ \prod_{j=1}^{N-1} \iint d^D\bar{\boldsymbol{x}}_j \; d^D\Delta\boldsymbol{x}_j \right\}
$$

$$
\times e^{\frac{i}{\hbar}\Delta t \sum_{j=1}^{N-1} \left(-\boldsymbol{m}\ddot{\bar{\boldsymbol{x}}}_j - \left(\frac{dV(\boldsymbol{x})}{d\boldsymbol{x}}\right)^T_{\boldsymbol{x}=\bar{\boldsymbol{x}}_j} \right)\bullet\Delta\boldsymbol{x}_j}
$$

$$
\times e^{\frac{i}{\hbar}\Delta t \left(-\frac{(\boldsymbol{m}(\bar{\boldsymbol{x}}_1 - \bar{\boldsymbol{x}}_0))\bullet\Delta\boldsymbol{x}_0}{(\Delta t)^2} + \frac{(\boldsymbol{m}(\bar{\boldsymbol{x}}_N - \bar{\boldsymbol{x}}_{N-1}))\bullet\Delta\boldsymbol{x}_N}{(\Delta t)^2} - \left(\frac{dV(\boldsymbol{x})}{d\boldsymbol{x}}\right)^T_{\boldsymbol{x}=\bar{\boldsymbol{x}}_0} \bullet\Delta\boldsymbol{x}_0 \right)} . \tag{2.51}
$$

Integrating over $\Delta\boldsymbol{x}_j$ then leads to delta functions,

$$
\left\langle \boldsymbol{x}_0 \middle| \mathrm{e}^{\frac{i\widehat{H}t}{\hbar}} \middle| \boldsymbol{x}_N \right\rangle \left\langle \boldsymbol{x}'_N \middle| \mathrm{e}^{-\frac{i\widehat{H}t}{\hbar}} \middle| \boldsymbol{x}'_0 \right\rangle
$$
$$
\approx \lim_{N\to\infty} \left(\frac{\det(\boldsymbol{m})}{(\Delta t\hbar)^D} \right)^N (2\pi)^{-D} \left\{ \prod_{j=1}^{N-1} \int \mathrm{d}^D\bar{\boldsymbol{x}}_j \right\}
$$
$$
\times \left(\prod_{j=1}^{N-1} \delta\left(\frac{\Delta t}{\hbar}\left(-\boldsymbol{m}\ddot{\bar{\boldsymbol{x}}}_j - \left(\frac{\mathrm{d}V(\boldsymbol{x})}{\mathrm{d}\boldsymbol{x}}\right)^T_{\boldsymbol{x}=\bar{\boldsymbol{x}}_j} \right) \right) \right)
$$
$$
\times \mathrm{e}^{\frac{i}{\hbar}\Delta t\left(-\frac{(\boldsymbol{m}(\bar{\boldsymbol{x}}_1-\bar{\boldsymbol{x}}_0))\bullet\Delta\boldsymbol{x}_0}{(\Delta t)^2} + \frac{(\boldsymbol{m}(\bar{\boldsymbol{x}}_N-\bar{\boldsymbol{x}}_{N-1}))\bullet\Delta\boldsymbol{x}_N}{(\Delta t)^2} - \left(\frac{\mathrm{d}V(\boldsymbol{x})}{\mathrm{d}\boldsymbol{x}}\right)^T_{\boldsymbol{x}=\bar{\boldsymbol{x}}_0}\bullet\Delta\boldsymbol{x}_0 \right)}
$$
$$
= \lim_{N\to\infty} \left(\frac{\det(\boldsymbol{m})}{(\Delta t)^{2D}} \right)^N \left(\frac{\Delta t}{2\pi\hbar} \right)^D \left\{ \prod_{j=1}^{N-1} \int \mathrm{d}^D\bar{\boldsymbol{x}}_j \right\}
$$
$$
\times \left(\prod_{j=1}^{N-1} \delta\left(-\boldsymbol{m}\ddot{\bar{\boldsymbol{x}}}_j - \left(\frac{\mathrm{d}V(\boldsymbol{x})}{\mathrm{d}\boldsymbol{x}}\right)^T_{\boldsymbol{x}=\bar{\boldsymbol{x}}_j} \right) \right)
$$
$$
\times \mathrm{e}^{\frac{i}{\hbar}\Delta t\left(-\frac{(\boldsymbol{m}(\bar{\boldsymbol{x}}_1-\bar{\boldsymbol{x}}_0))\bullet\Delta\boldsymbol{x}_0}{(\Delta t)^2} + \frac{(\boldsymbol{m}(\bar{\boldsymbol{x}}_N-\bar{\boldsymbol{x}}_{N-1}))\bullet\Delta\boldsymbol{x}_N}{(\Delta t)^2} - \left(\frac{\mathrm{d}V(\boldsymbol{x})}{\mathrm{d}\boldsymbol{x}}\right)^T_{\boldsymbol{x}=\bar{\boldsymbol{x}}_0}\bullet\Delta\boldsymbol{x}_0 \right)}.
$$
$$
(2.52)
$$

Returning to equation 2.44 we have

$$
\left\langle \boldsymbol{x}_0 \middle| \widehat{\boldsymbol{\Omega}}(t) \middle| \boldsymbol{x}'_0 \right\rangle = \left\langle \bar{\boldsymbol{x}}_0 - \frac{\Delta\boldsymbol{x}_0}{2} \middle| \widehat{\boldsymbol{\Omega}}(t) \middle| \bar{\boldsymbol{x}}_0 + \frac{\Delta\boldsymbol{x}_0}{2} \right\rangle
$$
$$
\approx \lim_{N\to\infty} \iint \mathrm{d}^D\bar{\boldsymbol{x}}_N\, \mathrm{d}^D\Delta\boldsymbol{x}_N \left\langle \bar{\boldsymbol{x}}_N - \frac{\Delta\boldsymbol{x}_N}{2} \middle| \widehat{\boldsymbol{\Omega}} \middle| \bar{\boldsymbol{x}}_N + \frac{\Delta\boldsymbol{x}_N}{2} \right\rangle
$$
$$
\times \left(\frac{\det(\boldsymbol{m})}{(\Delta t)^{2D}} \right)^N \left(\frac{\Delta t}{2\pi\hbar} \right)^D \left\{ \prod_{j=1}^{N-1} \int \mathrm{d}^D\bar{\boldsymbol{x}}_j \right\}
$$
$$
\times \left(\prod_{j=1}^{N-1} \delta\left(-\boldsymbol{m}\ddot{\bar{\boldsymbol{x}}}_j - \left(\frac{\mathrm{d}V(\boldsymbol{x})}{\mathrm{d}\boldsymbol{x}}\right)^T_{\boldsymbol{x}=\bar{\boldsymbol{x}}_j} \right) \right)
$$
$$
\times \mathrm{e}^{\frac{i}{\hbar}\Delta t\left(-\frac{(\boldsymbol{m}(\bar{\boldsymbol{x}}_1-\bar{\boldsymbol{x}}_0))\bullet\Delta\boldsymbol{x}_0}{(\Delta t)^2} + \frac{(\boldsymbol{m}(\bar{\boldsymbol{x}}_N-\bar{\boldsymbol{x}}_{N-1}))\bullet\Delta\boldsymbol{x}_N}{(\Delta t)^2} - \left(\frac{\mathrm{d}V(\boldsymbol{x})}{\mathrm{d}\boldsymbol{x}}\right)^T_{\boldsymbol{x}=\bar{\boldsymbol{x}}_0}\bullet\Delta\boldsymbol{x}_0 \right)}.
$$
$$
(2.53)
$$

Since

$$
\left[\widehat{\boldsymbol{\Omega}}\right]_{\mathrm{W}}\left(\bar{\boldsymbol{x}}_N, \frac{\boldsymbol{m}\left(\bar{\boldsymbol{x}}_N - \bar{\boldsymbol{x}}_{N-1}\right)}{\Delta t}\right)
$$
$$
= \int \mathrm{d}^D \Delta \boldsymbol{x}_N \; \mathrm{e}^{\frac{i}{\hbar} \frac{\left(\boldsymbol{m}\left(\bar{\boldsymbol{x}}_N - \bar{\boldsymbol{x}}_{N-1}\right)\right) \bullet \Delta \boldsymbol{x}_N}{\Delta t}}
$$
$$
\times \left\langle \bar{\boldsymbol{x}}_N - \frac{\Delta \boldsymbol{x}_N}{2} \left| \widehat{\boldsymbol{\Omega}} \right| \bar{\boldsymbol{x}}_N + \frac{\Delta \boldsymbol{x}_N}{2} \right\rangle \tag{2.54}
$$

equation 2.53 can be written as

$$
\left\langle \bar{\boldsymbol{x}}_0 - \frac{\Delta \boldsymbol{x}_0}{2} \left| \widehat{\boldsymbol{\Omega}}(t) \right| \bar{\boldsymbol{x}}_0 + \frac{\Delta \boldsymbol{x}_0}{2} \right\rangle
$$
$$
\approx \lim_{N \to \infty} \int \mathrm{d}^D \bar{\boldsymbol{x}}_N \left[\widehat{\boldsymbol{\Omega}}\right]_{\mathrm{W}}\left(\bar{\boldsymbol{x}}_N, \frac{\boldsymbol{m}\left(\bar{\boldsymbol{x}}_N - \bar{\boldsymbol{x}}_{N-1}\right)}{\Delta t}\right)
$$
$$
\times \left(\frac{\det\left(\boldsymbol{m}\right)}{\left(\Delta t\right)^{2D}}\right)^N \left(\frac{\Delta t}{2\pi\hbar}\right)^D \left\{ \prod_{j=1}^{N-1} \int \mathrm{d}^D \bar{\boldsymbol{x}}_j \right\}
$$
$$
\times \left(\prod_{j=1}^{N-1} \delta\left(-\boldsymbol{m}\ddot{\bar{\boldsymbol{x}}}_j - \left(\frac{\mathrm{d}V\left(\boldsymbol{x}\right)}{\mathrm{d}\boldsymbol{x}}\right)^T_{\boldsymbol{x}=\bar{\boldsymbol{x}}_j}\right) \right)
$$
$$
\times \mathrm{e}^{\frac{i}{\hbar}\Delta t\left(-\frac{\left(\boldsymbol{m}\left(\bar{\boldsymbol{x}}_1 - \bar{\boldsymbol{x}}_0\right)\right) \bullet \Delta \boldsymbol{x}_0}{\left(\Delta t\right)^2} - \left(\frac{\mathrm{d}V\left(\boldsymbol{x}\right)}{\mathrm{d}\boldsymbol{x}}\right)^T_{\boldsymbol{x}=\bar{\boldsymbol{x}}_0} \bullet \Delta \boldsymbol{x}_0\right)}. \tag{2.55}
$$

Defining the momentum vectors $\bar{\boldsymbol{p}}_N = \frac{m(\bar{x}_N - \bar{x}_{N-1})}{\Delta t}$ and $\bar{\boldsymbol{p}}_0 = \frac{m(\bar{x}_0 - \bar{x}_{-1})}{\Delta t}$, and thus also the position $\bar{\boldsymbol{x}}_{-1}$ at time $-\Delta t$, and multiplying both

sides of the "$\approx$" with $e^{\frac{i}{\hbar}\bar{\boldsymbol{p}}_0 \bullet \Delta \boldsymbol{x}_0}$ gives

$$
e^{\frac{i}{\hbar}\bar{\boldsymbol{p}}_0 \bullet \Delta \boldsymbol{x}_0} \left\langle \bar{\boldsymbol{x}}_0 - \frac{\Delta \boldsymbol{x}_0}{2} \middle| \widehat{\boldsymbol{\Omega}}(t) \middle| \bar{\boldsymbol{x}}_0 + \frac{\Delta \boldsymbol{x}_0}{2} \right\rangle
$$

$$
\approx \lim_{N \to \infty} \left(\frac{\det(\boldsymbol{m})}{(\Delta t)^{2D}} \right)^N \left(\frac{\Delta t}{2\pi\hbar} \right)^D \left\{ \prod_{j=1}^{N} \int d^D \bar{\boldsymbol{x}}_j \right\}
$$

$$
\times \left(\prod_{j=1}^{N-1} \delta \left(-\boldsymbol{m} \ddot{\bar{\boldsymbol{x}}}_j - \left(\frac{dV(\boldsymbol{x})}{d\boldsymbol{x}} \right)^T_{\boldsymbol{x}=\bar{\boldsymbol{x}}_j} \right) \right)
$$

$$
\times \left[\widehat{\boldsymbol{\Omega}} \right]_{\mathrm{W}} (\bar{\boldsymbol{x}}_N, \bar{\boldsymbol{p}}_N)
$$

$$
\times e^{\frac{i}{\hbar} \Delta t \left(\frac{\bar{\boldsymbol{p}}_0 \bullet \Delta \boldsymbol{x}_0}{\Delta t} - \frac{(\boldsymbol{m}(\bar{\boldsymbol{x}}_1 - \bar{\boldsymbol{x}}_0)) \bullet \Delta \boldsymbol{x}_0}{(\Delta t)^2} - \left(\frac{dV(\boldsymbol{x})}{d\boldsymbol{x}} \right)^T_{\boldsymbol{x}=\bar{\boldsymbol{x}}_0} \bullet \Delta \boldsymbol{x}_0 \right)}
$$

$$
= \lim_{N \to \infty} \left(\frac{\det(\boldsymbol{m})}{(\Delta t)^{2D}} \right)^N \left(\frac{\Delta t}{2\pi\hbar} \right)^D \left\{ \prod_{j=1}^{N} \int d^D \bar{\boldsymbol{x}}_j \right\}
$$

$$
\times \left(\prod_{j=1}^{N-1} \delta \left(-\boldsymbol{m} \ddot{\bar{\boldsymbol{x}}}_j - \left(\frac{dV(\boldsymbol{x})}{d\boldsymbol{x}} \right)^T_{\boldsymbol{x}=\bar{\boldsymbol{x}}_j} \right) \right)
$$

$$
\times \left[\widehat{\boldsymbol{\Omega}} \right]_{\mathrm{W}} (\bar{\boldsymbol{x}}_N, \bar{\boldsymbol{p}}_N)
$$

$$
\times e^{\frac{i}{\hbar} \Delta t \left(-\frac{(\boldsymbol{m}(\bar{\boldsymbol{x}}_1 - 2\bar{\boldsymbol{x}}_0 + \bar{\boldsymbol{x}}_{-1})) \bullet \Delta \boldsymbol{x}_0}{(\Delta t)^2} - \left(\frac{dV(\boldsymbol{x})}{d\boldsymbol{x}} \right)^T_{\boldsymbol{x}=\bar{\boldsymbol{x}}_0} \bullet \Delta \boldsymbol{x}_0 \right)}
$$

$$
= \lim_{N \to \infty} \left(\frac{\det(\boldsymbol{m})}{(\Delta t)^{2D}} \right)^N \left(\frac{\Delta t}{2\pi\hbar} \right)^D \left\{ \prod_{j=1}^{N} \int d^D \bar{\boldsymbol{x}}_j \right\}
$$

$$
\times \left(\prod_{j=1}^{N-1} \delta \left(-\boldsymbol{m} \ddot{\bar{\boldsymbol{x}}}_j - \left(\frac{dV(\boldsymbol{x})}{d\boldsymbol{x}} \right)^T_{\boldsymbol{x}=\bar{\boldsymbol{x}}_j} \right) \right)
$$

$$
\times \left[\widehat{\boldsymbol{\Omega}} \right]_{\mathrm{W}} (\bar{\boldsymbol{x}}_N, \bar{\boldsymbol{p}}_N) \, e^{\frac{i}{\hbar} \Delta t \left(-(\boldsymbol{m} \ddot{\bar{\boldsymbol{x}}}_0) \bullet \Delta \boldsymbol{x}_0 - \left(\frac{dV(\boldsymbol{x})}{d\boldsymbol{x}} \right)^T_{\boldsymbol{x}=\bar{\boldsymbol{x}}_0} \bullet \Delta \boldsymbol{x}_0 \right)} .
$$

$$
(2.56)
$$

Integrating over $\Delta \boldsymbol{x}_0$ on both sides of the "$\approx$" leads to

$$\int \mathrm{d}^D \Delta \boldsymbol{x}_0 \, \mathrm{e}^{\frac{i}{\hbar} \bar{\boldsymbol{p}}_0 \bullet \Delta \boldsymbol{x}_0} \left\langle \bar{\boldsymbol{x}}_0 - \frac{\Delta \boldsymbol{x}_0}{2} \middle| \widehat{\boldsymbol{\Omega}}(t) \middle| \bar{\boldsymbol{x}}_0 + \frac{\Delta \boldsymbol{x}_0}{2} \right\rangle$$

$$= \left[\widehat{\boldsymbol{\Omega}}(t) \right]_{\mathrm{W}} (\bar{\boldsymbol{x}}_0, \bar{\boldsymbol{p}}_0)$$

$$\approx \lim_{N \to \infty} \left(\frac{\det(\boldsymbol{m})}{(\Delta t)^{2D}} \right)^N \left(\frac{\Delta t}{2\pi\hbar} \right)^D \left\{ \prod_{j=1}^{N} \int \mathrm{d}^D \bar{\boldsymbol{x}}_j \right\}$$

$$\times \left(\prod_{j=1}^{N-1} \delta \left(-\boldsymbol{m} \ddot{\bar{\boldsymbol{x}}}_j - \left(\frac{\mathrm{d}V(\boldsymbol{x})}{\mathrm{d}\boldsymbol{x}} \right)^T_{\boldsymbol{x}=\bar{\boldsymbol{x}}_j} \right) \right)$$

$$\times \left[\widehat{\boldsymbol{\Omega}} \right]_{\mathrm{W}} (\bar{\boldsymbol{x}}_N, \bar{\boldsymbol{p}}_N)$$

$$\times \int \mathrm{d}^D \Delta \boldsymbol{x}_0 \, \mathrm{e}^{\frac{i}{\hbar} \Delta t \left(-\left(\boldsymbol{m} \ddot{\bar{\boldsymbol{x}}}_0 \right) \bullet \Delta \boldsymbol{x}_0 - \left(\frac{\mathrm{d}V(\boldsymbol{x})}{\mathrm{d}\boldsymbol{x}} \right)^T_{\boldsymbol{x}=\bar{\boldsymbol{x}}_0} \bullet \Delta \boldsymbol{x}_0 \right)}$$

$$= \lim_{N \to \infty} \left(\frac{\det(\boldsymbol{m})}{(\Delta t)^{2D}} \right)^N \left(\frac{\Delta t}{\hbar} \right)^D \left\{ \prod_{j=1}^{N} \int \mathrm{d}^D \bar{\boldsymbol{x}}_j \right\}$$

$$\times \left(\prod_{j=1}^{N-1} \delta \left(-\boldsymbol{m} \ddot{\bar{\boldsymbol{x}}}_j - \left(\frac{\mathrm{d}V(\boldsymbol{x})}{\mathrm{d}\boldsymbol{x}} \right)^T_{\boldsymbol{x}=\bar{\boldsymbol{x}}_j} \right) \right)$$

$$\times \left[\widehat{\boldsymbol{\Omega}} \right]_{\mathrm{W}} (\bar{\boldsymbol{x}}_N, \bar{\boldsymbol{p}}_N)$$

$$\times \delta \left(\frac{\Delta t}{\hbar} \left(-\boldsymbol{m} \ddot{\bar{\boldsymbol{x}}}_0 - \left(\frac{\mathrm{d}V(\boldsymbol{x})}{\mathrm{d}\boldsymbol{x}} \right)^T_{\boldsymbol{x}=\bar{\boldsymbol{x}}_0} \right) \right)$$

$$= \lim_{N \to \infty} \left(\frac{\det(\boldsymbol{m})}{(\Delta t)^{2D}} \right)^N \left\{ \prod_{j=1}^{N} \int \mathrm{d}^D \bar{\boldsymbol{x}}_j \right\}$$

$$\times \left(\prod_{j=0}^{N-1} \delta \left(-\boldsymbol{m} \ddot{\bar{\boldsymbol{x}}}_j - \left(\frac{\mathrm{d}V(\boldsymbol{x})}{\mathrm{d}\boldsymbol{x}} \right)^T_{\boldsymbol{x}=\bar{\boldsymbol{x}}_j} \right) \right)$$

$$\times \left[\widehat{\boldsymbol{\Omega}} \right]_{\mathrm{W}} (\bar{\boldsymbol{x}}_N, \bar{\boldsymbol{p}}_N). \tag{2.57}$$

The delta functions restrict the path from $\bar{\boldsymbol{x}}_0$ at time 0 to $\bar{\boldsymbol{x}}_N$ at time t to $\boldsymbol{m} \ddot{\bar{\boldsymbol{x}}}_j = -\left(\frac{\mathrm{d}V(\boldsymbol{x})}{\mathrm{d}\boldsymbol{x}} \right)^T_{\boldsymbol{x}=\bar{\boldsymbol{x}}_j}$. This is Newton's second law of motion. The factor $\left(\frac{\det(\boldsymbol{m})}{(\Delta t)^{2D}} \right)^N$ is a normalization to account for the fact that

the dimensions of $\mathrm{d}^D \bar{\boldsymbol{x}}_j$ and $-\boldsymbol{m}\ddot{\bar{\boldsymbol{x}}}_j - \left(\frac{\mathrm{d}V(\boldsymbol{x})}{\mathrm{d}\boldsymbol{x}}\right)^T_{\boldsymbol{x}=\bar{\boldsymbol{x}}_j}$ do not agree. Thus

$$
\begin{aligned}
&\left[\widehat{\boldsymbol{\Omega}}(t)\right]_{\mathrm{W}} (\bar{\boldsymbol{x}}_0, \bar{\boldsymbol{p}}_0) \\
&\approx \lim_{N\to\infty} \left(\frac{\det(\boldsymbol{m})}{(\Delta t)^{2D}}\right)^N \left\{\prod_{j=1}^{N} \int \mathrm{d}^D \bar{\boldsymbol{x}}_j\right\} \\
&\quad \times \left(\prod_{j=0}^{N-1} \delta\left(-\boldsymbol{m}\ddot{\bar{\boldsymbol{x}}}_j - \left(\frac{\mathrm{d}V(\boldsymbol{x})}{\mathrm{d}\boldsymbol{x}}\right)^T_{\boldsymbol{x}=\bar{\boldsymbol{x}}_j}\right)\right) \\
&\quad \times \left[\widehat{\boldsymbol{\Omega}}\right]_{\mathrm{W}} (\bar{\boldsymbol{x}}_N, \bar{\boldsymbol{p}}_N)
\end{aligned} \tag{2.58}
$$

is the classical Wigner method. The only approximation introduced in this derivation is the truncation, after the linear term, of the Taylor expansion of the potential energy in equation 2.49. This truncation does of course not affect systems with all higher order derivatives being zero. The classical Wigner method is thus proven to be exact for e.g. bilinearly coupled harmonic oscillators.

This is a linearization of a path integral and is therefore called linearized path integral (LPI).

It can be noted that the LPI derivation presented here avoids the use of $\lim_{\Delta t\to 0} \Delta t \left(\frac{\mathrm{d}V(\boldsymbol{x})}{\mathrm{d}\boldsymbol{x}}\right)^T_{\boldsymbol{x}=\bar{\boldsymbol{x}}_0} \bullet \Delta \boldsymbol{x}_0 \to 0$ that both Shi and Geva[21] and Poulsen, Nyman, and Rossky[22] use. As no other factor of Δt, in the derivation, is assumed to be 0 this could be seen as an advantage.

2.3   Chemical kinetics and thermal rate constants

> Kinetics is at the heart of physical chemistry, [...]

<div align="right">
G. Kristin Jonsson
(Lab.-report in kinetics, 2011)
</div>

In chemistry a chemical reaction such as

$$A + B \rightarrow C + D \tag{2.a}$$

has a rate of $\dfrac{d[C]}{dt}$, with the brackets denoting the concentration of the enclosed species $\left(\dfrac{d[C]}{dt} = \dfrac{d[D]}{dt} = -\dfrac{d[A]}{dt} = -\dfrac{d[B]}{dt} \right)$. For the simple kind of bimolecular (or more generally bispecies) reaction shown here the reaction rate can be expressed as

$$\frac{d[C]}{dt} = k_r(T)[A][B], \tag{2.59}$$

where $k_r(T)$ is called the reaction rate constant. Miller and coworkers[37,38] have shown how to calculate bimolecular reaction rate constants from three different traces:

$$k_r(T)$$

$$= \frac{1}{Q_R} \lim_{t \to \infty} \frac{d}{dt} \operatorname{Tr} \left\{ \theta \left(s - \widehat{x}_r \right) e^{-\beta \widehat{H}} e^{\frac{i \widehat{H} t}{\hbar}} \theta \left(\widehat{x}_r - s \right) e^{-\frac{i \widehat{H} t}{\hbar}} \right\} \tag{2.60}$$

$$= \frac{1}{Q_R} \lim_{t \to \infty} \operatorname{Tr} \left\{ \widehat{F} \left(\widehat{x}_r - s \right) e^{-\beta \widehat{H}} e^{\frac{i \widehat{H} t}{\hbar}} \theta \left(\widehat{x}_r - s \right) e^{-\frac{i \widehat{H} t}{\hbar}} \right\} \tag{2.61}$$

$$= \frac{1}{Q_R} \int_0^\infty dt \, \operatorname{Tr} \left\{ \widehat{F} \left(\widehat{x}_r - s \right) e^{-\beta \widehat{H}} e^{\frac{i \widehat{H} t}{\hbar}} \widehat{F} \left(\widehat{x}_r - s \right) e^{-\frac{i \widehat{H} t}{\hbar}} \right\}$$

$$= \frac{1}{Q_R} \frac{1}{2} \int_{-\infty}^\infty dt \, \operatorname{Tr} \left\{ \widehat{F} \left(\widehat{x}_r - s \right) e^{-\beta \widehat{H}} e^{\frac{i \widehat{H} t}{\hbar}} \widehat{F} \left(\widehat{x}_r - s \right) e^{-\frac{i \widehat{H} t}{\hbar}} \right\}, \tag{2.62}$$

where Q_{R} is the canonical partition function of the reactants, $\widehat{x}_{\mathrm{r}} = x_{\mathrm{r}}(\widehat{\boldsymbol{x}})$ is the reaction coordinate operator, $\widehat{\boldsymbol{x}}$ is the position operator, s is the position of a dividing surface that separates reactants and products, $\widehat{F}(x)$ is the probability flux operator, and $\theta(x)$ is the Heaviside step function.

The probability flux operator is

$$\widehat{F}(\widehat{x} - s) = \frac{1}{2} m^{-1} \left(\delta\left(\widehat{x} - s\right) \widehat{p} + \widehat{p}\delta\left(\widehat{x} - s\right) \right). \qquad (2.63)$$

To elucidate the physical meaning of the probability flux operator it can be pointed out that the Wigner transform of the operator is

$$\left[\widehat{F}(\widehat{x} - s) \right]_{\mathrm{W}} (x, p) = \frac{p}{m} \delta(x - s) \qquad (2.64)$$

which simply is the velocity with position fixed in the surface s.

For reaction rate calculations the dividing surface s could be placed e.g. in the transition state, but this is not a requirement. The dividing surface can formally be placed anywhere, as long as it separates reactants and products from each other. Certain choices, such as placing s in the transition state, may be beneficial for numerical convergence or even a requirement if approximations to the exact expressions are used. E.g., in the transition state theory limit, $t \to 0$, where it is assumed that no recrossings of the dividing surface occurs it makes a big difference if the dividing surface is placed on the top of a potential barrier or below it.

The expressions 2.60-2.62 are rather intuitive. The trace in equation 2.60 is proportional to the probability of being on the reactant side of the dividing surface at time $t = 0$ and later on the product side of the dividing surface at $t \to \infty$.

The trace in equation 2.61 is proportional to the flow of the probability density thought the dividing surface at time $t = 0$ multiplied with the probability of ending up on the product side of the dividing surface at $t \to \infty$.

The trace in equation 2.62 is proportional to the product of the flow of the probability density thought the dividing surface at the two times $t = 0$, or $t \to -\infty$, and $t \to \infty$.

A requirement for the validity of equations 2.60-2.62 is that if following the reaction coordinate far enough away from the dividing

surface there should not be any possibility of reflecting back a trajectory or wavepacket.

These traces, or more specificly the flux-Heaviside one in equation 2.61, are used for the calculation of reaction rate constants in paper IV, and section 3.3.

Another, older and more common, formulation for the reaction rate constant is collision theory. This theory is only valid for bispecies reactions of ideal gases. It assumes classical mechanics for the translational movement of chemical species.

$$
\begin{aligned}
k_{\mathrm{r}}(T) &= \int_0^\infty \mathrm{d}E\, \sigma(E) v_{\mathrm{rel}}(E) 2\beta^{\frac{3}{2}} \sqrt{\frac{E}{\pi}}\, \mathrm{e}^{-\beta E} \\
&= \sqrt{\frac{8}{\pi \mu_{\mathrm{A,B}}}}\, \beta^{\frac{3}{2}} \int_0^\infty \mathrm{d}E\, \sigma(E) E\, \mathrm{e}^{-\beta E},
\end{aligned}
\tag{2.65}
$$

where E is the collision energy, $\sigma(E)$ is the reaction cross section, $v_{\mathrm{rel}}(E) = \sqrt{2E/\mu}$ is the relative velocity of the colliding species, $2\beta^{\frac{3}{2}} \sqrt{E/\pi}\, \mathrm{e}^{-\beta E}$ is the Maxwell-Boltzmann distribution function of the energy, and $\mu_{\mathrm{A,B}} = \frac{m_{\mathrm{A}} m_{\mathrm{B}}}{m_{\mathrm{A}} + m_{\mathrm{B}}}$ is the reduced mass of the colliding species with masses m_{A} and m_{B}.

In the situation where the two species can be described as classical hard spheres, then if species A was trying to get past a stationary B the collision cross section would be the area that B covers so that the center of A can not pass through it without colliding with B, see figure 2.2. For hard spheres the collision cross section is simply the area of a circle with a radius that is the sum of the radii of the species. For non-spherical species the area they cover would of course depend on relative orientation, but the collision cross section would be an average over all orientations. The reaction cross section is similar to the collision cross section, but with the addition that a collision only counts if it leads to a reaction. In reality, it is not well defined where the borders of a chemical species are, so the species could be considered to come into proximity of each other, rather than to collide.

Thus the integral over collision energies in equation 2.65 has three parts: the Maxwell-Boltzmann distribution function, that takes account of the probability density of each particular collision energy,
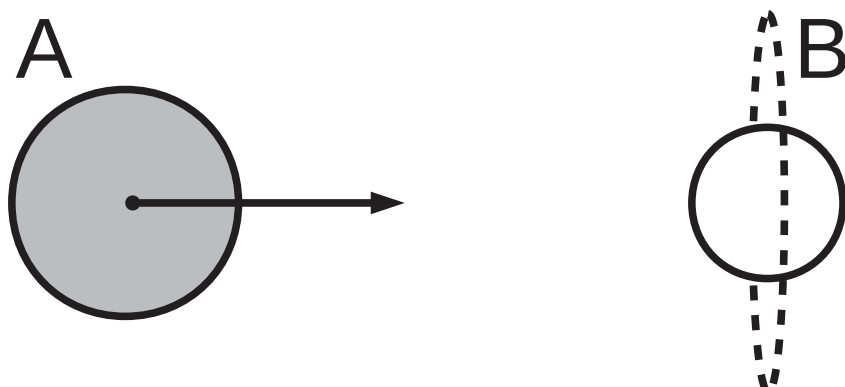
Figure 2.2: Illustration of the collision cross section of the two spherical particles A and B. The dashed line shows the area around particle B that the center of particle A, when moving in from the left of the figure, can not pass through without the two particles colliding.

the reaction cross section, that takes account of the probability of the species colliding and reacting, and the relative velocity, that determines at what rate collisions can occur.

Collision theory is used for the calculation of the radiative association rate constant in paper I, and section 3.1.

2.4   Common methods of approximate quantum dynamics

> It should be stressed that nuclei are heavy enough that quantum effects are almost negligible, i.e. they behave to a good approximation as classical particles. Indeed, if nuclei showed significant quantum aspects, the concept of molecular structure (i.e. different configurations and conformations) would not have any meaning, since the nuclei would simply tunnel through barriers and end up in the global minimum.
>
> Frank Jensen[39]

The quote that starts this section is from a standard textbook in computational chemistry. As already stated in chapter 1 of this thesis, and indeed also acknowledged by Jensen elsewhere in his book,[39] there are however situations in which quantum mechanics is necessary to accurately describe the behavior of the atomic nuclei.

Apart from the classical Wigner method, that has been extensively described in sections 2.1 and 2.2, there are many methods for approximate quantum dynamics. A few notable methods with a relation to the work presented in this thesis will be presented in this section, so that they can provide a context and serve as a comparison for some of the new developments that are presented in chapter 3.

Time correlation functions are important to describe the dynamics of physical systems. Examples of such functions can be found in equations 2.60-2.62. Those correlation functions are used to calculate reaction rate constants. The more general formulation of a thermal time correlation function of operator $\widehat{A}$ at time 0 and operator $\widehat{B}$ at time t is[†]

$$\left\langle \widehat{A}\widehat{B}(t) \right\rangle = \frac{1}{Z} \operatorname{Tr} \left\{ \widehat{A}\, \mathrm{e}^{-\beta\widehat{H}}\, \mathrm{e}^{\frac{i\widehat{H}t}{\hbar}}\, \widehat{B}\, \mathrm{e}^{-\frac{i\widehat{H}t}{\hbar}} \right\}. \tag{2.66}$$

[†]An even more general formulation of a time correlation function would have any number of operators at different times.

The Boltzmann operator can be placed on either side of $\widehat{\boldsymbol{A}}$. This will only change the sign of the imaginary part,

$$\frac{1}{Z} \operatorname{Tr} \left\{ \widehat{\boldsymbol{A}} \, \mathrm{e}^{-\beta \widehat{H}} \, \mathrm{e}^{\frac{i \widehat{H} t}{\hbar}} \, \widehat{\boldsymbol{B}} \, \mathrm{e}^{-\frac{i \widehat{H} t}{\hbar}} \right\} = \frac{1}{Z} \operatorname{Tr} \left\{ \mathrm{e}^{-\beta \widehat{H}} \, \widehat{\boldsymbol{A}} \, \mathrm{e}^{\frac{i \widehat{H} t}{\hbar}} \, \widehat{\boldsymbol{B}} \, \mathrm{e}^{-\frac{i \widehat{H} t}{\hbar}} \right\}^{*},$$
(2.67)

where * denotes complex conjugate.

Some quantum dynamical methods work with Kubo-transformed time correlation functions,[40]

$$\left\langle \widehat{\boldsymbol{A}} \widehat{\boldsymbol{B}}(t) \right\rangle_{\text{Kubo}}$$
$$= \frac{1}{Z} \operatorname{Tr} \left\{ \frac{1}{\beta} \int_0^\beta \mathrm{d}\zeta \, \mathrm{e}^{-\zeta \widehat{H}} \, \widehat{\boldsymbol{A}} \, \mathrm{e}^{-(\beta - \zeta) \widehat{H}} \, \mathrm{e}^{\frac{i \widehat{H} t}{\hbar}} \, \widehat{\boldsymbol{B}} \, \mathrm{e}^{-\frac{i \widehat{H} t}{\hbar}} \right\},$$
(2.68)

which have the benefit that the quantum correlation functions are more similar to their classical counterparts than is the case for the standard "physical" correlation functions.

Another alternative is symmetrized correlation functions,[41]

$$\left\langle \widehat{\boldsymbol{A}} \widehat{\boldsymbol{B}}(t) \right\rangle_{\text{Sym}} = \frac{1}{Z} \operatorname{Tr} \left\{ \mathrm{e}^{-\frac{\beta}{2} \widehat{H}} \, \widehat{\boldsymbol{A}} \, \mathrm{e}^{-\frac{\beta}{2} \widehat{H}} \, \mathrm{e}^{\frac{i \widehat{H} t}{\hbar}} \, \widehat{\boldsymbol{B}} \, \mathrm{e}^{-\frac{i \widehat{H} t}{\hbar}} \right\},$$
(2.69)

which have the benefit that they are real instead of complex quantities. The correlation functions, or technically just traces, presented in section 2.3 are of this type.

The standard, Kubo-transformed, and symmetrized versions of the same correlation function are equivalent in the sense that they contain the same information. Using the Fourier transform, $[f(t)]_{\text{F}}(\omega)$, the different correlation functions are related as:[40,41]

$$\left[\left\langle \widehat{\boldsymbol{A}} \widehat{\boldsymbol{B}}(t) \right\rangle \right]_{\text{F}}(\omega) = \mathrm{e}^{-\frac{\beta \hbar \omega}{2}} \left[\left\langle \widehat{\boldsymbol{A}} \widehat{\boldsymbol{B}}(t) \right\rangle_{\text{Sym}} \right]_{\text{F}}(\omega)$$
$$= \frac{\beta \hbar \omega}{\mathrm{e}^{\beta \hbar \omega} - 1} \left[\left\langle \widehat{\boldsymbol{A}} \widehat{\boldsymbol{B}}(t) \right\rangle_{\text{Kubo}} \right]_{\text{F}}(\omega).$$
(2.70)

These relations are only valid for exact quantum mechanics. If approximations to quantum mechanics are used, then equation 2.70

will also be approximate. As mentioned some methods work with a certain version of the correlation function. Other methods, e.g. the classical Wigner method, can be used for any of the versions of the correlation function. If one is not interested in the correlation function itself, but rather something that is calculated from it, the different versions may in some cases give the same result. In the case of equations 2.60-2.62, it is long time values and an integral that is interesting rather than the correlation functions themselves. For these equations the ordinary version of the correlation function, or the Kubo-transformed correlation function, would give the same result as the symmetrized version. However, as soon as one starts to approximate the correlation functions this does not necessarily apply any more.

Semi-classical initial value representation

The semi-classical initial value representation[18] (SC-IVR) has already been mentioned in connection to the classical Wigner method. It uses the IVR-representation of the time propagation operator:

$$
\begin{aligned}
\mathrm{e}^{-\frac{i\hat{H}t}{\hbar}} = \iint \frac{\mathrm{d}^D \boldsymbol{x}_0 \ \mathrm{d}^D \boldsymbol{p}_0}{(2\pi i \hbar)^{\frac{D}{2}}} \sqrt{\det\left(\frac{\partial \boldsymbol{x}_t\left(\boldsymbol{x}_0, \boldsymbol{p}_0\right)}{\partial \boldsymbol{p}_0}\right)} \\
\times \mathrm{e}^{\frac{i}{\hbar} S(\boldsymbol{x}_0, \boldsymbol{p}_0, t)} \left|\boldsymbol{x}_t\right\rangle \left\langle \boldsymbol{x}_0\right|,
\end{aligned}
\tag{2.71}
$$

where the index 0 denotes initial values, $\boldsymbol{x}_t\left(\boldsymbol{x}_0, \boldsymbol{p}_0\right)$ is the position at time t as a function of the initial values, and $S_{\mathrm{cl}}\left(\boldsymbol{x}_0, \boldsymbol{p}_0, t\right)$ is the classical action of the trajectory that connects $\boldsymbol{x}_0$ and $\boldsymbol{x}_t\left(\boldsymbol{x}_0, \boldsymbol{p}_0\right)$. There are some different implementations of SC-IVR. The interested reader is directed to a paper by Miller.[19]

Matsubara dynamics

Matsubara dynamics was rather recently (2015) developed by Hele et al.[42] and even more recently (2019) generalized from just single time correlation functions to multitime correlation functions.[43] It is a method for calculating Kubo-transformed correlation functions. Matsubara dynamics is based on the discretized imaginary time

path integral. Every bead in the path integral polymer is given a momentum and kinetic energy in real time. A normal mode analysis is made for the path integral polymer, in the limit where the number of beads goes to infinity, and the normal modes are divided into two groups. One group contains the so called Matsubara modes, i.e. the modes with the lowest frequencies, and the other group contains the non-Matsubara modes, i.e. the higher frequency modes. The propagation forward in time is made by using the quantum mechanical propagation operator for phase space distributions, $e^{\widehat{L}t}$, with the Liouvillian operator (here shown one-dimensional)

$$\widehat{L} = \frac{p}{m}\frac{\partial}{\partial x} - \frac{2V(x)}{\hbar}\sin\left(\frac{\overleftarrow{\partial}}{\partial x}\frac{\hbar}{2}\frac{\overrightarrow{\partial}}{\partial p}\right), \tag{2.72}$$

but only including derivatives of the Matsubara mode coordinates. By using this method of propagation the quantum Boltzmann distribution is conserved over time. The intention of this method is to find a more correct way of combining a quantum Boltzmann distribution with classical dynamics, compared to the classical Wigner method, which does not conserve the quantum Boltzmann distribution over time.

Matsubara dynamics is a fairly accurate method of approximate quantum dynamics, but it is not practical to use for chemical problems, as it is too computationally demanding. Approximations to Matsubara dynamics, to make it less demanding, have been studied.[44] Matsubara dynamics has also been used as a comparison for the classical Wigner method,[42] and as an intermediate point to derive RPMD and CMD from first principles.[45]

Centroid molecular dynamics

Centroid molecular dynamics (CMD) was first introduced by Cao and Voth.[35] CMD uses the discretized imaginary time path integral and gives Kubo-transformed correlation functions. In CMD the interesting quantities are measured as centroid variables. For the case of $\widehat{x}$ and $\widehat{p}$ the corresponding centroid variables are just the average position and momentum, respectively, of all the beads in the

path integral. A phase space centroid distribution, that gives the thermal distribution, and a quasi density operator, that is used to acquire centroid variables and their propagation in time, are defined.

CMD was also derived as a centroid mean-field approximation of Matsubara dynamics.[45]

For a harmonic oscillator, and an infinite number of beads in the polymer, the original CMD method is exact, but only for correlation functions where at least one of the operators, $\widehat{\boldsymbol{A}}$ or $\widehat{\boldsymbol{B}}$, is linear,[46]

$$\widehat{\boldsymbol{\Omega}} = \boldsymbol{\Omega}_0 + \boldsymbol{\Omega}_1 \widehat{\boldsymbol{x}} + \boldsymbol{\Omega}_2 \widehat{\boldsymbol{p}}, \tag{2.73}$$

where the $\boldsymbol{\Omega}$:s are constants. CMD works poorly for non-linear correlation functions for other potentials.[45] The CMD method has been extended to work better for correlation functions of non-linear operators,[46] but this is much more complicated than standard CMD.

One particular disadvantage of CMD is for vibrational spectra, where the peaks of a spectrum can be artificially broadened and shifted in frequency at low temperatures.[47] This is an example of what is called the curvature problem of CMD.

Ring polymer molecular dynamics

Ring polymer molecular dynamics (RPMD) was first introduced by Craig and Manolopoulos in 2004.[36] Just as the previous two methods, RPMD uses the discretized imaginary time path integral to calculate Kubo-transformed correlation functions. Contrary to CMD, the measurables of interest are evaluated at the position of every bead in the ring polymer and then taken as the mean of these values. To get a propagation in time every bead in the ring polymer is propagated according to classical mechanics, with the addition of the interactions with neighboring beads.

RPMD is restricted to the calculation of position correlation functions, meaning that correlation functions of operators containing momentum can not be directly obtained. Momentum correlation functions can, however, be calculated from time-derivatives of position correlation functions.[48,49] Thus, momentum correlation functions can be obtained, but for certain operators, such as high powers of $\widehat{\boldsymbol{p}}$, it may be impractical.

Hele et al.[45] showed that, RPMD can be derived from Matsubara dynamics by removing part of the Liouvillian operator.

For a harmonic oscillator, and an infinite number of beads in the polymer, the RPMD method is exact, but only for correlation functions where at least one of the operators, $\widehat{A}$ or $\widehat{B}$, is linear. If the correlation function happens to be $\langle \widehat{x}\widehat{x}(t)\rangle_{\text{Kubo}}$, then the RPMD method using any number of beads gives the exact result.[36] RPMD works worse for correlation functions of non-linear operators than for correlation functions of linear ones, also for other potentials than the harmonic oscillator.[45]

An RPMD correlation function is exact a time 0 and the ensemble is conserved during propagation.

One particular disadvantage of RPMD, as for CMD, is for vibrational spectra. In the case of RPMD, however, new spurious peaks can appear in a spectrum, and the peaks can be artificially broadened and split.[47] By thermostating the vibrational modes of the path integral polymer the RPMD method has been found to become better at handling vibrational spectra.[50]

RPMD is used as a comparison, for the new method that is developed, in papers III and IV, and section 3.3.

Dirac-Frenkel

The Dirac-Frenkel variational principle was first introduced by Dirac[51] and Frenkel,[52] and later a somewhat different form was derived by McLachlan.[53]

$$\left\langle \delta\Psi(t)\left|i\hbar\frac{\partial}{\partial t} - \widehat{H}\right|\Psi(t)\right\rangle = 0, \tag{2.74}$$

where $\delta\Psi(t)$ is a variation in the time dependent wavefunction. For wavefunctions or densities that have been written in a parametrized form this variational principle allows the derivation of equations of motion in these parameters, giving an approximate solution to the time dependent Schrödinger equation.

Among the methods that have been derived using the Dirac-Frenkel variational principle can be found e.g. the multi-configurational time dependent Hartree (MCTDH) method,[54] which is a very accurate method for time dependent quantum mechanics, but quickly

becomes computationally expensive as the size of the modeled system is increased.

A variational principle corresponding to the Dirac-Frenkel one, but for Wigner distributions in phase space, is used in paper II, and section 3.2.

Chapter 3

Developments

> The general who wins a battle makes many calculations in his temple ere the battle is fought. The general who loses a battle makes but few calculations beforehand. Thus do many calculations lead to victory, and few calculations to defeat: How much more do no calculation at all pave the way to defeat!
>
> Sun Tzu (transl. L. Giles)[55]

The new contributions to science from the research presented in this thesis are a reaction rate constant for a radiative association reaction and two methods of approximate quantum dynamics. The reaction rate constant is presented in section 3.1 (paper I). The two new quantum dynamical methods are presented in sections 3.2 (paper II) and 3.3 (papers III and IV) respectively. In section 3.4 suggestions are made for the direction of future research.

3.1 Formation of the Hydroxyl Radical by Radiative Association

In paper I[5] new values for the reaction rate constant of the radiative association reaction

$$O(^3P) + H(^2S) \rightarrow OH(X^2\Pi) + \gamma , \qquad (3.a)$$
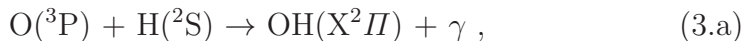
where γ is a photon, is presented for the temperature range 10 K - 30000 K.

The interest in this reaction comes from astrochemistry as the hydroxyl radical has been observed in the interstellar medium, i.e. the space between the stars, of the Milky Way[56] and two other galaxies.[57] Also the reactants of this reaction are the hydrogen atom and the oxygen atom. Hydrogen is the most abundant element and oxygen is the third most abundant element in our galaxy so there should not be a lack of reactants, from an interstellar point of view.

On earth it could be reasonable to believe that the formation of OH from O and H would happen through a three body collision, i.e. a third species colliding with the activated complex of O and H and carrying away some energy. However, the Earths atmosphere can, through a back-of-the-envelope calculation, be estimated to have a number density of $\sim 10^{19}$ cm^{-3} at the surface, while what is considered a dense cloud in the interstellar medium has number densities of between 10^3 cm^{-3} and 10^6 cm^{-3}.[58] It is therefore possible for reactions that would be completely irrelevant at the surface of the Earth to be very important in the interstellar medium.

Three body reactions do noticeably occur in the interstellar medium in the form of reactions between species adsorbed onto dust grains, but these reactions are not the subject of paper I.

The radiative association reaction can take place through a number of different pathways. The ones considered in paper I are the ones starting from the electronic ground states of the atoms.

The ground state atoms O(^{3}P) and H(^{2}S) can form the molecule in the electronic states OH(X$^2\Pi$), OH($1^2\Sigma^-$), OH(a$^4\Sigma^-$), and OH(b$^4\Pi$). The potential energy for these electronic states can be seen as a function of internuclear distance, x_{ind}, in figure 3.1. OH(X$^2\Pi$) is the only one of these electronic states that has bound
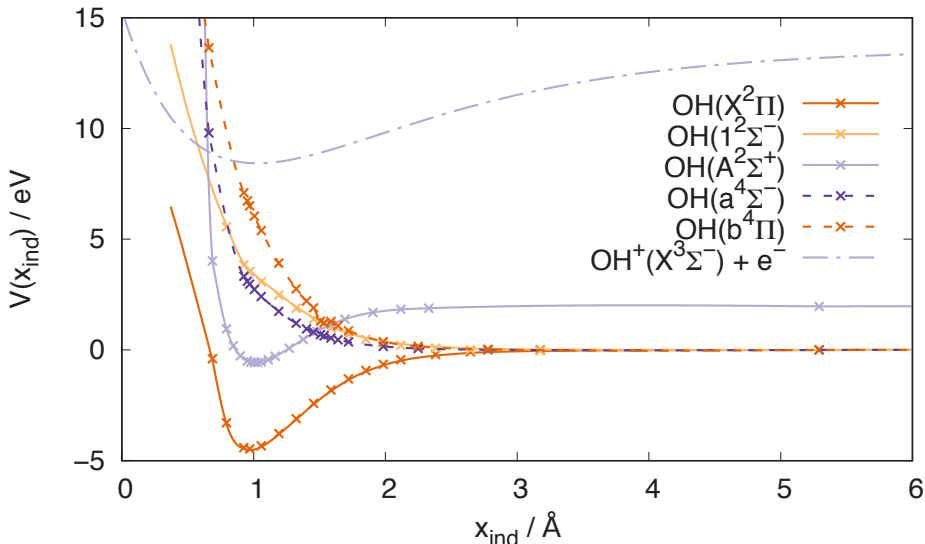
Figure 3.1: Potential energy surfaces for the electronic states $X^2\Pi$,[59] $1^2\Sigma^-$,[59] $A^2\Sigma^+$,[60] $a^4\Sigma^-$,[60] and $b^4\Pi$[60] of OH and a Morse potential for the electronic state $X^3\Sigma^-$ of OH^+[61,62] shifted to account for the hydrogen ionization energy.[63] The crosses show the original data points and the lines are inter- and extrapolations.

vibrational levels, and these bound levels are the product of the reaction. The free or quasi-bound vibrational states of $OH(X^2\Pi)$ will be denoted $OH(X^2\Pi)^*$.

The two most direct pathways for the reaction are

$$O(^3P) + H(^2S) \rightarrow OH(X^2\Pi)^* \rightarrow OH(X^2\Pi) + \gamma \qquad (3.b)$$

and

$$O(^3P) + H(^2S) \rightarrow OH(1^2\Sigma^-) \rightarrow OH(X^2\Pi) + \gamma . \qquad (3.c)$$
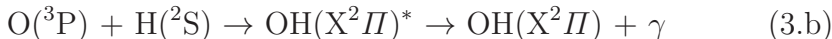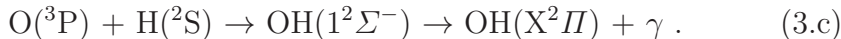
The atoms could also approach each other in any of the electronic states corresponding to the ground states of the atoms and couple, through e.g. spin-orbit-interactions, to the state $A^2\Sigma^+$, that can be seen in figure 3.1. From the quasibound vibrational levels of that state a radiative transition to a bound vibrational level of $X^2\Pi$ can happen. This, so called, inverse predissociation adds four possible pathways for the reaction

$$O(^3P) + H(^2S) \rightarrow OH(X^2\Pi)^* \rightarrow OH(A^2\Sigma^+)$$
$$\rightarrow OH(X^2\Pi) + \gamma \, , \tag{3.d}$$

$$O(^3P) + H(^2S) \rightarrow OH(1^2\Sigma^-) \rightarrow OH(A^2\Sigma^+)$$
$$\rightarrow OH(X^2\Pi) + \gamma \, , \tag{3.e}$$

$$O(^3P) + H(^2S) \rightarrow OH(a^4\Sigma^-) \rightarrow OH(A^2\Sigma^+)$$
$$\rightarrow OH(X^2\Pi) + \gamma \, , \tag{3.f}$$

and

$$O(^3P) + H(^2S) \rightarrow OH(b^4\Pi) \rightarrow OH(A^2\Sigma^+)$$
$$\rightarrow OH(X^2\Pi) + \gamma \, . \tag{3.g}$$
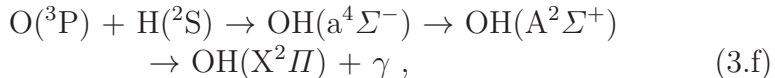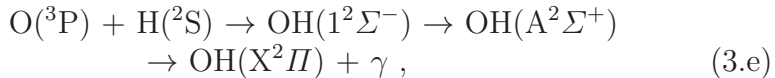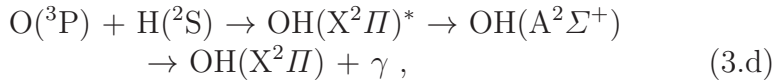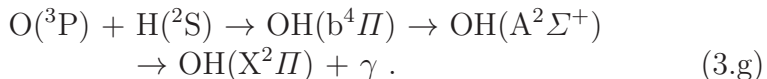
Only single-photon processes are considered, as two-photon processes are highly unlikely to occur.

Possible competing reactions are the electron detachment reaction

$$O(^3P) + H(^2S) \rightarrow OH(X^2\Pi/1^2\Sigma^-/a^4\Sigma^-/b^4\Pi)$$
$$\rightarrow OH^+(X^3\Sigma^-) + e^- \tag{3.h}$$

and the charge transfer reactions

$$O(^3P) + H(^2S) \rightarrow OH(X^2\Pi/1^2\Sigma^-/a^4\Sigma^-/b^4\Pi)$$
$$\rightarrow O^-(^2P) + H^+ \tag{3.i}$$

and

$$O(^3P) + H(^2S) \rightarrow OH(X^2\Pi/1^2\Sigma^-/a^4\Sigma^-/b^4\Pi)$$
$$\rightarrow O^+(^4S) + H^-(^1S) \, . \tag{3.j}$$
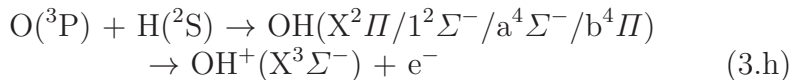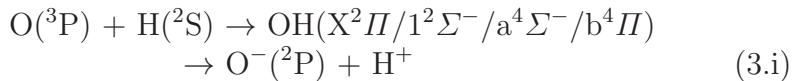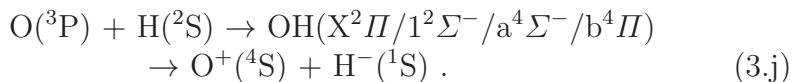
Theory and method

Several methods were used to calculate rate constants in this work. These used the potential energy surfaces shown in figure 3.1 together with the dipole moment of the state $X^2\Pi$ and the transition dipole moment of the transition $1^2\Sigma^- \rightarrow X^2\Pi$ that are shown in figure 3.2.
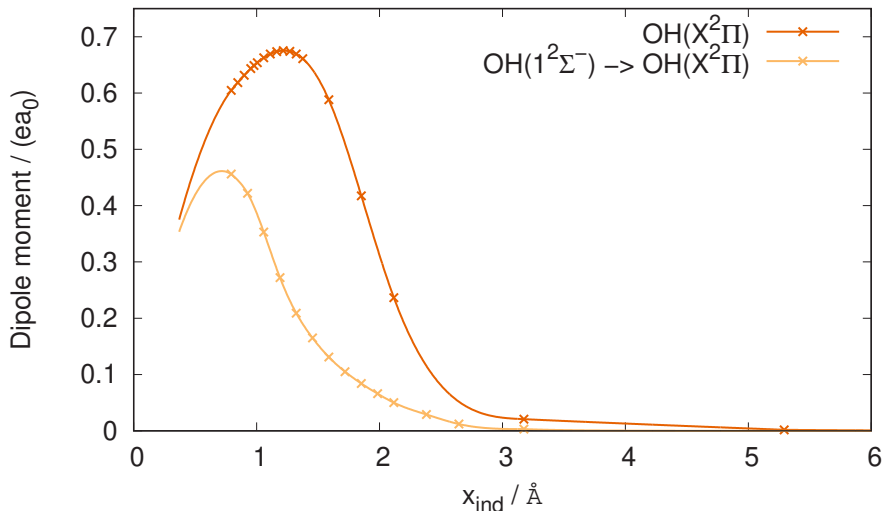
Figure 3.2: Electric dipole moment of the electronic state $X^2\Pi$[64] and transition dipole moment for the transition between electronic states $1^2\Sigma^-$ and $X^2\Pi$,[59] of OH. ea_0 is the elemental charge times the Bohr radius. The crosses show the original data points and the lines are inter- and extrapolations.

Quantum mechanical perturbation theory

To get quantum mechanical reaction cross sections a first order perturbation theory was used. The perturbation, that is added to the hamiltonian of the system, is in this case the interaction between the electric field of the emitted photon and the dipole moment of the molecular system. This perturbation theory for transition probabilities is sometimes called "Fermi's golden rule" or just the "golden rule". It is more thoroughly described in e.g. the textbook by Bransden and Joachain.[65] The application of this perturbation theory to get radiative association cross sections has been described in e.g. references 66 and 67. This method requires wavefunctions to be computed for both the unbound and bound states so that the matrix elements of the dipole moment operator can be obtained. Here the unbound wavefunctions were calculated with Numerov's method[68] and the bound wavefunctions were calculated with the

version of the discrete variable representation (DVR) of Colbert and Miller.[69]

Since molecules can rotate these calculations need to account for different rotational states. When rotation is added to the diatomic system a centrifugal potential, $\propto {}^1/x_{\mathrm{ind}}^2$, has to be added to the potential energy surface. When this, purely repulsive, centrifugal potential is added to the $X^2\Pi$ potential a barrier is obtained for some rotational quantum numbers. This barrier can cause quasibound vibrational states, i.e. states with an energy lower than the barrier but above the dissociation limit, so tunneling is necessary to enter or escape. The reaction cross section calculated with this method will look like a smooth function of energy, but when the collision energy coincides with the energy of a quasibound state there is a sudden peak in the function. (These peaks can be seen in figure 3.3.) The phenomenon is called resonance.

The quasibound states are long lived, compared with a wavepacket just bouncing off the repulsive part of the potential. Somewhat simplified, the system could be considered as getting stuck inside the barrier for a while. Thus, for a collision energy with a resonance there will be much more time for the radiative transition from the quasibound state to occur, compared to the simple bounce-off situation. These quasibound states have a finite lifetime, since there is the possibility of escaping them through tunneling or the emission of a photon. Due to this, there is a kind of uncertainty relation,

$$\Delta E_{\mathrm{res}} = \frac{\hbar}{\tau_{\mathrm{res}}},\tag{3.1}$$

where τ_{res} is the lifetime of the resonance and ΔE_{res} is the so called "width" of the resonance. The width is actually related to the width of the peaks in the reaction cross section.

A drawback of this perturbation theory is, as for all first order perturbation theories, that the perturbation has to be small. If the perturbation, in this case the interaction between the photon and the system, is large enough to significantly affect the bound or unbound wavefunctions, then this method will not work that well.

Another drawback of this perturbation theory method is that when putting it into collision theory and calculating the integral over energy, equation 2.65, that integral has to be done numerically

and the cross section has to be calculated on a grid of energies. If there are resonances to account for, the grid has to be fine enough to properly represent these possibly very thin peaks in the cross section function. If the grid is too coarse the peaks may be distorted in shape or may not be found at all.

Semiclassical method

An alternative to perturbation theory when it comes to calculating quantum mechanical cross sections is the use of an optical potential,

$$V_{\text{opt}}(x_{\text{ind}}) = -\frac{i\hbar}{2} A_{\text{Einstein}}(x_{\text{ind}}), \qquad (3.2)$$

where $A_{\text{Einstein}}(x_{\text{ind}})$ is the Einstein A coefficient, that is the probability of transition between two states per unit of time. This optical potential is added to the standard hamiltonian of the system. When the system is propagated forward in time the imaginary optical potential will absorb part of the probability of the unbound states. This means that there is no need to calculate the wavefunctions for the bound states, only for the unbound ones.

The method used in paper I is restricted by the Franck-Condon principle,[70–72] which states that during a transition between two electronic states in a molecule the electrons will move to the appropriate new configuration, but the nuclei are so slow that they will keep their position and momentum and only adapt after the transition has already happened. This is a predecessor to the Born-Oppenheimer approximation.[3] This optical potential method only works for radiative transitions between different electronic states, in this case reaction 3.c.

In this work the unbound wavefunctions were handled semiclassicaly with the Wentzel-Kramers-Brillouin (WKB) approximation.[73–75]

With the semiclassical approximation, this method can not account for resonances. But it can give the baseline of the reaction cross section.

Classical method

Since the semiclassical method described in the preceding section only handles transitions between two different electronic states , it can not be used for reaction 3.b. To get an alternative method to calculate cross sections for this reaction a purely classical method was used instead. This classical method was used in the form developed by Gustafsson.[76]

This classical method uses the classical equations of motion to compute the electric dipole moment of the system as a function of time. The frequency of the changes in dipole moment can be equated with the frequency of the emitted photon and the intensity of the emission can be calculated as the Larmor power,[77] that depends on the second time derivative of the dipole moment.

Since this method is based on the classical equations of motion, it can not account for resonances, but just as the semiclassical method, it can give the baseline of the reaction cross section.

Breit-Wigner theory and inverse predissociation

Breit-Wigner theory[78] allows the calculation of the contribution to the reaction rate constant that comes from the resonances. A certain shape is assumed for the resonance-peaks, and the contribution to the reaction cross section or rate constant from each resonance can be calculated from the width/lifetime of the resonance. This contribution is

$$\sigma_{\text{res}}(E) \propto \frac{\Delta E_{\text{res,rad}} \Delta E_{\text{res,tun}}}{\left(E - E_{\text{res}}\right)^2 + \frac{(\Delta E_{\text{res,tot}})^2}{4}} = \frac{\frac{1}{\tau_{\text{res,rad}} \tau_{\text{res,tun}}}}{\frac{(E - E_{\text{res}})^2}{\hbar^2} + \frac{1}{4\tau_{\text{res,tot}}^2}}$$

(3.3)

$$k_{\text{r,res}}(T) \propto \frac{\Delta E_{\text{res,rad}} \Delta E_{\text{res,tun}}}{\Delta E_{\text{res,tot}}} = \frac{\hbar \tau_{\text{res,tot}}}{\tau_{\text{res,rad}} \tau_{\text{res,tun}}}$$

$$= \frac{\hbar}{\tau_{\text{res,rad}} + \tau_{\text{res,tun}}},$$

(3.4)

where the relevant energy, E, is the collision energy compared to the asymptotic potential energy of $X^2\Pi$, and E_{res} is the energy of the quasibound state. The width/lifetime of the resonance has

been divided into one part for the radiative process of escaping the quasibound state and one part for the tunneling out of the quasibound state. The total process of escaping the quasibound state has $\Delta E_{\text{res,tot}} = \Delta E_{\text{res,rad}} + \Delta E_{\text{res,tun}}$ and $^1/_{\tau_{\text{res,tot}}} = ^1/_{\tau_{\text{res,rad}}} + ^1/_{\tau_{\text{res,tun}}}$.

As has already been mentioned, the quantum mechanical perturbation theory gives the reaction cross section as a function of energy, and the integral over energy in equation 2.65 has to be performed numerically. The ability of the perturbation theory to describe the contribution from the resonance is thus dependent on that the grid that the integration is conducted upon is fine enough to capture the position and shape of the very narrow peaks in the cross section. Breit-Wigner theory instead assumes a peak shape that is analytically integrable, and therefore does not have the same problems as the perturbation theory.

Of course computations are needed to find the energies of the quasibound states and calculate their widths/lifetimes. In this work the program LEVEL[79] was used. The methods to accomplish these computations will not be further explored here. The Breit-Wigner theory was used to add a resonance contribution to the cross section of reaction 3.b when it was calculated with the classical method.

The use of equations 3.3 and 3.4 is not restricted to quasibound vibrational states caused by tunneling. Reactions 3.d-3.g occur via quasibound vibrational states in $A^2\Sigma^+$ that can be entered and exited, not by tunneling through a potential barrier, but rather by coupling to the electronic states $X^2\Pi$, $1^2\Sigma^-$, $a^4\Sigma^-$, and $b^4\Pi$, e.g. through spin-orbit interactions.

This process is called inverse predissociation. Predissociation is when a bound molecule absorbs a photon and is excited to this kind of quasibound state and then changes electronic state and becomes unbound, dissociating. Inverse predissociation is thus the inverse of this.

As long as the energies of the quasibound states and the widths/lifetimes for the radiative process and the coupling between the electronic states can be obtained, a contribution to the reaction rate constant can be calculated through equations 3.3 and 3.4. In paper I these were taken from the literature.

Electron detachment

For reaction 3.h an upper bound to the reaction cross section was estimated through a method that has been used for $O^- + H$.[80] This approximate method assumes that, for a certain electronic state all classical trajectories that reach the point where the potential energy surface of this electronic state crosses the potential energy surface of the electronic state with a detached electron, x_{cross}, leads to a reaction,

$$\sigma_{\mathrm{Elec.det.}}(E) \propto \begin{cases} 0 & \text{if } E < V(x_{\mathrm{cross}}) \\ \pi x_{\mathrm{cross}}^2 \left(1 - \dfrac{V(x_{\mathrm{cross}})}{E}\right) & \text{if } E \geqslant V(x_{\mathrm{cross}}) \end{cases}.$$

$$(3.5)$$

Since the $X^2\Pi$ potential energy surface was not available at, nor extrapolated to, the point where it would cross the potential energy of the $X^3\Sigma^-$-state of OH^+ it was not counted in the total cross section. However, from looking at figure 3.1 it can be safely assumed that this $V(x_{\mathrm{cross}})$ will not be the crossing of potential energy surfaces that is lowest in energy, and only the one that is lowest in energy will determine the energy at which the electron detachment cross section starts being non-zero. As will be seen in the next section, only the energy at which the electron detachment may start to occur, rather than the estimated value of the cross section, is important. Not accounting for $X^2\Pi$ will thus not affect the end results of this work.

Results and discussion

In figure 3.3 the reaction cross section for reaction 3.b is shown. The difference between the cross section calculated with the perturbation theory and the classical method with the addition of Breit-Wigner theory can be seen. The baselines of the two approaches are very similar except at the highest and lowest energies. Thus, the classical method is a very good approximation for the non-resonant contribution to this cross section. It is visible that Breit-Wigner theory finds many more resonances than the perturbation theory does, particularly at high energies, where the perturbation theory does not
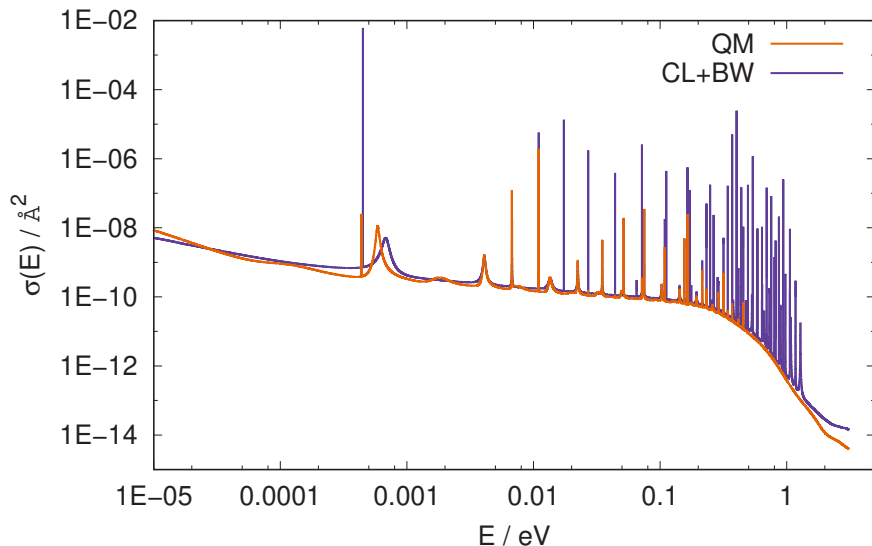
Figure 3.3: Reaction cross section for the reaction $OH(X^2\Pi)^* \rightarrow OH(X^2\Pi) + \gamma$ (3.b) calculated with the quantum mechanical perturbation theory (QM) and the classical method + Breit-Wigner theory (CL+BW).

find any resonances at all. The axes in the graph are logarithmic. To get a manageable number of grid points for the energy, the grid is coarser at higher energies than at lower ones. This can now be seen, as the perturbation theory is completely dependent on having a fine enough energy grid for finding the resonances. For the highest energies, where the grid is the coarsest, the perturbation theory does not find any resonances at all. Meanwhile the Breit-Wigner theory have found a lot of resonances, independent of the grid. Since the perturbation theory misses too many resonances, the cross section from the classical method with the addition of Breit-Wigner theory was used for the rate constant calculations, see figure 3.5.

In figure 3.4 the reaction cross section for reaction 3.c is shown. The difference between the cross section calculated with the perturbation theory and the semiclassical method can be seen. Since the electronic state $1^2\Sigma^-$ is purely repulsive, there are no quasi-bound vibrational states and thus no resonances. At low energies the pertur-
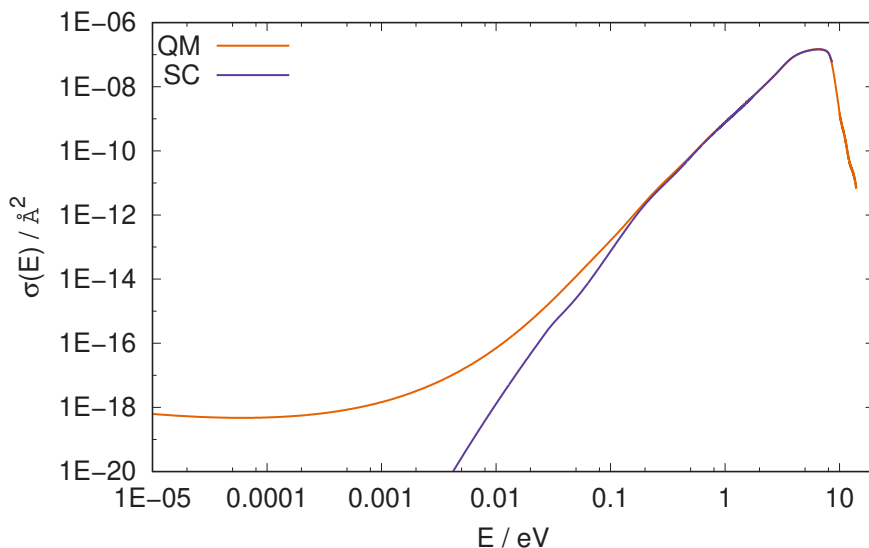
Figure 3.4: Reaction cross section for the reaction $OH(1^2\Sigma^-) \rightarrow OH(X^2\Pi) + \gamma$ (3.c) calculated with the quantum mechanical perturbation theory (QM) and the semiclassical method (SC).

bation theory cross sections are much higher than the semiclassical ones, due, at least in part, to tunneling into the classically forbidden short distances. At high energies the semiclassical cross section can not be calculated because the Franck-Condon principle restricts the energy of the emitted photon to the difference between the potential energy surfaces, and if this difference is lower than the collision energy the bound vibrational states are inaccessible. In figure 3.5 the reaction rate constants calculated from these cross sections are shown. The noticeable difference between the perturbation theory and semiclassical reaction rate constants is in the temperature range 200 K - 1000 K, where reaction 3.b dominates. This difference is thus not a problem.

It is reassuring, for reaction 3.c, that different methods give the same result for the reaction rate constant. This indicates that the result should be reliable.

In figure 3.6 the cross sections for reactions 3.b, 3.c, and 3.h has been gathered in the same graph. It can be seen that at low energies
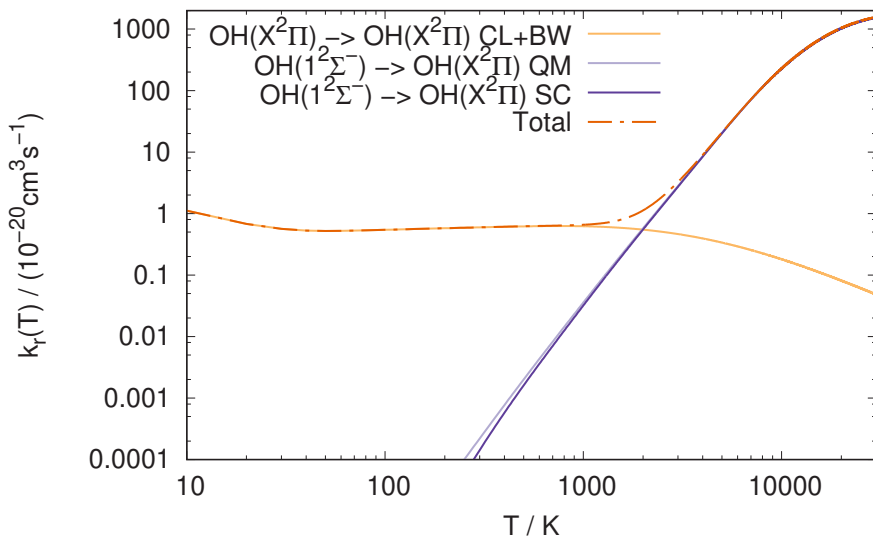
Figure 3.5: Reaction rate constant for the reactions $OH(X^2\Pi)^* \rightarrow OH(X^2\Pi) + \gamma$ (3.b), calculated with the classical method + Breit-Wigner theory (CL+BW), and $OH(1^2\Sigma^-) \rightarrow OH(X^2\Pi) + \gamma$ (3.c), calculated with the quantum mechanical perturbation theory (QM) and the semiclassical method (SC). Additionally a total reaction rate constant is shown.

the cross section for reaction 3.b is much higher than the cross section for reaction 3.c. At higher energies the processes have similar cross sections, and from around ~1 eV reaction 3.c gets the higher cross section. This is the same kind of trend as for the reaction rate constants for the two reactions that become equal around ~2000 K.

In figure 3.6 the estimate of the cross section for the electron detachment process, reaction 3.h, can also be seen. This approximate cross section is supposed to be an upper limit to the real cross section. The energies at which this reaction could interfere with the radiative association are the ones for which there is no calculated semiclassical cross section for reaction 3.c. The perturbation theory cross section does, however, have finite values at these high collision energies. The highest collision energies are most important at the highest temperatures. Since the rate constants calculated from the
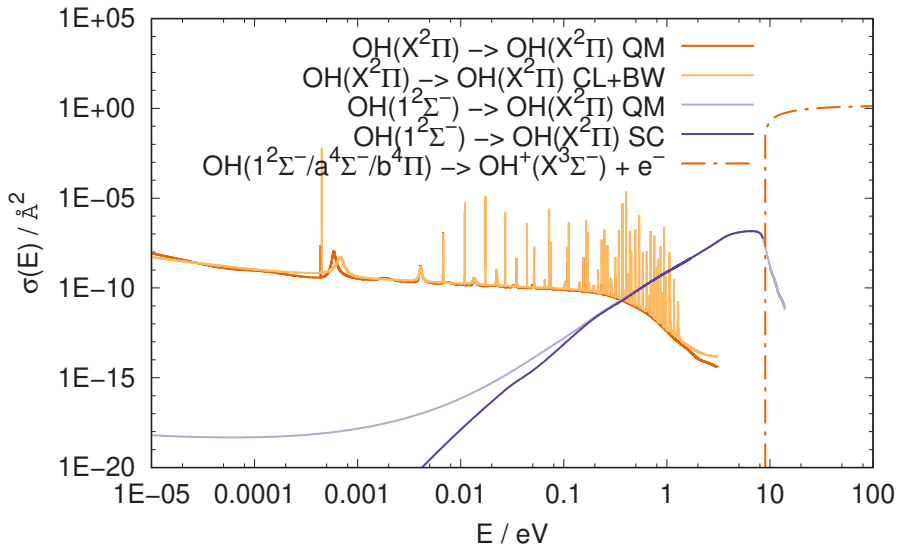
Figure 3.6: Reaction cross sections for the reactions $OH(X^2\Pi)^*$ $\to OH(X^2\Pi) + \gamma$ (3.b) and $OH(1^2\Sigma^-) \to OH(X^2\Pi) + \gamma$ (3.c), calculated with the quantum mechanical perturbation theory (QM), the classical method + Breit-Wigner theory (CL+BW), and the semiclassical method (SC). Estimate of reaction cross section for $OH(1^2\Sigma^-/a^4\Sigma^-/b^4\Pi) \to OH^+(X^3\Sigma^-) + e^-$ (3.h).

semiclassical and perturbation theory cross sections are indistinguishable at the high temperatures in figure 3.5, it can be concluded that the high collision energies where the two different cross sections are very different are not important at the temperatures studied in this work. If these collision energies are unimportant, then the competing electron detachment process will not affect the reaction rate constant studied here. Likewise, the charge transfer reactions, 3.i and 3.j, have threshold energies of >12 eV*, making also them negligible.

In figure 3.7 the total reaction rate constants for the processes 3.b and 3.c, and the total reaction rate constant for the inverse predissociation are shown. From around ~20 K to ~9000 K inverse

---

*These energies are acquired from an addition of ionization energies[63,81–83] and electron affinities.[84,85]
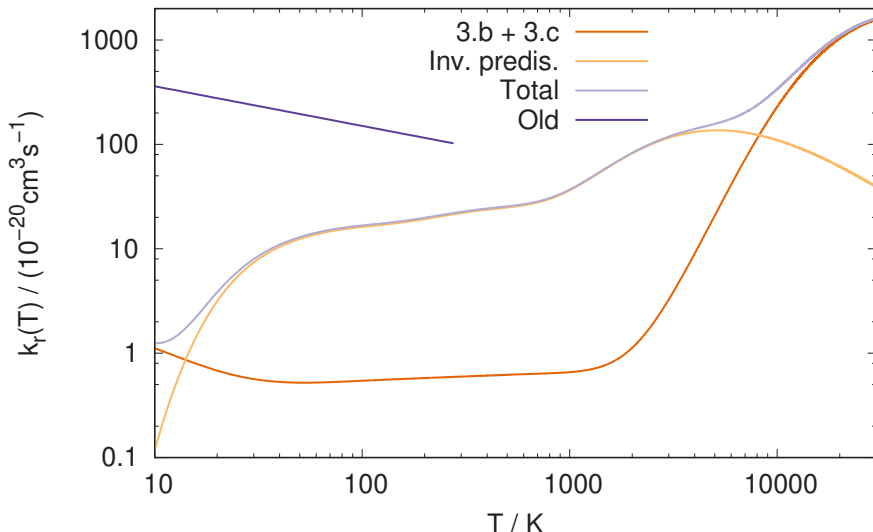
Figure 3.7: The total reaction rate constants for the radiative association reaction $O(^3P) + H(^2S) \rightarrow OH(X^2\Pi) + \gamma$ (3.a) through the processes 3.b + 3.c, the inverse predissociation processes (reactions 3.d-3.g), and the total sum of the processes. An older value for the same reaction rate constant, taken from KIDA,[86] is also shown.

predissociation dominates the reaction rate constant. At temperatures above ~10000 K process 3.c is, however, dominating.

This dominance by the process 3.c at high temperature means that the temperatures where the inverse predissociation makes a noticeable contribution to the total reaction rate constant will be temperatures where the highest collision energies will not matter. Thus, the high energy processes of electron detachment and charge transfer should not interfere with the inverse predissociation.

When it comes to possible interference between the processes 3.b and 3.c and inverse predissociation reactions 3.d-3.g, 3.f and 3.g goes via electronic states that are not involved with 3.b and 3.c and will not noticeably affect or be affected by them. 3.f is assumed to be the dominating process for inverse predissociation for most of the temperature interval studied.[60] Thus, it can also be assumed that inverse predissociaton will not interfere with 3.b and 3.c for most

temperatures. A possible problem is that both reactions 3.b and 3.d become important at low temperatures. However, none of the resonances in the two pathways overlap, so it is unlikely that they would affect each other.

If looking at collisions between O- and H-atoms that may have excited electronic states, discarding the excited states of hydrogen is unproblematic as they are very high in energy, ~ 10 eV.[87–89] The excited states of oxygen may however matter, at the higher temperatures studied here, as O(^{1}D) is only ~ 2 eV[87,90] above the ground state. This means that there are additional reaction pathways that could be significant at high temperatures, possibly increasing the rate constant.

There is an older value for the radiative association rate constant, shown in figure 3.7. This older value is the one found in the databases Kinetic Database for Astrochemistry[86] (KIDA) and UMIST database for astrochemistry[91] (UDfA). This older value is very different from the newly calculated one. The old value for the reaction rate constant is likely just a rough estimate[†]. With the above discussion indicating that the newly calculated rate constant should be relatively trustworthy, it is reasonable to assume that it is of higher quality than the old rate constant. Additionally, the new rate constant covers a much larger temperature interval.

[†]The author has been unsuccessful in locating the original source of the old reaction rate constant. As of writing this (20 April 2020) KIDA denotes the method for obtaining it as "estimation", which, according to KIDA, means that it is a guess, but possibly an educated one.

3.2 Dynamics of Gaussian basis functions

In 2011 Poulsen published a work where the Dirac-Frenkel variational principle, see section 2.4, was applied to Wigner functions.[92] In paper II[93] two new forms of basis functions to construct Wigner functions, for use with this variational principle are described and tested on a few model systems. The purpose is to evaluate if this could be a useful method for approximate quantum dynamics.

Theory and method

The Dirac-Frenkel variational principle for wavefunctions was briefly presented in section 2.4. The variational principle introduced by Poulsen[92] is the corresponding variational principle for Wigner distributions in phase space. In analogy with the Dirac-Frenkel variational principle the Wigner transformed operator can be written in a parametrized form. Here the parametrized Wigner functions will be called $\Phi_{\mathrm{W}}\left(\boldsymbol{x}, \boldsymbol{p}, \boldsymbol{\alpha}(t)\right)$, where $\boldsymbol{\alpha}(t)$ is the vector of parameters. The equation corresponding to equation 2.74 is

$$
\iint \mathrm{d}^D\boldsymbol{x}\, \mathrm{d}^D\boldsymbol{p}\, \left(\delta\Phi_{\mathrm{W}}\left(\boldsymbol{x}, \boldsymbol{p}, \boldsymbol{\alpha}(t)\right)\right)^*
$$
$$
\times \left(\widehat{L} - \frac{\mathrm{d}}{\mathrm{d}t}\right) \Phi_{\mathrm{W}}\left(\boldsymbol{x}, \boldsymbol{p}, \boldsymbol{\alpha}(t)\right) = 0, \tag{3.6}
$$

where $\delta\Phi_{\mathrm{W}}\left(\boldsymbol{x}, \boldsymbol{p}, \boldsymbol{\alpha}(t)\right)$ is a variation in $\Phi_{\mathrm{W}}\left(\boldsymbol{x}, \boldsymbol{p}, \boldsymbol{\alpha}(t)\right)$ corresponding to the variation $\delta\boldsymbol{\alpha}(t)$ in $\boldsymbol{\alpha}(t)$. These variations are complex, even though both the Wigner function, and the parameters, may be real. $\widehat{L}$ is the Liouvillian operator that was shown in equation 2.72. Since the time dependence of the Wigner function is contained in the parameters, the time derivative of the Wigner function is

$$
\frac{\mathrm{d}}{\mathrm{d}t}\Phi_{\mathrm{W}}\left(\boldsymbol{x}, \boldsymbol{p}, \boldsymbol{\alpha}(t)\right) = \dot{\boldsymbol{\alpha}}(t) \bullet \frac{\mathrm{d}}{\mathrm{d}\boldsymbol{\alpha}(t)}\Phi_{\mathrm{W}}\left(\boldsymbol{x}, \boldsymbol{p}, \boldsymbol{\alpha}(t)\right), \tag{3.7}
$$

where $\dot{\boldsymbol{\alpha}}(t)$ is the time derivative of $\boldsymbol{\alpha}(t)$. This means that the variational principle also can be written

$$\iint \mathrm{d}^D\boldsymbol{x}\,\mathrm{d}^D\boldsymbol{p}\,\left(\delta\Phi_{\mathrm{W}}\left(\boldsymbol{x},\boldsymbol{p},\boldsymbol{\alpha}(t)\right)\right)^*$$
$$\times\left(\widehat{L}-\dot{\boldsymbol{\alpha}}(t)\bullet\frac{\mathrm{d}}{\mathrm{d}\boldsymbol{\alpha}(t)}\right)\Phi_{\mathrm{W}}\left(\boldsymbol{x},\boldsymbol{p},\boldsymbol{\alpha}(t)\right)=0. \qquad (3.8)$$

From this, a formula for $\dot{\boldsymbol{\alpha}}(t)$ can be obtained,

$$\dot{\boldsymbol{\alpha}}(t)=\frac{\iint \mathrm{d}^D\boldsymbol{x}\,\mathrm{d}^D\boldsymbol{p}\,\left(\frac{\mathrm{d}}{\mathrm{d}\boldsymbol{\alpha}(t)}\Phi_{\mathrm{W}}\left(\boldsymbol{x},\boldsymbol{p},\boldsymbol{\alpha}(t)\right)\right)^*\widehat{L}\Phi_{\mathrm{W}}\left(\boldsymbol{x},\boldsymbol{p},\boldsymbol{\alpha}(t)\right)}{\iint \mathrm{d}^D\boldsymbol{x}\,\mathrm{d}^D\boldsymbol{p}\,\left(\frac{\mathrm{d}}{\mathrm{d}\boldsymbol{\alpha}(t)}\Phi_{\mathrm{W}}\left(\boldsymbol{x},\boldsymbol{p},\boldsymbol{\alpha}(t)\right)\right)^*\bullet\frac{\mathrm{d}}{\mathrm{d}\boldsymbol{\alpha}(t)}\Phi_{\mathrm{W}}\left(\boldsymbol{x},\boldsymbol{p},\boldsymbol{\alpha}(t)\right)},$$
$$(3.9)$$

which is an equation of motion for the parameters.

This variational principle can be written as a principle of least action,[92] with an action functional, $S\left(\boldsymbol{\alpha}(t)\right)$, that is

$$S\left(\boldsymbol{\alpha}(t)\right)=\int\mathrm{d}t\iint\mathrm{d}^D\boldsymbol{x}\,\mathrm{d}^D\boldsymbol{p}\,\left(\Phi_{\mathrm{W}}\left(\boldsymbol{x},\boldsymbol{p},\boldsymbol{\alpha}(t)\right)\right)^*$$
$$\times\left(\widehat{L}-\dot{\boldsymbol{\alpha}}(t)\bullet\frac{\mathrm{d}}{\mathrm{d}\boldsymbol{\alpha}(t)}\right)\Phi_{\mathrm{W}}\left(\boldsymbol{x},\boldsymbol{p},\boldsymbol{\alpha}(t)\right). \quad (3.10)$$

Here the principle of least action states that you should find the path in $\boldsymbol{\alpha}(t)$ that makes $S\left(\boldsymbol{\alpha}(t)\right)$ an extremum. This principle of least action is equivalent to equations 3.6 and 3.8.

In paper II[93] two new types of basis functions, ϕ, are suggested for building up the parametrized Wigner functions. As in the paper, the one-dimensional case will be shown here.

$$\Phi_{\mathrm{W}}\left(x,p,\boldsymbol{\alpha}(t)\right)=\overset{\text{num. of basis func.}}{\underset{j=0}{\sum}}w_j\phi_j\left(x,p,\boldsymbol{\alpha}_j(t)\right), \qquad (3.11)$$

where w_j is the weight coefficient of the basis function and $\boldsymbol{\alpha}_j(t)$ is the vector of parameters for each basis function. The basis functions suggested are a so called thawed real Gaussian function

$$\phi_j\left(x,p,\boldsymbol{\alpha}_j(t)\right)=\mathcal{N}\,\mathrm{e}^{-\begin{pmatrix}x-x_0(t)\\p-p_0(t)\end{pmatrix}^T\begin{pmatrix}a(t)&c(t)\\c(t)&b(t)\end{pmatrix}\begin{pmatrix}x-x_0(t)\\p-p_0(t)\end{pmatrix}}$$
$$(3.12)$$

and a frozen complex Gaussian function

$$\phi_j\left(x, p, \boldsymbol{\alpha}_j(t)\right) = e^{i\xi(t)} \, e^{-\begin{pmatrix} x - x_0\left(t\right) \\ p - p_0\left(t\right) \end{pmatrix}^T \begin{pmatrix} a & 0 \\ 0 & b \end{pmatrix} \begin{pmatrix} x - x_0\left(t\right) \\ p - p_0\left(t\right) \end{pmatrix}},$$
(3.13)

where $\mathcal{N}$ is a normalization constant, x_0 and p_0 are the average position and momentum of the basis function, and a, b, c, and ξ are other parameters of the basis function. The vectors $\boldsymbol{\alpha}_j(t)$ for the two kinds of basis functions are

$$\boldsymbol{\alpha}_{j,\text{Thawed}}(t) = \begin{pmatrix} x_0(t) \\ p_0(t) \\ a(t) \\ b(t) \\ c(t) \end{pmatrix}$$
(3.14)

$$\boldsymbol{\alpha}_{j,\text{Frozen}}(t) = \begin{pmatrix} x_0(t) \\ p_0(t) \\ a \\ b \\ \xi(t) \end{pmatrix}.$$
(3.15)

While all other parameters are real, the time dependent parameters for the frozen Gaussian, $x_0(t)$, $p_0(t)$, and $\xi(t)$, are complex numbers. Even though the individual frozen Gaussian functions are complex valued, the total Wigner function, that is the sum of them, should be real valued. The frozen Gaussian is called "frozen" because a and b have fixed values that do not change with time, and even though $\xi(t)$ change with time, it only affects the size and complex phase of the function. The frozen Gaussian thus preserves its shape, and only changes its average coordinate in phase space, its size, and its complex phase, when it evolves in time. In contrast, the thawed Gaussian is "thawed" (not frozen) because $a(t)$, $b(t)$, and $c(t)$ change with time. So the thawed Gaussian changes shape and average coordinate in phase space, but it conserves its size as it evolves in time.

A Wigner function constructed from one of the types of basis functions presented in paper II can be propagated in time by propagating the individual basis functions separately. For the thawed

Gaussian, the equations of motion, according to the variational principle, are

$$\dot{x}_0(t) = \frac{p_0(t)}{m} \tag{3.16}$$

$$\dot{p}_0(t) = -\frac{\mathrm{d}V_{\mathrm{Sm}}\left(x_0(t)\right)}{\mathrm{d}x_0(t)} \tag{3.17}$$

$$\dot{a}(t) = 2c(t)\frac{\mathrm{d}^2V_{\mathrm{Sm}}\left(x_0(t)\right)}{\mathrm{d}\left(x_0(t)\right)^2} \tag{3.18}$$

$$\dot{b}(t) = -\frac{2c(t)}{m} \tag{3.19}$$

$$\dot{c}(t) = b(t)\frac{\mathrm{d}^2V_{\mathrm{Sm}}\left(x_0(t)\right)}{\mathrm{d}\left(x_0(t)\right)^2} - \frac{a(t)}{m}, \tag{3.20}$$

where $V_{\mathrm{Sm}}\left(x_0(t)\right)$ is a smeared potential defined by

$$V_{\mathrm{Sm}}\left(x_0(t)\right) = \frac{1}{\hbar\sqrt{\pi b'(t)}} \int \mathrm{d}\eta\, V(\eta)\, e^{-\frac{(x_0(t)-\eta)^2}{\hbar^2 b'(t)}} \tag{3.21}$$

$$b'(t) = \frac{b(t)}{2}\left(\frac{1}{\hbar^2\left(a(t)b(t) - c(t)^2\right)} + 1\right). \tag{3.22}$$

$a(t)b(t) - c(t)^2$ is a constant of motion, and for a minimum uncertainty Wigner function, i.e. corresponding to a single state wavefunction, $a(t)b(t) - c(t)^2 = 1/\hbar^2$, resulting in $b'(t) = b(t)$. In this particular situation the proposed method is equivalent to methods that have been used before for Gaussian wavefunctions.[94,95]

For the frozen Gaussian, the equations of motion, according to

the variational principle, are

$$\dot{x}_{0,\mathrm{R}}(t) = \frac{p_{0,\mathrm{R}}(t)}{m} \tag{3.23}$$

$$\dot{x}_{0,\mathrm{I}}(t) = \frac{1}{2\hbar^2 ab} \frac{\mathrm{d}}{\mathrm{d}p_{0,\mathrm{I}}(t)}$$
$$\left(V_{\mathrm{Sm}} \left(x_{0,\mathrm{R}}(t) - \hbar b p_{0,\mathrm{I}}(t) \right) + V_{\mathrm{Sm}} \left(x_{0,\mathrm{R}}(t) + \hbar b p_{0,\mathrm{I}}(t) \right) \right) \tag{3.24}$$

$$\dot{p}_{0,\mathrm{R}}(t) = -\frac{1}{2} \frac{\mathrm{d}}{\mathrm{d}x_{0,\mathrm{R}}(t)}$$
$$\left(V_{\mathrm{Sm}} \left(x_{0,\mathrm{R}}(t) - \hbar b p_{0,\mathrm{I}}(t) \right) + V_{\mathrm{Sm}} \left(x_{0,\mathrm{R}}(t) + \hbar b p_{0,\mathrm{I}}(t) \right) \right) \tag{3.25}$$

$$\dot{p}_{0,\mathrm{I}}(t) = -\frac{a\dot{x}_{0,\mathrm{I}}(t)}{mb} \tag{3.26}$$

$$\dot{\xi}_{\mathrm{R}}(t) = \frac{1}{\hbar} \left(V_{\mathrm{Sm}} \left(x_{0,\mathrm{R}}(t) + \hbar b p_{0,\mathrm{I}}(t) \right) - V_{\mathrm{Sm}} \left(x_{0,\mathrm{R}}(t) - \hbar b p_{0,\mathrm{I}}(t) \right) \right)$$
$$- p_{0,\mathrm{I}}(t) b \frac{\mathrm{d}}{\mathrm{d}x_{0,\mathrm{R}}(t)}$$
$$\left(V_{\mathrm{Sm}} \left(x_{0,\mathrm{R}}(t) + \hbar b p_{0,\mathrm{I}}(t) \right) + V_{\mathrm{Sm}} \left(x_{0,\mathrm{R}}(t) - \hbar b p_{0,\mathrm{I}}(t) \right) \right) \tag{3.27}$$

$$\dot{\xi}_{\mathrm{I}}(t) = 2a x_{0,\mathrm{I}}(t) \dot{x}_{0,\mathrm{I}}(t) + 2b p_{0,\mathrm{I}}(t) \dot{p}_{0,\mathrm{I}}(t) \tag{3.28}$$

$$\dot{a} = \dot{b} = 0, \tag{3.29}$$

where $x_0(t)$, $p_0(t)$, and $\xi(t)$ have been divided into their real and imaginary parts, respectively denoted by R and I. $b'(t)$ for the smeared potential is for the frozen Gaussian defined as before, but with $c = 0$.

Both of the types of basis functions presented are mathematically complete, i.e. any function of $\boldsymbol{x}$ and $\boldsymbol{p}$ can be exactly expressed as a sum of such Gaussians. An additional useful property of the frozen Gaussians is that when summing them up to obtain the total Wigner function they can in principle account for quantum interference, due to their complex phase. Another effect of this complex phase is that the total Wigner function will not keep its normalization. Every time one wants to use the time evolved Wigner function it has to be renormalized. The thawed Gaussians will keep their individual normalization and they are completely positive real-valued, so the total Wigner function built from them will keep its nomalization over time, but they can not account for quantum interference.
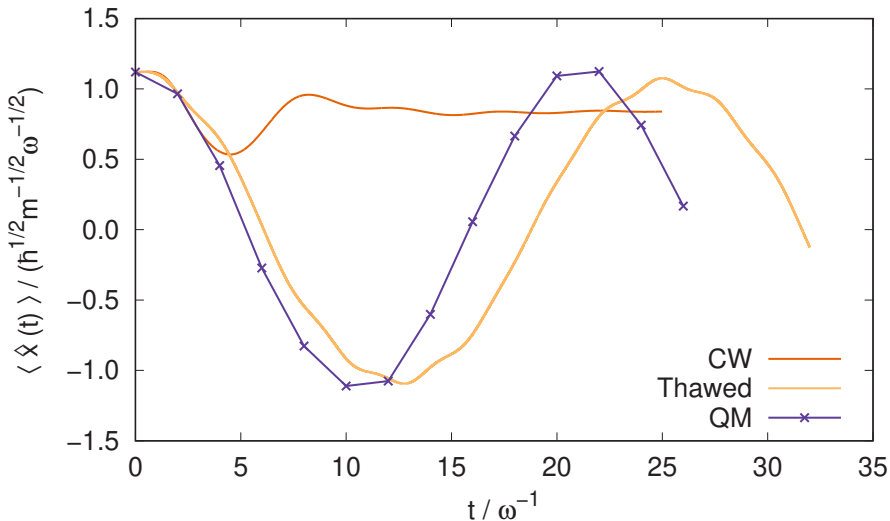
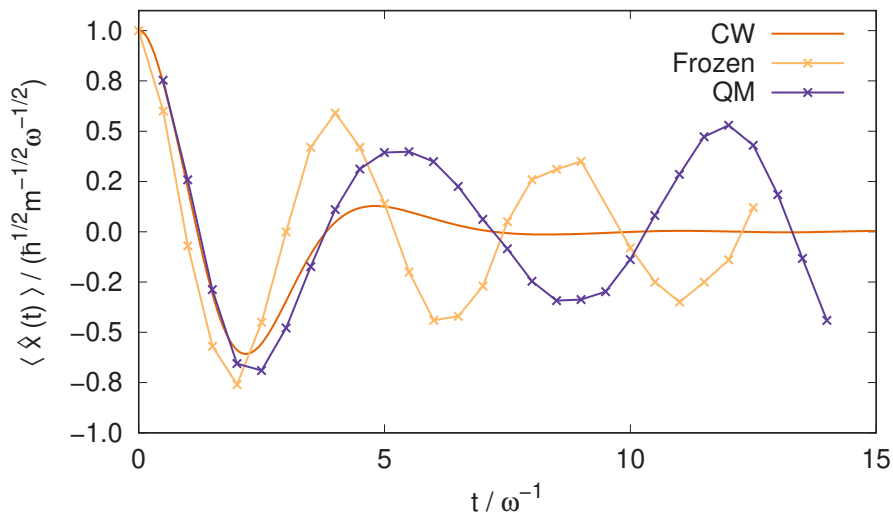Figure 3.8: Average position of a particle in the double well potential as a function of time. Results from the classical Wigner method (CW), a single thawed Gaussian function (Thawed), and accurate quantum mechanics (QM).

Both types of basis functions handle harmonic potentials exactly. For the frozen Gaussian basis functions the complex phase disappears for harmonic potentials, making the computations simpler. For potentials close to harmonic the complex phase factor, $e^{i\xi_R(t)}$, will be small.

Results and discussion

The new basis functions and equations of motion were tested for two different one-dimensional systems, a quartic double well potential, $V(x) = \dfrac{m^2\omega^3}{10\hbar}x^4 - \dfrac{m\omega^2}{2}x^2$, and a quartic potential $V(x) = \dfrac{m^2\omega^3}{4\hbar}x^4$, where ω is a unit of angular frequency. ω is also the absolute value of the angular frequency on top of the barrier in the double well.

For a Wigner function corresponding to the ground state of an oscillation in one of the wells in the double well, the average position as a function of time is shown in figure 3.8. Here a comparison can
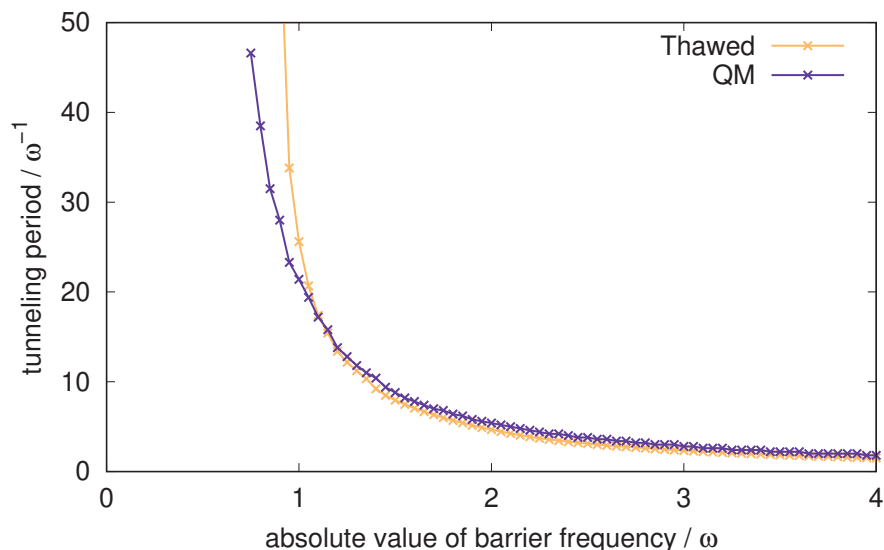
Figure 3.9: Tunneling periods of double well potentials with different barrier frequencies, but the same well depth. Results from thawed Gaussian functions (Thawed) and from accurate quantum mechanics (QM).

be made between the use of a single thawed Gaussian basis function, the classical Wigner method, and accurate quantum mechanics. The classical Wigner method and the exact quantum mechanics are only used to calculate the dynamics, the initial distribution is still the Gaussian basis function. It can be seen that the thawed Gaussians, quite well, account for the tunneling between the potential wells. The frequency of the oscillation is, however, a bit too slow. The dynamics of the thawed Gaussian function is a clear improvement over the classical Wigner method. The classical Wigner function can be seen to be stuck in the starting well, due to it not being able to account for dynamic tunneling.

The effect of adjusting the double well potential so that the frequency of barrier changed, but the depth of the wells stayed the same, was studied. In figure 3.9 the tunneling periods resulting from this are shown. The thawed Gaussian basis function gives good results for the tunneling period, except for the lowest frequency
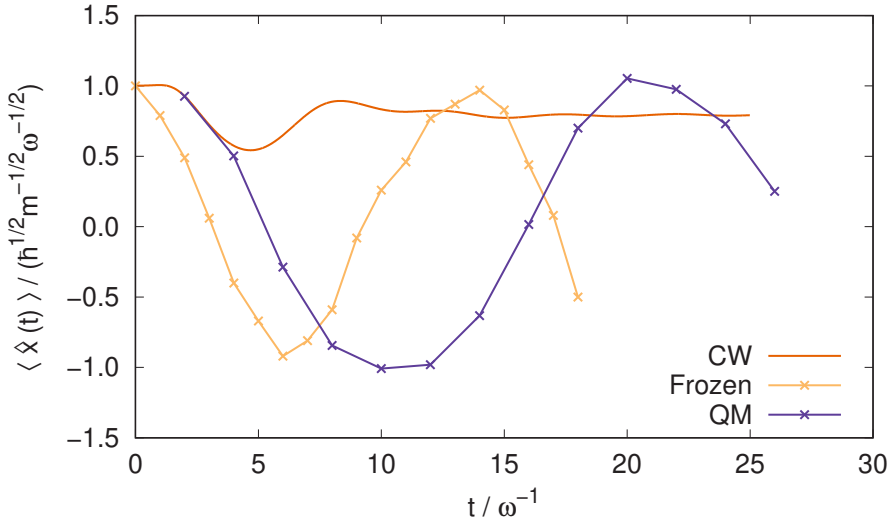
Figure 3.10: Average position of a particle in the double well potential as a function of time. Results from the classical Wigner method (CW), a Wigner function consisting of frozen Gaussian basis functions (Frozen), and accurate quantum mechanics (QM).

barriers, i.e. the widest ones.

Also, the frozen Gaussian basis functions were tested for the double well potential. For the standard double well the average position as a function of time for a Wigner function starting in one of the wells is shown in figure 3.10. As for figure 3.8, the classical Wigner method and the exact quantum mechanics are only used to calculate the dynamics, the initial distribution is the one described by the Gaussian basis functions. In contrast to the thawed Gaussian case, where only a single basis function was used, the Wigner function is here described by thousands of frozen Gaussian basis functions, making the variational dynamics much more computationally demanding. The frozen Gaussians, as the thawed ones, can be seen to account quite well for tunneling. For the frozen Gaussians the frequency of the oscillation is, however, significantly too fast. The frozen Gaussians definitely account for tunneling better than the classical Wigner method does, but it does not accurately reproduce

Figure 3.11: Average position of a particle in a quartic potential as a function of time. Results from the classical Wigner method (CW), a Wigner function consisting of frozen Gaussian basis functions (Frozen), and accurate quantum mechanics (QM).

quantum mechanical results for any time except $t = 0$.

The average position of a Wigner function, initialized as a Gaussian distribution on one side of the quartic potential, was calculated with the frozen Gaussian basis functions, and is displayed in figure 3.11. For this situation dynamic tunneling is not nearly as important as for the double well. For short times, the frozen Gaussian basis functions describe the accurate dynamics quite well, but worse than the classical Wigner method. The frequency of the dynamics of the frozen Gaussian functions is too high, but the correlation function retains a reasonable amplitude of the oscillation for much longer than the classical Wigner method does. In paper II it is shown that the frozen Gaussian basis functions describe the quantum interference on this quartic potential qualitatively, but not quantitatively.

Using the Feynman-Kleinert approximation[96] for the Boltzman operator, an analytic expression for the initial distribution for $\langle \widehat{x}\widehat{x}(t) \rangle_{\text{Kubo}}$, as described in section 2.4, for use with the thawed
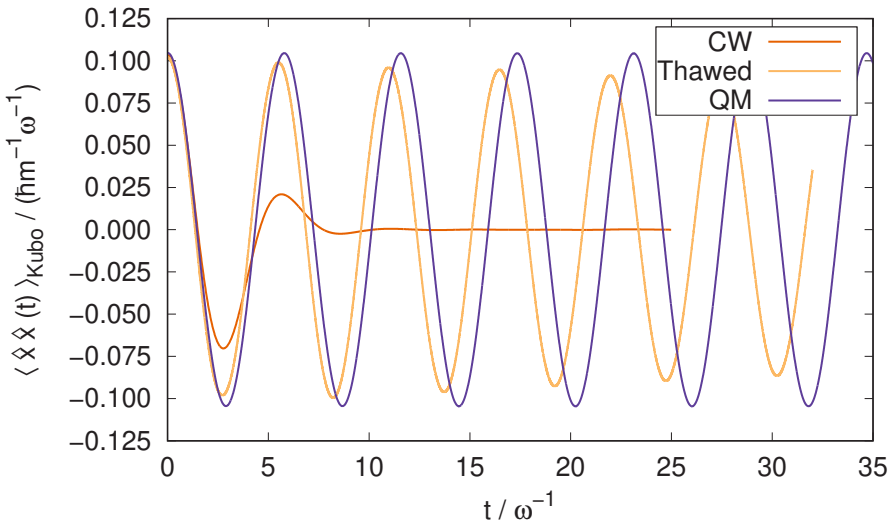
Figure 3.12: Kubo transformed position autocorrelation function for the quartic potential at $\beta\hbar\omega = 8$. Results from the classical Wigner method (CW), thawed Gaussian basis functions (Thawed), and accurate quantum mechanics (QM).

Gaussian basis functions, could be obtained. This expression was used to test the thawed Gaussian basis functions. In figures 3.12 and 3.13, $\langle \widehat{x}\widehat{x}(t) \rangle_{\text{Kubo}}$ for the quartic potential at temperatures $\beta\hbar\omega = 8$ and $\beta\hbar\omega = 1$ can be seen. At the lower temperature the thawed Gaussian basis functions give a good approximation to the quantum mechanical correlation function. At the higher temperature the thawed Gaussian basis functions, except for at very short times, fail to capture either the amplitude or the frequency of the correlation function. A similar situation for the double well potential is shown in the paper. That the thawed Gaussian functions from the Feynman-Kleinert approximation do not work well at high temperatures is due to that the division into basis functions, at high temperature, may lead to the propagation of individual basis functions that are unphysical according to Heisenbergs uncertainty principle, i.e. being too localized in both position and momentum simultaneously.

In summary the thawed Gaussian basis functions seem to be good
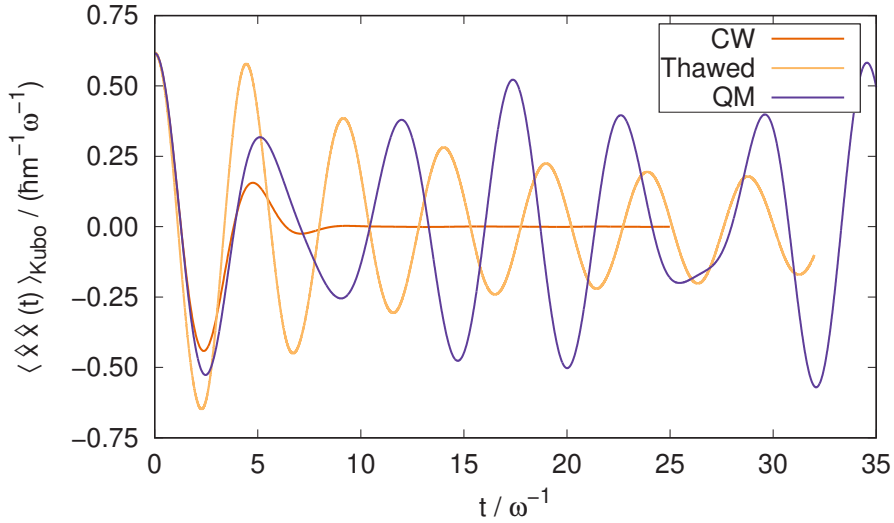
Figure 3.13: Kubo transformed position autocorrelation function for the quartic potential at $\beta\hbar\omega = 1$. Results from the classical Wigner method (CW), thawed Gaussian basis functions (Thawed), and accurate quantum mechanics (QM).

at describing tunneling, while the frozen Gaussian basis functions can describe interference. However, the dynamics of the frozen Gaussian basis functions are too fast.

3.3   The open polymer classical Wigner method

A new method of computing initial phase space distributions for the classical Wigner method, presented in sections 2.1 and 2.2, was published in paper III.[97] In this method a discretized imaginary time path integral, as presented in section 2.2, is used to sample a thermal quantum distribution. The new method was given the name "Open polymer classical Wigner". As can be surmised from the name, the polymer corresponding to the imaginary time path integral is not a closed ring, but have an opening. Paper IV is a manuscript in which the new variant of the classical Wigner method is applied to the calculation of reaction rate constants through the flux-Heaviside trace presented in section 2.3.

Derivation of the open polymer expression

The canonical correlation function $\left\langle \widehat{\boldsymbol{A}} \widehat{\boldsymbol{B}}\left(t\right)\right\rangle$ can be written

$$
\begin{aligned}
\left\langle \widehat{\boldsymbol{A}} \widehat{\boldsymbol{B}}\left(t\right)\right\rangle &= \frac{1}{Z}\operatorname{Tr}\left\{\widehat{\boldsymbol{A}}\,\mathrm{e}^{-\beta\widehat{H}}\,\mathrm{e}^{\frac{i\widehat{H}t}{\hbar}}\,\widehat{\boldsymbol{B}}\,\mathrm{e}^{-\frac{i\widehat{H}t}{\hbar}}\right\} \\
&= \frac{1}{Z}\int \mathrm{d}^D\boldsymbol{x}\,\left\langle \boldsymbol{x}\left|\widehat{\boldsymbol{A}}\,\mathrm{e}^{-\beta\widehat{H}}\,\mathrm{e}^{\frac{i\widehat{H}t}{\hbar}}\,\widehat{\boldsymbol{B}}\,\mathrm{e}^{-\frac{i\widehat{H}t}{\hbar}}\right|\boldsymbol{x}\right\rangle \\
&= \frac{1}{Z}\int \mathrm{d}^D\boldsymbol{x}\,\left\langle \boldsymbol{x}\left|\widehat{\boldsymbol{A}}\,\mathrm{e}^{-\beta\widehat{H}}\,\widehat{\boldsymbol{B}}(t)\right|\boldsymbol{x}\right\rangle. \quad (3.30)
\end{aligned}
$$

By inserting $N-1$ identity operators and dividing the Boltzmann operator into many parts, as was done in section 2.2, this can be changed into

$$
\begin{aligned}
\left\langle \widehat{\boldsymbol{A}} \widehat{\boldsymbol{B}}\left(t\right)\right\rangle &= \frac{1}{Z}\left\{\prod_{j=1}^{N}\int \mathrm{d}^D\boldsymbol{x}_j\right\}\left\langle \boldsymbol{x}_1\left|\widehat{\boldsymbol{A}}\,\mathrm{e}^{-\frac{\beta}{N}\widehat{H}}\right|\boldsymbol{x}_2\right\rangle \\
&\quad \times \left\langle \boldsymbol{x}_2\left|\mathrm{e}^{-\frac{\beta}{N}\widehat{H}}\right|\boldsymbol{x}_3\right\rangle \ldots \left\langle \boldsymbol{x}_{N-1}\left|\mathrm{e}^{-\frac{\beta}{N}\widehat{H}}\right|\boldsymbol{x}_N\right\rangle \\
&\quad \times \left\langle \boldsymbol{x}_N\left|\mathrm{e}^{-\frac{\beta}{N}\widehat{H}}\,\widehat{\boldsymbol{B}}(t)\right|\boldsymbol{x}_1\right\rangle. \quad (3.31)
\end{aligned}
$$

All the matrix elements can now be exchanged for inverse Fourier transforms of Wigner transforms, with the help of equation 2.26,

giving

$$
\left\langle \widehat{A}\widehat{B}\left(t\right)\right\rangle = \frac{1}{Z}\left\{\prod_{j=1}^{N}\iint \frac{\mathrm{d}^{D}\boldsymbol{x}_{j}\,\mathrm{d}^{D}\boldsymbol{p}_{j}}{\left(2\pi\hbar\right)^{D}}\,\mathrm{e}^{i\left(\boldsymbol{x}_{j}-\boldsymbol{x}_{(j\bmod N)+1}\right)\bullet\boldsymbol{p}_{j}/\hbar}\right\}
$$
$$
\times\left[\widehat{A}\,\mathrm{e}^{-\frac{\beta}{N}\widehat{H}}\right]_{\mathrm{W}}\left(\frac{\boldsymbol{x}_{1}+\boldsymbol{x}_{2}}{2},\boldsymbol{p}_{1}\right)
$$
$$
\times\left[\mathrm{e}^{-\frac{\beta}{N}\widehat{H}}\right]_{\mathrm{W}}\left(\frac{\boldsymbol{x}_{2}+\boldsymbol{x}_{3}}{2},\boldsymbol{p}_{2}\right)
$$
$$
\cdots\left[\mathrm{e}^{-\frac{\beta}{N}\widehat{H}}\right]_{\mathrm{W}}\left(\frac{\boldsymbol{x}_{N-1}+\boldsymbol{x}_{N}}{2},\boldsymbol{p}_{N-1}\right)
$$
$$
\times\left[\mathrm{e}^{-\frac{\beta}{N}\widehat{H}}\,\widehat{B}(t)\right]_{\mathrm{W}}\left(\frac{\boldsymbol{x}_{N}+\boldsymbol{x}_{1}}{2},\boldsymbol{p}_{N}\right). \tag{3.32}
$$

In the limit where $N \to \infty$, or equivalently the high temperature limit, the Trotter product,[32]

$$
\lim_{N\to\infty}\mathrm{e}^{-\frac{\beta}{N}\widehat{H}} = \mathrm{e}^{-\frac{\beta}{2N}\widehat{V}}\,\mathrm{e}^{-\frac{\beta}{N}\widehat{T}}\,\mathrm{e}^{-\frac{\beta}{2N}\widehat{V}}, \tag{3.33}
$$

can be used, meaning that

$$
\lim_{N\to\infty}\left[\mathrm{e}^{-\frac{\beta}{N}\widehat{H}}\right]_{\mathrm{W}}(\boldsymbol{x},\boldsymbol{p}) = \lim_{N\to\infty}\left[\mathrm{e}^{-\frac{\beta}{2N}\widehat{V}}\,\mathrm{e}^{-\frac{\beta}{N}\widehat{T}}\,\mathrm{e}^{-\frac{\beta}{2N}\widehat{V}}\right]_{\mathrm{W}}(\boldsymbol{x},\boldsymbol{p})
$$
$$
= \lim_{N\to\infty}\left[\mathrm{e}^{-\frac{\beta}{2N}\widehat{V}}\right]_{\mathrm{W}}(\boldsymbol{x},\boldsymbol{p})\,\mathrm{e}^{-\frac{i\hbar}{2}\left(\overleftarrow{\frac{\partial}{\partial\boldsymbol{p}}}\bullet\overrightarrow{\frac{\partial}{\partial\boldsymbol{x}}}-\overleftarrow{\frac{\partial}{\partial\boldsymbol{x}}}\bullet\overrightarrow{\frac{\partial}{\partial\boldsymbol{p}}}\right)}
$$
$$
\times\left[\mathrm{e}^{-\frac{\beta}{N}\widehat{T}}\right]_{\mathrm{W}}(\boldsymbol{x},\boldsymbol{p})\,\mathrm{e}^{-\frac{i\hbar}{2}\left(\overleftarrow{\frac{\partial}{\partial\boldsymbol{p}}}\bullet\overrightarrow{\frac{\partial}{\partial\boldsymbol{x}}}-\overleftarrow{\frac{\partial}{\partial\boldsymbol{x}}}\bullet\overrightarrow{\frac{\partial}{\partial\boldsymbol{p}}}\right)}\left[\mathrm{e}^{-\frac{\beta}{2N}\widehat{V}}\right]_{\mathrm{W}}(\boldsymbol{x},\boldsymbol{p}),
$$
$$
\tag{3.34}
$$

where equation 2.4 has been used. These Wigner transforms are easy to evaluate, as long as the potential is restricted to only depend

on the position.

$$\left[e^{-\frac{\beta}{N}\widehat{T}} \right]_{\mathrm{W}} (\boldsymbol{x}, \boldsymbol{p})$$

$$= \int \mathrm{d}^D \boldsymbol{\lambda} \; e^{i\boldsymbol{x}\bullet\boldsymbol{\lambda}/\hbar} \left\langle \boldsymbol{p} + \frac{\boldsymbol{\lambda}}{2} \left| e^{-\frac{\beta}{N}\frac{1}{2}\left(m^{-1}\widehat{\boldsymbol{p}}\right)\bullet\widehat{\boldsymbol{p}}} \right| \boldsymbol{p} - \frac{\boldsymbol{\lambda}}{2} \right\rangle$$

$$= \int \mathrm{d}^D \boldsymbol{\lambda} \; e^{i\boldsymbol{x}\bullet\boldsymbol{\lambda}/\hbar} \; e^{-\frac{\beta}{N}\frac{1}{2}\left(m^{-1}\left(\boldsymbol{p}+\frac{\boldsymbol{\lambda}}{2}\right)\right)\bullet\left(\boldsymbol{p}+\frac{\boldsymbol{\lambda}}{2}\right)} \; \delta \left(\boldsymbol{\lambda} \right)$$

$$= e^{-\frac{\beta}{N}\frac{1}{2}\left(m^{-1}\boldsymbol{p}\right)\bullet\boldsymbol{p}} \tag{3.35}$$

$$\left[e^{-\frac{\beta}{2N}\widehat{V}} \right]_{\mathrm{W}} (\boldsymbol{x}, \boldsymbol{p})$$

$$= \int \mathrm{d}^D \boldsymbol{\eta} \; e^{-i\boldsymbol{\eta}\bullet\boldsymbol{p}/\hbar} \left\langle \boldsymbol{x} + \frac{\boldsymbol{\eta}}{2} \left| e^{-\frac{\beta}{2N}V(\boldsymbol{x})} \right| \boldsymbol{x} - \frac{\boldsymbol{\eta}}{2} \right\rangle$$

$$= \int \mathrm{d}^D \boldsymbol{\eta} \; e^{-i\boldsymbol{\eta}\bullet\boldsymbol{p}/\hbar} \; e^{-\frac{\beta}{2N}V\left(\boldsymbol{x}+\frac{\boldsymbol{\eta}}{2}\right)} \; \delta \left(\boldsymbol{\eta} \right)$$

$$= e^{-\frac{\beta}{2N}V(\boldsymbol{x})} \tag{3.36}$$

Putting these results into equation 3.34 and Taylor expanding gives

$$
\lim_{N\to\infty}\left[e^{-\frac{\beta}{N}\widehat{H}}\right]_{\mathrm{W}}(\boldsymbol{x},\boldsymbol{p})
$$

$$
=\lim_{N\to\infty}e^{-\frac{\beta}{2N}V(\boldsymbol{x})}\,e^{-\frac{i\hbar}{2}\left(\frac{\overleftarrow{\partial}}{\partial\boldsymbol{p}}\bullet\frac{\overrightarrow{\partial}}{\partial\boldsymbol{x}}-\frac{\overleftarrow{\partial}}{\partial\boldsymbol{x}}\bullet\frac{\overrightarrow{\partial}}{\partial\boldsymbol{p}}\right)}\,e^{-\frac{\beta}{N}\frac{1}{2}\left(\boldsymbol{m}^{-1}\boldsymbol{p}\right)\bullet\boldsymbol{p}}
$$

$$
\times\,e^{-\frac{i\hbar}{2}\left(\frac{\overleftarrow{\partial}}{\partial\boldsymbol{p}}\bullet\frac{\overrightarrow{\partial}}{\partial\boldsymbol{x}}-\frac{\overleftarrow{\partial}}{\partial\boldsymbol{x}}\bullet\frac{\overrightarrow{\partial}}{\partial\boldsymbol{p}}\right)}\,e^{-\frac{\beta}{2N}V(\boldsymbol{x})}
$$

$$
=\lim_{N\to\infty}e^{-\frac{\beta}{2N}V(\boldsymbol{x})}\,e^{-\frac{i\hbar}{2}\left(\frac{\overleftarrow{\partial}}{\partial\boldsymbol{p}}\bullet\frac{\overrightarrow{\partial}}{\partial\boldsymbol{x}}-\frac{\overleftarrow{\partial}}{\partial\boldsymbol{x}}\bullet\frac{\overrightarrow{\partial}}{\partial\boldsymbol{p}}\right)}
$$

$$
\times\left(e^{-\frac{\beta}{N}\frac{1}{2}\left(\boldsymbol{m}^{-1}\boldsymbol{p}\right)\bullet\boldsymbol{p}}\left(1+\mathcal{O}\left(\frac{\beta^{2}}{N^{2}}\right)\right)e^{-\frac{\beta}{2N}V(\boldsymbol{x})}\right)
$$

$$
=\lim_{N\to\infty}e^{-\frac{\beta}{2N}V(\boldsymbol{x})}\left(1+\mathcal{O}\left(\frac{\beta^{2}}{N^{2}}\right)\right)e^{-\frac{\beta}{N}\frac{1}{2}\left(\boldsymbol{m}^{-1}\boldsymbol{p}\right)\bullet\boldsymbol{p}}\,e^{-\frac{\beta}{2N}V(\boldsymbol{x})}
$$

$$
+\frac{i\hbar}{2}e^{-\frac{\beta}{2N}V(\boldsymbol{x})}\mathcal{O}\left(\frac{\beta^{2}}{N^{2}}\right)e^{-\frac{\beta}{N}\frac{1}{2}\left(\boldsymbol{m}^{-1}\boldsymbol{p}\right)\bullet\boldsymbol{p}}\,e^{-\frac{\beta}{2N}V(\boldsymbol{x})}
$$

$$
+\mathcal{O}\left(\frac{\beta^{2}}{N^{2}}e^{-\frac{\beta}{N}H(\boldsymbol{x},\boldsymbol{p})}\right)
$$

$$
=\lim_{N\to\infty}e^{-\frac{\beta}{N}H(\boldsymbol{x},\boldsymbol{p})}+\mathcal{O}\left(\frac{\beta^{2}}{N^{2}}e^{-\frac{\beta}{N}H(\boldsymbol{x},\boldsymbol{p})}\right)
$$

$$
=\lim_{N\to\infty}e^{-\frac{\beta}{N}H(\boldsymbol{x},\boldsymbol{p})}, \tag{3.37}
$$

where $H\left(\boldsymbol{x},\boldsymbol{p}\right)$ is the classical Hamiltonian. $\mathcal{O}\left(\beta^{2}/N^{2}\right)$ shows the order of the error, using the big O notation. Using this result, the operator $\widehat{\boldsymbol{A}}$ can be separated from the Boltzmann operator in its

Wigner transform,

$$
\lim_{N \to \infty} \left[\widehat{A}\, \mathrm{e}^{-\frac{\beta}{N}\widehat{H}} \right]_{\mathrm{W}} (\boldsymbol{x}, \boldsymbol{p})
$$

$$
= \lim_{N \to \infty} \left[\widehat{A} \right]_{\mathrm{W}} (\boldsymbol{x}, \boldsymbol{p})\, \mathrm{e}^{-\frac{i\hbar}{2}\left(\frac{\overleftarrow{\partial}}{\partial \boldsymbol{p}} \bullet \frac{\overrightarrow{\partial}}{\partial \boldsymbol{x}} - \frac{\overleftarrow{\partial}}{\partial \boldsymbol{x}} \bullet \frac{\overrightarrow{\partial}}{\partial \boldsymbol{p}} \right)} \left[\mathrm{e}^{-\frac{\beta}{N}\widehat{H}} \right]_{\mathrm{W}} (\boldsymbol{x}, \boldsymbol{p})
$$

$$
= \lim_{N \to \infty} \left[\widehat{A} \right]_{\mathrm{W}} (\boldsymbol{x}, \boldsymbol{p})\, \mathrm{e}^{-\frac{i\hbar}{2}\left(\frac{\overleftarrow{\partial}}{\partial \boldsymbol{p}} \bullet \frac{\overrightarrow{\partial}}{\partial \boldsymbol{x}} - \frac{\overleftarrow{\partial}}{\partial \boldsymbol{x}} \bullet \frac{\overrightarrow{\partial}}{\partial \boldsymbol{p}} \right)}\, \mathrm{e}^{-\frac{\beta}{N}H(\boldsymbol{x}, \boldsymbol{p})}
$$

$$
= \lim_{N \to \infty} \left[\widehat{A} \right]_{\mathrm{W}} (\boldsymbol{x}, \boldsymbol{p}) \left(1 + \mathcal{O}\left(\frac{\beta}{N} \right) \right) \mathrm{e}^{-\frac{\beta}{N}H(\boldsymbol{x}, \boldsymbol{p})}
$$

$$
= \lim_{N \to \infty} \left[\widehat{A} \right]_{\mathrm{W}} (\boldsymbol{x}, \boldsymbol{p})\, \mathrm{e}^{-\frac{\beta}{N}H(\boldsymbol{x}, \boldsymbol{p})} + \mathcal{O}\left(\frac{\beta}{N}\, \mathrm{e}^{-\frac{\beta}{N}H(\boldsymbol{x}, \boldsymbol{p})} \right)
$$

$$
= \lim_{N \to \infty} \left[\widehat{A} \right]_{\mathrm{W}} (\boldsymbol{x}, \boldsymbol{p})\, \mathrm{e}^{-\frac{\beta}{N}H(\boldsymbol{x}, \boldsymbol{p})} . \tag{3.38}
$$

The same thing can be done for $\widehat{\boldsymbol{B}}(t)$,

$$
\lim_{N \to \infty} \left[\mathrm{e}^{-\frac{\beta}{N}\widehat{H}}\, \widehat{\boldsymbol{B}}(t) \right]_{\mathrm{W}} (\boldsymbol{x}, \boldsymbol{p})
$$

$$
= \lim_{N \to \infty} \mathrm{e}^{-\frac{\beta}{N}H(\boldsymbol{x}, \boldsymbol{p})} \left[\widehat{\boldsymbol{B}}(t) \right]_{\mathrm{W}} (\boldsymbol{x}, \boldsymbol{p}) . \tag{3.39}
$$

Inserting the simplifications of the Wigner transforms, equations 3.37-3.39, into equation 3.32 gives

$$
\left\langle \widehat{A}\widehat{B}(t) \right\rangle = \lim_{N \to \infty} \frac{1}{Z} \left\{ \prod_{j=1}^{N} \iint \frac{\mathrm{d}^{D}\boldsymbol{x}_{j}\, \mathrm{d}^{D}\boldsymbol{p}_{j}}{(2\pi\hbar)^{D}}\, \mathrm{e}^{i\left(\boldsymbol{x}_{j} - \boldsymbol{x}_{(j \bmod N)+1} \right) \bullet \boldsymbol{p}_{j}/\hbar} \right\}
$$

$$
\times \left[\widehat{A} \right]_{\mathrm{W}} \left(\frac{\boldsymbol{x}_{1} + \boldsymbol{x}_{2}}{2}, \boldsymbol{p}_{1} \right) \mathrm{e}^{-\frac{\beta}{N}H\left(\frac{\boldsymbol{x}_{1}+\boldsymbol{x}_{2}}{2}, \boldsymbol{p}_{1} \right)}
$$

$$
\times \mathrm{e}^{-\frac{\beta}{N}H\left(\frac{\boldsymbol{x}_{2}+\boldsymbol{x}_{3}}{2}, \boldsymbol{p}_{2} \right)} \dots \mathrm{e}^{-\frac{\beta}{N}H\left(\frac{\boldsymbol{x}_{N-1}+\boldsymbol{x}_{N}}{2}, \boldsymbol{p}_{N-1} \right)}
$$

$$
\times \mathrm{e}^{-\frac{\beta}{N}H\left(\frac{\boldsymbol{x}_{N}+\boldsymbol{x}_{1}}{2}, \boldsymbol{p}_{N} \right)} \left[\widehat{\boldsymbol{B}}(t) \right]_{\mathrm{W}} \left(\frac{\boldsymbol{x}_{N} + \boldsymbol{x}_{1}}{2}, \boldsymbol{p}_{N} \right) . \tag{3.40}
$$

The potential energy has already been assumed to only depend on position, not momentum, so

$$
\left\langle \widehat{A}\widehat{B}\left(t\right)\right\rangle = \lim_{N\to\infty} \frac{1}{Z} \left\{ \prod_{j=1}^{N} \iint \frac{\mathrm{d}^D \boldsymbol{x}_j \, \mathrm{d}^D \boldsymbol{p}_j}{(2\pi\hbar)^D} \, \mathrm{e}^{i\left(\boldsymbol{x}_j - \boldsymbol{x}_{(j \bmod N)+1}\right)\bullet \boldsymbol{p}_j/\hbar} \right\}
$$

$$
\times \left[\widehat{A}\right]_{\mathrm{W}} \left(\frac{\boldsymbol{x}_1 + \boldsymbol{x}_2}{2}, \boldsymbol{p}_1\right) \mathrm{e}^{-\frac{\beta}{N}\left(\frac{1}{2}\left(m^{-1}\boldsymbol{p}_1\right)\bullet\boldsymbol{p}_1 + V\left(\frac{\boldsymbol{x}_1+\boldsymbol{x}_2}{2}\right)\right)}
$$

$$
\times \mathrm{e}^{-\frac{\beta}{N}\left(\frac{1}{2}\left(m^{-1}\boldsymbol{p}_2\right)\bullet\boldsymbol{p}_2 + V\left(\frac{\boldsymbol{x}_2+\boldsymbol{x}_3}{2}\right)\right)}
$$

$$
\ldots \mathrm{e}^{-\frac{\beta}{N}\left(\frac{1}{2}\left(m^{-1}\boldsymbol{p}_{N-1}\right)\bullet\boldsymbol{p}_{N-1} + V\left(\frac{\boldsymbol{x}_{N-1}+\boldsymbol{x}_N}{2}\right)\right)}
$$

$$
\times \mathrm{e}^{-\frac{\beta}{N}\left(\frac{1}{2}\left(m^{-1}\boldsymbol{p}_N\right)\bullet\boldsymbol{p}_N + V\left(\frac{\boldsymbol{x}_N+\boldsymbol{x}_1}{2}\right)\right)}
$$

$$
\times \left[\widehat{B}(t)\right]_{\mathrm{W}} \left(\frac{\boldsymbol{x}_N + \boldsymbol{x}_1}{2}, \boldsymbol{p}_N\right). \tag{3.41}
$$

By integrating over the momenta, as in section 2.2 we obtain

$$
\left\langle \widehat{A}\widehat{B}\left(t\right)\right\rangle = \lim_{N\to\infty} \frac{1}{Z} \left\{ \prod_{j=1}^{N} \int \frac{\mathrm{d}^D \boldsymbol{x}_j}{(2\pi\hbar)^D} \right\}
$$

$$
\times \left(\left(\frac{2\pi N}{\beta}\right)^{\frac{D}{2}} \sqrt{\det(\boldsymbol{m})} \right)^{N-2}
$$

$$
\times \iint \mathrm{d}^D \boldsymbol{p}_1 \, \mathrm{d}^D \boldsymbol{p}_N
$$

$$
\times \mathrm{e}^{-\frac{\beta}{N}\left(\frac{1}{2}\left(m^{-1}\boldsymbol{p}_1\right)\bullet\boldsymbol{p}_1 + V\left(\frac{\boldsymbol{x}_1+\boldsymbol{x}_2}{2}\right) - \frac{iN}{\beta\hbar}(\boldsymbol{x}_1-\boldsymbol{x}_2)\bullet\boldsymbol{p}_1\right)}
$$

$$
\times \mathrm{e}^{-\frac{\beta}{N}\left(\frac{1}{2}\left(m^{-1}\boldsymbol{p}_N\right)\bullet\boldsymbol{p}_N + V\left(\frac{\boldsymbol{x}_N+\boldsymbol{x}_1}{2}\right) - \frac{iN}{\beta\hbar}(\boldsymbol{x}_N-\boldsymbol{x}_1)\bullet\boldsymbol{p}_N\right)}
$$

$$
\times \left[\widehat{A}\right]_{\mathrm{W}} \left(\frac{\boldsymbol{x}_1 + \boldsymbol{x}_2}{2}, \boldsymbol{p}_1\right)
$$

$$
\times \mathrm{e}^{-\frac{\beta}{N}\sum_{j=2}^{N-1}\left(\frac{N^2}{2\beta^2\hbar^2}(m(\boldsymbol{x}_j-\boldsymbol{x}_{j+1}))\bullet(\boldsymbol{x}_j-\boldsymbol{x}_{j+1}) + V\left(\frac{\boldsymbol{x}_j+\boldsymbol{x}_{j+1}}{2}\right)\right)}
$$

$$
\times \left[\widehat{B}(t)\right]_{\mathrm{W}} \left(\frac{\boldsymbol{x}_N + \boldsymbol{x}_1}{2}, \boldsymbol{p}_N\right). \tag{3.42}
$$

Here $\boldsymbol{p}_1$ and $\boldsymbol{p}_N$ have not been integrated out since they occur in $\left[\widehat{A}\right]_{\mathrm{W}}\left(\frac{\boldsymbol{x}_1+\boldsymbol{x}_2}{2},\boldsymbol{p}_1\right)$ and $\left[\widehat{B}(t)\right]_{\mathrm{W}}\left(\frac{\boldsymbol{x}_N+\boldsymbol{x}_1}{2},\boldsymbol{p}_N\right)$, which are unknown functions. For the method derived here to work, we must restrict $\widehat{A}$ to

operators whose Wigner transforms are such functions of $\boldsymbol{p}_1$ that the integral

$$\int \mathrm{d}^D \boldsymbol{p}_1 \; \mathrm{e}^{-\frac{\beta}{N}\left(\frac{1}{2}\left(\boldsymbol{m}^{-1}\boldsymbol{p}_1\right)\bullet\boldsymbol{p}_1 - \frac{iN}{\beta\hbar}(\boldsymbol{x}_1 - \boldsymbol{x}_2)\bullet\boldsymbol{p}_1\right)} \left[\widehat{\boldsymbol{A}}\right]_{\mathrm{W}} \left(\frac{\boldsymbol{x}_1 + \boldsymbol{x}_2}{2}, \boldsymbol{p}_1\right)$$

$$(3.43)$$

is analytically solvable, giving yet another spring term. This is not such a severe restriction since at least all $\left[\widehat{\boldsymbol{A}}\right]_{\mathrm{W}}\left(\frac{\boldsymbol{x}_1+\boldsymbol{x}_2}{2},\boldsymbol{p}_1\right)$ that are polynomials with regard to $\boldsymbol{p}_1$ work fine. To simplify later expressions, a new function is defined:

$$\boldsymbol{A}'\left(\frac{\boldsymbol{x}_1 + \boldsymbol{x}_2}{2}, \boldsymbol{x}_1 - \boldsymbol{x}_2\right)$$

$$= \frac{\int \mathrm{d}^D \boldsymbol{p}_1 \; \mathrm{e}^{-\frac{\beta}{N}\left(\frac{1}{2}\left(\boldsymbol{m}^{-1}\boldsymbol{p}_1\right)\bullet\boldsymbol{p}_1 - \frac{iN}{\beta\hbar}(\boldsymbol{x}_1 - \boldsymbol{x}_2)\bullet\boldsymbol{p}_1\right)} \left[\widehat{\boldsymbol{A}}\right]_{\mathrm{W}} \left(\frac{\boldsymbol{x}_1 + \boldsymbol{x}_2}{2}, \boldsymbol{p}_1\right)}{\int \mathrm{d}^D \boldsymbol{p}_1 \; \mathrm{e}^{-\frac{\beta}{N}\left(\frac{1}{2}\left(\boldsymbol{m}^{-1}\boldsymbol{p}_1\right)\bullet\boldsymbol{p}_1 - \frac{iN}{\beta\hbar}(\boldsymbol{x}_1 - \boldsymbol{x}_2)\bullet\boldsymbol{p}_1\right)}}$$

$$(3.44)$$

Proving that equation 3.44 can be solved for all polynomials in $\boldsymbol{p}_1$ can be done by first calculating $\boldsymbol{A}'$ for a Wigner transform $\left[\widehat{\boldsymbol{A}}\right]_{\mathrm{W}}\left(\frac{\boldsymbol{x}_1+\boldsymbol{x}_2}{2},\boldsymbol{p}_1\right) = f\left(\frac{\boldsymbol{x}_1+\boldsymbol{x}_2}{2}\right)\sum_{j''=1}^{D} p_{j'',1}^n$, where $f\left(\frac{\boldsymbol{x}_1+\boldsymbol{x}_2}{2}\right)$ is any func-

tion or constant and n is a positive integer.

$$
\boldsymbol{A}'_{\boldsymbol{p}_1,n}\left(\frac{\boldsymbol{x}_1+\boldsymbol{x}_2}{2}, \boldsymbol{x}_1-\boldsymbol{x}_2\right)
$$

$$
= \frac{\int \mathrm{d}^D\boldsymbol{p}_1\ \mathrm{e}^{-\frac{\beta}{N}\left(\frac{1}{2}\left(\boldsymbol{m}^{-1}\boldsymbol{p}_1\right)\bullet\boldsymbol{p}_1 - \frac{iN}{\beta\hbar}(\boldsymbol{x}_1-\boldsymbol{x}_2)\bullet\boldsymbol{p}_1\right)}\ f\left(\frac{\boldsymbol{x}_1+\boldsymbol{x}_2}{2}\right)\sum_{j''=1}^D p_{j'',1}^n}{\int \mathrm{d}^D\boldsymbol{p}_1\ \mathrm{e}^{-\frac{\beta}{N}\left(\frac{1}{2}(\boldsymbol{m}^{-1}\boldsymbol{p}_1)\bullet\boldsymbol{p}_1 - \frac{iN}{\beta\hbar}(\boldsymbol{x}_1-\boldsymbol{x}_2)\bullet\boldsymbol{p}_1\right)}}
$$

$$
= \frac{f\left(\frac{\boldsymbol{x}_1+\boldsymbol{x}_2}{2}\right)}{\left(\frac{2\pi N}{\beta}\right)^{\frac{D}{2}}\sqrt{\det(\boldsymbol{m})}\ \mathrm{e}^{-\frac{\beta}{N}\frac{N^2}{2\beta^2\hbar^2}(\boldsymbol{m}(\boldsymbol{x}_1-\boldsymbol{x}_2))\bullet(\boldsymbol{x}_1-\boldsymbol{x}_2)}}
$$

$$
\times \left(-\frac{\hbar}{i}\right)^n\left\{\sum_{j''=1}^D \frac{\mathrm{d}^n}{\mathrm{d}(x_{j'',1}-x_{j'',2})^n}\right\}
$$

$$
\times \int \mathrm{d}^D\boldsymbol{p}_1\ \mathrm{e}^{-\frac{\beta}{N}\left(\frac{1}{2}\left(\boldsymbol{m}^{-1}\boldsymbol{p}_1\right)\bullet\boldsymbol{p}_1 - \frac{iN}{\beta\hbar}(\boldsymbol{x}_1-\boldsymbol{x}_2)\bullet\boldsymbol{p}_1\right)}
$$

$$
= \frac{f\left(\frac{\boldsymbol{x}_1+\boldsymbol{x}_2}{2}\right)}{\left(\frac{2\pi N}{\beta}\right)^{\frac{D}{2}}\sqrt{\det(\boldsymbol{m})}\ \mathrm{e}^{-\frac{\beta}{N}\frac{N^2}{2\beta^2\hbar^2}(\boldsymbol{m}(\boldsymbol{x}_1-\boldsymbol{x}_2))\bullet(\boldsymbol{x}_1-\boldsymbol{x}_2)}}
$$

$$
\times (i\hbar)^n\left\{\sum_{j''=1}^D \frac{\mathrm{d}^n}{\mathrm{d}(x_{j'',1}-x_{j'',2})^n}\right\}
$$

$$
\times \left(\frac{2\pi N}{\beta}\right)^{\frac{D}{2}}\sqrt{\det(\boldsymbol{m})}\ \mathrm{e}^{-\frac{\beta}{N}\frac{N^2}{2\beta^2\hbar^2}(\boldsymbol{m}(\boldsymbol{x}_1-\boldsymbol{x}_2))\bullet(\boldsymbol{x}_1-\boldsymbol{x}_2)}
$$

$$
= \frac{f\left(\frac{\boldsymbol{x}_1+\boldsymbol{x}_2}{2}\right)(i\hbar)^n}{\mathrm{e}^{-\frac{\beta}{N}\frac{N^2}{2\beta^2\hbar^2}(\boldsymbol{m}(\boldsymbol{x}_1-\boldsymbol{x}_2))\bullet(\boldsymbol{x}_1-\boldsymbol{x}_2)}}
$$

$$
\times \left\{\sum_{j''=1}^D \frac{\mathrm{d}^n}{\mathrm{d}(x_{j'',1}-x_{j'',2})^n}\right\}\mathrm{e}^{-\frac{\beta}{N}\frac{N^2}{2\beta^2\hbar^2}(\boldsymbol{m}(\boldsymbol{x}_1-\boldsymbol{x}_2))\bullet(\boldsymbol{x}_1-\boldsymbol{x}_2)}
$$

(3.45)

Here the variable $\zeta_{j''} = \sqrt{\dfrac{m_{j''}N}{2\beta}}\dfrac{1}{\hbar}\left(x_{j'',1}-x_{j'',2}\right)$ can be introduced,

giving

$$
\boldsymbol{A'}_{\boldsymbol{p}_1, n} \left(\frac{\boldsymbol{x}_1 + \boldsymbol{x}_2}{2}, \boldsymbol{x}_1 - \boldsymbol{x}_2 \right)
$$

$$
= \frac{f \left(\frac{\boldsymbol{x}_1 + \boldsymbol{x}_2}{2} \right) (i\hbar)^n}{e^{- \sum_{j''=1}^{D} \zeta_{j''}^2}}
$$

$$
\times \left\{ \sum_{j''=1}^{D} \left(\frac{m_{j''} N}{2\beta} \right)^{\frac{n}{2}} \frac{1}{\hbar^n} \frac{\mathrm{d}^n}{\mathrm{d}\zeta_{j''}^n} \right\} e^{- \sum_{j''=1}^{D} \zeta_{j''}^2}
$$

$$
= \frac{f \left(\frac{\boldsymbol{x}_1 + \boldsymbol{x}_2}{2} \right) i^n}{e^{- \sum_{j''=1}^{D} \zeta_{j''}^2}}
$$

$$
\times \left(\sum_{j''=1}^{D} \left(\frac{m_{j''} N}{2\beta} \right)^{\frac{n}{2}} (-1)^n \mathsf{H}_n \left(\zeta_{j''} \right) \right) e^{- \sum_{j''=1}^{D} \zeta_{j''}^2}
$$

$$
= f \left(\frac{\boldsymbol{x}_1 + \boldsymbol{x}_2}{2} \right) (-i)^n
$$

$$
\times \sum_{j''=1}^{D} \left(\frac{m_{j''} N}{2\beta} \right)^{\frac{n}{2}} \mathsf{H}_n \left(\sqrt{\frac{m_{j''} N}{2\beta}} \frac{(x_{j'', 1} - x_{j'', 2})}{\hbar} \right) \tag{3.46}
$$

where H_n is the nth order Hermite polynomial. This result can easily be extended to n^{th} order polynomials in $\boldsymbol{p}_1$, $\left[\widehat{\boldsymbol{A}} \right]_{\mathrm{W}} \left(\frac{\boldsymbol{x}_1 + \boldsymbol{x}_2}{2}, \boldsymbol{p}_1 \right) = \sum_{j'=0}^{n} f_{j'} \left(\frac{\boldsymbol{x}_1 + \boldsymbol{x}_2}{2} \right) \sum_{j''=1}^{D} p_{j'', 1}^n$, as a sum,

$$
\boldsymbol{A'}_{\text{polynomial}} \left(\frac{\boldsymbol{x}_1 + \boldsymbol{x}_2}{2}, \boldsymbol{x}_1 - \boldsymbol{x}_2 \right)
$$

$$
= \sum_{j'=0}^{n} f_{j'} \left(\frac{\boldsymbol{x}_1 + \boldsymbol{x}_2}{2} \right) (-i)^{j'}
$$

$$
\times \sum_{j''=1}^{D} \left(\frac{m_{j''} N}{2\beta} \right)^{\frac{j'}{2}} \mathsf{H}_{j'} \left(\sqrt{\frac{m_{j''} N}{2\beta}} \frac{(x_{j'', 1} - x_{j'', 2})}{\hbar} \right). \tag{3.47}
$$

Using the the definition of $\boldsymbol{A'}$ in equation 3.44 equation 3.40 can

be written as

$$\left\langle \widehat{\boldsymbol{A}}\widehat{\boldsymbol{B}}\left(t\right)\right\rangle = \lim_{N\to\infty}\frac{1}{Z}\left\{\prod_{j=1}^{N}\int\frac{\mathrm{d}^{D}\boldsymbol{x}_{j}}{\left(2\pi\hbar\right)^{D}}\right\}$$

$$\times\left(\left(\frac{2\pi N}{\beta}\right)^{\frac{D}{2}}\sqrt{\det\left(\boldsymbol{m}\right)}\right)^{N-1}\int\mathrm{d}^{D}\boldsymbol{p}_{N}$$

$$\times\,\mathrm{e}^{-\frac{\beta}{N}\left(\frac{1}{2}\left(\boldsymbol{m}^{-1}\boldsymbol{p}_{N}\right)\bullet\boldsymbol{p}_{N}+V\left(\frac{\boldsymbol{x}_{N}+\boldsymbol{x}_{1}}{2}\right)-\frac{iN}{\beta\hbar}\left(\boldsymbol{x}_{N}-\boldsymbol{x}_{1}\right)\bullet\boldsymbol{p}_{N}\right)}$$

$$\times\,\boldsymbol{A}'\left(\frac{\boldsymbol{x}_{1}+\boldsymbol{x}_{2}}{2},\boldsymbol{x}_{1}-\boldsymbol{x}_{2}\right)$$

$$\times\,\mathrm{e}^{-\frac{\beta}{N}\sum_{j=1}^{N-1}\left(\frac{N^{2}}{2\beta^{2}\hbar^{2}}\left(\boldsymbol{m}\left(\boldsymbol{x}_{j}-\boldsymbol{x}_{j+1}\right)\right)\bullet\left(\boldsymbol{x}_{j}-\boldsymbol{x}_{j+1}\right)+V\left(\frac{\boldsymbol{x}_{j}+\boldsymbol{x}_{j+1}}{2}\right)\right)}$$

$$\times\,\left[\widehat{\boldsymbol{B}}(t)\right]_{\mathrm{W}}\left(\frac{\boldsymbol{x}_{N}+\boldsymbol{x}_{1}}{2},\boldsymbol{p}_{N}\right). \tag{3.48}$$

$\left[\widehat{\boldsymbol{B}}(t)\right]_{\mathrm{W}}\left(\frac{\boldsymbol{x}_{N}+\boldsymbol{x}_{1}}{2},\boldsymbol{p}_{N}\right)$ is most often much more tricky to calculate compared to $\left[\widehat{\boldsymbol{A}}\right]_{\mathrm{W}}\left(\frac{\boldsymbol{x}_{1}+\boldsymbol{x}_{2}}{2},\boldsymbol{p}_{1}\right)$, since it includes propagation in time. For a general potential there will not be an analytic integral over $\boldsymbol{p}_{N}$. $\left[\widehat{\boldsymbol{B}}(t)\right]_{\mathrm{W}}\left(\frac{\boldsymbol{x}_{N}+\boldsymbol{x}_{1}}{2},\boldsymbol{p}_{N}\right)$ will thus be kept as it is.

Some reordering of equation 3.48 can be done, to make it a bit more readable,

$$\left\langle \widehat{\boldsymbol{A}}\widehat{\boldsymbol{B}}\left(t\right)\right\rangle = \lim_{N\to\infty}\frac{1}{Z}\left(\frac{N}{2\pi\beta}\right)^{\frac{(N-1)D}{2}}\left(\det\left(\boldsymbol{m}\right)\right)^{\frac{N-1}{2}}\hbar^{-ND}\left(2\pi\right)^{-D}$$

$$\times\left\{\prod_{j=1}^{N}\int\mathrm{d}^{D}\boldsymbol{x}_{j}\right\}\int\mathrm{d}^{D}\boldsymbol{p}_{N}\,\mathrm{e}^{\frac{i}{\hbar}\left(\boldsymbol{x}_{N}-\boldsymbol{x}_{1}\right)\bullet\boldsymbol{p}_{N}}$$

$$\times\,\mathrm{e}^{-\frac{\beta}{N}\left(\frac{1}{2}\left(\boldsymbol{m}^{-1}\boldsymbol{p}_{N}\right)\bullet\boldsymbol{p}_{N}+\sum_{j=1}^{N}\left(V\left(\frac{\boldsymbol{x}_{j}+\boldsymbol{x}_{(j\bmod N)+1}}{2}\right)\right)\right)}$$

$$\times\,\mathrm{e}^{-\frac{\beta}{N}\sum_{j=1}^{N-1}\left(\frac{N^{2}}{2\beta^{2}\hbar^{2}}\left(\boldsymbol{m}\left(\boldsymbol{x}_{j}-\boldsymbol{x}_{j+1}\right)\right)\bullet\left(\boldsymbol{x}_{j}-\boldsymbol{x}_{j+1}\right)\right)}$$

$$\times\,\boldsymbol{A}'\left(\frac{\boldsymbol{x}_{1}+\boldsymbol{x}_{2}}{2},\boldsymbol{x}_{1}-\boldsymbol{x}_{2}\right)$$

$$\times\,\left[\widehat{\boldsymbol{B}}(t)\right]_{\mathrm{W}}\left(\frac{\boldsymbol{x}_{N}+\boldsymbol{x}_{1}}{2},\boldsymbol{p}_{N}\right). \tag{3.49}$$
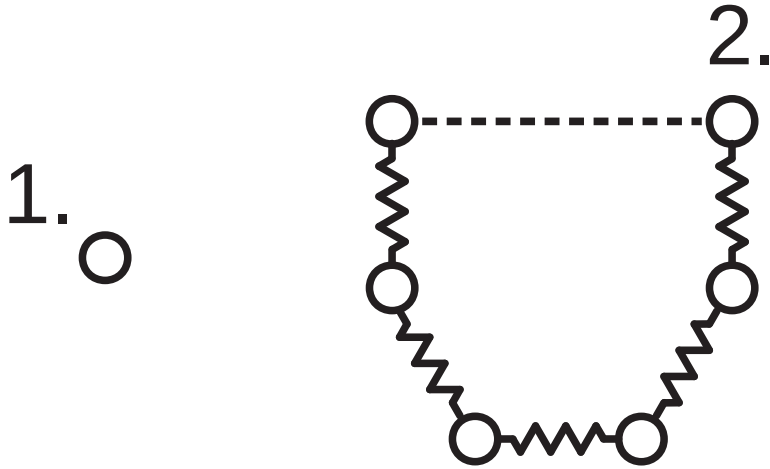
Figure 3.14: Illustration of a classical particle (1.) and its corresponding imaginary time path integral open polymer (2.). The zigzag lines represent the spring terms. The dashed line represent the opening in the polymer, which has a corresponding complex phase factor.

This is an exact expression for a quantum time correlation function. It is written as a discretized imaginary time path integral, as in section 2.2, but the usual ring polymer is instead an open polymer, as the last spring term is missing. Instead of a spring term, the opening in the polymer has a complex phase factor $e^{\frac{i}{\hbar}(\boldsymbol{x}_N - \boldsymbol{x}_1) \bullet \boldsymbol{p}_N}$. In figure 3.14 the open polymer is illustrated in comparison to a classical particle. This figure can be compared with the ring polymer in figure 2.1. Another, minor, difference compared to the imaginary time path integral in section 2.2 is that there the potential energy is evaluated at the beads, $V(\boldsymbol{x}_j)$, while here it is evaluated at the midpoint between two beads, $V\left(\frac{\boldsymbol{x}_j + \boldsymbol{x}_{(j \bmod N)+1}}{2}\right)$. This difference does not matter when $N \to \infty$, and it is caused by the different handling of the Boltzmann operators in this section compared to section 2.2.

To make equation 3.49 useful in actual computations two approxi-

mations are made. The first one is to approximate $\left[\widehat{\boldsymbol{B}}(t)\right]_{\mathrm{W}}\left(\dfrac{\boldsymbol{x}_N + \boldsymbol{x}_1}{2}, \boldsymbol{p}_N\right)$ with the classical Wigner model,

$$
\begin{aligned}
&\left[\widehat{\boldsymbol{B}}(t)\right]_{\mathrm{W}}\left(\frac{\boldsymbol{x}_N + \boldsymbol{x}_1}{2}, \boldsymbol{p}_N\right) \\
&\approx \left[\widehat{\boldsymbol{B}}\right]_{\mathrm{W}}\left(\boldsymbol{x}\left(\frac{\boldsymbol{x}_N + \boldsymbol{x}_1}{2}, \boldsymbol{p}_N, t\right), \boldsymbol{p}\left(\frac{\boldsymbol{x}_N + \boldsymbol{x}_1}{2}, \boldsymbol{p}_N, t\right)\right).
\end{aligned}
\tag{3.50}
$$

The second approximation is to restrict N to finite numbers. These two approximations lead to

$$
\begin{aligned}
\left\langle \widehat{\boldsymbol{A}}\widehat{\boldsymbol{B}}(t)\right\rangle &\approx \left\langle \widehat{\boldsymbol{A}}\widehat{\boldsymbol{B}}(t)\right\rangle_{OPCW, y} \\
&= \frac{1}{Z}\left(\frac{N}{2\pi\beta}\right)^{\frac{(N-1)D}{2}} \left(\det\left(\boldsymbol{m}\right)\right)^{\frac{N-1}{2}} \hbar^{-ND}(2\pi)^{-D} \\
&\quad \times \left\{\prod_{j=1}^{N}\int \mathrm{d}^D\boldsymbol{x}_j\right\}\int \mathrm{d}^D\boldsymbol{p}_N \; \mathrm{e}^{\frac{i}{\hbar}(\boldsymbol{x}_N - \boldsymbol{x}_1)\bullet\boldsymbol{p}_N} \\
&\quad \times \mathrm{e}^{-\frac{\beta}{N}\left(\frac{1}{2}\left(\boldsymbol{m}^{-1}\boldsymbol{p}_N\right)\bullet\boldsymbol{p}_N + \sum_{j=1}^{N}\left(V\left(\frac{\boldsymbol{x}_j + \boldsymbol{x}_{(j \bmod N)+1}}{2}\right)\right)\right)} \\
&\quad \times \mathrm{e}^{-\frac{\beta}{N}\sum_{j=1}^{N-1}\left(\frac{N^2}{2\beta^2\hbar^2}(\boldsymbol{m}(\boldsymbol{x}_j - \boldsymbol{x}_{j+1}))\bullet(\boldsymbol{x}_j - \boldsymbol{x}_{j+1})\right)} \\
&\quad \times \boldsymbol{A}'\left(\frac{\boldsymbol{x}_1 + \boldsymbol{x}_2}{2}, \boldsymbol{x}_1 - \boldsymbol{x}_2\right) \\
&\quad \times \left[\widehat{\boldsymbol{B}}\right]_{\mathrm{W}}\left(\boldsymbol{x}\left(\frac{\boldsymbol{x}_N + \boldsymbol{x}_1}{2}, \boldsymbol{p}_N, t\right), \boldsymbol{p}\left(\frac{\boldsymbol{x}_N + \boldsymbol{x}_1}{2}, \boldsymbol{p}_N, t\right)\right),
\end{aligned}
\tag{3.51}
$$

where $\boldsymbol{x}\left(\frac{\boldsymbol{x}_N + \boldsymbol{x}_1}{2}, \boldsymbol{p}_N, t\right)$ and $\boldsymbol{p}\left(\frac{\boldsymbol{x}_N + \boldsymbol{x}_1}{2}, \boldsymbol{p}_N, t\right)$ are the positions and momenta of a classical trajectory starting with $\frac{\boldsymbol{x}_N + \boldsymbol{x}_1}{2}$ and $\boldsymbol{p}_N$. This is the open polymer classical Wigner (OPCW) method published in paper III.[97] When $N \to \infty$ the initial distribution converges toward exact quantum mechanics, and the correlation function converges toward the exact classical Wigner method.

In papers III and IV the methods used to numerically evaluate equation 3.51 are Metropolis Monte Carlo[98] for the integrals and

molecular dynamics, using the velocity Verlet algorithm,[99,100] for the time evolution.

As is indicated with the subscript y, the $\left\langle \widehat{\boldsymbol{A}}\widehat{\boldsymbol{B}}\left(t\right)\right\rangle_{OPCW,y}$ in equation 3.51 is only one version of the OPCW method. Another, slightly different, version was also published in the same paper. This other version arises from the fact that if all dependence on $\widehat{\boldsymbol{x}}$ in $\widehat{\boldsymbol{A}}$ is to the left of all dependence on $\widehat{\boldsymbol{p}}$, then the $\widehat{\boldsymbol{x}}$-parts of $\widehat{\boldsymbol{A}}$ can operate on $\langle\boldsymbol{x}_1|$ in equation 3.31 and avoid being enclosed in the Wigner transform in equation 3.32. After that step the derivation would move on exactly as before, but $\boldsymbol{A}'$ would of course not depend on $\frac{\boldsymbol{x}_1+\boldsymbol{x}_2}{2}$ anymore. An $\boldsymbol{A}'_x\left(\boldsymbol{x}_1,\boldsymbol{x}_1-\boldsymbol{x}_2\right)$ can be defined to be the product of the function of $\boldsymbol{x}_1$ and the $\boldsymbol{A}'\left(\boldsymbol{x}_1-\boldsymbol{x}_2\right)$ resulting from the $\widehat{\boldsymbol{p}}$-dependent parts of $\widehat{\boldsymbol{A}}$. Then, this version of OPCW can be written as

$$
\left\langle \widehat{\boldsymbol{A}}\widehat{\boldsymbol{B}}\left(t\right)\right\rangle \approx \left\langle \widehat{\boldsymbol{A}}\widehat{\boldsymbol{B}}\left(t\right)\right\rangle_{OPCW,x}
$$

$$
= \frac{1}{Z}\left(\frac{N}{2\pi\beta}\right)^{\frac{(N-1)D}{2}}\left(\det\left(\boldsymbol{m}\right)\right)^{\frac{N-1}{2}}\hbar^{-ND}(2\pi)^{-D}
$$

$$
\times\left\{\prod_{j=1}^{N}\int \mathrm{d}^D\boldsymbol{x}_j\right\}\int \mathrm{d}^D\boldsymbol{p}_N\ \mathrm{e}^{\frac{i}{\hbar}(\boldsymbol{x}_N-\boldsymbol{x}_1)\bullet\boldsymbol{p}_N}
$$

$$
\times \mathrm{e}^{-\frac{\beta}{N}\left(\frac{1}{2}\left(\boldsymbol{m}^{-1}\boldsymbol{p}_N\right)\bullet\boldsymbol{p}_N+\sum_{j=1}^{N}\left(V\left(\frac{\boldsymbol{x}_j+\boldsymbol{x}_{(j\ \mathrm{mod}\ N)+1}}{2}\right)\right)\right)}
$$

$$
\times \mathrm{e}^{-\frac{\beta}{N}\sum_{j=1}^{N-1}\left(\frac{N^2}{2\beta^2\hbar^2}(\boldsymbol{m}(\boldsymbol{x}_j-\boldsymbol{x}_{j+1}))\bullet(\boldsymbol{x}_j-\boldsymbol{x}_{j+1})\right)}
$$

$$
\times \boldsymbol{A}'_x\left(\boldsymbol{x}_1,\boldsymbol{x}_1-\boldsymbol{x}_2\right)
$$

$$
\times\left[\widehat{\boldsymbol{B}}\right]_{\mathrm{W}}\left(\boldsymbol{x}\left(\frac{\boldsymbol{x}_N+\boldsymbol{x}_1}{2},\boldsymbol{p}_N,t\right),\boldsymbol{p}\left(\frac{\boldsymbol{x}_N+\boldsymbol{x}_1}{2},\boldsymbol{p}_N,t\right)\right),
$$
$$(3.52)$$

where it can now be understood that the subscript x in $\left\langle \widehat{\boldsymbol{A}}\widehat{\boldsymbol{B}}\left(t\right)\right\rangle_{OPCW,x}$ denotes that the function corresponding to operator $\widehat{\boldsymbol{A}}$ is evaluated at $\boldsymbol{x}_1$. The y in $\left\langle \widehat{\boldsymbol{A}}\widehat{\boldsymbol{B}}\left(t\right)\right\rangle_{OPCW,y}$ denotes that the function corresponding to operator $\widehat{\boldsymbol{A}}$ is evaluated at $\boldsymbol{y}_1$, which is the symbol used for $\frac{\boldsymbol{x}_1+\boldsymbol{x}_2}{2}$ in paper III.

For some simple cases it is easy to see what $\boldsymbol{A}'_x (\boldsymbol{x}_1, \boldsymbol{x}_1 - \boldsymbol{x}_2)$ will be.

- If $\widehat{\boldsymbol{A}}$ only depends on $\widehat{\boldsymbol{p}}$ and not on $\widehat{\boldsymbol{x}}$, then $\boldsymbol{A}'_x (\boldsymbol{x}_1, \boldsymbol{x}_1 - \boldsymbol{x}_2) = \boldsymbol{A}' (\frac{\boldsymbol{x}_1 + \boldsymbol{x}_2}{2}, \boldsymbol{x}_1 - \boldsymbol{x}_2)$.

- If $\widehat{\boldsymbol{A}}$ is only a function of $\widehat{\boldsymbol{x}}$, $\widehat{\boldsymbol{A}} = f(\widehat{\boldsymbol{x}})$, then $\boldsymbol{A}'_x (\boldsymbol{x}_1, \boldsymbol{x}_1 - \boldsymbol{x}_2) = f(\boldsymbol{x}_1)$ and $\boldsymbol{A}' (\frac{\boldsymbol{x}_1 + \boldsymbol{x}_2}{2}, \boldsymbol{x}_1 - \boldsymbol{x}_2) = f(\frac{\boldsymbol{x}_1 + \boldsymbol{x}_2}{2})$.

- If $\widehat{\boldsymbol{A}}$ is the product of a function of $\widehat{\boldsymbol{x}}$, $f(\widehat{\boldsymbol{x}})$, and a function of $\widehat{\boldsymbol{p}}$, $g(\widehat{\boldsymbol{p}})$, such that $\widehat{\boldsymbol{A}} = f(\widehat{\boldsymbol{x}}) g(\widehat{\boldsymbol{p}})$ and $\boldsymbol{A}'_g$ is the $\boldsymbol{A}'$ when $\widehat{\boldsymbol{A}} = g(\widehat{\boldsymbol{p}})$, then $\boldsymbol{A}'_x (\boldsymbol{x}_1, \boldsymbol{x}_1 - \boldsymbol{x}_2) = f(\boldsymbol{x}_1) \boldsymbol{A}'_g (\frac{\boldsymbol{x}_1 + \boldsymbol{x}_2}{2}, \boldsymbol{x}_1 - \boldsymbol{x}_2)$ and $\boldsymbol{A}' (\frac{\boldsymbol{x}_1 + \boldsymbol{x}_2}{2}, \boldsymbol{x}_1 - \boldsymbol{x}_2) = f(\frac{\boldsymbol{x}_1 + \boldsymbol{x}_2}{2}) \boldsymbol{A}'_g (\frac{\boldsymbol{x}_1 + \boldsymbol{x}_2}{2}, \boldsymbol{x}_1 - \boldsymbol{x}_2)$.

If $\widehat{\boldsymbol{A}}$ has $\widehat{\boldsymbol{p}}$-dependence to the left of an $\widehat{\boldsymbol{x}}$-dependence, then a rearrangement of the expression for $\widehat{\boldsymbol{A}}$ may possible, such as for

$$\widehat{p}\widehat{x} = \widehat{x}\widehat{p} + [\widehat{p}, \widehat{x}] = \widehat{x}\widehat{p} + [\widehat{p}, \widehat{x}] = \widehat{x}\widehat{p} - i\hbar. \tag{3.53}$$

These kind of operators will lead to a more complicated derivation of $\left\langle \widehat{\boldsymbol{A}}\widehat{\boldsymbol{B}}(t) \right\rangle_{OPCW,x}$ and a general formula for them will not be given here. In paper IV the flux-Heaviside trace, equation 2.61, from section 2.3 is handled, and the flux operator, equation 2.63, needs the kind of treatment illustrated. The interested reader is directed to the paper for an example of how a complicated $\widehat{\boldsymbol{A}}$ can be handled.

In the limit $N \to \infty$ the y-version and the x-version of OPCW will be equivalent, but in practical numerical calculations they can behave differently. The OPCW method is interesting for running the classical Wigner method, because the main difficulty of any classical Wigner method is to obtain the initial quantum distribution. Sampling a discretized imaginary path integral should be relatively cheap, computationally, but the complex phase factor makes the integrand oscillatory, which makes the sampling more demanding. For multidimensional systems the complex phase factor becomes even worse, since each degree of freedom contributes to it. In paper III it was suggested to describe only the most important, or most quantum mechanical, degrees of freedom with the open polymer. For the less important, or less quantum mechanical, degrees of freedom

the polymer would be collapsed into a single classical particle, but keeping the couplings to all beads in degrees of freedom that still have a quantum description. This could reduce the computational cost significantly, but at the cost of correlation functions not converging toward exact classical Wigner as the number of beads is increased.

Here, the OPCW method is only derived for the standard correlation function. In appendix B of paper III a version of the OPCW method for Kubo transformed correlation functions is presented. Paper IV contains derivations for symmetrized correlation functions, specifically the flux-Heaviside trace, equation 2.61.

It should be noted that the OPCW method is related to an expression published, but not further explored, by Bose and Makri.[101][‡] OPCW is also related to a version of a method published by Bonella et al.[102][§].

Results and discussion

In paper III OPCW was tested on the same two one-dimensional potentials as was used in paper II, see section 3.2, i.e. a quartic potential, $V(x) = \frac{m^2\omega^3}{4\hbar}x^4$, and a double well potential, $V(x) = \frac{m^2\omega^3}{10\hbar}x^4 - \frac{m\omega^2}{2}x^2$. Additionally, OPCW was tested on the same quartic potential, but bilinearly coupled to a bath of harmonic oscillators.[48,104] These tests were done with position, position-squared, momentum, and momentum-squared autocorrelation functions.

In paper IV OPCW was tested for a parabolic barrier, $V(x) = -\frac{m\omega^2}{2}x^2$, and an Eckart potential, $V(x) = \frac{6\hbar\omega}{\pi} \operatorname{sech}^2\left(\sqrt{\frac{\pi m\omega}{12\hbar}}x\right)$. These tests where done with the symmetrized flux-Heaviside trace, equation 2.61, and resulted in rate constants and tunneling factors for the Eckart potential.

Some illustrative results from both papers III and IV are reproduced here to illustrate the conclusions from the papers.

Common methods for approximating the initial distribution for the classical Wigner model use a harmonic approximation.[22,23,105] For comparison a representative from this group of methods is used

---

[‡]Equation 2.7 in reference 101.

[§]The $L = 1$ version of the method published in reference 102. The relation is more clear in a later paper by Bonella and Ciccotti, reference 103.
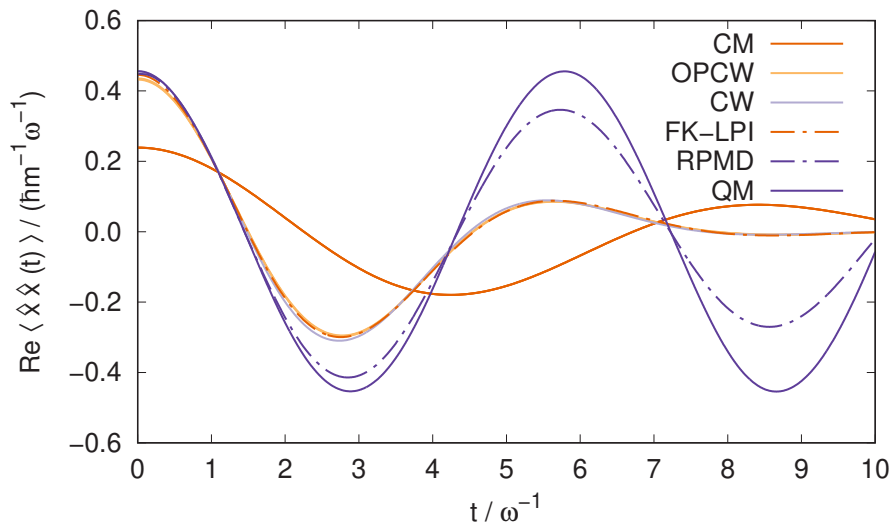
Figure 3.15: The real part of the position autocorrelation function for a quartic oscillator calculated at $\beta\hbar\omega = 8$. Results for classical mechanics (CM), OPCW, exact classical Wigner (CW), FK-LPI, RPMD, and exact quantum mechanics (QM).

as a comparison in the graphs. This method is the Feynman-Kleinert linearized path integral (FK-LPI) method.[22] It uses the Feynman-Kleinert approximation,[96] which is a local harmonic approximation, for the initial quantum distribution.

In both papers III and IV it was found that, as the number of beads in the polymer is increased, the correlation functions (or trace) calculated with OPCW converge toward exact quantum mechanics at time $t = 0$ and exact classical Wigner correlation functions for all times. This is as expected from the derivations.

In figures 3.15 and 3.16 Re $\langle \widehat{x}\widehat{x}(t) \rangle$ for the quartic oscillator at $\beta\hbar\omega = 8$ and $\beta\hbar\omega = 1$ can be seen, respectively. For both these cases OPCW, as well as FK-LPI, has been converged to very near the exact classical Wigner correlation function. In this case the y- and x-versions of OPCW give very similar correlation functions, and only the y-version is shown in the graph. These OPCW calculations use 160 beads at $\beta\hbar\omega = 8$ and 80 beads at $\beta\hbar\omega = 1$. It was found
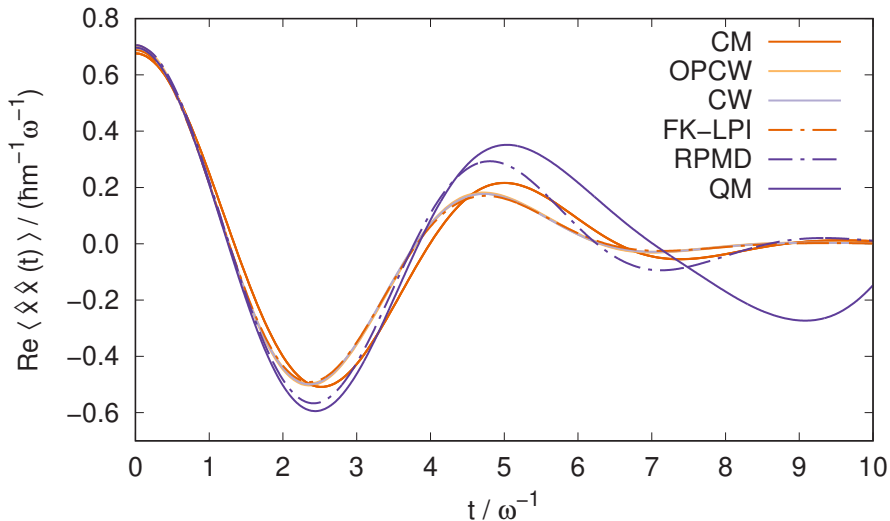
Figure 3.16: The real part of the position autocorrelation function for a quartic oscillator calculated at $\beta\hbar\omega = 1$. Results for classical mechanics (CM), OPCW, exact classical Wigner (CW), FK-LPI, RPMD, and exact quantum mechanics (QM).

in paper III that fewer beads are needed for convergence, of OPCW, at higher temperatures but that the Monte Carlo integration also becomes more demanding per bead, for the higher temperature.

In figures 3.17 and 3.18 $\mathrm{Re}\,\langle\widehat{x}\widehat{x}\,(t)\rangle$ and $\mathrm{Re}\,\langle\widehat{x}^2\widehat{x}^2\,(t)\rangle$ for the double well potential at $\beta\hbar\omega = 8$ can be seen. This potential is interesting to test since it contains some negative curvature. As before only the y-version of OPCW is shown, in this case using 160 beads. For $\mathrm{Re}\,\langle\widehat{x}\widehat{x}\,(t)\rangle$ both OPCW and FK-LPI have more or less converged to the exact classical Wigner result. For $\mathrm{Re}\,\langle\widehat{x}^2\widehat{x}^2\,(t)\rangle$, however, OPCW has converged close to the exact classical Wigner result, but FK-LPI has a significantly different behavior. This illustrates a possible benefit of OPCW compared to FK-LPI. OPCW works equally well regardless of the potential energy surface it is applied to, even if some will be more numerically demanding than others. Methods, such as FK-LPI, that use approximations for the potential energy surface will work differently well, depending on how
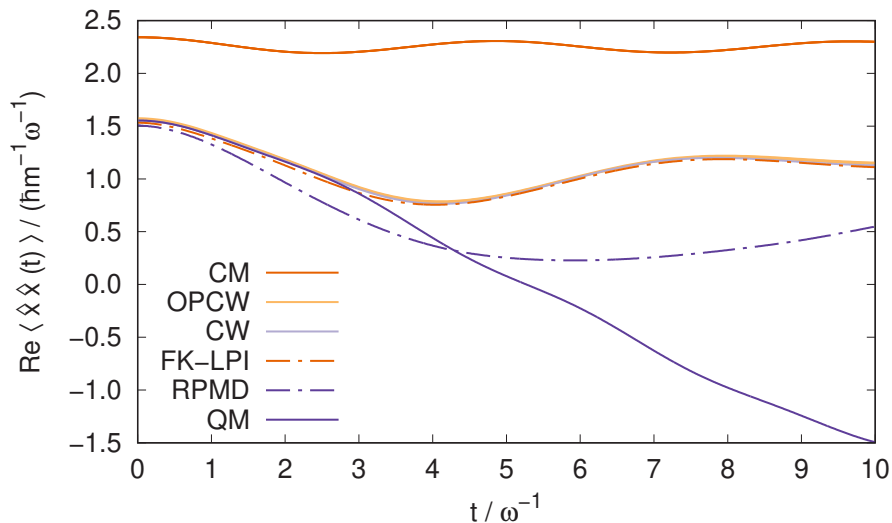
Figure 3.17: The real part of the position autocorrelation function for a double well potential calculated at $\beta\hbar\omega = 8$. Results for classical mechanics (CM), OPCW, exact classical Wigner (CW), FK-LPI, RPMD, and exact quantum mechanics (QM).

			$k_{\mathrm{r}}/(\hbar^{\frac{1}{2}}\omega^{\frac{1}{2}}m^{-\frac{1}{2}})$		
$\beta\hbar\omega$	CM	OPCW	CW	RPMD	QM
1	5.9084E-2	6.10E-2	6.0986E-2	6.17E-2	6.2856E-2
3	7.4821E-4	1.009E-3	1.0087E-3	1.07E-3	1.1409E-3
6	1.7186E-6	7.391E-6	7.5092E-6	7.55E-6	8.9347E-6

Table 3.1: Rate constant for the Eckart potential at different inverse temperatures. Values for OPCW, RPMD, classical mechanics (CM), exact classical Wigner (CW), and exact quantum mechanics (QM).

well the approximation describes the surface. It is however worth noting that in figure 3.18 both OPCW and FK-LPI follow exact classical Wigner well for as long as the classical Wigner results follow exact quantum mechanics. It would thus be misleading to claim that OPCW describes this double well better than FK-LPI does.

Another potential with a region of negative curvature is the
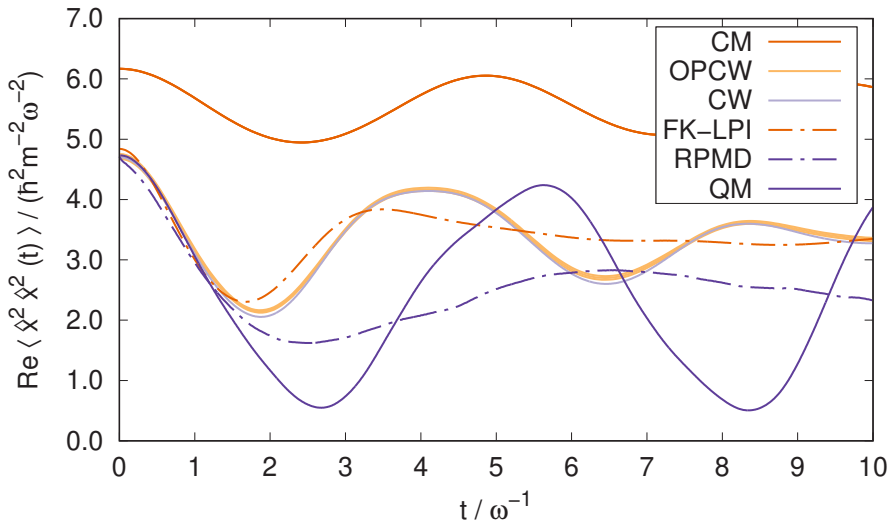
Figure 3.18: The real part of the position-squared autocorrelation function for a double well potential calculated at $\beta\hbar\omega = 8$. Results for classical mechanics (CM), OPCW, exact classical Wigner (CW), FK-LPI, RPMD, and exact quantum mechanics (QM). The increased thickness of the OPCW line shows the standard deviation.

Eckart potential, studied in paper IV. In table 3.1 rate constants, taken from the long time values of the flux-Heaviside trace, equation 2.61, for the Eckart barrier at different temperatures can be found. In this case results from the x-version of OPCW, with 40 beads, are shown. It can be seen that for these rate constants the OPCW results are close to the exact classical Wigner value. For $\beta\hbar\omega = 1$, as little as 6 beads can be enough to get an accurate classical Wigner result. The classical Wigner rate constants, as could be expected, place themselves between the classical and the quantum mechanical ones. At $\beta\hbar\omega = 1$ the difference between the classical and quantum rate constants is only $\sim 6\,\%$, so there is not much benefit from using the classical Wigner method, which accounts for half of that difference. At $\beta\hbar\omega = 3$ and $\beta\hbar\omega = 6$ the differences between classical and quantum rate constants are $\sim 50\,\%$ and a factor ~ 5, respectively. At these temperatures the classical Wigner rate
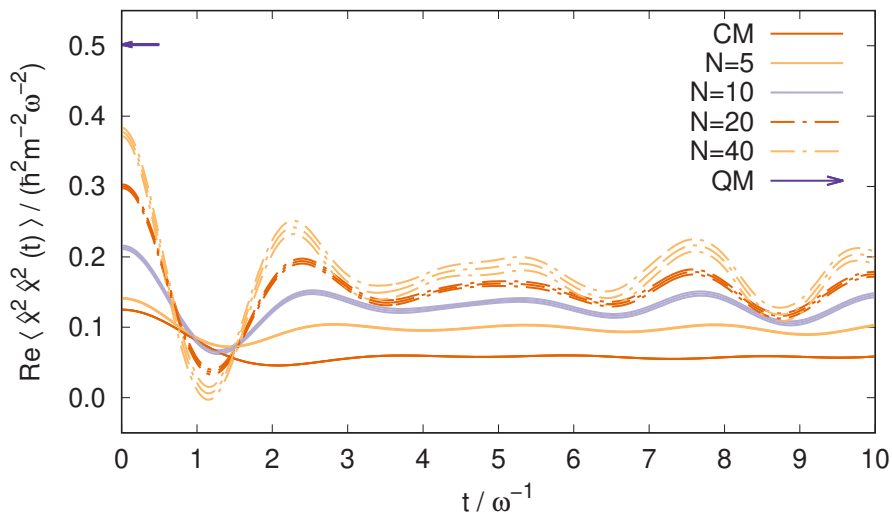
Figure 3.19: The real part of the position-squared autocorrelation function for a quartic potential bilinearly coupled to a bath of 3 harmonic oscillators, calculated at $\beta\hbar\omega = 8$. Results for classical mechanics (CM) and the y-version of OPCW, with different numbers of beads (N). Exact quantum mechanics (QM) is shown at time $t = 0$. The top and bottom lines of each type show the standard deviation.

constants are significant improvements over pure classical mechanics. The same thing can be seen for the position autocorrelation function for the quartic oscillator in figures 3.15 and 3.16, for the higher temperature the classical Wigner method is hardly an improvement over classical mechanics, but for the lower temperature it is a clear improvement.

In figures 3.19 and 3.20 $\mathrm{Re}\left\langle\widehat{x}^2\widehat{x}^2\left(t\right)\right\rangle$ for the quartic potential coupled to a bath of 3 harmonic oscillators can be seen. These figures illustrate the difference in convergence of $\mathrm{Re}\left\langle\widehat{x}^2\widehat{x}^2\left(t\right)\right\rangle_{\mathrm{OPCW},y}$ and $\mathrm{Re}\left\langle\widehat{x}^2\widehat{x}^2\left(t\right)\right\rangle_{\mathrm{OPCW},x}$, as the number of beads used is increased. For this multidimensional system no exact classical Wigner correlation function was readily calculable and the exact quantum mechanical result is only the time 0 value, not the entire correlation function. At
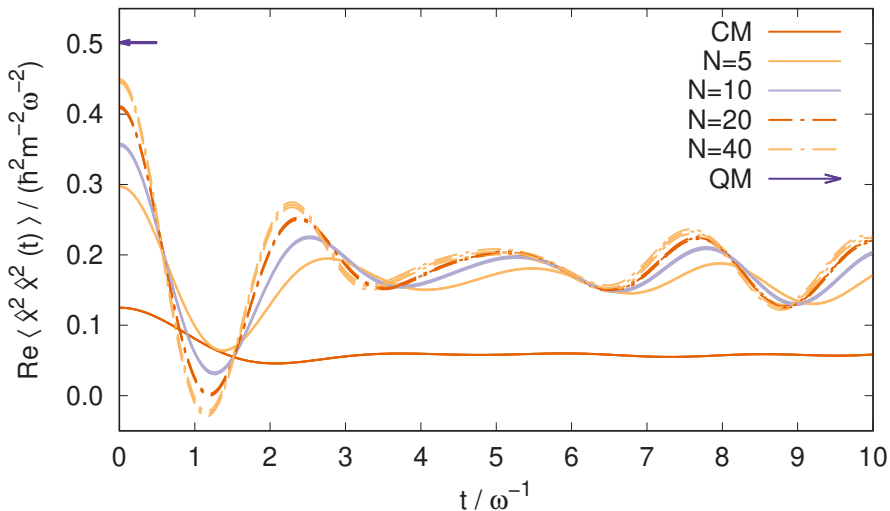
Figure 3.20: The real part of the position-squared autocorrelation function for a quartic potential bilinearly coupled to a bath of 3 harmonic oscillators, calculated at $\beta\hbar\omega = 8$. Results for classical mechanics (CM) and the x-version of OPCW, with different numbers of beads (N). Exact quantum mechanics (QM) is shown at time $t = 0$. The top and bottom lines of each type show the standard deviation.

time zero the classical Wigner method should however yield the exact quantum mechanical result, so this is still a useful comparison for OPCW. As can be seen, Re $\langle \hat{x}^2 \hat{x}^2 (t) \rangle_{\text{OPCW},x}$ converges significantly faster toward the exact quantum result, when the number of beads is increased, than Re $\langle \hat{x}^2 \hat{x}^2 (t) \rangle_{\text{OPCW},y}$ does. That the x-version of OPCW converges faster toward exact classical Wigner than the y-version was also observed for all other correlation functions, or traces, where comparisons were made in papers III and IV. For the calculations using the same number of beads in figures 3.19 and 3.20 the same number of Monte Carlo steps were used. Thus, the standard deviations illustrate another point from paper III. That is that the x-version of OPCW tend to converge better with respect to the number of Monte Carlo steps used than the y-version does.
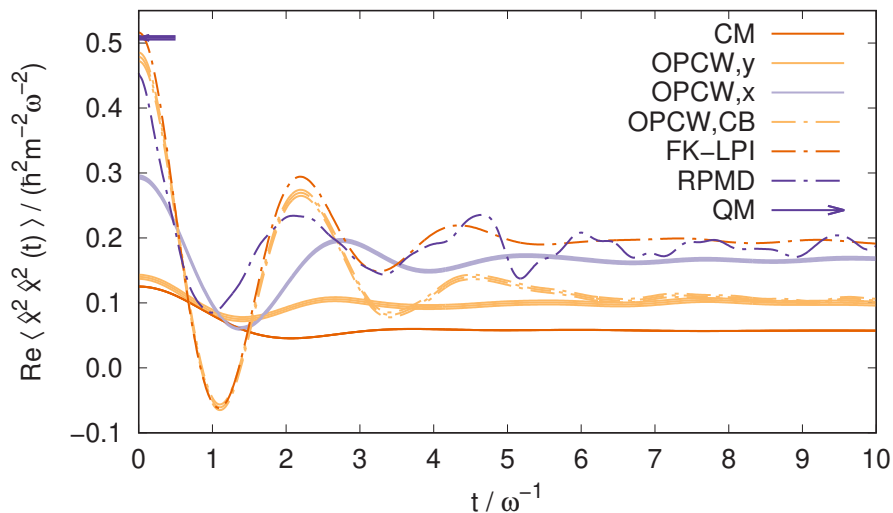
Figure 3.21: The real part of the position-squared autocorrelation function for a quartic potential bilinearly coupled to a bath of 9 harmonic oscillators, calculated at $\beta\hbar\omega = 8$. Results for classical mechanics (CM), OPCW, FK-LPI, and RPMD. The exact quantum mechanical result (QM) is shown at time $t = 0$. The OPCW method is shown for the y-version, the x-version, and the x-version with a classical bath (CB). The top and bottom lines of each type show the standard deviation.

Both these observations of course make the x-version seem more promising as a useful computational method than the y-version, but there is no guarantee that these convergence behaviors will be the same for every system and correlation function.

In figure 3.21 $\operatorname{Re}\left\langle \widehat{x}^2 \widehat{x}^2(t) \right\rangle$ for the quartic oscillator coupled to a bath of 9 harmonic oscillators can be seen. Due to the demanding computations, only results using 5 beads are shown for $\operatorname{Re}\left\langle \widehat{x}^2 \widehat{x}^2(t) \right\rangle_{\text{OPCW},y}$ and $\operatorname{Re}\left\langle \widehat{x}^2 \widehat{x}^2(t) \right\rangle_{\text{OPCW},x}$. It can, as for figures 3.19 and 3.20 be seen that the x-version of OPCW is closer to the exact result than the y-version is. Both are however far off. Figure 3.21 also shows how much of an improvement it can be to make the harmonic bath classical and just let the quartic oscillator be

sampled by an open polymer. In this classical bath calculation it was feasible to have 320 beads in the polymer in the quartic potential. The OPCW, with a classical bath, correlation function follows FK-LPI quite well for the first 3 ω^{-1}. After that the classical bath result continues toward a different long time value. If assuming that Re $\left\langle \widehat{x}^2 \widehat{x}^2 (t) \right\rangle_{\text{OPCW},x}$ is closer to the exact classical Wigner result than Re $\left\langle \widehat{x}^2 \widehat{x}^2 (t) \right\rangle_{\text{OPCW},y}$ is, then the long time value of the classical bath calculation should not be close to the exact classical Wigner value. Since the long time value of Re $\left\langle \widehat{x}^2 \widehat{x}^2 (t) \right\rangle_{\text{OPCW},x}$ is in the neighborhood of well converged FK-LPI results, this is a fair assumption.

When a classical Wigner calcluation is run, all degrees of freedom start off with some zero point energy. Since the evolution in time is classical, this zero point energy leaks between the degrees of freedom, degrading the results over time. This phenomenon was mentioned in section 2.1. If only one degree of freedom has zero point energy and the others do not, then the leakage of zero point energy from that single degree of freedom should be even bigger and it would only go one way, making the effect even larger. This is a reason why the long time values of classical bath OPCW correlation functions should not necessarily be trusted to converge toward the exact classical Wigner result. Another observation that can be made in figure 3.21 is that the OPCW, with classical bath, value at time zero is a bit below the exact quantum mechanical result. There is no guarantee that any number of beads in the quartic degree of freedom would make the OPCW value come any closer, due to the classical bath. In paper III it it can be seen that the classical bath approximation of OPCW seems to give a good approximation to exact classical Wigner for short times, for the quartic potential coupled to a harmonic bath, and that it is computationally much cheaper than standard OPCW.

In figures 3.15, 3.16, 3.17, 3.18, and 3.21, and table 3.1 the classical Wigner results can be compared with RPMD. For most of these cases, and most of the cases in papers III and IV, RPMD gives results that are better than, or equally good as, the classical Wigner results. Notable exceptions to this are the correlation functions from the double well potential, figures 3.17 and 3.18. For short times the classical bath OPCW method also gives better results

than RPMD for the position-squared autocorrelation function, for the quartic potential with a harmonic bath. Since the classical Wigner method, and OPCW, give better results than RPMD for the double well potential, and this is also the system where OPCW shows good potential compared to FK-LPI, the double well potential, and possibly other potentials with regions of negative curvature, are interesting for further studies.

3.4   Future outlook

The research presented in this thesis contains a rate constant for the formation of the hydroxyl radical through radiative association, two new types of basis functions for use with a variational principle for the time evolution of Wigner functions, and a method for sampling the initial distributions in the classical Wigner method. After the summation of all this research, the question that remain is: Where to go from here?

The new reaction rate constant was published in 2015, but has still not[¶] been included in any astrochemical database and none of its citations indicates that it has been used for astrochemical modeling.

The database KIDA[86] has instructions for suggesting new additions to their database. It is an oversight by the author that no such suggestion has been sent. To make this rate constant actually benefit the astrochemical community, the first thing that has to be done is to actually suggest that it is included in a database.

The calculation of reaction rate constants for other radiative association reactions and the development of the methods to conduct these calculations has continued in the research group, and among collaborators, of the author since the publication of paper I.[106–114] One of the main directions that further research is going toward is the calculation of radiative association rate constants for systems larger than diatoms. As radiative association generally becomes more likely the larger the molecule, due to a more long lived activated complex, as explained e.g. in the textbook by Tielens,[115] this seems to be the right way to go.

For the Gaussian basis functions for use with a variational principle for the time propagation of Wigner functions, presented in paper II, more testing would be needed to know in what situations they could be a beneficial route to go for calculations. Further testing could also help to find ways of improving the current methods. Multidimensional potentials and other correlation functions than the position autocorrelation function, would be the obvious first steps in such testing. As was suggested in the paper, a way of improving

---

[¶]When writing this, 30 April 2020.

the dynamics of the frozen Gaussian basis functions could be to give them a semiclassical prefactor that approximately would account for coupling between the separate basis functions.

When it comes to the OPCW method published in paper III and studied for rate constants in paper IV, again, further testing is the way forward. Since OPCW should be able to converge toward the exact classical Wigner method, as the number of beads in the path integral is increased, for any physical potential energy surface, it would be interesting to try it against other approximate classical Wigner methods, apart from FK-LPI, to see if the method is an improvement compared to what is already available. Since negative curvature of the potential energy surface can be problematic for other methods, this is of course one kind of system that is extra interesting to look at. The rate constant calculations should be extended to multidimensional systems, such as a double well potential with a bath of harmonic oscillators, as a step of getting closer to real molecular systems.

Improving the numerical performance of the OPCW method is also an important aspect to consider, if the method is to be practical for large systems.

Bibliography

[1] M. Shelley, *Frankenstein, or The Modern Prometheus.* 1831.

[2] P. A. M. Dirac, "Quantum mechanics of many-electron systems," *Proceedings of the Royal Society of London. Series A, Containing Papers of a Mathematical and Physical Character*, vol. 123, pp. 714–733, Apr 1929.

[3] M. Born and R. Oppenheimer, "Zur Quantentheorie der Molekeln," *Annalen der Physik*, vol. 389, no. 20, pp. 457–484, 1927.

[4] T. E. Markland, S. Habershon, and D. E. Manolopoulos, "Quantum diffusion of hydrogen and muonium atoms in liquid water and hexagonal ice," *The Journal of Chemical Physics*, vol. 128, p. 194506, May 2008.

[5] S. K.-M. Svensson, M. Gustafsson, and G. Nyman, "Formation of the hydroxyl radical by radiative association," *The Journal of Physical Chemistry A*, vol. 119, pp. 12263–9, Dec 2015.

[6] L. Wang, S. D. Fried, S. G. Boxer, and T. E. Markland, "Quantum delocalization of protons in the hydrogen-bond network of an enzyme active site," *Proceedings of the National Academy of Sciences*, vol. 111, pp. 18454–18459, Dec 2014.

[7] E. Schrödinger, "Quantisierung als Eigenwertproblem," *Annalen der Physik*, vol. 384, pp. 361–376, Jan 1926.

[8] E. Schrödinger, "Quantisierung als Eigenwertproblem," *Annalen der Physik*, vol. 384, pp. 489–527, Feb 1926.

[9] E. Schrödinger, "Über das Verhältnis der Heisenberg-Born-Jordanschen Quantenmechanik zu der meinem," *Annalen der Physik*, vol. 384, pp. 734–756, Mar 1926.

[10] E. Schrödinger, "Quantisierung als Eigenwertproblem," *Annalen der Physik*, vol. 385, pp. 437–490, May 1926.

[11] E. Schrödinger, "Quantisierung als Eigenwertproblem," *Annalen der Physik*, vol. 386, pp. 109–139, Jun 1926.

[12] E. Schrödinger, "Der stetige Übergang von der Mikro- zur Makromechanik," *Die Naturwissenschaften*, vol. 14, pp. 664–666, Jul 1926.

[13] E. Schrödinger, "An undulatory theory of the mechanics of atoms and molecules," *Physical Review*, vol. 28, pp. 1049–1070, Dec 1926.

[14] E. J. Heller, "Wigner phase space method: Analysis for semiclassical applications," *The Journal of Chemical Physics*, vol. 65, pp. 1289–1298, Aug 1976.

[15] E. Wigner, "On the quantum correction for thermodynamic equilibrium," *Physical Review*, vol. 40, pp. 749–759, Jun 1932.

[16] J. E. Moyal, "Quantum mechanics as a statistical theory," *Mathematical Proceedings of the Cambridge Philosophical Society*, vol. 45, pp. 99–124, Jan 1949.

[17] H. Wang, X. Sun, and W. H. Miller, "Semiclassical approximations for the calculation of thermal rate constants for chemical reactions in complex molecular systems," *The Journal of Chemical Physics*, vol. 108, pp. 9726 – 9736, Jun 1998.

[18] W. H. Miller, "Classical S matrix: Numerical application to inelastic collisions," *The Journal of Chemical Physics*, vol. 53, pp. 3578–3587, Nov 1970.

[19] W. H. Miller, "The semiclassical initial value representation: a potentially practical way for adding quantum effects to classical molecular dynamics simulations," *The Journal of Physical Chemistry A*, vol. 105, pp. 2942–2955, Mar 2001.

[20] X. Sun, H. Wang, and W. H. Miller, "On the semiclassical description of quantum coherence in thermal rate constants," *The Journal of Chemical Physics*, vol. 109, pp. 4190–4200, Sep 1998.

[21] Q. Shi and E. Geva, "A relationship between semiclassical and centroid correlation functions," *The Journal of Chemical Physics*, vol. 118, pp. 8173–8184, May 2003.

[22] J. A. Poulsen, G. Nyman, and P. J. Rossky, "Practical evaluation of condensed phase quantum correlation functions: A Feynman–Kleinert variational linearized path integral method," *The Journal of Chemical Physics*, vol. 119, pp. 12179–12193, Dec 2003.

[23] Q. Shi and E. Geva, "Semiclassical theory of vibrational energy relaxation in the condensed phase," *The Journal of Physical Chemistry A*, vol. 107, pp. 9059–9069, Oct 2003.

[24] Q. Shi and E. Geva, "Vibrational energy relaxation in liquid oxygen from a semiclassical molecular dynamics simulation," *The Journal of Physical Chemistry A*, vol. 107, pp. 9070–9078, Oct 2003.

[25] J. A. Poulsen, J. Scheers, G. Nyman, and P. J. Rossky, "Quantum density fluctuations in liquid neon from linearized path-integral calculations," *Physical Review B*, vol. 75, p. 224505, Jun 2007.

[26] J. A. Poulsen, G. Nyman, and P. J. Rossky, "Static and dynamic quantum effects in molecular liquids: A linearized path integral description of water," *Proc Natl Acad Sci U S A*, vol. 102, pp. 6709–6714, May 2005.

[27] N. Marković and J. A. Poulsen, "A linearized path integral description of the collision process between a water molecule and a graphite surface," *The Journal of Physical Chemistry A*, vol. 112, pp. 1701–1711, Feb 2008.

[28] S. Habershon and D. E. Manolopoulos, "Zero point energy leakage in condensed phase dynamics: An assessment of quantum simulation methods for liquid water," *The Journal of Chemical Physics*, vol. 131, p. 244518, Dec 2009.

[29] K. Boye, "In motion." Karin Boye: Complete poems, Trans. D. McDuff, Bloodaxe Books, 1994.

[30] R. P. Feynman, "Space-time approach to non-relativistic quantum mechanics," *Reviews of Modern Physics*, vol. 20, pp. 367–387, Apr 1948.

[31] R. P. Feynman and A. R. Hibbs, *Quantum Mechanics and Path Integrals*. McGraw-Hill Companies, Inc., New York, 1965.

[32] H. F. Trotter, "On the product of semi-groups of operators," *Proceedings of the American Mathematical Society*, vol. 10, pp. 545–551, Aug 1959.

[33] J. A. Barker, "A quantum-statistical Monte Carlo method; path integrals with boundary conditions," *The Journal of Chemical Physics*, vol. 70, pp. 2914–2918, Mar 1979.

[34] M. Parrinello and A. Rahman, "Study of an F center in molten KCl," *The Journal of Chemical Physics*, vol. 80, pp. 860–867, Jan 1984.

[35] J. Cao and G. A. Voth, "A new perspective on quantum time correlation functions," *The Journal of Chemical Physics*, vol. 99, pp. 10070–10073, Dec 1993.

[36] I. R. Craig and D. E. Manolopoulos, "Quantum statistics and classical mechanics: real time correlation functions from ring polymer molecular dynamics," *The Journal of Chemical Physics*, vol. 121, pp. 3368–73, Aug 2004.

[37] W. H. Miller, "Quantum mechanical transition state theory and a new semiclassical model for reaction rate constants," *The Journal of Chemical Physics*, vol. 61, pp. 1823–1834, Sep 1974.

[38] W. H. Miller, S. D. Schwartz, and J. W. Tromp, "Quantum mechanical rate constants for bimolecular reactions," *The Journal of Chemical Physics*, vol. 79, pp. 4889–4898, Nov 1983.

[39] F. Jensen, *Introduction to Computational Chemistry*. England: John Wiley & Sons Ltd, 2nd ed., 2007.

[40] R. Kubo, "Statistical-mechanistical theory of irreversible processes. I. general theory and simple application to magnetic and conduction problems," *Journal of the Physical Society of Japan*, vol. 12, pp. 570–586, Jun 1957.

[41] P. Schofield, "Space-time correlation function formalism for slow neutron scattering," *Physical Review Letters*, vol. 4, pp. 239–240, Mar 1960.

[42] T. J. H. Hele, M. J. Willatt, A. Muolo, and S. C. Althorpe, "Boltzmann-conserving classical dynamics in quantum time-correlation functions: "Matsubara dynamics"," *The Journal of Chemical Physics*, vol. 142, p. 134103, Apr 2015.

[43] K. A. Jung, P. E. Videla, and V. S. Batista, "Multi-time formulation of Matsubara dynamics," *The Journal of Chemical Physics*, vol. 151, p. 034108, Jul 2019.

[44] M. J. Willatt, M. Ceriotti, and S. C. Althorpe, "Approximating Matsubara dynamics using the planetary model: Tests on liquid water and ice," *The Journal of Chemical Physics*, vol. 148, p. 102336, Jan 2018.

[45] T. J. H. Hele, M. J. Willatt, A. Muolo, and S. C. Althorpe, "Communication: Relation of centroid molecular dynamics and ring-polymer molecular dynamics to exact quantum dynamics," *The Journal of Chemical Physics*, vol. 142, p. 191101, May 2015.

[46] D. R. Reichman, P.-N. Roy, S. Jang, and G. A. Voth, "A Feynman path centroid dynamics approach for the computation of time correlation functions involving nonlinear operators," *The Journal of Chemical Physics*, vol. 113, pp. 919–929, Jul 2000.

[47] A. Witt, S. D. Ivanov, M. Shiga, H. Forbert, and D. Marx, "On the applicability of centroid and ring polymer path integral molecular dynamics for vibrational spectroscopy," *The Journal of Chemical Physics*, vol. 130, p. 194510, May 2009.

[48] I. R. Craig and D. E. Manolopoulos, "Chemical reaction rates from ring polymer molecular dynamics," *The Journal of Chemical Physics*, vol. 122, p. 084106, Feb 2005.

[49] T. F. Miller and D. E. Manolopoulos, "Quantum diffusion in liquid para-hydrogen from ring-polymer molecular dynamics," *The Journal of Chemical Physics*, vol. 122, p. 184503, May 2005.

[50] M. Rossi, M. Ceriotti, and D. E. Manolopoulos, "How to remove the spurious resonances from ring polymer molecular dynamics," *The Journal of Chemical Physics*, vol. 140, p. 234116, Jun 2014.

[51] P. A. M. Dirac, "Note on exchange phenomena in the Thomas atom," *Mathematical Proceedings of the Cambridge Philosophical Society*, vol. 26, pp. 376–385, Jul 1930.

[52] J. I. Frenkel, *Wave Mechanics; Advanced General Theory*. Oxford: Clarendon Press, 1934.

[53] A. McLachlan, "A variational solution of the time-dependent Schrodinger equation," *Molecular Physics*, vol. 8, no. 1, pp. 39–44, 1964.

[54] H.-D. Meyer, U. Manthe, and L. Cederbaum, "The multi-configurational time-dependent Hartree approach," *Chemical Physics Letters*, vol. 165, pp. 73–78, Jan 1990.

[55] S. Tzu, *The Art of War, Trans. L. Giles*. London: Luzac & Co., 1910.

[56] S. Weinreb, A. H. Barrett, M. L. Meeks, and J. C. Henry, "Radio observations of OH in the interstellar medium," *Nature*, vol. 200, pp. 829–831, Nov 1963.

[57] L. Weliachew, "Detection of interstellar OH in two external galaxies," *The Astrophysical Journal*, vol. 167, pp. L47–L52, Jul 1971.

[58] E. Herbst, "Chemistry in the interstellar medium," *Annual Review of Physical Chemistry*, vol. 46, pp. 27–54, Oct 1995.

[59] E. F. van Dishoeck, S. R. Langhoff, and A. Dalgarno, "The low-lying $2\Sigma^-$ states of OH," *The Journal of Chemical Physics*, vol. 78, pp. 4552–4561, Apr 1983.

[60] D. R. Yarkony, "A theoretical treatment of the predissociation of the individual rovibronic levels of OH/OD(A $^2\Sigma^+$)," *The Journal of Chemical Physics*, vol. 97, pp. 1838–1849, Aug 1992.

[61] H. van Lonkhuyzen and C. A. de Lange, "U.V. photoelectron spectroscopy of OH and OD radicals," *Molecular Physics*, vol. 51, pp. 551–568, Sep 1984.

[62] K. P. Huber and G. Herzberg, *Constants of diatomic molecules*, vol. 4 of *Molecular Spectra and Molecular Structure*. Springer, Boston, MA, USA, 1979.

[63] A. Kramida, Y. Ralchenko, J. Reader, and NIST ASD Team, "Atomic spectra database, ver. 5.2." National Institute of Standards and Technology, Gaitersburg, MD, USA, Sep 2014.

[64] S. R. Langhoff, C. W. Bauschlicher Jr., and P. R. Taylor, "Theoretical study of the dipole moment function of OH(X $^2\Pi$)," *The Journal of Chemical Physics*, vol. 91, pp. 5953–5959, Nov 1989.

[65] B. H. Bransden and C. J. Joachain, *Quantum Mechanics*. Harlow; England: Pearson Education Limited, 2nd ed., 2000.

[66] J. F. Babb and A. Dalgarno, "Radiative association and inverse predissociation of oxygen atoms," *Physical Review A*, vol. 51, pp. 3021–3026, Apr 1995.

[67] Ğ. Barinovs and M. C. van Hemert, "CH$^+$ radiative association," *The Astrophysical Journal*, vol. 636, pp. 923–926, Jan 2006.

[68] B. V. Noumerov, "A method of extrapolation of perturbations," *Monthly Notices of the Royal Astronomical Society*, vol. 84, pp. 592–602, Jun 1924.

[69] D. T. Colbert and W. H. Miller, "A novel discrete variable representation for quantum mechanical reactive scattering via the S-matrix Kohn method," *The Journal of Chemical Physics*, vol. 96, pp. 1982–1991, Feb 1992.

[70] J. Franck and E. G. Dymond, "Elementary processes of photochemical reactions," *Transactions of the Faraday Society*, vol. 21, pp. 536–542, Feb 1926.

[71] E. U. Condon, "A theory of intensity distribution in band systems," *Physical Review*, vol. 28, pp. 1182–1201, Dec 1926.

[72] E. U. Condon, "Nuclear motions associated with electron transitions in diatomic molecules," *Physical Review*, vol. 32, pp. 858–872, Dec 1928.

[73] G. Wentzel, "Eine Verallgemeinerung der Quantenbedingungen für die Zwecke der Wellenmechanik," *Zeitschrift für Physik*, vol. 38, pp. 518–529, Jun 1926.

[74] H. A. Kramers, "Wellenmechanik und halbzahlige Quantisierung," *Zeitschrift für Physik*, vol. 39, pp. 828–840, Oct 1926.

[75] L. Brillouin, "La mécanique ondulatoire de Schrödinger: une méthode générale de résolution par approximations successives," *Comptes Rendus de l'Académie des Sciences*, vol. 183, pp. 24–26, 1926.

[76] M. Gustafsson, "Classical calculations of radiative association in absence of electronic transitions," *The Journal of Chemical Physics*, vol. 138, pp. 074308–1–074308–7, Feb 2013.

[77] J. Larmor, "On the theory of the magnetic influence on spectra; and on the radiation from moving ions," *The London, Edinburgh, and Dublin Philosophical Magazine and Journal of Science, Series 5*, vol. 44, no. 271, pp. 503–512, 1897.

[78] G. Breit and E. Wigner, "Capture of slow neutrons," *Physical Review*, vol. 49, pp. 519–531, Apr 1936.

[79] R. J. Le Roy, "LEVEL 8.0 a computer program for solving the radial Schrödinger equation for bound and quasibound levels, including corrections as of December 2012." University of Waterloo Chemical Physics Research Report CP-663, Apr 2007.

[80] J. A. Fedchak, M. A. Huels, L. D. Doverspike, and R. L. Champion, "Electron detachment and charge transfer for collisions of O^- and S^- with H," *Physical Review A*, vol. 47, pp. 3796–3800, May 1993.

[81] U. Jentschura, S. Kotochigova, E. LeBigot, P. Mohr, and B. Taylor, "The energy levels of hydrogen and deuterium, ver. 2.1." National Institute of Standards and Technology, Gaitersburg, MD, USA, Jul 2005.

[82] K. Eriksson and H. Isberg, "New measurements in the spectrum of atomic oxygen, O I," *Arkiv för fysik*, vol. 37, pp. 221–230, 1968.

[83] C. E. Moore, *Selected Tables of Atomic Spectra, Atomic Energy Levels and Multiplet Tables – O I*, vol. 3 of *National Standard Reference Data System*. National Bureau of Standards, U.S., Apr 1976.

[84] K. R. Lykke, K. K. Murray, and W. C. Lineberger, "Threshold photodetachment of H⁻," *Physical Review A*, vol. 43, pp. 6104–6107, Jun 1991.

[85] D. Neumark, K. R. Lykke, T. Andersen, and W. C. Lineberger, "Laser photodetachment measurement of the electron affinity of atomic oxygen," *Physical Review A*, vol. 32, pp. 1890–1892, Sep 1985.

[86] V. Wakelam, E. Herbst, J.-C. Loison, I. Smith, V. Chandrasekaran, B. Pavone, N. Adams, M.-C. Bacchus-Motabonel, A. Bergeat, K. Béroff, V. Bierbaum, M. Chabot, A. Dalgarno, E. F. van Dishoeck, A. Faure, W. Geppert, D. Gerlich, D. Galli, E. Hébrard, F. Hersant, K. Hickson, P. Honvault, S. Klippenstein, S. Le Picard, G. Nyman, P. Pernot, S. Schlemmer, F. Selsis, I. Sims, D. Talbi, J. Tennyson, J. Troe, R. Wester, and L. Wiesenfeld, "A KInetic Database for Astrochemistry (KIDA)," *The Astrophysical Journal Supplement Series*, vol. 199, p. 21, Mar 2012.

[87] A. Kramida, Y. Ralchenko, J. Reader, and NIST ASD Team, "NIST atomic spectra database, ver. 5.7.1." National Institute of Standards and Technology, Gaitersburg, MD, USA, Apr 2020.

[88] A. Kramida, "A critical compilation of experimental data on spectral lines and energy levels of hydrogen, deuterium, and tritium," *Atomic Data and Nuclear Data Tables*, vol. 96, pp. 586–644, Nov 2010.

[89] A. Kramida, "Erratum to "a critical compilation of experimental data on spectral lines and energy levels of hydrogen, deuterium, and tritium" [At. Data Nucl. Data Tables 96 (2010) 586–644]," *Atomic Data and Nuclear Data Tables*, vol. 126, pp. 295–298, Mar 2019.

[90] C. E. Moore, *Tables of Spectra of Hydrogen, Carbon, Nitrogen, and Oxygen Atoms and Ions.* CRC Series in Evaluated Data in Atomic Physics, Boca Raton, Florida, U.S.A.: CRC Press, 1993.

[91] D. McElroy, C. Walsh, A. J. Markwick, M. A. Cordiner, K. W. Smith, and T. J. Millar, "The UMIST database for astrochemistry 2012," *Astronomy and Astrophysics*, vol. 550, p. A36, Feb 2013.

[92] J. A. Poulsen, "A variational principle in Wigner phase-space with applications to statistical mechanics," *The Journal of Chemical Physics*, vol. 134, p. 034118, Jan 2011.

[93] J. A. Poulsen, S. K.-M. Svensson, and G. Nyman, "Dynamics of Gaussian Wigner functions derived from a time-dependent variational principle," *AIP Advances*, vol. 7, pp. 115018–1–115018–12, Nov 2017.

[94] R. D. Coalson and M. Karplus, "Multidimensional variational Gaussian wave packet dynamics with application to photodissociation spectroscopy," *The Journal of Chemical Physics*, vol. 93, pp. 3919–3930, Sep 1990.

[95] D. J. Coughtrie and D. P. Tew, "A Gaussian wave packet phase-space representation of quantum canonical statistics," *The Journal of Chemical Physics*, vol. 143, p. 044102, Jul 2015.

[96] R. P. Feynman and H. Kleinert, "Effective classical partition functions," *Physical Review A*, vol. 34, pp. 5080–5084, Dec 1986.

[97] S. K.-M. Svensson, J. A. Poulsen, and G. Nyman, "Classical Wigner model based on a Feynman path integral open polymer," *The Journal of Chemical Physics*, vol. 152, p. 094111, Mar 2020.

[98] N. Metropolis, A. W. Rosenbluth, M. N. Rosenbluth, A. H. Teller, and E. Teller, "Equation of state calculations by fast computing

machines," *The Journal of Chemical Physics*, vol. 21, pp. 1087–1092, Jun 1953.

[99] L. Verlet, "Computer "experiments´´ on classical fluids. I. thermodynamical properties of Lennard-Jones molecules," *Physical Review*, vol. 159, pp. 98–103, Jul 1967.

[100] W. C. Swope, H. C. Andersen, P. H. Berens, and K. R. Wilson, "A computer simulation method for the calculation of equilibrium constants for the formation of physical clusters of molecules: Application to small water clusters," *The Journal of Chemical Physics*, vol. 76, pp. 637–649, Jan 1982.

[101] A. Bose and N. Makri, "Coherent state-based path integral methodology for computing the Wigner phase space distribution," *The Journal of Physical Chemistry A*, vol. 123, pp. 4284–4294, Apr 2019.

[102] S. Bonella, M. Monteferrante, C. Pierleoni, and G. Ciccotti, "Path integral based calculations of symmetrized time correlation functions. II," *The Journal of Chemical Physics*, vol. 133, p. 164105, Oct 2010.

[103] S. Bonella and G. Ciccotti, "Approximating time-dependent quantum statistical properties," *Entropy*, vol. 16, pp. 86–109, Dec 2013.

[104] A. O. Caldeira and A. J. Leggett, "Quantum tunnelling in a dissipative system," *Annals of Physics*, vol. 149, pp. 374–456, September 1983.

[105] J. Liu and W. H. Miller, "Using the thermal Gaussian approximation for the Boltzmann operator in semiclassical initial value time correlation functions," *The Journal of Chemical Physics*, vol. 125, p. 224104, Dec 2006.

[106] J. Öström, D. S. Bezrukov, G. Nyman, and M. Gustafsson, "Reaction rate constant for radiative association of CF^+," *The Journal of Chemical Physics*, vol. 144, p. 044302, Jan 2016.

[107] J. Öström, D. S. Bezrukov, G. Nyman, and M. Gustafsson, "Erratum: "Reaction rate constant for radiative association of CF^+" [J. Chem. Phys. 144, 044302 (2016)]," *The Journal of Chemical Physics*, vol. 150, p. 249901, Jun 2019.

[108] R. K. Kathir, G. Nyman, and M. Gustafsson, "The rate constant for formation of HCl through radiative association," *Monthly Notices of the Royal Astronomical Society*, vol. 470, pp. 3068–3070, Jun 2017.

[109] P. Szabó and M. Gustafsson, "A surface-hopping method for semiclassical calculations of cross sections for radiative association with electronic transitions," *The Journal of Chemical Physics*, vol. 147, p. 094308, Sep 2017.

[110] T. Stoecklin, P. Halvick, H.-G. Yu, G. Nyman, and Y. Ellinger, "On the gas-phase formation of the HCO radical: accurate quantum study of the H+CO radiative association," *Monthly Notices of the Royal Astronomical Society*, vol. 475, pp. 2545–2552, Jan 2018.

[111] M. Záměčníková, P. Soldán, M. Gustafsson, and G. Nyman, "Formation of CO^+ by radiative association," *Monthly Notices of the Royal Astronomical Society*, vol. 489, pp. 2954–2960, Aug 2019.

[112] M. Gustafsson and R. C. Forrey, "Semiclassical methods for calculating radiative association rate constants for different thermodynamic conditions: Application to formation of CO, CN, and SiN," *The Journal of Chemical Physics*, vol. 150, p. 224301, Jun 2019.

[113] D. Burdakova, G. Nyman, and T. Stoecklin, "Formation of Na-containing complex molecules in the gas phase in dense molecular clouds: quantum study of the $Na^+ + H_2$ and $Na^+ + D_2$ radiative association step," *Monthly Notices of the Royal Astronomical Society*, vol. 485, pp. 5874–5879, Mar 2019.

[114] M. Záměčníková, M. Gustafsson, G. Nyman, and P. Soldán, "Formation of CO^+ by radiative association II," *Monthly Notices*

of the Royal Astronomical Society, vol. 492, pp. 3794–3802, Jan 2020.

[115] A. G. G. M. Tielens, *The Physics and Chemistry of the Interstellar Medium.* Cambridge, UK: Cambridge University Press, 2005.

Papers

Paper I

Formation of the Hydroxyl Radical by Radiative Association

Article

Formation of the Hydroxyl Radical by Radiative Association

S. Karl-Mikael Svensson,[†] Magnus Gustafsson,[‡] and Gunnar Nyman*,[†]

[†]Department of Chemistry and Molecular Biology, University of Gothenburg, SE-41296 Gothenburg, Sweden

[‡]Applied Physics, Division of Material Science, Department of Engineering Science and Mathematics, Luleå University of Technology, SE-97187 Luleå, Sweden

ABSTRACT: The reaction rate constant for the radiative association of $O(^3P)$ and $H(^2S)$ has been calculated by combining a few different methods and taking account of both direct and resonance-mediated pathways. The latter includes both shape resonances and Feshbach type inverse predissociation. The reaction rate constant is expressed as a function of temperature in the interval 10−30000 K. This reaction may be astrochemically relevant and is expected to be of use in astrochemical networks.
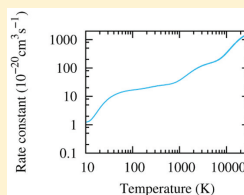
INTRODUCTION

The hydroxyl radical (OH) has been observed in the interstellar medium both in the Milky Way[1] and in other galaxies.[2] OH is also thought to have been an important species in the early universe, when heavy elements were more rare than in present-day molecular clouds.[3]

Due to the low density of the interstellar medium (for the most common element hydrogen it is usually <1 cm^{-3}),[4] three-body collisions essentially do not occur. This allows for two-body collisions with low reaction probabilities, such as radiative association, to be important. The atoms needed to form the hydroxyl radical by this type of reaction are hydrogen (H) and oxygen (O), which respectively are the atoms of the most and third most abundant elements in our galaxy and may have atomic densities of approximately 0.35[4] and 0.0001 cm^{-3}, respectively.[5] Therefore, it is of interest to see if this type of reaction could be a possible path for the formation of the hydroxyl radical.

When the ground state atoms $O(^3P)$ and $H(^2S)$ collide, the molecular states that are possible for them to form are $OH(X^2\Pi)$, $OH(1^2\Sigma^-)$, $OH(a^4\Sigma^-)$, and $OH(b^4\Pi)$, whose potential energies can be seen in Figure 1. The states $X^2\Pi$ and $1^2\Sigma^-$ can radiate to give $OH(X^2\Pi)$ in a bound rovibrational energy level. Explicitly written, these reactions are ($OH(X^2\Pi)*$ denotes a free or quasibound state)

$$O(^3P) + H(^2S) \rightarrow OH(X^2\Pi)* \rightarrow OH(X^2\Pi) + h\nu \qquad (I)$$

and

$$O(^3P) + H(^2S) \rightarrow OH(1^2\Sigma^-) \rightarrow OH(X^2\Pi) + h\nu \qquad (II)$$
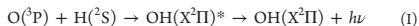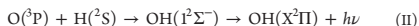
Alternatively, the two colliding atoms, in any of the formerly mentioned states, may undergo a radiationless transition to the excited quasibound $A^2\Sigma^+$ state of OH from where a radiative transition to $X^2\Pi$ can be made. This type of radiative association reaction mechanism is called inverse predissociation and can occur via any of the pathways
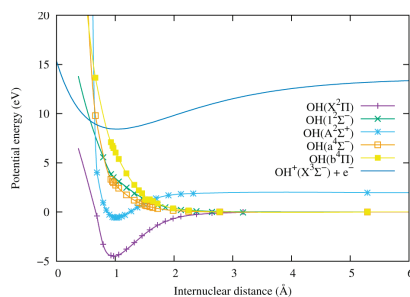
Figure 1. Potential energies for the $X^2\Pi$ and $1^2\Sigma^-$ states of OH from van Dishoeck et al.,[6] the potential energies for the $A^2\Sigma^+$, $a^4\Sigma^-$, and $b^4\Pi$ from Yarkony,[7] and a Morse potential for the potential energy of the $X^3\Sigma^-$ state of OH$^+$ (with parameters from van Lonkhuyzen and de Lange[8] and Huber and Herzberg[9]) placed one ionization energy of hydrogen[10] above OH. The points are the original data and the lines (except the Morse potential) are inter- and extrapolations.
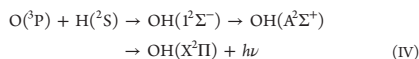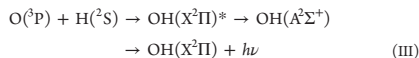
$$O(^3P) + H(^2S) \rightarrow OH(X^2\Pi)* \rightarrow OH(A^2\Sigma^+)$$
$$\rightarrow OH(X^2\Pi) + h\nu \qquad (III)$$

$$O(^3P) + H(^2S) \rightarrow OH(1^2\Sigma^-) \rightarrow OH(A^2\Sigma^+)$$
$$\rightarrow OH(X^2\Pi) + h\nu \qquad (IV)$$

$$O(^3P) + H(^2S) \rightarrow OH(a^4\Sigma^-) \rightarrow OH(A^2\Sigma^+)$$
$$\rightarrow OH(X^2\Pi) + h\nu \qquad (V)$$

or

$$O(^3P) + H(^2S) \rightarrow OH(b^4\Pi) \rightarrow OH(A^2\Sigma^+)$$
$$\rightarrow OH(X^2\Pi) + h\nu \qquad (VI)$$
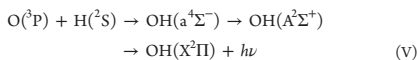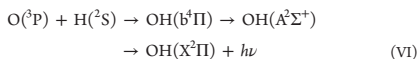
The rate constants for formation of OH through inverse predissociation III−VI have been estimated previously.[11,12] The radiative association reactions I and II have not been studied prior to this work.

The aim of this study is to compute a reliable reaction rate constant for OH formation through radiative association that can be incorporated into chemical models of the interstellar medium (through, e.g., KIDA[13] and the UMIST database for astrochemistry[14]). This includes calculations of rate constants corresponding to reactions I and II, and an improved estimate of the contribution from the inverse predissociation reactions III−VI. Attention is also paid to possible influence from electron detachment and charge transfer processes.

■ THEORETICAL METHODS

For a binary collisional process, such as radiative association where the orbital electronic angular momentum quantum number changes from Λ to Λ', an expression for the thermal rate constant is

$$k_{\Lambda \rightarrow \Lambda'}(T)$$
$$= \left(\frac{8}{\pi\mu}\right)^{1/2} \left(\frac{1}{k_B T}\right)^{3/2} \int_0^\infty E\sigma_{\Lambda \rightarrow \Lambda'}(E) \exp(-E/k_B T) \, dE \qquad (1)$$

where $k_{\Lambda \rightarrow \Lambda'}(T)$ is the thermal rate constant, T is the absolute temperature, μ is the reduced mass of the colliding particles, k_B is Boltzmann's constant, E is the kinetic energy of the colliding particles, and $\sigma_{\Lambda \rightarrow \Lambda'}(E)$ is the cross-section for the process. There are a few different ways to calculate this cross-section. Four such approaches were used for reaction pathways I and II in this work: a quantum mechanical perturbation theory, a semiclassical method, a classical method, and Breit−Wigner theory.

Quantum Mechanical Perturbation Theory. The perturbation theory employed here physically means that we approximately account for the interaction between the electric field of the photon produced in the reaction and the electric dipole moment of the molecule. When the quantum mechanical perturbation theory is used, a Fermi Golden rule cross-section is obtained and can be written as (as described by, e.g., refs 15 and 16)

$$\sigma_{\Lambda \rightarrow \Lambda'}(E)$$
$$= \sum_{Jv'J'} \frac{32}{3} \frac{\pi^5 \hbar^2}{(4\pi\epsilon_0)c^3} \frac{1}{\mu E} P_\Lambda \nu_{E\Lambda'v'J'}^3 S_{\Lambda J \rightarrow \Lambda' J'} |M_{\Lambda E J \Lambda' v' J'}|^2 \qquad (2)$$

where J and J' are the total angular momentum quantum numbers before and after the process, respectively, v' is the vibrational quantum number for the bound state, $\hbar$ is the reduced Planck constant, ϵ_0 is the permittivity of vacuum, c is the speed of light, P_Λ is a factor for statistical weight, $\nu_{E\Lambda'v'J'}$ is the frequency of the emitted photon, $S_{\Lambda J \rightarrow \Lambda' J'}$ is the Hönl−

London factor (rotational line intensity factor),[17] and $M_{\Lambda E J \Lambda' v' J'}$ is the matrix element of the transition dipole moment operator. The sum is over all J, v', and J'. It is assumed in these calculations that the electronic spin quantum number (S) is much smaller than J, so that for the operators $\mathbf{J} - \mathbf{S} \approx \mathbf{J}$. $M_{\Lambda E J \Lambda' v' J'}$ is defined as

$$M_{\Lambda E J \Lambda' v' J'} = \int_0^\infty F_{\Lambda E J}(R) \, D_{\Lambda \Lambda'}(R) \, \Psi_{\Lambda' v' J'}(R) \, dR \qquad (3)$$

where R is the distance between the particles, $F_{\Lambda E J}(R)$ is the collision-energy-normalized wave function of the unbound state, $\Psi_{\Lambda' v' J'}(R)$ is the normalized wave function of the bound state, and $D_{\Lambda \Lambda'}(R)$ is the electric dipole moment operator for the transition between the electronic states of Λ and Λ'. P_Λ is defined as

$$P_\Lambda = \frac{(2S + 1)(2 - \delta_{0,\Lambda})}{(2L_A + 1)(2S_A + 1)(2L_B + 1)(2S_B + 1)} \qquad (4)$$

where $\delta_{0,\Lambda}$ is the Kronecker delta, L_A and L_B are the electronic orbital angular momentum quantum numbers of particles A and B, respectively, and S_A and S_B are the electronic spin quantum numbers of particles A and B, respectively.

Semiclassical Method. The semiclassical method can be seen as the time integral of the transition rate between two electronic states, as it is given by the Einstein A coefficient.[18] This can also be formulated as an integral over internuclear separation, which is done here. This method only works for transitions between different electronic states and has a cross-section according to the formula[19,20]

$$\sigma_{\Lambda \rightarrow \Lambda'}(E)$$
$$= 4\pi \sqrt{\frac{\mu}{2E}} P_\Lambda \int_0^\infty b \int_{R_c}^\infty \frac{A_{\Lambda \rightarrow \Lambda'}^{Eb}(R)}{\sqrt{1 - \frac{V_\Lambda(R)}{E} - \frac{b^2}{R^2}}} \, dR \, db \qquad (5)$$

where b is the impact parameter, R_c is the outer classical turning point, $V_\Lambda(R)$ is the potential energy of the electronic state characterized by Λ, and $A_{\Lambda \rightarrow \Lambda'}^{Eb}(R)$ is the probability of transition between the states characterized by Λ and Λ', respectively, per unit of time. $A_{\Lambda \rightarrow \Lambda'}^{Eb}(R)$ is given by[21]

$$A_{\Lambda \rightarrow \Lambda'}^{Eb}(R) = \begin{cases} A_{\Lambda \rightarrow \Lambda'}(R) & \text{if } E < V_\Lambda(R) - V_\Lambda(R) \text{ and} \\ & V_{\Lambda'}(R) + \frac{Eb^2}{R^2} < 0 \\ 0 & \text{otherwise} \end{cases} \qquad (6)$$

where $V_{\Lambda'}(R)$ is the potential energy of the electronic state characterized by Λ', and $A_{\Lambda \rightarrow \Lambda'}(R)$ is defined by

$$A_{\Lambda \rightarrow \Lambda'}(R)$$
$$= \frac{64}{3} \frac{\pi^4}{(4\pi\epsilon_0)hc^3} \left(\frac{2 - \delta_{0,\Lambda+\Lambda'}}{2 - \delta_{0,\Lambda}}\right) \nu_{\Lambda \rightarrow \Lambda'}^3(R) \, D_{\Lambda \Lambda'}^2(R) \qquad (7)$$

with

$$\nu_{\Lambda \rightarrow \Lambda'}(R) = \frac{\max(0, V_\Lambda(R) - V_{\Lambda'}(R))}{h} \qquad (8)$$

Classical Method. The classical method only applies to transitions within one electronic state and therefore complements the semiclassical method. The method essentially takes the frequency at which the electric dipole moment of the

system changes, by using classical mechanics, and equates that frequency to that of the emitted photon. The intensity of the emission is given by the Larmor power[22] and the radiative association cross section is given by[23]

$$\sigma_{\Lambda \to \Lambda}(E)$$
$$= \frac{4}{3c^3\hbar(4\pi\epsilon_0)}P_\Lambda \int_0^\infty b \int_0^\infty \omega^3 \left| \int_{-\infty}^\infty e^{i\omega t} \mathbf{D}(b,E,t)\, dt \right|^2 d\omega\, db$$

(9)

where ω is the angular frequency of the emitted photon, t is time, and $\mathbf{D}(b,E,t)$ is the time-dependent electric dipole moment vector of the system. $\mathbf{D}(b,E,t)$ can be found from $D_{\Lambda\Lambda}(R)$ by solving the equations of motion,

$$\frac{dR}{dt} = \sqrt{\frac{2}{\mu}\left(E - V_\Lambda(R) - \frac{Eb^2}{R^2}\right)}$$

(10)

$$\frac{d\theta}{dt} = \frac{b}{R^2}\sqrt{\frac{2E}{\mu}}$$

(11)

where θ is the polar angle of the system.

Breit−Wigner Theory. Radiative association cross sections will in many cases have peaks due to resonances and the shape of these resonances will not always be correct when the quantum mechanical perturbation theory is used.[24] The semiclassical and classical methods on the contrary cannot take resonances into account at all, but only give the direct contribution to the cross-section. Breit−Wigner theory accounts only for resonances and therefore can work as a complement to the semiclassical or classical method and, when combined with either of these, in some cases give better results than the quantum mechanical perturbation theory.

The Breit−Wigner theory assumes that the rate constant can be divided into a direct contribution, $k_{\Lambda \to \Lambda'}^{\text{direct}}(T)$, and a contribution from resonances, $k_{\Lambda \to \Lambda'}^{\text{res}}(T)$,

$$k_{\Lambda \to \Lambda'}(T) = k_{\Lambda \to \Lambda'}^{\text{direct}}(T) + k_{\Lambda \to \Lambda'}^{\text{res}}(T)$$

(12)

The resonance contribution to the rate constant is given by[25,26]

$$k_{\Lambda \to \Lambda'}^{\text{res}}(T) = \hbar^2 P_\Lambda \left(\frac{2\pi}{\mu k_B T}\right)^{3/2}$$
$$\times \sum_{vJ}(2J+1)\frac{\Gamma_{\Lambda vJ}^{\text{tun}}\Gamma_{\Lambda vJ \to \Lambda'}^{\text{rad}}}{\Gamma_{\Lambda vJ \to \Lambda'}^{\text{rad}} + \Gamma_{\Lambda vJ}^{\text{tun}}} \exp(-E_{\Lambda vJ}/k_B T)$$

(13)

where v is the vibrational quantum number of a quasibound state, $E_{\Lambda vJ}$ is the energy of a quasibound state with quantum numbers Λ, v, and J, $\Gamma_{\Lambda vJ \to \Lambda'}^{\text{rad}}$ is the total width of the radiative decay to any of the bound levels, and $\Gamma_{\Lambda vJ}^{\text{tun}}$ is the width of tunnelling out of the quasibound state. An alternate way to formulate eq 13 for calculating the speed of inverse predissociation is[11]

$$k_{\Lambda \to \Lambda'}^{\text{ip}}(T) = \hbar^2 P_\Lambda \left(\frac{2\pi}{\mu k_B T}\right)^{3/2}$$
$$\times \sum_{vJ}(2J+1)\frac{\Gamma_{\Lambda J \to \Lambda'' vJ}^{\text{pre}}\Gamma_{\Lambda'' vJ \to \Lambda'}^{\text{rad}}}{\Gamma_{\Lambda'' vJ \to \Lambda' \text{or} \Lambda J}^{\text{tot}}} \exp(-E_{\Lambda'' vJ}/k_B T)$$

(14)

where Λ'' is the orbital electronic angular momentum quantum number for the predissociatied (quasibound) state, $\Gamma_{\Lambda'' vJ \to \Lambda'}^{\text{rad}}$ is

the total width of the radiative transition from the predissociated state with vibrational quantum number v and rotational quantum number J to any of the bound states, $\Gamma_{\Lambda J \to \Lambda'' vJ}^{\text{pre}}$ is the width of escaping the quasibound state by radiationless transitions to another electronic state, $\Gamma_{\Lambda'' vJ \to \Lambda' \text{or} \Lambda J}^{\text{tot}} = \Gamma_{\Lambda'' vJ \to \Lambda'}^{\text{rad}} + \sum_\Lambda \Gamma_{\Lambda J \to \Lambda'' vJ}^{\text{pre}}$, and $E_{\Lambda'' vJ}$ is the energy of the quasibound vibrational state with Λ'', v, and J.

Electron Detachment. A reaction that possibly could compete with the radiative association processes is electron detachment,

$$O(^3P) + H(^2S) \to OH(1^2\Sigma^-) \to OH^+(X^3\Sigma^-) + e^-$$

(VII)

$$O(^3P) + H(^2S) \to OH(a^4\Sigma^-) \to OH^+(X^3\Sigma^-) + e^-$$

(VIII)

and

$$O(^3P) + H(^2S) \to OH(b^4\Pi) \to OH^+(X^3\Sigma^-) + e^-$$

(IX)
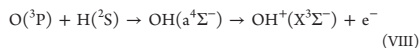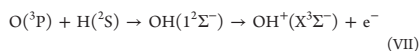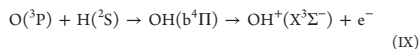
A method to approximate an upper limit to the cross-section of electron detachment can be found in an experimental study on $O^- + H$.[27] In this approximation it is assumed that in all cases when the classical trajectory reaches a point in space where the potential energy surface of the reactants cross the potential energy surface of the ground state of the products, the reaction occurs. According to this approximation the cross-section, $\sigma_{\text{detachment}}(E)$, is

$$\sigma_{\text{detachment}}(E) = \sum_\Lambda P_\Lambda \pi(R_\Lambda^\times)^2 \left[1 - \frac{V_\Lambda(R_\Lambda^\times)}{E}\right]$$

(15)

where $R_\Lambda^\times$ is the distance at which the potential energy surface of the reactant state characterized by Λ and the product state cross. The sum is over all relevant Λ.

Charge Transfer. Apart from electron detachment, another reaction that could compete with the radiative association is charge transfer:

$$O + H \to O^+ + H^-$$

(X)

and

$$O + H \to O^- + H^+$$

(XI)

The threshold energies for these reactions are 12.863880 and 12.13736 eV, respectively (using electron affinities from Lykke et al.[28] and Neumark et al.[29] and ionization energies from Kramida et al.[10]).

Computational Details. For the calculations of the cross sections of reactions I, II, and VII−IX the necessary data were taken from the literature. Potential energy data points for the $X^2\Pi$ and $1^2\Sigma^-$ states and the electrical transition dipole moment between $X^2\Pi$ and $1^2\Sigma^-$ were taken from van Dishoeck et al.[6] The electrical dipole moment of the $X^2\Pi$ state was taken from Langhoff et al.[30] These data points were splined and extrapolated. At long distances the potentials were extrapolated as $\propto 1/R^6$. At short distances the potential energy of the $X^2\Pi$ state was extrapolated as a Morse potential with equilibrium distance and dissociation energy from Huber and Herzberg.[9] The potential energy of the $1^2\Sigma^-$ state was at short distances extrapolated as an exponential function.

The dipole moments were extrapolated as exponential functions going toward zero at long distances and as second-order polynomials going toward zero at short distances. The forms for the extrapolations toward short internuclear distances

were chosen to be simple forms that behave qualitatively correct. Different forms were tested, and it was found that the extrapolation was not important for the resulting reaction rate constant.[31]

The potential energy of the $X^3\Sigma^-$ state of OH^+ was approximated by a Morse potential ($V(R) = D_e\{1 - \exp[a(R - R_e)]\}^2$) with equilibrium distance (R_e) and dissociation energy (D_e) from van Lonkhuyzen and de Lange[8] and a from Huber and Herzberg.[9] The difference in asymptotic energy between $X^2\Pi$ of OH and $X^3\Sigma^-$ of OH^+ was taken to be the ionization energy of hydrogen.[10] All the potential energies and dipole moments used can be seen in Figures 1 and 2.
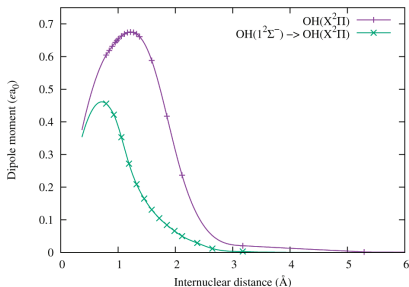
Figure 2. Electric dipole moment of the $X^2\Pi$ state of OH from Langhoff et al.[30] and the electrical transition dipole moment between the $X^2\Pi$ and $1^2\Sigma^-$ states of OH from van Dishoeck et al.[6] e is the elemental charge, and a_0 is the Bohr radius. The points are the original data and the lines are inter- and extrapolations.

The widths of the inverse predissociation (reactions III, IV, V, and VI) were gathered from many different sources. Vibrational quantum numbers up to 4 and rotational quantum numbers up to a maximum of 30 were considered. Total,

radiative, and predissociation lifetimes were mostly taken from Yarkony.[7] Total lifetimes not available in that article were taken from Brzozowski et al.[33] and, where available, predissociation lifetimes were taken from Parlant and Yarkony[34] instead. These lifetimes do not take account of nonradiative coupling between the continuum of $X^2\Pi$ and $A^2\Sigma^+$, so the predissociation widths from Julienne and Krauss[11] taking account of only that coupling were added, and for $v = 1$ they were interpolated. The contributions from different rovibrational states to the predissociation widths for vibrational quantum numbers 3 and 4 were taken from the golden rule calculations for rotational quantum numbers 0 and 14 in Parlant and Yarkony[34] and interpolated for the rotational quantum numbers in between.

Radiative widths were interpolated and a few widths were found by the use of $\Gamma^{tot}_{\Lambda''vJ\to\Lambda'\text{or}\Lambda J} = \Gamma^{rad}_{\Lambda''vJ\to\Lambda'} + \sum_\Lambda \Gamma^{pre}_{\Lambda J\to\Lambda''vJ}$. Energies of the quasibound states were calculated with the spectroscopic constants from Luque and Crosley.[35]

The cross sections for reactions I and II were calculated with the quantum mechanical perturbation theory. The bound wave functions were calculated with discrete variable representation[36] and the unbound wave functions were calculated with Numerov's method.[37]

The cross-section for reaction I was also calculated by combining the classical method with Breit−Wigner theory. The outer classical turning point, R_G, was found by the bisection method, the range of time was found by Romberg integration[38] of dt/dR from R_c to an outer distance limit. dR/dt and $d\theta/dt$ were integrated with the fourth-order Runge−Kutta method,[38] the Fourier transforms were done by fast Fourier transform,[38] the integral over ω was made with Simpson's 1/3 rule,[38] and the integral over b was evaluated with the trapezoidal rule. The cross-section and reaction rate constant for the resonance contribution were calculated by using quasibound state parameters obtained with the program LEVEL, developed by LeRoy.[39]

The cross-section for reaction II was additionally calculated by the semiclassical method. The bisection method was used to

Table 1. Hönl−London Factors $S_{\Lambda J\Omega\epsilon\to\Lambda'J'\Omega'\epsilon'}$ Calculated by the Method of Watson[17] for Hund's Case a[a]

$^{2S+1}\Lambda$	Ω	ϵ	$^{2S+1}\Lambda'$	Ω'	ϵ'	$J' = J - 1$	$J' = J$	$J' = J + 1$
$^1\Pi$	1	± 1	$^1\Pi$	1	± 1	$\frac{(J+1)(J-1)}{J} \approx J$	0	$\frac{J(J+2)}{J+1} \approx J$
$^1\Pi$	1	± 1	$^1\Pi$	1	∓ 1	0	$\frac{2J+1}{J(J+1)} \approx 0$	0
$^1\Sigma^-$	0	-1	$^1\Pi$	1	1	0	$2J+1 \approx 2J$	0
$^1\Sigma^-$	0	-1	$^1\Pi$	1	-1	$J-1 \approx J$	0	$J+2 \approx J$
$^2\Pi$	1/2	± 1	$^2\Pi$	1/2	± 1	$\frac{(J+1/2)(J-1/2)}{J} \approx J$	0	$\frac{(J+3/2)(J+1/2)}{J+1} \approx J$
$^2\Pi$	1/2	± 1	$^2\Pi$	1/2	∓ 1	0	$\frac{J+1/2}{2(J+1)} \approx 0$	0
$^2\Pi$	3/2	± 1	$^2\Pi$	3/2	± 1	$\frac{(J+3/2)(J-3/2)}{J} \approx J$	0	$\frac{(J+5/2)(J-1/2)}{J+1} \approx J$
$^2\Pi$	3/2	± 1	$^2\Pi$	3/2	∓ 1	0	$\frac{9(J+1/2)}{2(J+1)} \approx 0$	0
$^2\Sigma^-$	1/2	± 1	$^2\Pi$	1/2	± 1	$\frac{(J+1/2)(J-1/2)}{2J} \approx \frac{J}{2}$	0	$\frac{(J+3/2)(J+1/2)}{2(J+1)} \approx \frac{J}{2}$
$^2\Sigma^-$	1/2	± 1	$^2\Pi$	1/2	∓ 1	0	$\frac{(J+1/2)^3}{J(J+1)} \approx J$	0
$^2\Sigma^-$	1/2	± 1	$^2\Pi$	3/2	± 1	$\frac{(J-1/2)(J-3/2)}{2J} \approx \frac{J}{2}$	0	$\frac{(J+5/2)(J+3/2)}{2(J+1)} \approx \frac{J}{2}$
$^2\Sigma^-$	1/2	± 1	$^2\Pi$	3/2	∓ 1	0	$\frac{(J+3/2)(J+1/2)(J-1/2)}{J(J+1)} \approx J$	0

[a]The approximations are valid for large J. ϵ is parity and Ω is the quantum number of the projection of the total electronic angular momentum on the internuclear axis.

find the classical turning point, the integral over R was evaluated with the Romberg method,[38] and the integral over b was calculated with the trapezoidal rule.

The direct (nonresonant) contribution to the rate constants acquired by integration of the cross-section over the energy (eq 1) was calculated with the trapezoidal rule.

The programs used here are available with Hönl−London factors for singlets. Looking at Table 1, we can see that for the transitions relevant here this is a good approximation for large J, except for $\Sigma \rightarrow \Pi$ transitions where an extra factor of 0.5 appears. This factor is, however, accounted for by summation over $\Omega'\epsilon'$. The summation over $\Omega\epsilon$ is not done explicitly in the calculations of the cross sections, but it is instead taken care of by multiplication by the factor P_Λ. In Table 2 the Hönl-London factors and P_Λ used in the calculations can be seen.

Table 2. Hönl−London Factors $S_{\Delta J \rightarrow \Lambda' J'}$ and Statistical Weight Factors P_Λ Used for the Calculations of the Rate Constant for Reactions I and II

	$S_{\Lambda\ J \rightarrow \Lambda' J-1}$	$S_{\Lambda\ J \rightarrow \Lambda' J}$	$S_{\Lambda\ J \rightarrow \Lambda' J+1}$	P_Λ
$X^2\Pi \rightarrow X^2\Pi$	$\frac{(J+1)(J-1)}{J}$	$\frac{2J+1}{J(J+1)}$	$\frac{J(J+2)}{J+1}$	4/18
$1^2\Sigma^- \rightarrow X^2\Pi$	$J-1$	$2J+1$	$J+2$	2/18

When the cross sections were calculated, they were considered converged when the corresponding reaction rate constant at all considered temperatures had converged to within 0.5% with respect to the individual computational parameters.

■ RESULTS AND DISCUSSION

The calculated cross sections can be seen in Figure 3. For the $X^2\Pi \rightarrow X^2\Pi$ pathway the quantum mechanical perturbation
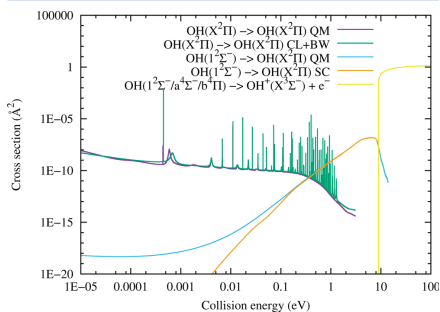
Figure 3. Reaction cross sections for reaction I calculated by the quantum mechanical method (QM) and the classical method with Breit−Wigner theory added (CL+BW), for reaction II calculated by the quantum mechanical method (QM) and the semiclassical method (SC), and for reactions VII−IX by the use of eq 15.

theory and the combined classical/Breit−Wigner methods for calculating the cross-section result in very similar baselines, apart from at high and low energies. With the Breit−Wigner theory we have, however, found many more resonances than with the quantum mechanical perturbation theory. This is likely

to be due to the energy resolution of the quantum calculation, but for the purpose of this work the comparison is satisfactory.

For the $1^2\Sigma^- \rightarrow X^2\Pi$ pathway the semiclassical and quantum mechanical cross sections are almost identical for a large range of energies. The semiclassical program could not calculate cross sections at as high energies as the quantum mechanical program due to limitations in the semiclassical computational procedure. The semiclassical cross-section will, however, approach zero very quickly for the high energies where it is not plotted, due to the Franck−Condon principle.[40,41] It can be seen in Figure 4
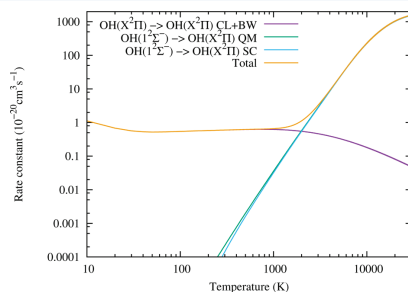
Figure 4. Reaction rate constants for reaction I calculated with the classical method and Breit−Wigner theory (CL+BW), for reaction II calculated with the golden rule (QM) and semiclassical method (SC), and for both reactions summed (Total).

that the semiclassical and quantum mechanical rate constants are nearly indistinguishable, so the differences in cross-section at high energies do not affect the rate constant at the studied temperatures. Further the electron detachment reaction only matters at energies above 9 eV. Also because the charge transfer reactions X and XI have threshold energies of >12 eV, which is noticeably higher than the energy where the electron detachment starts to dominate, they are not important for our study.

At most temperatures we assume $a^4\Sigma^-$ to be the most important collision state for the inverse predissociation process,[7] and this electronic state is not relevant for the other radiative association pathways, meaning that even if reactions I and III, or II and IV would interfere with each other, it would not affect the total reaction rate noticeably for those temperatures. For low temperatures both reactions I and III make noticeable contributions to the total reaction rate. Because both these reactions occur via the state $X^2\Pi$ they could possibly affect one another. However, the interference between the processes will most likely not give a noticeable difference, because none of the resonances in the different pathways overlap.

The total reaction rate constant is plotted versus temperature in Figure 5, where the importance of the inverse predissociation is seen. The previous estimation for the rate constant for inverse predissociation[12] was obtained up to 400 K and stayed below 3×10^{-20} cm^3 s^{-1} at those temperatures. The parameters obtained by fitting the total rate constant to the Kooij formula,[42] which is the form on which this kind of rate constants are often presented in databases such as KIDA, can be seen in Table 3. The fit is within 5% of the rate constant. As shown in Figure 5, the rate constant already present in, for
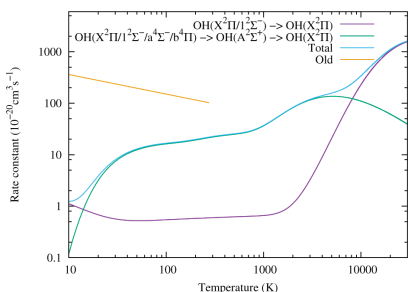
Figure 5. Reaction rate constant for the combination of reactions I and II, for the combination of reactions III−VI, and for the total of all these reactions. Also an older total reaction rate constant, taken from KIDA,[13] is shown.

Table 3. Reaction Rate Constants Fitted to the Kooij Formula[42] [Written as $k_{\Lambda \to \Lambda'}(T) = \alpha(T/300 \text{ K})^\beta \exp(-\gamma/T)$] in a Few Different Temperature Intervals[a]

temp interval (K)	α (10^{-20} cm^3 s^{-1})	β	γ (K)
10−20	249551	4.90741	−44.3485
20−100	18.4379	−0.366037	50.6067
100−500	22.7637	0.259761	4.71068
500−2000	2.17451	1.72564	−776.051
2000−5000	262.168	−0.0290599	2184.05
5000−15000	0.00646257	2.78182	−11183.4
15000−30000	85814.4	−0.593255	37216

[a]The fit is within 5% of the original reaction rate constant.

example, KIDA is larger than the one calculated in this study.[43] The rate constant calculated in the present work should be an improvement over the old one, because this new rate constant includes all the reactions I−VI and has values for a larger temperature interval.

CONCLUSIONS

The reaction rate constant for the radiative association of O(^{3}P) and H(^{2}S) into OH(X^{2}Π) has been calculated for the temperature range 10−30000 K. The calculation includes direct and shape-resonance-mediated radiative association, as well as inverse predissociation, and has been conducted by using a few different methods for the different pathways of the reaction. This rate constant is expected to be interesting for inclusion in astrochemical databases, because it has a much larger temperature interval than the rate constant already available in for example KIDA[13] and the UMIST database for astrochemistry.[14]

AUTHOR INFORMATION

Corresponding Author

*G. Nyman. E-mail: nyman@chem.gu.se. Phone: +46 (0)31 7869035.

Notes

The authors declare no competing financial interest.

REFERENCES

(1) Weinreb, S.; Barret, A.; Meeks, M.; Henry, J. Radio Observations of OH in the Interstellar Medium. *Nature* **1963**, *200*, 829−831.

(2) Weliachew, L. Detection of Interstellar OH in Two External Galaxies. *Astrophys. J.* **1971**, *167*, L47−L52.

(3) Sternberg, A.; Dalgarno, A.; Pei, Y.; Herbst, E. In *Conditions and Impact of Star Formation*; Röllig, M., Simon, R., Ossenkopf, V., Stutzki, J., Eds.; EAS Publications Series, 52; European Astronomical Society: Geneva, 2011; pp 43−46.

(4) Bohlin, R. C.; Savage, B. D.; Drake, J. F. A Survey of Interstellar H I from L$_\alpha$ Absorption Measurments. II. *Astrophys. J.* **1978**, *224*, 132−142.

(5) Meyer, D. M.; Jura, M.; Cardelli, J. A. The Definite Abundance of Interstellar Oxygen. *Astrophys. J.* **1998**, *493*, 222−229.

(6) van Dishoeck, E. F.; Langhoff, S. R.; Dalgarno, A. The Low-Lying $^2\Sigma^-$ States of OH. *J. Chem. Phys.* **1983**, *78*, 4552−4561.

(7) Yarkony, D. A Theoretical Treatment of the Predissociation of the Individual Rovibronic Levels of OH/OD($A^2\Sigma^+$). *J. Chem. Phys.* **1992**, *97*, 1838−1849.

(8) van Lonkhuyzen, H.; de Lange, C. A. U. V. Photoelectron Spectroscopy of OH and OD Radicals. *Mol. Phys.* **1984**, *51*, 551−568.

(9) Huber, K. P.; Herzberg, G. *Constants of Diatomic Molecules*; Molecular Spectra and Molecular Structure; Van Nostrand Reinhold Co.: New York, 1979; Vol. 4.

(10) Kramida, A.; Ralchenko, Y.; Reader, J.; Team, N. A. NIST Atomic Spectra Database, ver. 5.2. http://physics.nist.gov/asd (accessed 150309), 2014; National Institute of Standards and Technology, Gaithersburg, MD.

(11) Julienne, P. S.; Krauss, M. In *Molecules in the Galactic Environment*; Gordon, M. A., Snyder, L. E., Eds.; John Wiley & Sons: New York, 1973; pp 353−373.

(12) Julienne, P. S.; Krauss, M.; Donn, B. Formation of OH Through Inverse Predissociation. *Astrophys. J.* **1971**, *170*, 65−70.

(13) Wakelam, V.; Herbst, E.; Loison, J.-C.; Smith, I. W. M.; Chandrasekaran, V.; Pavone, B.; Adams, N. G.; Bacchus-Montabonel, M.-C.; Bergeat, A.; Béroff, K.; et al. A Kinetic Database for Astrochemistry (KIDA). *Astrophys. J. Suppl. Ser.* **2012**, *199*, 21-1−21-10 (the actual database can be found at the URL http://kida.obs.u-bordeaux1.fr).

(14) McElroy, D.; Walsh, C.; Markwick, A. J.; Cordiner, M. A.; Smith, K.; Millar, T. J. The UMIST Database for Astrochemistry 2012. *Astron. Astrophys.* **2013**, *550*, A36-1−A36-13 (the actual database can be found at the URL http://www.udfa.net/).

(15) Babb, J. F.; Dalgarno, A. Radiative Association and Inverse Predissociation of Oxygen Atoms. *Phys. Rev. A: At., Mol., Opt. Phys.* **1995**, *51*, 3021−3026.

(16) Barinovs, Ģ.; van Hemert, M. C. CH$^+$ Radiative Association. *Astrophys. J.* **2006**, *636*, 923−926.

(17) Watson, J. K. G. Hönl-London Factors for Multiplet Transitions in Hund's Case a or b. *J. Mol. Spectrosc.* **2008**, *252*, 5−8.

(18) Julienne, P. S. Theory of Rare Gas-Group VI 1 S-1 D Collision-Induced Transitions. *J. Chem. Phys.* **1978**, *68*, 32−41.

(19) Bates, D. R. Rate of Formation of Molecules by Radiative Association. *Mon. Not. R. Astron. Soc.* **1951**, *111*, 303−314.

(20) Zygelman, B.; Dalgarno, A. Radiative Quenching of He(2 ^{1}S) Induced by Collisions with Ground-State Helium Atoms. *Phys. Rev. A: At., Mol., Opt. Phys.* **1988**, *38*, 1877−1884.

(21) Gustafsson, M.; Antipov, S. V.; Franz, J.; Nyman, G. Refined Theoretical Study of Radiative Association: Cross Sections and Rate Constants for the Formation of SiN. *J. Chem. Phys.* **2012**, *137*, 104301.

(22) Jackson, J. D. *Classical Electrodynamics*; John Wiley and Sons Ltd.: New York, 1962.

(23) Gustafsson, M. Classical Calculations of Radiative Association in Absence of Electronic Transitions. *J. Chem. Phys.* **2013**, *138*, 074308.

(24) Bennett, O.; Dickinson, A.; Leininger, T.; Gadéa, F. Radiative Association in Li+H Revisited: The Role of Quasi-Bound States. *Mon. Not. R. Astron. Soc.* **2003**, *341*, 361–368.

(25) Bain, R. A.; Bardsley, J. N. Shape Resonances in Atom-Atom Collisions - I. Radiative Association. *J. Phys. B: At. Mol. Phys.* **1972**, *5*, 277–285.

(26) Breit, G.; Wigner, E. Capture of Slow Neutrons. *Phys. Rev.* **1936**, *49*, 519–531.

(27) Fedchak, J. A.; Huels, M. A.; Doverspike, L. D.; Champion, R. L. Electron Detachment and Charge Transfer for Collisions of O^- and S^- with H. *Phys. Rev. A: At., Mol., Opt. Phys.* **1993**, *47*, 3796–3800.

(28) Lykke, K. R.; Murray, K. K.; Lineberger, W. C. Threshold Photodetachment of H^-. *Phys. Rev. A: At., Mol., Opt. Phys.* **1991**, *43*, 6104–6107.

(29) Neumark, D. M.; Lykke, K. R.; Andersen, T.; Lineberger, W. C. Laser Photodetachment Measurment of the Electron Affinity of Atomic Oxygen. *Phys. Rev. A: At., Mol., Opt. Phys.* **1985**, *32*, 1890–1892.

(30) Langhoff, S. R.; Bauschlicher, C. W.; Taylor, P. R. Theoretical Study of the Dipole Moment Function of OH($X^2\Pi$. *J. Chem. Phys.* **1989**, *91*, 5953–5959.

(31) It has come to our attention that there are more recent calculations of the potential energies and transition dipole moments for OH than those used here.[32] Most notably these have values for shorter internuclear distances than those used in the present study, meaning that we could have extrapolated less. However, because the forms of the extrapolations were not important for the reaction rate constants, the use of the newer and better potentials and transition dipole moments would most likely not have changed the results of this study noticeably.

(32) van der Loo, M. P. J.; Groenenboom, G. C. Ab Initio Calculation of (2 + 1) Resonance Enhanced Multiphoton Ionization Spectra and Lifetimes of the (D,3) $^2\Sigma^-$ States of OH and OD. *J. Chem. Phys.* **2005**, *123*, 074310.

(33) Brzozowski, J.; Erman, P.; Lyyra, M. Precision Estimates of the Predissociation Rates of the OH $A^2\Sigma$ State ($v \leq 2$). *Phys. Scr.* **1978**, *17*, 507–511.

(34) Parlant, G.; Yarkony, D. A Theoretical Analysis of the State-Specific Decomposition of OH($A^2\Sigma^+$,v',N',F1/F2) Levels, Including the Effects of Spin-Orbit and Coriolis Interactions. *J. Chem. Phys.* **1999**, *110*, 363–376.

(35) Luque, J.; Crosley, D. Transition Probabilities in the $A^2\Sigma^+ - X^2\Pi_i$ Electronic System of OH. *J. Chem. Phys.* **1998**, *109*, 439–448.

(36) Colbert, D. T.; Miller, W. H. A Novel Discrete Variable Representation for Quantum Mechanical Reactive Scattering via the Smatrix Kohn Method. *J. Chem. Phys.* **1992**, *96*, 1982–1991.

(37) Noumerov, B. A Method of Extrapolation of Perturbations. *Mon. Not. R. Astron. Soc.* **1924**, *84*, 592–602.

(38) Press, W. H.; Teukolsky, S. A.; Vetterling, W. T.; Flannery, B. P. *Numerical Recipes in FORTRAN - The Art of Scientific Computing*, 2nd ed.; Cambridge University Press: Cambridge, U.K., 1992.

(39) Roy, R. J. L. LEVEL 8.0 A Computer Program for Solving the Radial Schrödinger Equation for Bound and Quasibound Levels. University of Waterloo Chemical Physics Research Report CP-663, 2007; Including corrections as of December 2012.

(40) Franck, J.; Dymond, E. G. Elementary Processes of Photochemical Reactions. *Trans. Faraday Soc.* **1926**, *21*, 536–542.

(41) Condon, E. U. Nuclear Motions Associated with Electron Transitions in Diatomic Molecules. *Phys. Rev.* **1928**, *32*, 858–872.

(42) Kooij, D. M. Über die Zersetzung des Gasförmigen Phosphorwasserstoffs. *Z. Phys. Chem.* **1893**, *12*, 155–161.

(43) We have unsuccessfully tried to trace the original source of the rate constant available in KIDA.

Paper II

Dynamics of Gaussian Wigner functions derived from a time-dependent variational principle

---

Dynamics of Gaussian Wigner functions derived from a time-dependent variational principle

Jens Aage Poulsen,[a] S. Karl-Mikael Svensson,[b] and Gunnar Nyman[c]
*Department of Chemistry and Molecular Biology, University of Gothenburg,
41296 Gothenburg, Sweden*

By using a time-dependent variational principle formulated for Wigner phase-space functions, we obtain the optimal time-evolution for two classes of Gaussian Wigner functions, namely those of either thawed real-valued or frozen but complex Gaussians. It is shown that tunneling effects are approximately included in both schemes. © 2017 Author(s). *All article content, except where otherwise noted, is licensed under a Creative Commons Attribution (CC BY) license (http://creativecommons.org/licenses/by/4.0/).* https://doi.org/10.1063/1.5004757

I. INTRODUCTION

Many times, the correct description of processes in molecular systems requires inclusion of quantum statistical effects. An obvious example is that of chemical reactions in small molecular systems that may be treated accurately (see e.g. Refs. 1 and 2). However, for processes in much larger systems, quantum effects still may play an important role, but here one must resort to more approximate methods. Molecular diffusion at low temperature[3] is one such example. For such problems, many approximate schemes have been put forth. Among these we mention the family of path integral-based approches such as Ring Polymer Molecular Dynamics,[4] Centroid Molecular Dynamics[5] and Path Integral Liouville dynamics.[6] Also, various implementations of the so-called Classical Wigner model or Linearized Semi-Classical Initial Value Representation[7–10] have been quite successful. Common for all these methods is that they are exact in the high temperature limit, but also that they are unable to account for some genuine quantum effects, such as tunneling through barriers. The interested reader may consult e.g. Ref. 10 where some of these methods were tested on model problems. In this article we consider a computational method, which is also aimed at modeling dynamical quantum effects in many-body systems. It adopts a variational principle for minimizing the error between exact and approximate quantum dynamics. The variational principle is put to work in Wigners phase-space formulation of quantum mechanics.[11,12]

The Wigner phase-space formulation of quantum mechanics[12] represents an alternative to path integral methods. This formulation has a mathematical structure which closely resembles that found in classical statistical mechanics. Indeed, operator averages may instead be computed using classical-like phase-space averages over so-called Wigner distribution functions, and the dynamics of Wigner functions follow equations of motion which are extensions of those of Newton. Given these desirable properties, a large body of litterature on Wigners formulation of quantum mechanics has been published, and we refer to the famous articles collected in the textbook by Zachos et al.[12]

In Wigners formulation, the Wigner function representation of the density operator plays a central role:

$$[\hat{\rho}]_W(q, p; t) \equiv \int_{-\infty}^{\infty} d\eta \, e^{-ip\eta/\hbar} \left\langle q + \frac{\eta}{2} \left| \hat{\rho}(t) \right| q - \frac{\eta}{2} \right\rangle. \tag{1}$$

[a]jens72@chem.gu.se
[b]karl.mikael.svensson@chem.gu.se
[c]nyman@chem.gu.se

The density operator may be time-dependent and its Wigner distribution evolves according to the Wigner-Moyal equation:[12]

$$\frac{d}{dt}[\hat{\rho}]_W(q,p;t) = \mathcal{L}[\hat{\rho}]_W(q,p;t), \tag{2}$$

where the Liouvillian is given by

$$\mathcal{L} = -\frac{p}{m}\frac{\partial}{\partial q} + V'(q)\frac{\partial}{\partial p} - \frac{\hbar^2}{24}V'''(q)\frac{\partial^3}{\partial p^3} + .. \tag{3}$$

This evolution equation is general and applies to all time-dependent Wigner functions. Also, the important problem of computing quantum correlation functions can be formulated in Wigner phase-space. To see this, we use the identity,

$$\left\langle \hat{A}(t)\hat{B}(0) \right\rangle = \frac{1}{Z} Tr \left(e^{i\hat{H}t/\hbar} e^{-\hat{H}/k_B T} \hat{A} \, e^{-i\hat{H}t/\hbar} \hat{B} \right)$$

$$= \frac{1}{Z}\frac{1}{2\pi\hbar} \int_{-\infty}^{\infty} dpdq \, [e^{-\hat{H}/k_B T}\hat{A}]_W(q,p;t)[\hat{B}]_W(q,p). \tag{4}$$

Thus the calculation of correlation functions is equivalent to the problem of evolving the more general functions $[e^{-\hat{H}/k_B T}\hat{A}]_W(q,p;t)$ in Wigner phase-space. In Ref. 13 we derived a time-dependent variational principle that enables one to propagate a general parameter-dependent Wigner-function in an optimal way. This principle can be considered as a generalization of the Dirac-Frenkel variational principle for wavefunctions.[14]

In this paper we consider two different classes of Wigner functions that are parameter-dependent. Using the variational principle, we derive the equations of motion for their variational parameters and apply the dynamical theory for calculating various time-dependent expectation values for a particle in a quartic and a double well potential.

This paper is organized as follows: An introduction to the variational principle is presented in Section II. Sections III and IV apply the theory for calculating the time propagation of two different forms of Gaussian Wigner functions. Various applications of the theory and comparison to accurate results are also presented in these Sections. The conclusions are presented in Section V.

II. FORMULATION OF VARIATIONAL PRINCIPLE

Consider the propagation of a Wigner function through Eq.2. We will assume that the Wigner function is time-dependent through a vector of parameters $\vec{\theta}$. Hence, our problem is to find the optimum time evolution of $\vec{\theta}(t)$. This was the problem we solved in Ref. 13 by utilizing the time-dependent variational principle. The principle can be explained by considering the functional

$$J[\vec{\theta}, \dot{\vec{\theta}}] = \int_0^t ds \left\langle \rho(q,p;\vec{\theta}(s)), \{\mathcal{L} - \frac{\partial}{\partial s}\}\rho(q,p;\vec{\theta}(s)) \right\rangle$$

$$= \int_0^t ds \left\langle \rho(q,p;\vec{\theta}(s)), \{\mathcal{L} - \dot{\vec{\theta}} \cdot \nabla_{\vec{\theta}}\}\rho(q,p;\vec{\theta}(s)) \right\rangle. \tag{5}$$

Here, $\mathcal{L}$ is the Liouvillian and the general scalar-product between two Wigner functions has been introduced:

$$\langle A_W(q,p;t), B_W(q,p;t) \rangle = \int\int \frac{dqdp}{2\pi\hbar} A_W^*(q,p;t)B_W(q,p;t). \tag{6}$$

The time integration in Eq.5 goes from $s = 0$ to $s = t$, which is the time-window of interest. The action principle states that $J[\vec{\theta}, \dot{\vec{\theta}}]$ is stationary with respect to *complex* variations $\delta\vec{\theta}(s)$ (that vanish at end-points) if and only if $\vec{\theta}(s)$ is the optimum "path" in a least squares sense, i.e. so that the error

$$Error = \left\langle \{\mathcal{L} - \frac{\partial}{\partial s}\}\rho(q,p;\vec{\theta}(s)), \{\mathcal{L} - \frac{\partial}{\partial s}\}\rho(q,p;\vec{\theta}(s)) \right\rangle \tag{7}$$

is minimized along the path. To find the path that extremizes the functional, we use the Euler-Lagrange equations:

$$\frac{\partial}{\partial s}\{\frac{\partial}{\partial \dot{\theta}_i}\}J[\vec{\theta}, \dot{\vec{\theta}}] = \frac{\partial}{\partial \theta_i}J[\vec{\theta}, \dot{\vec{\theta}}], \tag{8}$$

where $\dot{\theta}_i$ is the time-derivative of the $i'th$ entry of the θ vector, θ_i etc. We notice that the Wigner function should be an analytic - differentiable - function of its complex variational parameters, otherwise, the equivalence between Eq.5 and Eq.7 does not hold.

III. VARIATIONAL PRINCIPLE FOR THAWED REAL-VALUED GAUSSIANS

A. Equations of motion

In this Section we consider the following ansatz for the variational "Wigner packet":

$$\rho(q, p; t) = \rho(q, p; q_0(t), p_0(t), \alpha(t), \gamma(t), \beta(t))$$

$$= N(t) \exp\{-\begin{pmatrix} q - q_0(t) \\ p - p_0(t) \end{pmatrix}^T \begin{pmatrix} \alpha(t) & \gamma(t) \\ \gamma(t) & \beta(t) \end{pmatrix} \begin{pmatrix} q - q_0(t) \\ p - p_0(t) \end{pmatrix}\}, \tag{9}$$

where $N(t)$ is a normalization constant. Thus, the variational parameters are $\alpha(t)$, $\beta(t)$, $\gamma(t)$, $q_0(t)$ and $p_0(t)$. We will be interested in real-valued parameter "trajectories" $\vec{\theta}(s)$ and, as we will see, a real-valued initial set of parameters stay real for all times. By substituting Eq.9 into Eq.5 and evaluating the Euler-Lagrange equations, we derive the equation of motions for the five parameters. We refer the interested reader to the supplementary material. Here, we simply state the result:

$$\begin{pmatrix} \dot{q}_0(t) \\ \dot{p}_0(t) \\ \dot{\alpha}(t) \\ \dot{\gamma}(t) \\ \dot{\beta}(t) \end{pmatrix} = \begin{pmatrix} p_0(t)/M \\ -\dfrac{d}{dq_0} V_{sm}(q_0(t)) \\ 2\gamma(t) \times M\Omega^2(q_0(t)) \\ \beta(t) \times M\Omega^2(q_0(t)) - \dfrac{\alpha(t)}{M} \\ -2\dfrac{\gamma(t)}{M} \end{pmatrix}, \tag{10}$$

where the effective frequency $\Omega(q_0)$ has been defined by:

$$M\Omega^2(q_0) = \frac{d^2}{dq_0^2} V_{sm}(q_0). \tag{11}$$

In these equations, the time-dependent smeared potential

$$V_{sm}(q_0) = \frac{1}{\sqrt{\pi \hbar^2 \beta'(t)}} \int_{-\infty}^{+\infty} dy V(y) \exp\left(-\frac{(q_0 - y)^2}{\beta'(t)\hbar^2}\right), \tag{12}$$

where

$$\beta'(t) = \frac{1}{2\hbar^2} \frac{\beta(t)}{\alpha(t)\beta(t) - \gamma(t)^2} + \frac{1}{2}\beta(t), \tag{13}$$

has appeared. As is easily shown, the product $\alpha(t)\beta(t) - \gamma(t)^2$ is a constant of motion. In the special case of a minimum uncertainty Wigner-function (which corresponds to a wave-function), we have $\alpha(t)\beta(t) - \gamma(t)^2 = 1/\hbar^2$ and then $\beta'(t) = \beta(t)$. Also, the above solution is exact for quadratic potentials. We notice that the Dirac-Frenkel principle has been applied for complex Gaussian wavefunctions in Ref. 16 in the context of photodissociation spectroscopy. Also, see Ref. 17. In the case, $\alpha(t)\beta(t) - \gamma(t)^2 = 1/\hbar^2$, these methods and our are equivalent.

B. Kubo position auto correlation function

Here we show that the thawed Gaussians via Eq.9 can be used for calculating so-called Kubo transformed thermal position auto correlation functions. Because the variational principle is formulated in Wigner phase-space we can solve quantum-statistical problems with no reference to wave functions. As shown in Appendix A, by adopting the so-called Feynman-Kleinert approximation to

the Boltzmann-operator, one can derive an approximate expression for the Kubo transformed position auto correlation function:

$$\langle xx(t) \rangle_{Kubo} = \frac{1}{Z_{FK}} \int dx_c x_c \exp(-W_1(x_c)/k_B T)$$

$$\times \frac{1}{(2\pi\hbar)^2} \int \int dq dp q \exp(t\mathcal{L}) 2 \sqrt{\frac{\pi 2 M k_B T \tanh(\frac{\hbar\Omega(x_c)}{2k_B T})}{\alpha(x_c)}}$$

$$\times \exp(-\frac{M\Omega(x_c)}{\hbar\alpha(x_c)}(q - x_c)^2) \exp(-\frac{\tanh(\frac{\hbar\Omega(x_c)}{2k_B T})}{\hbar M \Omega(x_c)} p^2). \tag{14}$$

This expression is exact to the extent that the Feynman-Kleinert approximation is. The equation is evaluated by Monte Carlo sampling using the weight function derived from the centroid potential: $\exp(-W_1(x_c)/k_B T)$. Clearly, the problem is to propagate the normalized Gaussian Wigner function:

$$\rho_{x_c}(q,p) = 2 \sqrt{\frac{\tanh(\frac{\hbar\Omega(x_c)}{2k_B T})}{\alpha(x_c)}} \exp(-\frac{M\Omega(x_c)}{\hbar\alpha(x_c)}(q - x_c)^2) \exp(-\frac{\tanh(\frac{\hbar\Omega(x_c)}{2k_B T})}{\hbar M \Omega(x_c)} p^2), \tag{15}$$

which is similar to Eq.9 and so can be propagated using Eq.10.

C. Application to double well potential

We first test the method against a model problem where tunneling dynamics is important. We consider the double well potential $V(x) = -0.5x^2 + 0.1x^4$. We adopt natural units: $\hbar = k_B = m = 1$. First, we will consider a pure state, i.e. the propagation of a Wigner function corresponding to a wave-function. The initial Wigner function or wave function is chosen as follows. We approximate the ground state wave function as a sum of two Gaussian wave functions:

$$\psi(x) = N[\exp(-\frac{\lambda}{2}(x - x_0)^2) + \exp(-\frac{\lambda}{2}(x + x_0)^2)]. \tag{16}$$

By minimizing the energy of this wave function with respect to λ and x_0 we obtain $\lambda = 1.23$ and $x_0 = 1.12$. We next consider the intial Wigner function to be equivalent to one half of the above wavefunction, i.e. the Gaussian in the right well. Its Wigner function thus becomes as in Eq.9 with $\alpha = 1.23$, $\beta = 1/1.23$, $\gamma = 0$, $q_0 = 1.12$ and $p_0 = 0$. The time-dependent effective potential is

$$V_{sm}(x) = -0.5(x^2 + \frac{1}{2}\beta(t)\hbar^2) + 0.1x^4 + 0.3\beta(t)\hbar^2 x^2 + 0.1\frac{3}{4}\beta(t)^2\hbar^4. \tag{17}$$

In Figure 1, the time-dependent average position of the Wigner function based on the variational method is shown. Also shown are accurate results as well as the predictions of the so-called classical
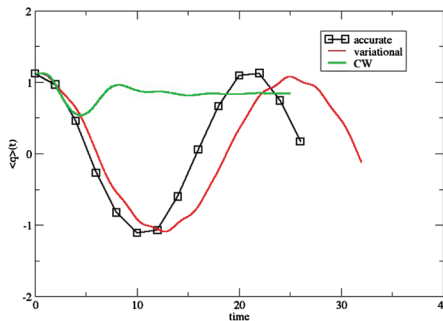
FIG. 1. Average position for a particle in the double well starting from a single Gaussian using $q_0 = 1.12$, $p_0 = \gamma(0) = 0$, $\alpha(0) = 1.23$ and $\beta(0) = 1/1.23$.
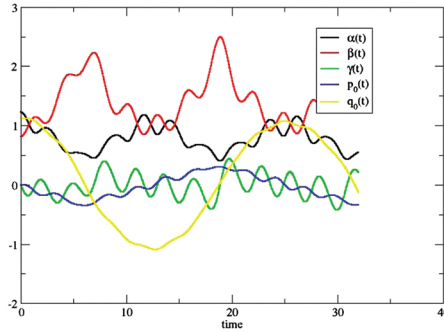
FIG. 2. Time-development of variational parameters.

Wigner approximation, where the Wigner function is propagated classically assuming (falsely) that Liouvilles theorem holds: $\rho(q, p; t) = \rho(q_{-t}, p_{-t}; 0)$. While the latter method clearly fails dramatically, it is seen that the variational method is capable of accounting for tunneling through the barrier. In Figure 2 is shown the time-development of the variational parameters. We see that $\beta'(t) = \beta(t)$ grows in magnitude which in turn lowers the smeared potential barrier thereby making it possible to pass the barrier. To further investigate the performance of the variational method, we repeated the above test with different double well potentials on the form $V(x) = -ax^2 + bx^4$. Thus a sequence of potentials were generated, keeping the potential height as above, but using different widths. For each case, the tunneling period was extracted from accurate and variational dynamics. The results are presented in Figure 3. We see that the variational method does a good job for narrow potentials but eventually fails as the barrier widens.

We next consider the calculation of the Kubo-transformed position correlation function of the double well. We show results from variational theory, accurate calculations as well as the classical Wigner model. In Figures 4 and 5 are results for an inverse temperature of 8 and 1, respectively. For $1/k_B T = 8$ it is seen that the variational method is in fairly good agreement with the accurate results. Again, the classical Wigner model performs badly. At $1/k_B T = 1$, the variational method actually performs less well as compared to $1/k_B T = 8$: It correctly predicts tunneling but roughly twice as fast as it should be.
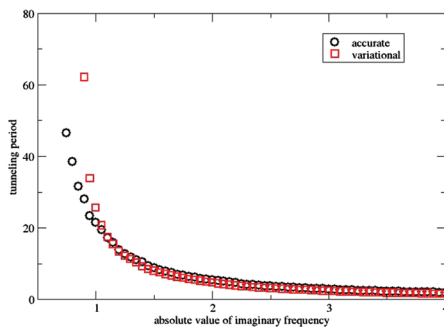
FIG. 3. Vibrational period of double well potential as a function of barrier width (imaginary frequency).
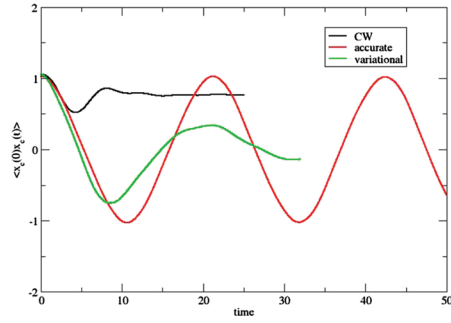
FIG. 4. Kubo double well position correlation function at $1/k_B T = 8$.
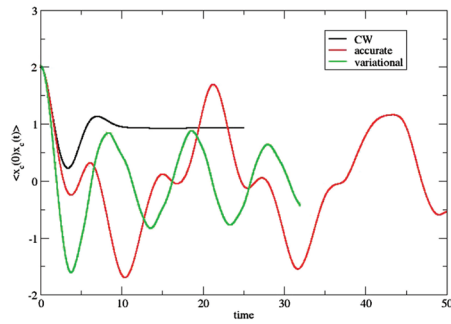
FIG. 5. Kubo double well position correlation function at $1/k_B T = 1$.
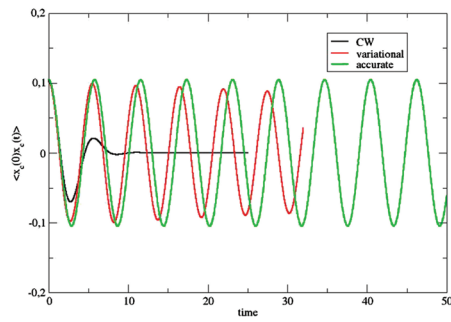
FIG. 6. Kubo quartic position correlation function at $1/k_B T = 8$.
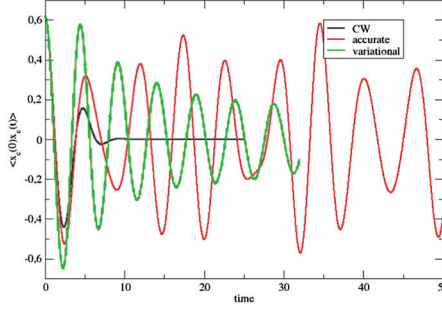
FIG. 7. Kubo quartic position correlation function at $1/k_B T = 1$.

D. Application to quartic potential

We consider the potential $V(x) = 0.25x^4$. We again adopt natural units: $\hbar = k_B = m = 1$. In Figures 6 and 7 are shown the Kubo-transformed correlation functions obtained from variational theory, accurate calculations and the classical Wigner model. We observe a good agreement between accurate and variational methods at $1/k_B T = 8$, while at $1/k_B T = 1$ the amplitude given by the variational method is too large before it dephases.

IV. VARIATIONAL PRINCIPLE FOR COMPLEX-VALUED FROZEN GAUSSIANS

A. Equations of motion

In this Section we consider the following ansatz for the variational "Wigner packet":

$$\rho(q, p; t) = \rho(q, p; \xi(t), q_0(t), p_0(t)) = \exp\{i\xi(t)\}$$
$$\times \exp\{-\binom{q - q_0(t)}{p - p_0(t)}^T \begin{pmatrix} \alpha & 0 \\ 0 & \beta \end{pmatrix} \binom{q - q_0(t)}{p - p_0(t)}\}. \tag{18}$$

The variational parameters are $(\xi(t), q_0(t), p_0(t))$. Let us write $\theta = (\xi, q_0, p_0)$, and introduce the writing: $\rho(q, p; t) = \rho(q, p; \xi(t), q_0(t), p_0(t)) = \rho(q, p; \theta(t))$. The parameters will be considered complex and hence we write $q_0(t) = q_r(t) + iq_i(t)$ etc. As shown in the supplementary material, when substituting Eq. 18 into Eq. 5 the resulting equations of motion are

$$\begin{pmatrix} \dot{q}_r \\ \dot{p}_r \\ \dot{q}_i \\ \dot{p}_i \\ \dot{\xi}_r \\ \dot{\xi}_i \end{pmatrix} = \begin{pmatrix} p_r/M \\ -\dfrac{d}{dq_r} \dfrac{V_{sm}(q_r - \hbar p_i \beta) + V_{sm}(q_r + \hbar p_i \beta)}{2} \\ \dfrac{1}{\alpha \beta \hbar^2} \dfrac{d}{dp_i} \dfrac{V_{sm}(q_r - \hbar p_i \beta) + V_{sm}(q_r + \hbar p_i \beta)}{2} \\ -\dfrac{\alpha}{\beta M} q_i \\ \dfrac{V_{sm}(q_r + \hbar p_i \beta) - V_{sm}(q_r - \hbar p_i \beta)}{\hbar} - 2\beta \dfrac{V'_{sm}(q_r - \hbar p_i \beta) + V'_{sm}(q_r + \hbar p_i \beta)}{2} p_i \\ \dfrac{d}{dt}\{\beta p_i^2 + \alpha q_i^2\} \end{pmatrix}. \tag{19}$$

Here, V'_{sm} means $\frac{d}{dq_r} V_{sm}$. The smeared potential is calculated as in Eq. 12 but now with $\beta' = \frac{1}{2\hbar^2} \frac{1}{\alpha} + \frac{1}{2}\beta$. It is not hard to demonstrate that if $q_0(t)$ and $p_0(t)$ are allowed to be complex, then the set of Wigner packets in Eq. 18 is mathematically complete, i.e. any function $f(q, p)$ can be expanded in them, using

the dot product in Eq.6:

$$f(q,p) = \int \int \int \int \frac{dq_r dq_i dp_r dp_i}{(\pi \hbar)^2} \exp(-2\alpha q_i^2 - 2\beta p_i^2) \rho(q,p;\theta) \langle \rho(q,p;\theta), f(q,p) \rangle . \qquad (20)$$

In this expression, the ξ variable in θ is zero. This expansion is a desirable property since all Wigner functions can then be time-evolved, at least approximately. The complex Wigner packet in Eq.18 has several interesting properties. First, let us consider dynamics in a harmonic potential. It turns out that an expansion-propagation scheme based on Eq.19 and Eq.20 is almost exact for a harmonic potential. More precisely, if we compute (again with $\xi = 0$):

$$f(q,p;t) = \int \int \int \int \frac{dq_r dq_i dp_r dp_i}{(\pi \hbar)^2} \exp(-2\alpha q_i^2 - 2\beta p_i^2) \rho(q,p;\theta(t)) \langle \rho(q,p;\theta(0)), f(q,p;0) \rangle$$
$$(21)$$

where the Wigner-packets $\rho(q, p; \theta(t))$ are time-evolved using Eq.19, then the result is exact apart from an overall scaling factor of the final Wigner function. This is of course easy to fix. It is a general property of the above expansion-propagation scheme, that the phase-space integral over the time-evolved Wigner function ("norm") is not equal to unity, but instead is a function of time. Hence, the Wigner function always has to be renormalized. A further interesting property is that since the Wigner-packets include a phase-factor $\exp(i\xi_r(t)/\hbar)$, the method can in principle account for interference effects, see below. From the equations of motion we also notice that this factor $\exp(i\xi_r(t)/\hbar)$ is always unity for a harmonic potential. This means that the method does not have oscillatory phases that causes problems for near-harmonic systems. This is clearly important if one is interested in multi-dimensional problems. We finally observe that the variables q_i and p_i determine the amount of off-diagonal character of the density operator of $\rho(q, p; \theta(t))$ in the momentum and position representation, respectively.

B. Application to double well potential

We consider again the double well potential from the previous section. We will consider the propagation of a Wigner packet with non-complex initial conditions, i.e. $q_r = 1$. and $p_r = p_i = q_i = \xi_r = \xi_i = 0$. We further set $\alpha = \beta = 1$. We compute its average position as a function of time. Our Wigner-packet is propagated through Eq.21 using some 45000 functions in the integral. The result is shown in Figure 8. As opposed to the classical Wigner model, we see that the variational Wigner-packet indeed tunnels through however a bit too fast. One also sees that the norm of the Wigner-packet quickly decays to around 0.10. In Figure 9 is shown the propagated Wigner functions after a time of 2. It is seen that the variational result reproduces the two blue, negative bassins "north" and "south" of the central positive yellow peak. Indeed, closer inspection shows that both Wigner
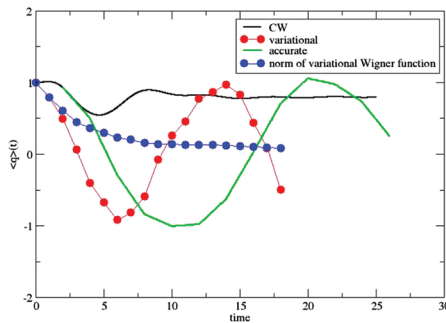
FIG. 8. Average position for a particle in the double well starting from a single Gaussian. $q_0 = 1., p_0 = 0$ and $\alpha = \beta = 1$.
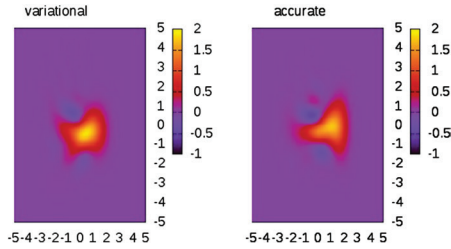
FIG. 9. Variational and accurate Wigner functions in the double well after a time of $t = 2$.
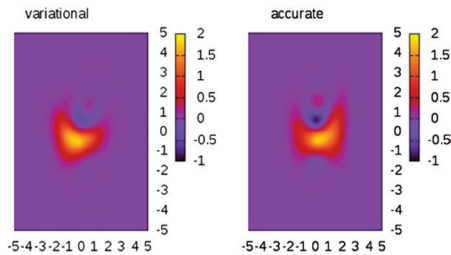
FIG. 10. Variational and accurate Wigner functions in the double well after a time of $t = 4$.

functions have negative values down to some -0.5. Similar results are shown in Figure 10 now for a time of 4. Here the agreement is less good and while the accurate function has a negative bassin with a "probability" of about -1., the corresponding variational "dip" only goes down to some -0.5.

C. Application to quartic potential

Here we revisit the quartic potential from the previous section. Again, we study the propagation of the Wigner packet with the initial conditions, $q_r = 1.$, $p_r = p_i = q_i = \xi_r = \xi_i = 0.$ and $\alpha = \beta = 1$. In Figure 11 is shown the average position of the quantum particle. We see a good agreement between
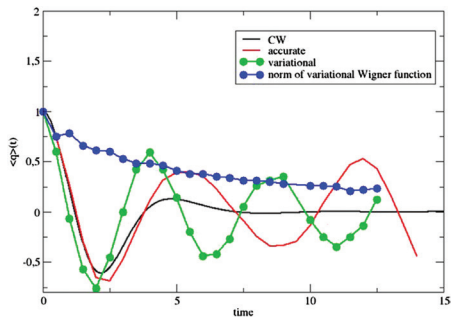
FIG. 11. Average position for a particle in the quartic potential starting from a single Gaussian. $q_0 = 1.$, $p_0 = 0$ and $\alpha = \beta = 1$.
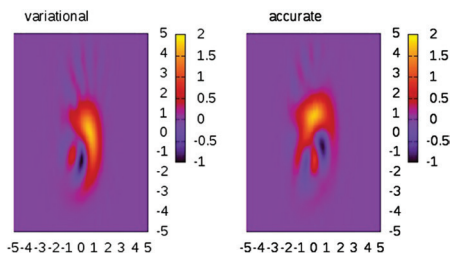
FIG. 12. Variational and accurate Wigner functions in the quartic potential after a time of $t = 4$.

the accurate and variational scheme for short times, but we also note a too fast oscillation predicted in the variational result. The good thing is that the normalized Wigner function clearly is more coherent than the classical Wigner result. Again the classical Wigner result erroneously decays on a fast time-scale. Finally, we show the time-evolved variational Wigner-packet for a time of 4. and compare to the accurate result in Figure 12. We see that the interference pattern is clearly qualitatively reproduced by the variational method. Indeed in both plots are clearly seen a black "dip" with probability of some -1.

V. DISCUSSION AND CONCLUSION

Let us first consider the variational method based on thawed Gaussians. It should be clear that this method is computationally simple and can be generalized to many dimensions. Also, as opposed to many other practical methods, it does seem to account for tunneling effects which is indeed encouraging. It is interesting to compare this method with Hellers now classic method for propagating thawed Gaussian wavefunctions.[15] His method allows for complex widths of the wavepackets meaning that the corresponding Wigner function is identical to our thawed Wigner functions, see Eq.9. In his paper, however, one expands the classical potential to second order around the center of the wavepacket. Thus the method does not use a smeared potential as in this work. Here, we found it essential to do so in order to account for tunneling effects through the barrier of the double well. It was observed that the thawed Gaussian method did not perform well at $1/k_B T = 1$ when used together with the Feynman-Kleinert model. Inspection of the equations of motion in Eq.10 and numerical experimentation reveals that the problem is the smeared potential. If β' is put equal to 0 then we essentially get the classical Wigner result, which is not a good result either. So β' is somewhat too big. The problem is as follows: At high temperature, the factor $\frac{M\Omega(x_c)}{\hbar\alpha(x_c)}$ in Eq.15 is initially large, since $\alpha(x_c)$ is small. From Eq.10 it follows that after a transient time, γ turns into a big negative number which again makes β and thereby β' big. Thus after a transient time, the effective potential is lowered and the particle is tunneling through. To conclude, in the high-temperature limit, we do not obtain dynamics for q_0 and p_0 "on" the classical potential if we use the Feynman-Kleinert sampling. At first this seems counter intuitive but the variational principle is actually acting correctly! To see this, we notice that a large β value means a very localized Wigner distribution along the momentum direction in phase-space. It trivially follows that the corresponding density operator has large off-diagonal elements in the position representation. It is well-known that in such a case, quantum effects are important when considering the dynamics of the Wigner function. So it is correct that q_0 and p_0 evolve non-classically. The classical high-temperature limit is only obtained if we use the variational principle for time-evolving a distribution function being broad in phase-space both along the q and p directions. Then both α and β are small all the time and the effective potential will be close to the classical one. The problem is then the form of the Feynman-Kleinert Gaussian functions that are too localized at high temperatures. Indeed they are quantum mechanically "illegal" since they violate Heisenbergs uncertainty relation. We should mention that this discussion is not relevant for harmonic potentials where the method is always exact: Here the smearing of the potential does not have any effect on the dynamics.

Let us next discuss the variational method based on complex frozen Gaussians. It was observed to keep coherence for a longer time than the classical Wigner model, but unfortunately, also predicts a somewhat too fast time-dynamics. Also, the propagated Wigner function does not keep its norm, although this is easily fixed afterwards. We notice that the method we use is a fully uncoupled approach: We expand a Wigner function in our set of complex Wigner packets which are afterwards driven forward in time individually. This method could be improved by including a semi-classical prefactor multiplied onto the Wigner packets. Such a factor accounts for coupling between the evolving Wigner-packets but it is evaluated in an approximate way. It could be evaluated in a similar manner as in the derivation of the Herman-Kluk semi-classical initial value representation[18–20] used for propagating wave functions. Here, the prefactor is evaluated by linearizing the dynamics around the orbit of the coherent state of interest. Such an analysis will be the subject of future research.

SUPPLEMENTARY MATERIAL

See supplementary material for a derivation of the equations of motion of the variational Wigner functions.

ACKNOWLEDGMENTS

APPENDIX A

In the following, the symbol β means $1/k_B T$. We will use the so-called Feynman-Kleinert approximation to the Boltzmann operator:

$$\exp(-\beta \hat{H}) \approx \int \int dx_c dp_c \rho(x_c, p_c) \hat{\delta}_{FK}(x_c, p_c), \tag{A1}$$

where

$$\rho(x_c, p_c) = \frac{1}{2\pi\hbar} \exp(-\beta \frac{p_c^2}{2m}) \exp(-\beta W_1(x_c)) \tag{A2}$$

and

$$\hat{\delta}_{FK}(x_c, p_c) = \int \int dx dx' |x'\rangle \langle x| \sqrt{\frac{M\Omega(x_c)}{\pi\hbar\alpha(x_c)}} \exp(\frac{i}{\hbar} p_c(x' - x))$$
$$\times \exp(-\frac{M\Omega(x_c)}{\hbar\alpha(x_c)}(\frac{x + x'}{2} - x_c)^2 - \frac{M\Omega(x_c)\alpha(x_c)}{4\hbar}(x - x')^2). \tag{A3}$$

In reference 7 it is shown how to determine the centroid potential $W_1(x_c)$, the effective frequency $\Omega(x_c)$ and $\alpha(x_c)$. Using Eq.A1 enables us to establish the following approximate identity:[21]

$$\frac{1}{\beta\hbar} \frac{1}{Z} \int_0^{\beta\hbar} ds \exp(-(\beta - s)\hat{H})\hat{x} \exp(-s\hat{H}) \approx \frac{1}{Z_{FK}} \int \int dx_c dp_c x_c \rho_{FK}(x_c, p_c) \hat{\delta}_{FK}(x_c, p_c), \tag{A4}$$

which would be exact if Eq.A1 were. By multiplying this equation with the Heisenberg operator $\hat{x}(t)$ followed by taking the trace, we obtain an expression for the Kubo-transformed position auto correlation function:

$$\langle xx(t)\rangle_{Kubo} = \tag{A5}$$

$$\frac{1}{\beta\hbar} \frac{1}{Z} \int_0^{\beta\hbar} ds Tr\{\exp(-(\beta - s)\hat{H})\hat{x} \exp(-s\hat{H})\hat{x}(t)\} \tag{A6}$$

$$\simeq \frac{1}{Z_{FK}} \int \int dx_c dp_c x_c \rho_{FK}(x_c, p_c) \frac{1}{2\pi\hbar}$$

$$\times \int \int dq dp (\exp(-it\hat{H}/\hbar)\hat{\delta}_{FK}(x_c, p_c) \exp(it\hat{H}/\hbar))_W[q, p]q.$$

II

We may explore the fact that $\hat{\delta}_{FK}(x_c, p_c)$ is an operator which has a Wigner-transform that is a Gaussian function of p_c. Hence we may integrate out p_c:

$$\langle xx(t) \rangle_{Kubo} = \tag{A7}$$

$$\frac{1}{Z_{FK}} \int dx_c x_c \rho_{FK}(x_c) \times \frac{1}{2\pi\hbar} \int\int dqdp \left(\exp(-it\hat{H}/\hbar) \right.$$

$$\times \int dp_c \exp(-\beta \frac{p_c^2}{2m}) \hat{\delta}_{FK}(x_c, p_c) \exp(it\hat{H}/\hbar))_W [q, p] q$$

$$= \frac{1}{Z_{FK}} \int dx_c x_c \rho_{FK}(x_c) \frac{1}{2\pi\hbar} \int\int dqdpq \exp(t\mathcal{L})$$

$$\times \int dp_c (\exp(-\beta \frac{p_c^2}{2m}) \hat{\delta}_{FK}(x_c, p_c))_W [q, p]$$

$$= \frac{1}{Z_{FK}} \int dx_c x_c \rho_{FK}(x_c) \times \frac{1}{2\pi\hbar} \int\int dqdpq \times \exp(t\mathcal{L})$$

$$2\sqrt{\frac{\pi 2M \tanh(\frac{\hbar\Omega(x_c)\beta}{2})}{\beta\alpha(x_c)}} \exp(-\frac{M\Omega(x_c)}{\hbar\alpha(x_c)}(q - x_c)^2) \tag{A8}$$

$$\times \exp(-\frac{\tanh(\frac{\hbar\Omega(x_c)\beta}{2})}{\hbar M\Omega(x_c)} p^2).$$

It is the last equation that can be evaluated using the varational method of Section II. It is calculated by sampling x_c by Monte Carlo and for each x_c, we propagate the local Gaussian Wigner distribution

$$\rho_{x_c}(q, p) = 2\sqrt{\frac{\tanh(\frac{\hbar\Omega(x_c)\beta}{2})}{\alpha(x_c)}} \exp(-\frac{M\Omega(x_c)}{\hbar\alpha(x_c)}(q - x_c)^2) \exp(-\frac{\tanh(\frac{\hbar\Omega(x_c)\beta}{2})}{\hbar M\Omega(x_c)} p^2). \tag{A9}$$

[1] Y. Zhao, T. Yamamoto, and W. H. Miller, J. Chem. Phys. **120**, 3100 (2004).
[2] R. V. Harrevelt, G. Nyman, and U. Manthe, J. Chem. Phys. **126**, 084303 (2007).
[3] T. D. Hone, J. A. Poulsen, P. J. Rossky, and D. E. Manolopoulos, J. Phys. Chem. B **112**, 294–300 (2008).
[4] I. R. Craig and D. E. Manolopoulos, J. Chem. Phys. **121**, 3368–3373 (2004).
[5] G. A. Voth, Adv. Chem. Phys. **93**, 135 (1996).
[6] J. Liu, J. Chem. Phys. **140**, 224107 (2014).
[7] J. A. Poulsen, G. Nyman, and P. J. Rossky, J. Chem. Phys. **119**, 12179 (2003).
[8] Q. Shi and E. Geva, J. Phys. Chem. B **107**, 9059 (2003).
[9] H. Wang, X. Sun, and W. H. Miller, J. Chem. Phys. **108**, 9726 (1998).
[10] K. K. G. Smith, J. A. Poulsen, G. Nyman, and P. J. Rossky, J. Chem. Phys. **142**, 244113 (2015).
[11] E. Wigner, Phys. Rev. **40**, 749 (1932).
[12] *Quantum Mechanics in Phase Space*, edited by C. K. Zachos, D. B. Fairlie, and T. L. Curtright, World Scientic Series in 20th Century Physics, Vol. 34, World Scientific (2005).
[13] J. A. Poulsen, J. Chem. Phys. **134**, 034118 (2011).
[14] A. Raab, Chem. Phys. Lett. **319**, 674–678 (2000).
[15] E. J. Heller, J. Chem. Phys. **64**, 63 (1976).
[16] R. D. Coalson and M. Karplus, J. Chem. Phys. **93**, 3919 (1990).
[17] D. J. Coughtrie and D. P. Tew, J. Chem. Phys. **143**, 044102 (2015).
[18] M. F. Herman and E. Kluk, Chem. Phys. **91**, 27 (1984).
[19] W. H. Miller, J. Phys. Chem. **106**, 8132 (2002).
[20] D. V. Shalashilin and M. S. Child, Chem. Phys. **304**, 103–120 (2004).
[21] J. A. Poulsen, G. Nyman, and P. J. Rossky, J. Phys. Chem. B **108**, 19799–19808 (2004).

II

Supplementary material: Quantum effects as modeled by "Wigner packets"

October 25, 2017

Abstract

The optimum time-evolution of uncoupled Gaussian Wigner packets in phase space is derived and studied through the time-dependent action principle.

Introduction

Wigner-packets

The goal of this work is to derive equations of motion for time-dependent Gaussian Wigner functions in phase space. The form of Wigner functions - Wigner packets - will be taken as

$$\rho(q,p;t) = \rho(q,p;\xi(t),q_0(t),p_0(t)) \tag{1}$$

$$= \exp\{i\xi(t)\}\exp\{-\begin{pmatrix} q-q_0(t) \\ p-p_0(t) \end{pmatrix}^T \begin{pmatrix} \alpha & 0 \\ 0 & \beta \end{pmatrix} \begin{pmatrix} q-q_0(t) \\ p-p_0(t) \end{pmatrix}\}$$

or

$$\rho(q,p;t) = \rho(q,p;q_0(t),p_0(t),\alpha(t),\gamma(t),\beta(t)) \tag{2}$$

$$= \exp\{-\begin{pmatrix} q-q_0(t) \\ p-p_0(t) \end{pmatrix}^T \begin{pmatrix} \alpha(t) & \gamma(t) \\ \gamma(t) & \beta(t) \end{pmatrix} \begin{pmatrix} q-q_0(t) \\ p-p_0(t) \end{pmatrix}\}.$$

All variational parameters are considered complex. A real-valued normalization constant, $N(t)$, will be included in Eq.2. $N(t)$ is not a variational parameter; it is determined by requiring that the Wigner packet is normalized with respect to a square norm:

$$\langle \rho(q,p;t), \rho(q,p;t) \rangle = \int\int \frac{dqdp}{2\pi\hbar} \rho^*(q,p;t)\rho(q,p;t)) = 1. \tag{3}$$

A general scalar-product between two Wigner functions will be useful:

$$\langle A_W(q,p;t), B_W(q,p;t) \rangle = \int\int \frac{dqdp}{2\pi\hbar} A_W^*(q,p;t)B_W(q,p;t)). \tag{4}$$

If we allow q_0 and p_0 to be complex, it can be shown that the set of packets in Eq.1 is complete, i.e. any Wigner function can be expanded in them. Hence, if we know how to propagate these packets, we can propagate every Wigner function. Observe for these Wigner packets the following points which will be clear later:

- The real part of $\xi(t)$, i.e. the phase $\xi_r(t)$, is always zero if the Wigner packet constitutes an exact propagation. Hence it picks up an (diagonal) error in the method in some sense. For a system with a harmonic potential, $\xi_r(t)$ is also zero. Hence, $\xi_r(t)$ is a measure of the anharmonicity of the problem.

- The phase $\xi(t)$ is only non-zero for complex trajectories $q_0(t)$ and $p_0(t)$.

The factor $\exp\{i\xi(t)\}$ will allow interference effects, i.e. negative bassins of the Wigner function to develop. This is seen as follows: First imagine expanding the initial Wigner funtion in the complex set $\mathcal{F}$. Then propagate these. Each Wigner packet will develop its own phase factor and in the end they will interfere when you sum them together.

The time-dependent action principle

Consider e.g. the propagation of Wigner packets given by Eq.2. We will then find the optimum time evolution of $\rho(q, p; q(t), p_0(t), \alpha(t), \gamma(t), \beta(t))$ by utilizing the time-dependent action principle. Before proceeding, introduce the short-hand notation: $\vec{\theta}(t) = \{q_0(t), p_0(t), \alpha(t), \gamma(t), \beta(t)\}$. Then, the variational principle can be explained by considering the functional

$$J[\vec{\theta}, \dot{\vec{\theta}}] = \int_0^t ds \left\langle \rho(q, p; \vec{\theta}(s)), \{\mathcal{L} - \frac{\partial}{\partial s}\}\rho(q, p; \vec{\theta}(s)) \right\rangle \tag{5}$$

$$= \int_0^t ds \left\langle \rho(q, p; \vec{\theta}(s)), \{\mathcal{L} - \dot{\vec{\theta}} \cdot \nabla_{\vec{\theta}}\}\rho(q, p; \vec{\theta}(s)) \right\rangle.$$

Here, $\mathcal{L}$ is the Liouvillian. The time integration goes from $s = 0$ to $s = t$, which is the time-window of interest. The action principle states that $J[\vec{\theta}, \dot{\vec{\theta}}]$ is stationary with respect to complex variations $\delta\vec{\theta}(s)$ (except at end-points) if and only if $\vec{\theta}(s)$ is the optimum "path" in a least squares sense, i.e. so that the error

$$Error = \left\langle \{\mathcal{L} - \frac{\partial}{\partial s}\}\rho(q, p; \vec{\theta}(s)), \{\mathcal{L} - \frac{\partial}{\partial s}\}\rho(q, p; \vec{\theta}(s)) \right\rangle \tag{6}$$

is minimized along the path. To find the path that extremizes the functional, we use the Euler-Lagrange equation:

$$\frac{\partial}{\partial s}\{\frac{\partial}{\partial \dot{\theta}_i}\}J[\vec{\theta}, \dot{\vec{\theta}}] = \frac{\partial}{\partial \theta_i}J[\vec{\theta}, \dot{\vec{\theta}}], \tag{7}$$

where $\dot{\theta}_i$ is the time-derivative of the $i'th$ entry of the θ vector etc. We notice that the wigner packet should be an analytic - differentiable - function of its complex variational parameters, otherwise, the equivalence between Eq.5 and Eq.6 does not hold.

The linearity of the variational principle.

There is an explicit solution to the Euler-Lagrange equations, namely

$$\dot{\vec{\theta}} = \left\langle \nabla_{\vec{\theta}}\rho(q, p; \vec{\theta}), \nabla_{\vec{\theta}}\rho(q, p; \vec{\theta}) \right\rangle^{-1} \left\langle \nabla_{\vec{\theta}}\rho(q, p; \vec{\theta}), \mathcal{L}\rho(q, p; \vec{\theta}) \right\rangle. \tag{8}$$

This equation is linear in $\mathcal{L}$. From this it follows that if we write $\mathcal{L} = \mathcal{L}_1 + \mathcal{L}_2$ then the optimum solution corresponding to $\mathcal{L}$ is the sum of optimum solutions to $\mathcal{L}_1$ and $\mathcal{L}_2$: $\dot{\vec{\theta}} = \dot{\vec{\theta}}_1 + \dot{\vec{\theta}}_2$. How does this help us? It wil enable us to find $\dot{\vec{\theta}}$ for a general potential in a simple way. The strategy is as follows: We decompose the potential in Fourier components:

$$V(x) = \int_{-\infty}^{+\infty} dk a(k) \exp(ikx). \tag{9}$$

Imagine that we have propagated the variables up to a time t, so that we know $\vec{\theta}(t)$. Using $\vec{\theta}(t)$ as input we solve the "local" Euler-Lagrange equations for $\mathcal{L}_k$ defined by

$$\mathcal{L}_k = V_k'(q)\frac{\partial}{\partial p} - \frac{\hbar^2}{24}V_k'''(q)\frac{\partial^3}{\partial p^3} + ..,\qquad(10)$$

with $V_k(x) = \exp(ikx)$ at time t. Call this "local" solution $\dot{\vec{\theta}}(k,t)$. So the "local" EL - J_k- may be denoted by

$$\frac{\partial}{\partial s}\{\frac{\partial}{\partial \dot{\theta}(k)_i}\}J_k[\vec{\theta},\dot{\vec{\theta}}(k,t)] = \frac{\partial}{\partial \theta_i}J_k[\vec{\theta},\dot{\vec{\theta}}(k,t)].\qquad(11)$$

Then the solution to our original problem is

$$\dot{\vec{\theta}}(t) = \dot{\vec{\theta}}(free,t) + \int_{-\infty}^{+\infty}dka(k)\dot{\vec{\theta}}(k,t),\qquad(12)$$

where $\dot{\vec{\theta}}(free,t)$ is the solution for $\mathcal{L} = -\frac{p}{M}\frac{\partial}{\partial q}$.

The action principle for a thawed Wigner packet.

Here we will let $\alpha(t)$, $\beta(t)$, $\gamma(t)$, $q_0(t)$ and $p_0(t)$ be variational parameters, i.e. we are considering Eq.2. As already stated, we should regard the variational parameters as complex under the search for the optimum "path". We will adopt the notation $q_0 = q_r + iq_i$ etc when writing complex numbers. As will be apparant later, we will need no phase-factor $\xi(t)$. Thus our variational Wigner packet is

$$\rho(q,p;t) = N(t)\exp\{-(\begin{array}{c}q-q_0(t)\\p-p_0(t)\end{array})^T(\begin{array}{cc}\alpha(t)&\gamma(t)\\\gamma(t)&\beta(t)\end{array})(\begin{array}{c}q-q_0(t)\\p-p_0(t)\end{array})\}.\qquad(13)$$

The normalization factor can be evaluated explicitly:

$$N(t) = 2\sqrt{\frac{\hbar}{\Lambda}}(\alpha_r\beta_r - \gamma_r^2)^{1/4}\qquad(14)$$

with

$$\ln\Lambda = \frac{1}{2}\{B^*(\begin{array}{c}q_0^*\\p_0^*\end{array}) + c.c.\}^T\underline{A}^{-1}\{\underline{B}^*(\begin{array}{c}q_0^*\\p_0^*\end{array}) + c.c.\}$$
$$- (\begin{array}{c}q_0^*\\p_0^*\end{array})^T\underline{B}^*(\begin{array}{c}q_0^*\\p_0^*\end{array}) - (\begin{array}{c}q_0\\p_0\end{array})^T\underline{B}(\begin{array}{c}q_0\\p_0\end{array}),\qquad(15)$$

with

$$\underline{A} = (\begin{array}{cc}\alpha_r&\gamma_r\\\gamma_r&\beta_r\end{array}),\quad \underline{B} = (\begin{array}{cc}\alpha&\gamma\\\gamma&\beta\end{array}).\qquad(16)$$

Notice that $\Lambda = 1$ if both the two sets $\{q_0(t),p_0(t)\}$, $\{\alpha(t),\beta(t),\gamma(t)\}$ are real-valued. The alert reader have by now noticed that - apart from its N factor

- $\rho(q, p; t)$ is analytic in its variational parameters. However, as shown in Appendix A, including a non-analytical *normalization factor* into the Wigner function does not change the solution to the Euler-Lagrange equations provided the solution is a real-valued path with a constant normalization factor (as will be the case here). So in this case, it is permissible to keep the N factor. From the previous section, it follows that we should consider the variational problem

$$J[\vec{\theta}, \dot{\vec{\theta}}] = \int_0^t ds \left\langle \rho(q, p; \vec{\theta}(s)), \{\mathcal{L}_k - \frac{\partial}{\partial s}\}\rho(q, p; \vec{\theta}(s)) \right\rangle, \qquad (17)$$

with $\mathcal{L}_k$ defined in Eq.10. Inserting Eq.13 into Eq.17 yields

$$J[\vec{\theta}, \dot{\vec{\theta}}] =$$

$$\frac{1}{i\hbar} \int_0^t ds \exp(-\frac{k^2}{8}\frac{\beta_r}{\alpha_r\beta_r - \gamma_r^2}[\hbar^2\gamma_i^2 + 1] - \frac{\hbar^2 k^2}{8}\frac{\beta_i}{\alpha_r\beta_r - \gamma_r^2}[\alpha_r\beta_i - 2\gamma_r\gamma_i])$$

$$\exp(-\frac{\hbar^2 k^2}{8}\beta_r)\exp(ik(\lambda_q + q_r))$$

$$\times\{\exp(-\frac{\hbar k^2}{4}\frac{\gamma_i\beta_r - \beta_i\gamma_r}{\alpha_r\beta_r - \gamma_r^2} - i\hbar k(q_i\gamma_r + p_i\beta_r - \gamma_i\lambda_q - \beta_i\lambda_p))$$

$$-\exp(+\frac{\hbar k^2}{4}\frac{\gamma_i\beta_r - \beta_i\gamma_r}{\alpha_r\beta_r - \gamma_r^2} + i\hbar k(q_i\gamma_r + p_i\beta_r - \gamma_i\lambda_q - \beta_i\lambda_p))\} \qquad (18)$$

$$+i\int_0^t ds 2\alpha_r\dot{q}_r q_i + 2\gamma_r\dot{q}_r p_i + 2\beta_r\dot{p}_r p_i + 2\gamma_r\dot{p}_r q_i$$

$$+\frac{1}{4}\frac{\dot{\beta}_i\alpha_r + \dot{\alpha}_i\beta_r - 2\dot{\gamma}_i\gamma_r}{\alpha_r\beta_r - \gamma_r^2} - 2\lambda_q\{\alpha_r\dot{q}_i + \dot{\alpha}_r q_i + \dot{\gamma}_r p_i + \gamma_r\dot{p}_i\}$$

$$-2\lambda_p\{\gamma_r\dot{q}_i + \dot{\beta}_r p_i + \dot{\gamma}_r q_i + \beta_r\dot{p}_i\}$$

$$-2\dot{q}_i\alpha_i q_i - \dot{\alpha}_i q_i^2 - 2\dot{p}_i\beta_i p_i - \dot{\beta}_i p_i^2 - 2\dot{q}_i\gamma_i p_i - 2\dot{p}_i\gamma_i q_i - 2p_i\dot{\gamma}_i q_i.$$

Two additional quantitites have appeared in Eq.18.

$$\begin{pmatrix} \lambda_q \\ \lambda_p \end{pmatrix} = \frac{-1}{\alpha_r\beta_r - \gamma_r^2} \begin{pmatrix} \beta_r & -\gamma_r \\ -\gamma_r & \alpha_r \end{pmatrix} \begin{pmatrix} \alpha_i & \gamma_i \\ \gamma_i & \beta_i \end{pmatrix} \begin{pmatrix} q_i \\ p_i \end{pmatrix}. \qquad (19)$$

Eq.18 looks very complicated. Fortunately, things will simplify directly. First we note that the seven terms in the last line of Eq.18 corresponds to a total time-derivative and therefore do not contribute to the variation of the integral and can therefore be neglected in the EL equations.

We will show that a real-valued path $\vec{\theta} = \{q_0(t), p_0(t), \alpha(t), \beta(t), \gamma(t)\}$ fullfills the Euler-Lagrange (EL) equations for the *full Liouvillian* $\mathcal{L}$ if the point $\vec{\theta}$ is real at $t = 0$. This means that the parameters $\vec{\theta}$ that the local EL equation is to be evaluated in, defined through Eq.11 are taken as real. We still allow for a complex time-change of this point when solving the local Eq.11, however the

superposition of these solutions through Eq.12 will remain real-valued. The fact that we evaluate the local EL equations in a real-valued point will simplify the mathematics. In fact - since the EL equations only involve variable first order differentiations, an inspection of Eq.18 reveals that all terms in this equation that are of second order or more in imaginary variables can be discarded. For example, different first-order derivatives working on the λ_q variable is zero when afterwards evaluated in a real-valued point $\vec{\theta}$. So instead of Eq.18 we are left with the much simpler expression:

$$J[\vec{\theta}, \dot{\vec{\theta}}] = \frac{1}{i\hbar} \int_0^t ds \exp(-\frac{k^2}{8}\frac{\beta_r}{\alpha_r\beta_r - \gamma_r^2} - \frac{\hbar^2 k^2}{8}\beta_r)\exp(ikq_r)$$

$$\times \{\exp(-\frac{\hbar k^2}{4}\frac{\gamma_i\beta_r - \beta_i\gamma_r}{\alpha_r\beta_r - \gamma_r^2} - i\hbar k(q_i\gamma_r + p_i\beta_r))$$

$$-\exp(+\frac{\hbar k^2}{4}\frac{\gamma_i\beta_r - \beta_i\gamma_r}{\alpha_r\beta_r - \gamma_r^2} + i\hbar k(q_i\gamma_r + p_i\beta_r))\} \tag{20}$$

$$+i\int_0^t ds 2\alpha_r\dot{q}_r q_i + 2\gamma_r\dot{q}_r p_i + 2\beta_r\dot{p}_r p_i + 2\gamma_r\dot{p}_r q_i$$

$$+\frac{1}{4}\frac{\dot{\beta}_i\alpha_r + \dot{\alpha}_i\beta_r - 2\dot{\gamma}_i\gamma_r}{\alpha_r\beta_r - \gamma_r^2}.$$

Consider now the Euler-Lagrange equations. First we consider the variable q_r. We get (remember it is evaluated for a real path, so in the end all complex terms are set to zero):

$$\frac{\partial}{\partial q_r}J = \frac{d}{dt}\frac{\partial}{\partial \dot{q}_r}J \iff 0 = \frac{d}{dt}[\alpha_r q_i + \gamma_r p_i]. \tag{21}$$

This is fullfilled if q_i and p_i and their time-derivatives are zero for all times. Next we consider p_r. We get

$$\frac{\partial}{\partial p_r}J = \frac{d}{dt}\frac{\partial}{\partial \dot{p}_r}J \iff 0 = \frac{d}{dt}[2\beta_r p_i + 2\gamma_r q_i]. \tag{22}$$

Again this is satisfied if q_i and p_i and their time-derivatives are zero. We next look at q_i:

$$\frac{\partial}{\partial q_i}J = \frac{d}{dt}\frac{\partial}{\partial \dot{q}_i}J \iff$$

$$-2k\gamma_r\exp(-\frac{k^2}{8}\frac{\beta_r}{\alpha_r\beta_r - \gamma_r^2} - \frac{\hbar^2 k^2}{8}\beta_r)\exp(ikq_r) + 2i\alpha_r\dot{q}_r + 2i\gamma_r\dot{p}_r = 0. \tag{23}$$

Next consider p_i:

$$\frac{\partial}{\partial p_i}J = \frac{d}{dt}\frac{\partial}{\partial \dot{p}_i}J \iff$$

$$-2k\beta_r\exp(-\frac{k^2}{8}\frac{\beta_r}{\alpha_r\beta_r - \gamma_r^2} - \frac{\hbar^2 k^2}{8}\beta_r)\exp(ikq_r) + i2\gamma_r\dot{q}_r + i2\beta_r\dot{p}_r = 0. \tag{24}$$

The solution to Eqs. 23-24 is: $\dot{q}_r = 0$ and $\dot{p}_r = -ik\exp(-\frac{k^2}{8}\frac{\beta_r}{\alpha_r\beta_r-\gamma_r^2} - \frac{\hbar^2 k^2}{8}\beta_r)\exp(ikq_r) = -\frac{d}{dq_r}\exp(-\frac{k^2}{8}\frac{\beta_r}{\alpha_r\beta_r-\gamma_r^2} - \frac{\hbar^2 k^2}{8}\beta_r)\exp(ikq_r)$, the latter which has the form of a force. Here it seems that we run into trouble: Clearly, the equation of motion for p_r appears to turn this variable into a complex quantity, which appears to contradict that $\dot{p}_i = 0$! But remember: What matters is the equations of motion that we obtain for p_r after having summed over all Fourier modes of the potential plus the free particle Liouvillian. And that will keep p_r real. Next we consider α_i. We have

$$\frac{\partial}{\partial \alpha_i}J = \frac{d}{dt}\frac{\partial}{\partial \dot{\alpha}_i}J \;\Leftrightarrow$$

$$0 = \frac{d}{dt}\frac{\beta_r}{\alpha_r\beta_r-\gamma_r^2} \;\Leftrightarrow \dot{\beta}_r = 0, \tag{25}$$

where we have assumed that $\alpha_r\beta_r - \gamma_r^2$ is independent of time; a fact that will be shown to hold for our stationary path. For β_i we get

$$\frac{\partial}{\partial \beta_i}J = \frac{d}{dt}\frac{\partial}{\partial \dot{\beta}_i}J \;\Leftrightarrow$$

$$\frac{1}{i}\exp(-\frac{k^2}{8}\frac{\beta_r}{\alpha_r\beta_r-\gamma_r^2} - \frac{\hbar^2 k^2}{8}\beta_r)\exp(ikq_r)\frac{k^2}{2}\frac{\gamma_r}{\alpha_r\beta_r-\gamma_r^2} = \frac{i}{4}\frac{d}{dt}\frac{\alpha_r}{\alpha_r\beta_r-\gamma_r^2}$$

or

$$\dot{\alpha}_r = 2\gamma_r \times \frac{d^2}{dq_r^2}\exp(-\frac{k^2}{8}\frac{\beta_r}{\alpha_r\beta_r-\gamma_r^2} - \frac{\hbar^2 k^2}{8}\beta_r)\exp(ikq_r) \tag{26}$$

For γ_i we get

$$\frac{\partial}{\partial \gamma_i}J = \frac{d}{dt}\frac{\partial}{\partial \dot{\gamma}_i}J \;\Leftrightarrow$$

$$\frac{-1}{i}\exp(-\frac{k^2}{8}\frac{\beta_r}{\alpha_r\beta_r-\gamma_r^2} - \frac{\hbar^2 k^2}{8}\beta_r)\exp(ikq_r)\frac{k^2}{2}\frac{\beta_r}{\alpha_r\beta_r-\gamma_r^2} = -\frac{i}{2}\frac{d}{dt}\frac{\gamma_r}{\alpha_r\beta_r-\gamma_r^2}$$

or

$$\dot{\gamma}_r = \beta_r \times \frac{d^2}{dq_r^2}\exp(-\frac{k^2}{8}\frac{\beta_r}{\alpha_r\beta_r-\gamma_r^2} - \frac{\hbar^2 k^2}{8}\beta_r)\exp(ikq_r). \tag{27}$$

Next we look at α_r. The EL equations

$$\frac{\partial}{\partial \alpha_r}J = \frac{d}{dt}\frac{\partial}{\partial \dot{\alpha}_r}J$$

is fulfilled since the left-hand side is zero for a real valued variational parameters, and the right-hand side is trivially zero. The same comment applies to β_r and γ_r and so these last three EL equations bring us nothing new. So, to summarize, we have found a real-valued solution provided the variational parameters are real-valued at $t = 0$. We are now ready to demonstrate that the time derivative of $\alpha_r\beta_r - \gamma_r^2$ is zero:

$$\frac{d}{dt}\{\alpha_r\beta_r - \gamma_r^2\}$$

$$= \dot{\alpha}_r \beta_r + \alpha_r \dot{\beta}_r - 2\gamma_r \dot{\gamma}_r$$

$$= 2\gamma_r \times \frac{d^2}{dq_r^2} \exp(-\frac{k^2}{8}\frac{\beta_r}{\alpha_r \beta_r - \gamma_r^2} - \frac{\hbar^2 k^2}{8}\beta_r)\exp(ikq_r)\beta_r \tag{28}$$

$$+\alpha_r \cdot 0 - 2\gamma_r \beta_r \times \frac{d^2}{dq_r^2}\exp(-\frac{k^2}{8}\frac{\beta_r}{\alpha_r\beta_r - \gamma_r^2} - \frac{\hbar^2 k^2}{8}\beta_r)\exp(ikq_r) = 0.$$

We next turn to the free-particle problem. The variational problem is

$$J[\vec{\theta}, \dot{\vec{\theta}}] = \int_0^t ds \left\langle \rho(q,p;\vec{\theta}(s)), \{-\frac{p}{M}\frac{\partial}{\partial q} - \frac{\partial}{\partial s}\}\rho(q,p;\vec{\theta}(s)) \right\rangle \tag{29}$$

$$= i\int_0^t ds 2\alpha_r(\dot{q}_r - \frac{p_r}{M})q_i + 2\gamma_r(\dot{q}_r - \frac{p_r}{M})p_i + 2\beta_r\dot{p}_r p_i + 2\gamma_r\dot{p}_r q_i$$

$$+\frac{1}{2M}\frac{\gamma_i\alpha_r - \alpha_i\gamma_r}{\alpha_r\beta_r - \gamma_r^2} + \frac{1}{4}\frac{\dot{\beta}_i\alpha_r + \dot{\alpha}_i\beta_r - 2\dot{\gamma}_i\gamma_r}{\alpha_r\beta_r - \gamma_r^2}.$$

Here we have again assumed that the solution is a real-valued path so that second-order imaginary terms can be discarded, as in Eq.20. The Euler-Lagrange (EL) equations are again evaluated. First q_r:

$$\frac{\partial}{\partial q_r}J = \frac{d}{dt}\frac{\partial}{\partial \dot{q}_r}J \Leftrightarrow 0 = \frac{d}{dt}[\alpha_r q_i + \gamma_r p_i]. \tag{30}$$

This is fullfilled if q_i and p_i and their time-derivatives are zero for all times. Next, we consider p_r:

$$\frac{\partial}{\partial p_r}J = \frac{d}{dt}\frac{\partial}{\partial \dot{p}_r}J \Leftrightarrow 0 = \frac{d}{dt}[2\beta_r p_i + 2\gamma_r q_i]. \tag{31}$$

Again this is satisfied if q_i and p_i and their time-derivatives are zero. We next look at q_i:

$$\frac{\partial}{\partial q_i}J = \frac{d}{dt}\frac{\partial}{\partial \dot{q}_i}J \Leftrightarrow$$

$$\alpha_r(\dot{q}_r - \frac{p_r}{M}) + \gamma_r\dot{p}_r = 0. \tag{32}$$

The EL equations for p_i yields

$$\frac{\partial}{\partial p_i}J = \frac{d}{dt}\frac{\partial}{\partial \dot{p}_i}J \Leftrightarrow$$

$$\gamma_r(\dot{q}_r - \frac{p_r}{M}) + \beta_r\dot{p}_r = 0. \tag{33}$$

These two equations are fullfilled if $\dot{q}_r - \frac{p_r}{M}$ and $\dot{p}_r = 0$. Next we consider α_i. The EL equations are

$$\frac{\partial}{\partial \alpha_i}J = \frac{d}{dt}\frac{\partial}{\partial \dot{\alpha}_i}J \Leftrightarrow$$

$$-\frac{1}{2M}\frac{\gamma_r}{\alpha_r\beta_r - \gamma_r^2} = \frac{1}{4}\frac{d}{dt}\frac{\beta_r}{\alpha_r\beta_r - \gamma_r^2} \Leftrightarrow \dot\beta_r = -\frac{2\gamma_r}{M}, \tag{34}$$

if we again assume that the denominator is time-independent. For β_i we obtain

$$\frac{\partial}{\partial\beta_i}J = \frac{d}{dt}\frac{\partial}{\partial\dot\beta_i}J \Leftrightarrow \dot\alpha_r = 0.$$

Finally, we consider γ_i:

$$\frac{\partial}{\partial\gamma_i}J = \frac{d}{dt}\frac{\partial}{\partial\dot\gamma_i}J \Leftrightarrow$$

$$\frac{\alpha_r}{2M} = -\frac{1}{2}\dot\gamma_r \Leftrightarrow \dot\gamma_r = -\frac{\alpha_r}{M}. \tag{35}$$

Again, for these solutions, we may easily verify that $\frac{d}{dt}\{\alpha_r\beta_r - \gamma_r^2\}$ is indeed zero. Let us consider α_r. The EL equation becomes

$$\frac{\partial}{\partial\alpha_r}J = \frac{d}{dt}\frac{\partial}{\partial\dot\alpha_r}J$$

or

$$2(\dot q_r - \frac{p_r}{M})q_i + \frac{1}{2M}\frac{\partial}{\partial\alpha_r}\frac{\gamma_i\alpha_r - \alpha_i\gamma_r}{\alpha_r\beta_r - \gamma_r^2} = 0, \tag{36}$$

which is fullfilled for a real-valued path. The EL equations for β_r and γ_r are similar; they are fullfilled for real-valued paths.

We can now revert to Eq.12 and find the equations of motion for a general potential. We have

$$\frac{d}{dt}\begin{pmatrix} q_r \\ p_r \\ \alpha_r \\ \gamma_r \\ \beta_r \end{pmatrix} \tag{37}$$

$$= \begin{pmatrix} p_r/M \\ 0 \\ 0 \\ -\frac{\alpha_r}{M} \\ -\frac{2\gamma_r}{M} \end{pmatrix} + \int_{-\infty}^{+\infty} dk a(k)\begin{pmatrix} 0 \\ -\frac{d}{dq_r}\exp(-\frac{k^2}{8}\frac{\beta_r}{\alpha_r\beta_r-\gamma_r^2} - \frac{\hbar^2 k^2}{8}\beta_r)\exp(ikq_r) \\ 2\gamma_r \times \frac{d^2}{dq_r^2}\exp(-\frac{k^2}{8}\frac{\beta_r}{\alpha_r\beta_r-\gamma_r^2} - \frac{\hbar^2 k^2}{8}\beta_r)\exp(ikq_r) \\ \beta_r \times \frac{d^2}{dq_r^2}\exp(-\frac{k^2}{8}\frac{\beta_r}{\alpha_r\beta_r-\gamma_r^2} - \frac{\hbar^2 k^2}{8}\beta_r)\exp(ikq_r) \\ 0 \end{pmatrix}.$$

Let us write $\beta_r'(t) = \frac{\beta_r}{2}\{1 + \frac{1}{\hbar^2(\alpha_r\beta_r - \gamma_r^2)}\}$. Then Eq.37 becomes

$$\frac{d}{dt}\begin{pmatrix} q_r \\ p_r \\ \alpha_r \\ \gamma_r \\ \beta_r \end{pmatrix} \tag{38}$$

$$
= \begin{pmatrix} p_r/M \\ 0 \\ 0 \\ -\frac{\alpha_r}{M} \\ -\frac{2\gamma_r}{M} \end{pmatrix} + \int_{-\infty}^{+\infty} dk a(k) \exp(-\frac{\hbar^2 k^2}{4}\beta_r') \begin{pmatrix} 0 \\ -\frac{d}{dq_r}\exp(ikq_r) \\ 2\gamma_r \times \frac{d^2}{dq_r^2}\exp(ikq_r) \\ \beta_r \times \frac{d^2}{dq_r^2}\exp(ikq_r) \\ 0 \end{pmatrix}.
$$

The second part may be evaluated by noting that $(a(k) = \frac{1}{2\pi}\int_{-\infty}^{+\infty} dy V(y)\exp(-iky))$:

$$
\int_{-\infty}^{+\infty} dk a(k)\exp(-\frac{\hbar^2 k^2}{4}\beta_r')\exp(ikq_r)
$$

$$
= \int_{-\infty}^{+\infty} dk \exp(-\frac{\hbar^2 k^2}{4}\beta_r')\exp(ikq_r)\frac{1}{2\pi}\int_{-\infty}^{+\infty} dy V(y)\exp(-iky)
$$

$$
= \frac{1}{2\pi}\int_{-\infty}^{+\infty} dy V(y)\int_{-\infty}^{+\infty} dk \exp(-\frac{\hbar^2 k^2}{4}\beta_r' + ik(q_r - y))
$$

$$
= \frac{1}{2\pi}\int_{-\infty}^{+\infty} dy V(y)\int_{-\infty}^{+\infty} dk \exp(-\beta_r'\frac{\hbar^2}{4}(k - 2i\frac{(q_r - y)}{\beta_r'\hbar^2})^2 - \frac{(q_r - y)^2}{\beta_r'\hbar^2})
$$

$$
= \frac{1}{\sqrt{\pi\hbar^2\beta_r'}}\int_{-\infty}^{+\infty} dy V(y)\exp(-\frac{(q_r - y)^2}{\beta_r'\hbar^2})
$$

$$
\equiv V_{sm}(q_r). \tag{39}
$$

Eq.38 then finally has a very simple appealing form:

$$
\frac{d}{dt}\begin{pmatrix} q_r \\ p_r \\ \alpha_r \\ \gamma_r \\ \beta_r \end{pmatrix} = \begin{pmatrix} p_r/M \\ 0 \\ 0 \\ -\frac{\alpha_r}{M} \\ -2\frac{\gamma_r}{M} \end{pmatrix} + \begin{pmatrix} 0 \\ -\frac{d}{dq_r}V_{sm}(q_r) \\ 2\gamma_r \times \frac{d^2}{dq_r^2}V_{sm}(q_r) \\ \beta_r \times \frac{d^2}{dq_r^2}V_{sm}(q_r) \\ 0 \end{pmatrix}, \tag{40}
$$

or

$$
\frac{d}{dt}\begin{pmatrix} q_r \\ p_r \\ \alpha_r \\ \gamma_r \\ \beta_r \end{pmatrix} = \begin{pmatrix} p_r/M \\ -\frac{d}{dq_r}V_{sm}(q_r) \\ 2\gamma_r \times M\Omega^2(q_r) \\ \beta_r \times M\Omega^2(q_r) - \frac{\alpha_r}{M} \\ -2\frac{\gamma_r}{M} \end{pmatrix}, \tag{41}
$$

where the effective frequency $\Omega(q_r)$ has been defined by:

$$
M\Omega^2(q_r) = \frac{d^2}{dq_r^2}V_{sm}(q_r). \tag{42}
$$

Clearly this is the equation of motion for a real-valued path. It is not hard to demonstrate that Eq.41 is identical to the exact result for a harmonic potential. To summarize: We have shown that the time-dependent variational principle

leads to very simple equations of motion for the Wigner-packet: Only a smeared potential and its first and second-derivatives are required. Let us apply the result to the potential

$$V(x) = -0.5x^2 + 0.1x^4. \tag{43}$$

For a minimum uncertainty Wigner packet, the smeared potential in Eq.39 is calculated to

$$V_{sm}(x) = -0.5(x^2 + \frac{1}{2}\beta_r\hbar^2) + 0.1x^4 + 0.1 * 3\beta_r\hbar^2 x^2 + 0.1 * \frac{3}{4}(\beta_r\hbar^2)^2. \tag{44}$$

The force thus becomes

$$F(x) = -V'_{sm}(x) = x - 4 * 0.1x^3 - 0.1 * 6\beta_r\hbar^2 x. \tag{45}$$

If we put $\beta_r\hbar^2 = 1$, then we recognize this potential as the one we used in Ref.[1] , where we considered tunneling of a particle through this barrier. Here, we explicitly utilized Eq.8. Hence our new general way of solving the variational equations is consistent with previous results.

From Eq.39, it follows that the smearing of the classical potential increases as $\beta_r\hbar^2 = \hbar^2/\{2\langle p^2 \rangle\}$. Thus the larger momentum of the particle, the more classically it behaves.

The action principle for a complex Gaussian.

Here we consider the ansatz in Eq.1:

$$\rho(q,p;t) = 2\exp\{i\xi(t) - (\begin{array}{c} q - q_0(t) \\ p - p_0(t) \end{array})^T \left(\begin{array}{cc} \alpha & 0 \\ 0 & \beta \end{array} \right) (\begin{array}{c} q - q_0(t) \\ p - p_0(t) \end{array})\}. \tag{46}$$

The number of complex variational parameters are three: $q_0(t)$, $p_0(t)$ and $\xi(t)$. We write $\xi(t) = \xi_r(t) + i\xi_i(t)$ etc. The Wigner packet is analytic in its variables but not normalized with respect to Eq.3:

$$\langle\rho(q,p;t), \rho(q,p;t)\rangle = \int\int \frac{dqdp}{2\pi\hbar}\rho^*(q,p;t)\rho(q,p;t)) = \exp(2[\alpha q_i^2 + \beta p_i^2 - \xi_i]). \tag{47}$$

Inserting Eq.46 into Eq.17 gives

$$J[\vec{\theta}, \dot{\vec{\theta}}] = \tag{48}$$

$$\frac{1}{i\hbar}\int_0^t ds \exp(-\frac{\hbar^2 k^2}{4}\beta')\exp(ikq_r)$$

$$\times\{\exp(-i\hbar kp_i\beta) - \exp(i\hbar kp_i\beta)\} \times \exp(2[\alpha q_i^2 + \beta p_i^2 - \xi_i])$$

$$+i\int_0^t ds[2\alpha\dot{q}_r q_i + 2\beta\dot{p}_r p_i + 2i\alpha\dot{q}_i q_i + 2\beta i\dot{p}_i p_i - i\dot{\xi}_i - \dot{\xi}_r] \times \exp(2[\alpha q_i^2 + \beta p_i^2 - \xi_i]).$$

Here $\beta' = \frac{1}{2\alpha\hbar^2} + \frac{\beta}{2}$. After having removed terms corresponding to a total time-derivative we get

$$J[\vec{\theta}, \dot{\vec{\theta}}] = \tag{49}$$

$$\frac{1}{i\hbar} \int_0^t ds \exp(-\frac{\hbar^2 k^2}{4}\beta') \exp(ikq_r)$$

$$\times \{\exp(-i\hbar k p_i \beta) - \exp(i\hbar k p_i \beta)\} \times \exp(2[\alpha q_i^2 + \beta p_i^2 - \xi_i])$$

$$+i \int_0^t ds[2\alpha \dot{q}_r q_i + 2\beta \dot{p}_r p_i - \dot{\xi}_r] \times \exp(2[\alpha q_i^2 + \beta p_i^2 - \xi_i]).$$

The EL equations are now solved. First for q_i:

$$\frac{\partial}{\partial q_i} J = \frac{d}{dt} \frac{\partial}{\partial \dot{q}_i} J \iff$$

$$i2\alpha \dot{q}_r \times \exp(2[\alpha q_i^2 + \frac{p_i^2}{\alpha\hbar^2} - \xi_i]) \tag{50}$$

$$+4\alpha q_i \{\frac{1}{i\hbar} \exp(-\frac{\hbar^2 k^2}{4}\beta') \exp(ikq_r)\{\exp(-i\hbar k p_i \beta) - \exp(i\hbar k p_i \beta)\}$$

$$+i[2\alpha \dot{q}_r q_i + 2\beta \dot{p}_r p_i - \dot{\xi}_r]\} \times \exp(2[\alpha q_i^2 + \beta p_i^2 - \xi_i]) = 0.$$

We solve this by setting $\dot{q}_r = 0$ and

$$\dot{\xi}_r =$$

$$-\frac{1}{\hbar} \exp(-\frac{\hbar^2 k^2}{4}\beta') \exp(ikq_r)\{\exp(-i\hbar k p_i \beta) - \exp(i\hbar k p_i \beta)\} + 2\beta \dot{p}_r p_i. \tag{51}$$

Next with respect to p_i:

$$\{-\exp(-\frac{\hbar^2 k^2}{4}\beta') \exp(ikq_r)k\beta\{\exp(-i\hbar k p_i \beta) + \exp(i\hbar k p_i \beta)\} + 2i\beta \dot{p}_r\}$$

$$\times \exp(2[\alpha q_i^2 + \beta p_i^2 - \xi_i]) \tag{52}$$

$$+2\beta p_i \{\frac{1}{i\hbar} \exp(-\frac{\hbar^2 k^2}{4}\beta') \exp(ikq_r)\{\exp(-i\hbar k p_i \beta) - \exp(i\hbar k p_i \beta)\}$$

$$+i[2\alpha \dot{q}_r q_i + 2\beta \dot{p}_r p_i - \dot{\xi}_r]\} \times \exp(2[\alpha q_i^2 + \frac{p_i^2}{\alpha\hbar^2} - \xi_i]) = 0.$$

We shall solve this by ensuring that the first and second terms vanish each, i.e. we set

$$\dot{p}_r = -ik \exp(ikq_r) \exp(-\frac{\hbar^2 k^2}{4}\beta') \frac{\exp(-i\hbar k p_i \beta) + \exp(i\hbar k p_i \beta)}{2}$$

$$= -\frac{d}{dq_r} \frac{\exp(ik(q_r - \hbar p_i \beta)) + \exp(ik(q_r + \hbar p_i \beta))}{2} \exp(-\frac{\hbar^2 k^2}{4}\beta'), \tag{53}$$

and
$$\dot{\xi}_r =$$

$$-\frac{1}{\hbar}\exp(-\frac{\hbar^2 k^2}{4}\beta')\exp(ikq_r)\{\exp(-i\hbar kp_i\beta) - \exp(i\hbar kp_i\beta)\} + 2\beta\dot{p}_r p_i \quad (54)$$

$$= -\frac{1}{\hbar}\exp(-\frac{\hbar^2 k^2}{4}\beta')\{\exp(ik(q_r - \hbar p_i\beta)) - \exp(ik(q_r + \hbar p_i\beta)) + 2\beta\dot{p}_r p_i,$$

which is again Eq.51. Next we look at the EL with respect to ξ_i.

$$\frac{\partial}{\partial \xi_i}J = \frac{d}{dt}\frac{\partial}{\partial \dot{\xi}_i}J \quad (55)$$

The right side is clearly zero. The same applies to the left-hand side, due to the choice of $\dot{\xi}_r$. Next we consider q_r. The EL equations are

$$\frac{\partial}{\partial q_r}J = \frac{d}{dt}\frac{\partial}{\partial \dot{q}_r}J \iff \quad (56)$$

$$\frac{k}{\hbar}\exp(-\frac{\hbar^2 k^2}{4}\beta')\exp(ikq_r)$$

$$\times\{\exp(-i\hbar kp_i\beta) - \exp(i\hbar kp_i\beta)\} \times \exp(2[\alpha q_i^2 + \beta p_i^2 - \xi_i])$$

$$= i2\alpha\dot{q}_i \times \exp(2[\alpha q_i^2 + \beta p_i^2 - \xi_i]) + i2\alpha q_i \frac{d}{dt}\exp(2[\alpha q_i^2 + \beta p_i^2 - \xi_i]).$$

We set

$$\xi_i = \alpha q_i^2 + \beta p_i^2 \quad (57)$$

then we get the equation:

$$\dot{q}_i = -\frac{ik}{2\alpha\hbar}\exp(-\frac{\hbar^2 k^2}{4}\beta')\exp(ikq_r) \times \{\exp(-i\hbar kp_i\beta) - \exp(i\hbar kp_i\beta)\} \quad (58)$$

$$= -\frac{1}{2\alpha\hbar}\exp(-\frac{\hbar^2 k^2}{4}\beta')\frac{d}{dq_r}\{\exp(ik(q_r - \hbar p_i\beta) - \exp(ik(q_r + \hbar p_i\beta))\}$$

$$= \frac{1}{\alpha\beta\hbar^2}\exp(-\frac{\hbar^2 k^2}{4}\beta')\frac{d}{dp_i}\frac{\{\exp(ik(q_r - \hbar p_i\beta) + \exp(ik(q_r + \hbar p_i\beta))\}}{2}.$$

Next we consider the EL equations with respect to p_r:

$$\frac{\partial}{\partial p_r}J = \frac{d}{dt}\frac{\partial}{\partial p_r}J \iff$$

$$0 = 2\beta\dot{p}_i \iff \dot{p}_i = 0. \quad (59)$$

Finally we consider ξ_r. The EL is

$$\frac{\partial}{\partial \xi_r}J = \frac{d}{dt}\frac{\partial}{\partial \dot{\xi}_r}J \iff$$

13

$$0 = -\frac{d}{dt}\exp(2[\alpha q_i^2 + \beta p_i^2 - \xi_i]), \tag{60}$$

which is ensured by Eq.57.

We next turn to the free-particle problem. The variational problem is

$$J[\vec{\theta}, \dot{\vec{\theta}}] = \int_0^t ds \left\langle \rho(q,p;\vec{\theta}(s)), \{-\frac{p}{M}\frac{\partial}{\partial q} - \frac{\partial}{\partial s}\}\rho(q,p;\vec{\theta}(s)) \right\rangle \tag{61}$$

$$= i\int_0^t ds 2[-\frac{\alpha}{M}p_r q_i + \alpha \dot{q}_r q_i + \beta \dot{p}_r p_i - \dot{\xi}_r] \times \exp(2[\alpha q_i^2 + \beta p_i^2 - \xi_i]).$$

First EL with respect to ξ_i:

$$\frac{\partial}{\partial \xi_i}J = \frac{d}{dt}\frac{\partial}{\partial \dot{\xi}_i}J \iff$$

$$\dot{\xi}_r = -\frac{\alpha}{M}p_r q_i + \alpha \dot{q}_r q_i + \beta \dot{p}_r p_i. \tag{62}$$

EL with respect to q_i:

$$\frac{\partial}{\partial q_i}J = \frac{d}{dt}\frac{\partial}{\partial \dot{q}_i}J \iff$$

$$\dot{q}_r - \frac{p_r}{M} = 0, \tag{63}$$

where we have used Eq.62. EL with respect to p_i:

$$\frac{\partial}{\partial p_i}J = \frac{d}{dt}\frac{\partial}{\partial \dot{p}_i}J \iff \dot{p}_r = 0. \tag{64}$$

Next EL with respect to ξ_r:

$$\frac{\partial}{\partial \xi_r}J = \frac{d}{dt}\frac{\partial}{\partial \dot{\xi}_r}J \iff$$

$$0 = -\frac{d}{dt}\exp(2[\alpha q_i^2 + \beta p_i^2 - \xi_i]), \tag{65}$$

which again leads to Eq.57. EL with respect to q_r:

$$\frac{\partial}{\partial q_r}J = \frac{d}{dt}\frac{\partial}{\partial \dot{q}_r}J \iff$$

$$\dot{q}_i = 0. \tag{66}$$

EL with respect to p_r:

$$\frac{\partial}{\partial p_r}J = \frac{d}{dt}\frac{\partial}{\partial \dot{p}_r}J \iff$$

$$-\frac{\alpha}{M}q_i = \beta \dot{p}_i \iff \dot{p}_i = -\frac{\alpha}{\beta M}q_i. \tag{67}$$

14

We are now in a position to write down the complete solution by adding Fourier components and the free particle solution:

$$
\begin{pmatrix} \dot{q}_r \\ \dot{p}_r \\ \dot{q}_i \\ \dot{p}_i \\ \dot{\xi}_r \\ \dot{\xi}_i \end{pmatrix} = \begin{pmatrix} p_r/M \\ 0 \\ 0 \\ -\frac{\alpha}{\beta M} q_i \\ 0 \\ 2\beta p_i \dot{p}_i \end{pmatrix} + \int_{-\infty}^{+\infty} dk\, a(k) \exp(-\frac{\hbar^2 k^2}{4}\beta') \times \qquad (68)
$$

$$
\begin{pmatrix} 0 \\ -\frac{d}{dq_r} \frac{\exp(ik(q_r-\hbar p_i\beta))+\exp(ik(q_r+\hbar p_i\beta))}{2} \\ \frac{1}{\alpha\beta\hbar^2}\frac{d}{dp_i}\frac{\{\exp(ik(q_r-\hbar p_i\beta))+\exp(ik(q_r+\hbar p_i\beta))\}}{2} \\ 0 \\ -\frac{1}{\hbar}\exp(ikq_r)\{\exp(-i\hbar kp_i\beta)-\exp(i\hbar kp_i\beta)\} - 2\beta\frac{d}{dq_r}\frac{\exp(ik(q_r-\hbar p_i\beta))+\exp(ik(q_r+\hbar p_i\beta))}{2}p_i \\ 2\alpha q_i\dot{q}_i \end{pmatrix}.
$$

Again the convolution can be done using Eq.39. The result is

$$
\begin{pmatrix} \dot{q}_r \\ \dot{p}_r \\ \dot{q}_i \\ \dot{p}_i \\ \dot{\xi}_r \\ \dot{\xi}_i \end{pmatrix} = \qquad (69)
$$

$$
\begin{pmatrix} p_r/M \\ -\frac{d}{dq_r}\frac{V_{sm}(q_r-\hbar p_i\beta)+V_{sm}(q_r+\hbar p_i\beta)}{2} \\ \frac{1}{\alpha\beta\hbar^2}\frac{d}{dp_i}\frac{V_{sm}(q_r-\hbar p_i\beta)+V_{sm}(q_r+\hbar p_i\beta)}{2} \\ -\frac{\alpha}{\beta M}q_i \\ \frac{V_{sm}(q_r+\hbar p_i\beta)-V_{sm}(q_r-\hbar p_i\beta)}{\hbar} - 2\beta\frac{d}{dq_r}\frac{V_{sm}(q_r-\hbar p_i\beta)+V_{sm}(q_r+\hbar p_i\beta)}{2}p_i \\ \frac{d}{dt}\{\beta p_i^2 + \alpha q_i^2\} \end{pmatrix}.
$$

Let us rewrite the Wigner packet as:

$$
\rho(q,p;t) = 2\exp\{i\xi_r(t) - \alpha(q-q_r(t))^2 + 2i\alpha q_i(t)(q-q_r(t))\} \qquad (70)
$$

$$
\times \exp\{-\beta(p-p_r(t))^2 + 2i\beta p_i(t)(p-p_r(t))\}
$$

$$
\times \exp\{\alpha q_i^2(t) + \beta p_i^2(t) - \xi_i(t)\}.
$$

The expression for the time-derivative of $\dot{\xi}_i$ allow us to write this propagated form of this variational Wigner packet as

$$
\rho(q,p;t) = 2\exp\{i\xi_r(t) - \alpha(q-q_r(t))^2 + 2i\alpha q_i(t)(q-q_r(t))\} \qquad (71)
$$

$$
\times \exp\{-\beta(p-p_r(t))^2 + 2i\beta p_i(t)(p-p_r(t))\}
$$

15

$$\times \exp\{\alpha q_i^2(0) + \beta p_i^2(0) - \xi_i(0)\}.$$

Hence, if we initially pick $\xi_i(0) = \alpha q_i^2(0) + \beta p_i^2(0)$, then the Wigner packet will always have the simpler form:

$$\rho(q, p; t) = 2 \exp\{i\xi_r(t) - \alpha(q - q_r(t))^2 + 2i\alpha q_i(t)(q - q_r(t))\} \qquad (72)$$

$$\times \exp\{-\beta(p - p_r(t))^2 + 2i\beta p_i(t)(p - p_r(t))\}.$$

Thus we have completely eliminated the ξ_i variable from the Wigner packet which thus takes a simpler form. It further follows that this function is normalized according to Eq.3 (see Eq.47).

Example A: The harmonic oscillator.

Consider a harmonic oscillator with $V(x) = \frac{M}{2}\Omega^2 x^2$. The smeared potential is the same up to an unimportant additive constant. Therefore we have

$$
\begin{pmatrix}
\dot{q}_r \\
\dot{p}_r \\
\dot{q}_i \\
\dot{p}_i \\
\dot{\xi}_r \\
\dot{\xi}_i
\end{pmatrix}
=
\begin{pmatrix}
p_r/M \\
-M\Omega^2 q_r \\
\beta/\alpha M\Omega^2 p_i \\
-\frac{\alpha}{\beta M} q_i \\
0 \\
2q_i p_i(-\frac{\alpha}{M} + \beta M\Omega^2)
\end{pmatrix}.
\qquad (73)
$$

This result have also been derived using the harmonic potential explicitly in the action functional.

Appendix A.

Consider the wigner packet $\rho(q, p; \vec{\theta})$ which we assume is analytic in its variational parameters. Assume it satisfies the EL equations with a real-valued path:

$$\frac{\partial}{\partial s}\{\frac{\partial}{\partial\dot{\theta}_i}\}\left\langle \rho(q, p; \vec{\theta}(s)), \{\mathcal{L}_k - \frac{\partial}{\partial s}\}\rho(q, p; \vec{\theta}(s))\right\rangle \qquad (74)$$

$$= \frac{\partial}{\partial\theta_i}\left\langle \rho(q, p; \vec{\theta}(s)), \{\mathcal{L}_k - \frac{\partial}{\partial s}\}\rho(q, p; \vec{\theta}(s))\right\rangle.$$

Next, consider the modified wigner packet $N(\vec{\theta}) \times \rho(q, p; \vec{\theta})$, where $N(\vec{\theta})$ is a possible non-analytical normalization constant. It satisfies the EL equations with the *same* real-valued path provided $N(\vec{\theta})$ is found to be time-independent. To see this we compute

$$\left\langle N(\vec{\theta}) \times \rho(q, p; \vec{\theta}(s)), \{\mathcal{L} - \frac{\partial}{\partial s}\}N(\vec{\theta}) \times \rho(q, p; \vec{\theta}(s))\right\rangle$$

$$= N^*(\vec{\theta})N(\vec{\theta})\left\langle \rho(q, p; \vec{\theta}(s)), \{\mathcal{L} - \frac{\partial}{\partial s}\}\rho(q, p; \vec{\theta}(s))\right\rangle$$

16

$$-N^*(\vec{\theta}) \left\langle \rho(q,p;\vec{\theta}(s)), \rho(q,p;\vec{\theta}(s))\frac{\partial}{\partial s}\}N(\vec{\theta}) \right\rangle \tag{75}$$

$$= \left|N(\vec{\theta})\right|^2 \left\langle \rho(q,p;\vec{\theta}(s)), \{\mathcal{L} - \frac{\partial}{\partial s}\}\rho(q,p;\vec{\theta}(s)) \right\rangle$$

$$-\frac{d}{dt}\ln N(\vec{\theta}).$$

The last line is thrown away since it corresponds to a total time-derivative. So we have to apply the EL equation to

$$J = \left|N(\vec{\theta})\right|^2 \left\langle \rho(q,p;\vec{\theta}(s)), \{\mathcal{L}_k - \frac{\partial}{\partial s}\}\rho(q,p;\vec{\theta}(s)) \right\rangle. \tag{76}$$

The EL equations for J is

$$\frac{\partial}{\partial s}\{\frac{\partial}{\partial \dot{\theta}_i}\} \left|N(\vec{\theta})\right|^2 \left\langle \rho(q,p;\vec{\theta}(s)), \{\mathcal{L} - \frac{\partial}{\partial s}\}\rho(q,p;\vec{\theta}(s)) \right\rangle$$

$$= \frac{\partial}{\partial \theta_i} \left|N(\vec{\theta})\right|^2 \left\langle \rho(q,p;\vec{\theta}(s)), \{\mathcal{L} - \frac{\partial}{\partial s}\}\rho(q,p;\vec{\theta}(s)) \right\rangle \tag{77}$$

or

$$\frac{\partial}{\partial s} \left|N(\vec{\theta})\right|^2 \{\frac{\partial}{\partial \dot{\theta}_i}\} \left\langle \rho(q,p;\vec{\theta}(s)), \{\mathcal{L} - \frac{\partial}{\partial s}\}\rho(q,p;\vec{\theta}(s)) \right\rangle$$

$$= \frac{\partial}{\partial \theta_i} \left|N(\vec{\theta})\right|^2 \left\langle \rho(q,p;\vec{\theta}(s)), \{\mathcal{L} - \frac{\partial}{\partial s}\}\rho(q,p;\vec{\theta}(s)) \right\rangle. \tag{78}$$

If $N(\vec{\theta})$ is time-independent, then we may rewrite this equation as

$$\left|N(\vec{\theta})\right|^2 \frac{\partial}{\partial s}\{\frac{\partial}{\partial \dot{\theta}_i}\} \left\langle \rho(q,p;\vec{\theta}(s)), \{\mathcal{L} - \frac{\partial}{\partial s}\}\rho(q,p;\vec{\theta}(s)) \right\rangle$$

$$= \{\frac{\partial}{\partial \theta_i} \left|N(\vec{\theta})\right|^2\} \left\langle \rho(q,p;\vec{\theta}(s)), \{\mathcal{L} - \frac{\partial}{\partial s}\}\rho(q,p;\vec{\theta}(s)) \right\rangle + \tag{79}$$

$$\left|N(\vec{\theta})\right|^2 \frac{\partial}{\partial \theta_i} \left\langle \rho(q,p;\vec{\theta}(s)), \{\mathcal{L} - \frac{\partial}{\partial s}\}\rho(q,p;\vec{\theta}(s)) \right\rangle.$$

The first term on the right is zero due to the real-valued path assumption which makes the bracket zero. The remaing equation is simply Eq.74.

On the other hand, assume that $N(\vec{\theta})\times\rho(q,p;\vec{\theta})$ has a real-valued stationary path solution with constant normalization factor. Then Eq.76-79 also has such an solution and Eq.79 shows that the same solution also satisfies Eq.74.

References

[1] Poulsen, J. Aa., *Journal of Chemical Physics* **2011**, 134, 034118.

Paper III

Classical Wigner Model Based on a Feynman Path Integral Open Polymer

III

Classical Wigner model based on a Feynman path integral open polymer

View Online   Export Citation   CrossMark

S. Karl-Mikael Svensson, Jens Aage Poulsen,[a] and Gunnar Nyman[b]

AFFILIATIONS

Department of Chemistry and Molecular Biology, University of Gothenburg, SE 405 30 Gothenburg, Sweden

[a]Electronic mail: jens.poulsen@gu.se
[b]Author to whom correspondence should be addressed: nyman@chem.gu.se

ABSTRACT

The classical Wigner model is one way to approximate the quantum dynamics of atomic nuclei. Here, a new method is presented for sampling the initial quantum mechanical distribution that is required in the classical Wigner model. The new method is tested for the position, position-squared, momentum, and momentum-squared autocorrelation functions for a one-dimensional quartic oscillator and double well potential as well as a quartic oscillator coupled to harmonic baths of different sizes. Two versions of the new method are tested and shown to possibly be useful. Both versions always converge toward the classical Wigner limit. For the one-dimensional cases, some results that are essentially converged to the classical Wigner limit are acquired and others are not far off. For the multi-dimensional systems, the convergence is slower, but approximating the sampling of the harmonic bath with classical mechanics was found to greatly improve the numerical performance. For the double well, the new method is noticeably better than the Feynman–Kleinert linearized path integral method at reproducing the exact classical Wigner results, but they are equally good at reproducing exact quantum mechanics. The new method is suggested as being interesting for future tests on other correlation functions and systems.

Published under license by AIP Publishing. https://doi.org/10.1063/1.5126183

I. INTRODUCTION

When studying molecular systems computationally, a problem that can arise is how to account for the quantum mechanical behavior of the atomic nuclei without having to solve the time dependent Schrödinger equation using wavefunctions and, instead, work with, e.g., trajectories, which has the potential to be significantly cheaper computationally for many chemically interesting problems. Several different methods exist, which can be used to address this problem, such as centroid molecular dynamics (CMD)[1] that has been well explained by Jang and Voth,[2] ring polymer molecular dynamics (RPMD),[3] semi-classical initial value representation (SC-IVR)[4] that has been well explained by Miller,[5] Matsubara dynamics,[6] and the classical Wigner (CW) method[7,8] [also called linearized semi-classical initial value representation (LSC-IVR), and linearized path integral (LPI)]. A new implementation of the classical Wigner method is the topic of the present article.

The classical Wigner method starts with a quantum mechanical phase space distribution, which is propagated forward in time classically. Finding the initial distribution is typically problematic. In this work, a new way to sample the initial phase space distribution is presented and tested for some simple problems.

The classical Wigner method, CMD, and RPMD can all be seen as approximations to Matsubara dynamics and give worse results than Matsubara dynamics.[6,9] However, for large systems, Matsubara dynamics would be too computationally demanding to be practical.[6]

Comparing CMD and RPMD to the classical Wigner method, one major advantage of the former two is that the quantum mechanical ensemble is conserved during the dynamics, while it is not in the classical Wigner method. On the other hand, for a harmonic oscillator, the classical Wigner method is exact for any correlation function,[7] while CMD can formally be done for non-linear operators,[10] but it is a much more complicated process than for linear operators, and RPMD is only exact for correlation functions where at least one operator is linear.[3]

The classical Wigner method can be seen as an approximation of the semi-classical initial value representation. In this approximation, quantum real time coherence is, however, lost, which may not be very important in large or condensed phase systems since these

typically decohere rapidly.[11] An advantage with the approximation is less oscillatory integrands to handle numerically.[11]

From the above comparisons, it can be seen that one of the reasons for using the classical Wigner method is that it may better handle non-linear correlation functions at a reasonable expense of computational resources, compared to the other available methods.

In the new implementation of the classical Wigner method that is presented in this paper, the initial phase space distribution is sampled with an imaginary time path integral polymer similar to those that can be found in CMD and RPMD, but in those cases, these polymers are closed rings and in the present implementation of the classical Wigner method, the polymer has an opening. The open polymer presented here is more closely related to those that can be found in the work of Bose and Makri[12] and Bonella *et al.*[13,14]

In what follows, first, the classical Wigner method is explained (Sec. II), and a new path integral open polymer implementation of it is presented (Sec. III). After that, the computational details (Sec. IV) and the results (Sec. V) are presented, and conclusions (Sec. VI) are drawn.

II. CLASSICAL WIGNER METHOD

The classical Wigner method was in its first form introduced, but not necessarily recommended by Heller.[7] In its current more general form, which is applicable to correlation functions, it was introduced by Wang, Sun, and Miller.[8] The classical Wigner method has as its basis the Wigner phase space distribution.[15,16] In one dimension, easily generalized to any number of dimensions, the Wigner transform is

$$\left(\hat{\Omega}\right)_{\mathrm{W}}[x, p] = \int_{-\infty}^{\infty} \mathrm{d}\eta\ \mathrm{e}^{-i\eta p/\hbar}\left\langle x + \frac{\eta}{2}\middle|\hat{\Omega}\middle|x - \frac{\eta}{2}\right\rangle, \quad (1)$$

where $\hat{\Omega}$ is an arbitrary operator, x is the position, p is the momentum, η is a variable with the dimension of the length, $\hbar$ is the reduced Planck constant, and i is the imaginary unit. The Wigner function is the Wigner transform of the probability density operator $\frac{1}{2\pi\hbar}|\Psi\rangle\langle\Psi|$, where $|\Psi\rangle$ is the ket of the state of the system. This distribution is an exact quantum mechanical quasi-probability distribution and can be used to calculate expectation values,

$$\left\langle\hat{\Omega}\right\rangle = \int_{-\infty}^{\infty} \mathrm{d}x \int_{-\infty}^{\infty} \mathrm{d}p \left(\tfrac{1}{2\pi\hbar}|\Psi\rangle\langle\Psi|\right)_{\mathrm{W}}[x, p]\left(\hat{\Omega}\right)_{\mathrm{W}}[x, p]. \quad (2)$$

The classical Wigner method consists of taking the quantum mechanical transformed quantity and propagating it forward in time with classical mechanics (CM), i.e.,

$$\left(\mathrm{e}^{\frac{i\hat{H}t}{\hbar}}\hat{\Omega}\,\mathrm{e}^{-\frac{i\hat{H}t}{\hbar}}\right)_{\mathrm{W}}[x, p] \simeq \left(\hat{\Omega}\right)_{\mathrm{W}}[x(t), p(t)], \quad (3)$$

where $\hat{H}$ is the Hamiltonian operator and t is time. Thus, the classical Wigner method works by initiating with a quantum mechanical distribution and then propagating it classically, thereby taking account of all equilibrium quantum effects e.g., zero-point energy, but overlooking e.g., dynamic tunneling and quantum interference within the dynamics. The method is exact for potentials up to and including harmonic terms.[7] For a detailed derivation of the classical Wigner method, the review by Liu[17] can be recommended.

The classical Wigner method has been applied successfully to, e.g., calculating the kinetic energy and density fluctuation spectrum in liquid neon[18] and vibrational energy relaxation rate constants,[19,20] but the classical Wigner method has also been found to have limitations for calculating the self-diffusion coefficient of liquid water[21] or handling anisotropic materials.[22]

III. FEYNMAN PATH INTEGRAL OPEN POLYMER

Let us assume that the quantity of interest for a system is the canonical time correlation function,

$$\left\langle\hat{A}\hat{B}(t)\right\rangle = \frac{1}{Z}\,\mathrm{Tr}\left\{\hat{A}\,\mathrm{e}^{-\beta\hat{H}}\,\mathrm{e}^{\frac{i\hat{H}t}{\hbar}}\hat{B}\,\mathrm{e}^{-\frac{i\hat{H}t}{\hbar}}\right\}, \quad (4)$$

where $\hat{A}$ and $\hat{B}$ are arbitrary operators, β is the inverse of Boltzmann's constant times the absolute temperature, Z is the partition function, and Tr denotes a trace. The choice of placing the Boltzmann operator after $\hat{A}$, instead of before, is arbitrary and only determines the sign of the imaginary part of the correlation function, since we have,

$$\frac{1}{Z}\,\mathrm{Tr}\left\{\mathrm{e}^{-\beta\hat{H}}\hat{A}\,\mathrm{e}^{\frac{i\hat{H}t}{\hbar}}\hat{B}\,\mathrm{e}^{-\frac{i\hat{H}t}{\hbar}}\right\} = \frac{1}{Z}\left(\mathrm{Tr}\left\{\hat{A}\,\mathrm{e}^{-\beta\hat{H}}\,\mathrm{e}^{\frac{i\hat{H}t}{\hbar}}\hat{B}\,\mathrm{e}^{-\frac{i\hat{H}t}{\hbar}}\right\}\right)^{*}. \quad (5)$$

The trace can be written as an integral over the position, x_1, eigenkets,

$$\left\langle\hat{A}\hat{B}(t)\right\rangle = \frac{1}{Z}\int_{-\infty}^{\infty}\mathrm{d}x_1\left\langle x_1\middle|\hat{A}\,\mathrm{e}^{-\beta\hat{H}}\,\mathrm{e}^{\frac{i\hat{H}t}{\hbar}}\hat{B}\,\mathrm{e}^{-\frac{i\hat{H}t}{\hbar}}\middle|x_1\right\rangle. \quad (6)$$

By dividing the Boltzmann operator $\mathrm{e}^{-\beta\hat{H}}$ into N factors $\mathrm{e}^{-\frac{\beta}{N}\hat{H}}$ and inserting $N-1$ identity operators, $\hat{I} = \int_{-\infty}^{\infty}\mathrm{d}x_j\,|x_j\rangle\langle x_j|$, the correlation function can be written as

$$\begin{aligned}\left\langle\hat{A}\hat{B}(t)\right\rangle = \frac{1}{Z}\Bigg\{\prod_{j=1}^{N}\int_{-\infty}^{\infty}\mathrm{d}x_j\Bigg\}&\left\langle x_1\middle|\hat{A}\,\mathrm{e}^{-\frac{\beta}{N}\hat{H}}\middle|x_2\right\rangle\\ \times&\left\langle x_2\middle|\mathrm{e}^{-\frac{\beta}{N}\hat{H}}\middle|x_3\right\rangle\ldots\left\langle x_{N-1}\middle|\mathrm{e}^{-\frac{\beta}{N}\hat{H}}\middle|x_N\right\rangle\\ \times&\left\langle x_N\middle|\mathrm{e}^{-\frac{\beta}{N}\hat{H}}\,\mathrm{e}^{\frac{i\hat{H}t}{\hbar}}\hat{B}\,\mathrm{e}^{-\frac{i\hat{H}t}{\hbar}}\middle|x_1\right\rangle,\end{aligned} \quad (7)$$

which can be recognized as a Feynman path integral[23] in imaginary time $(-i\hbar\beta)$, and this in turn can be rewritten as Wigner transforms,

$$\begin{aligned}\left\langle\hat{A}\hat{B}(t)\right\rangle = \frac{1}{Z}\Bigg\{\prod_{j=1}^{N}&\int_{-\infty}^{\infty}\int_{-\infty}^{\infty}\frac{\mathrm{d}x_j\,\mathrm{d}p_j}{2\pi\hbar}\Bigg\}\,\mathrm{e}^{-\frac{i}{\hbar}\sum_{j=1}^{N}p_j(x_{j+1}-x_j)}\\ \times&\left(\hat{A}\,\mathrm{e}^{-\frac{\beta}{N}\hat{H}}\right)_{\mathrm{W}}\left[\frac{x_1+x_2}{2}, p_1\right]\left(\mathrm{e}^{-\frac{\beta}{N}\hat{H}}\right)_{\mathrm{W}}\left[\frac{x_2+x_3}{2}, p_2\right]\\ \ldots&\left(\mathrm{e}^{-\frac{\beta}{N}\hat{H}}\right)_{\mathrm{W}}\left[\frac{x_{N-1}+x_N}{2}, p_{N-1}\right]\\ \times&\left(\mathrm{e}^{-\frac{\beta}{N}\hat{H}}\,\mathrm{e}^{\frac{i\hat{H}t}{\hbar}}\hat{B}\,\mathrm{e}^{-\frac{i\hat{H}t}{\hbar}}\right)_{\mathrm{W}}\left[\frac{x_N+x_1}{2}, p_N\right],\end{aligned} \quad (8)$$

where $x_{N+1} = x_1$ so that the coordinates make a loop.

If $\frac{\beta}{N}$ is approaching 0 and only finite temperatures are of interest, i.e., N is approaching infinity, then the Wigner transform of the Boltzmann operator is simply the classical Boltzmann factor. In this same limit, the Boltzmann operators can be separated from the transforms involving $\hat{A}$ and $\hat{B}$ and thus make up their own Wigner transforms, without consequence,

$$
\langle \hat{A}\hat{B}(t) \rangle = \lim_{N\to\infty} \frac{1}{Z} \left\{ \prod_{j=1}^{N} \int_{-\infty}^{\infty} \int_{-\infty}^{\infty} \frac{dx_j \, dp_j}{2\pi\hbar} \right\}
$$
$$
\times \, e^{-\frac{i}{\hbar}\sum_{j=1}^{N} p_j(x_{j+1}-x_j)} \left(\hat{A}\right)_W [y_1, p_1]
$$
$$
\times \, e^{-\frac{\beta}{N}\sum_{j=1}^{N} H(y_j, p_j)} \left(e^{\frac{i\hat{H}t}{\hbar}} \hat{B} \, e^{-\frac{i\hat{H}t}{\hbar}}\right)_W [y_N, p_N], \quad (9)
$$

where $y_j = \frac{x_j + x_{j+1}}{2}$, $y_N = \frac{x_N + x_1}{2}$, and $H(y_j, p_j)$ is the classical Hamiltonian. Now, assuming that the potential energy $V(y_j)$ is independent of momentum, whereby most of the momenta only occur in the kinetic energy term of the classical Hamiltonians, $\frac{p_j^2}{2m}$, and the symplectic area, $\sum_{j=1}^{N} p_j(x_{j+1} - x_j)$, it is easy to integrate those momenta out analytically. The momenta that occur in other places in Eq. (9) are p_1 and p_N. p_1 can occur within the Wigner transform of $\hat{A}$. Depending on how $\left(\hat{A}\right)_W[y_1, p_1]$ depends on p_1, the integration over p_1 will turn out differently. As long as $\int_{-\infty}^{\infty} dp_1 \left(\hat{A}\right)_W[y_1, p_1] \, e^{-\frac{\beta}{N} H(y_1, p_1)} \, e^{-\frac{i}{\hbar} p_1(x_2 - x_1)}$ can be evaluated analytically, e.g., for $\left(\hat{A}\right)_W[y_1, p_1]$ being any polynomial of p_1 (see Appendix A), all momenta except p_N can be integrated out analytically. p_N can usually not be integrated out analytically since if $\hat{B}$ includes either position or momentum, then $\left(e^{\frac{i\hat{H}t}{\hbar}} \hat{B} \, e^{-\frac{i\hat{H}t}{\hbar}}\right)_W [y_N, p_N]$ will depend on both, unless the potential is constant, and typically this dependence will be such that the integral is not easily evaluated analytically. Hence, these integrations lead to

$$
\langle \hat{A}\hat{B}(t) \rangle = \lim_{N\to\infty} \frac{1}{Z} \left(\frac{mN}{2\pi\beta}\right)^{\frac{N}{2}} \sqrt{\frac{\beta}{2\pi mN}} \, \hbar^{-N} \left\{ \prod_{j=1}^{N} \int_{-\infty}^{\infty} dx_j \right\}
$$
$$
\times \int_{-\infty}^{\infty} dp_N \, e^{-\frac{i}{\hbar} p_N(x_1 - x_N)} A'(y_1, x_2 - x_1)
$$
$$
\times \, e^{-\frac{mN}{2\hbar^2\beta}\sum_{j=1}^{N-1}(x_{j+1}-x_j)^2} \, e^{-\frac{\beta}{N}\sum_{j=1}^{N} V(y_j)}
$$
$$
\times \, e^{-\frac{\beta}{N}\frac{p_N^2}{2m}} \left(e^{\frac{i\hat{H}t}{\hbar}} \hat{B} \, e^{-\frac{i\hat{H}t}{\hbar}}\right)_W [y_N, p_N], \quad (10)
$$

where $A'(y_1, x_2 - x_1)$ is

$$
A'(y_1, x_2 - x_1) = \frac{\int_{-\infty}^{\infty} dp_1 \left(\hat{A}\right)_W[y_1, p_1] \, e^{-\frac{\beta}{N}\frac{p_1^2}{2m}} e^{-\frac{i}{\hbar} p_1(x_2 - x_1)}}{\int_{-\infty}^{\infty} dp_1 \, e^{-\frac{\beta}{N}\frac{p_1^2}{2m}} e^{-\frac{i}{\hbar} p_1(x_2 - x_1)}}
$$
$$
= \frac{\int_{-\infty}^{\infty} dp_1 \left(\hat{A}\right)_W[y_1, p_1] \, e^{-\frac{\beta}{N}\frac{p_1^2}{2m}} e^{-\frac{i}{\hbar} p_1(x_2 - x_1)}}{\sqrt{\frac{2\pi mN}{\beta}} \, e^{-\frac{\beta}{N}\frac{mN^2(x_2 - x_1)^2}{2\hbar^2\beta^2}}} \quad (11)
$$

and may depend on y_1 and/or $x_2 - x_1$.

Finally, the Wigner transform of the time-evolved operator $\hat{B}$ can be very difficult to derive. This is where the classical Wigner method comes in through the approximation $\left(e^{\frac{i\hat{H}t}{\hbar}} \hat{B} \, e^{-\frac{i\hat{H}t}{\hbar}}\right)_W[y_N, p_N] \approx \left(\hat{B}\right)_W[x(y_N, p_N, t), p(y_N, p_N, t)]$ [as in Eq. (3)] giving the final expression,

$$
\langle \hat{A}\hat{B}(t) \rangle \approx \frac{1}{Z} \left(\frac{mN}{2\pi\beta}\right)^{\frac{N}{2}} \sqrt{\frac{\beta}{2\pi mN}} \, \hbar^{-N} \left\{ \prod_{j=1}^{N} \int_{-\infty}^{\infty} dx_j \right\}
$$
$$
\times \int_{-\infty}^{\infty} dp_N \, e^{-\frac{i}{\hbar} p_N(x_1 - x_N)}
$$
$$
\times \, e^{-\frac{\beta}{N}\left(\frac{p_N^2}{2m} + \sum_{j=1}^{N} V(y_j) + \frac{mN^2}{2\hbar^2\beta^2}\sum_{j=1}^{N-1}(x_{j+1}-x_j)^2\right)}
$$
$$
\times A'(y_1, x_2 - x_1)\left(\hat{B}\right)_W[x(y_N, p_N, t), p(y_N, p_N, t)], \quad (12)
$$

where $x(y_N, p_N, t)$ and $p(y_N, p_N, t)$ are the position and momentum coordinates describing the classical trajectory starting with y_N and p_N, and where also for practical reasons the limit of $N \to \infty$ has been removed, thereby making the value of the correlation function at $t = 0$ approximate. When referring to this expression, it will be called $\langle \hat{A}\hat{B}(t) \rangle_{y_1}$. It is noted that Eq. (12) is closely related to an expression recently published by Bose and Makri[12] [Eq. (2.7) in the reference], but not further explored by them. The main difference is that they use a Boltzmann operator that is symmetrized around $\hat{A}$, i.e., $e^{-\frac{\beta}{2}\hat{H}} \hat{A} \, e^{-\frac{\beta}{2}\hat{H}}$. Equation (12) is also related to the $L = 1$ version of the method published by Bonella et al.,[13] more clearly seen in the paper by Bonella and Ciccotti.[14] This method also handles symmetrized Boltzmann operators but uses sum and difference variables for the polymer.

Apart from the asymmetric placement of the Boltzmann operator explored in this paper and the symmetric placement explored in the cited papers, another common handling of the Boltzmann operator is the Kubo transform.[24] This will not be further explored here; however, the Kubo transform of the new method can be found in Appendix B.

It can be noted that in Eq. (12), the effective equilibrium Hamiltonian has terms $\frac{mN^2}{2\hbar^2\beta^2}(x_{j+1} - x_j)^2$. These look exactly like the potential energy of harmonic springs and are, therefore, called "spring terms." This kind of model for a system is usually described as beads on a necklace, with the beads placed at the positions of the x_j:s and connected by springs. The ends of this polymer are connected via the imaginary exponential $-\frac{i}{\hbar} p_N(x_1 - x_N)$, thus making it "open" in the sense that there is no force keeping the ends together, in contrast to other path integral methods such as path integral molecular dynamics,[25] ring polymer molecular dynamics,[3] or path integral Monte Carlo.[26] Even such a method as the open chain imaginary time path integral of Cendagorta et al.[27] would be considered a closed polymer from this point of view. A graphical representation of the open polymer in this work is shown in Fig. 1. This is the polymer advertised in the title of this paper.

Looking back at Eq. (7), it can be seen that if $\hat{A}$ only depends on the position, then $\hat{A}$ can operate to the left and transform into a function of x_1, $A(x_1)$, thereby leaving a matrix element of the Boltzmann operator. This operation removes the approximation of separating the Wigner transforms of $\hat{A}$ and $e^{-\frac{\beta}{N}\hat{H}}$, making this derivation less approximate than the previous one. This means that a new version
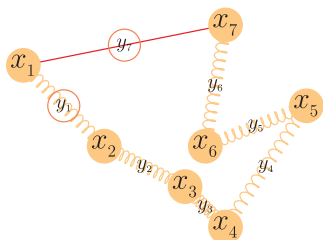
III

FIG. 1. A drawing to exemplify a 7-bead open polymer, where the positions of all the x:s and y:s have been marked. The springs represent the separations that give a spring-term, and the line is the separation that gives the imaginary exponential. y_1 and y_7 (in the circles) are where $A'(y_1, x_2 - x_1)$ and $(\hat{B})_{\mathrm{W}}[x(y_7, p_7, t), p(y_7, p_7, t)]$ are evaluated, respectively.

of Eq. (12) is

$$
\begin{aligned}
\langle \hat{A}\hat{B}(t) \rangle \approx {} & \frac{1}{Z}\left(\frac{mN}{2\pi\beta}\right)^{\frac{N}{2}} \sqrt{\frac{\beta}{2\pi mN}}\, \hbar^{-N} \left\{ \prod_{j=1}^{N} \int_{-\infty}^{\infty} \mathrm{d}x_j \right\} \\
& \times \int_{-\infty}^{\infty} \mathrm{d}p_N\; e^{-\frac{i}{\hbar}p_N(x_1 - x_N)} \\
& \times e^{-\frac{\beta}{N}\left(\frac{p_N^2}{2m} + \sum_{j=1}^{N} V(y_j) + \frac{mN^2}{2\hbar^2\beta^2}\sum_{j=1}^{N-1}(x_{j+1} - x_j)^2\right)} \\
& \times A(x_1)\,(\hat{B})_{\mathrm{W}}[x(y_N, p_N, t), p(y_N, p_N, t)], \quad (13)
\end{aligned}
$$

where the only change compared to before is that $A'(y_1, x_2 - x_1)$ has been replaced by $A(x_1)$. This expression will be referred to as $\langle \hat{A}\hat{B}(t) \rangle_{x_1}$. If $\hat{A}$ depends on both position and momentum, it is in many cases possible to reorder operators so that all position dependence is to the left of all momentum dependence, and then let the position dependent parts operate to the left in Eq. (7), keeping the momentum dependent parts in the matrix element. Of course this would lead to a more complicated expression than $A(x_1)$. Operators of both position and momentum will, however, not be further discussed in this article.

If $\hat{A}$ depends only on momentum, then Eq. (12) will be equivalent to Eq. (13) so that $\langle \hat{A}\hat{B}(t) \rangle_{x_1} = \langle \hat{A}\hat{B}(t) \rangle_{y_1}$. For this situation, the notation $\langle \hat{A}\hat{B}(t) \rangle_{y_1, x_1}$ will be used.

For simplicity of notation, the path integral open polymer method will usually be called Open Polymer Classical Wigner, or OPCW for short, in this paper.

For multidimensional systems, the path integral open polymer method for sampling initial conditions can potentially get a severe sign problem due to the factor $e^{-\frac{i}{\hbar}p_N(x_1 - x_N)}$ appearing in each degree of freedom. The way this problem will be tackled in this article is to sample the initial distribution of the most quantum mechanical or most important degrees of freedom by the path integral open polymer method and the other degrees of freedom by classical mechanics, coupling each bead in the quantum mechanical part(s) with the single bead in the classical parts.

IV. COMPUTATIONAL DETAILS

Equations (12) and (13) were evaluated by Monte Carlo for the integrals over x_j and p_N and with molecular dynamics for the time propagation of $(\hat{B})_{\mathrm{W}}[x(y_N, p_N, t), p(y_N, p_N, t)]$.

The correlation functions studied in this paper are autocorrelation functions of position, position-squared, momentum, and momentum-squared for a one-dimensional quartic potential. In addition, a one-dimensional double well potential and a quartic potential with many-dimensional harmonic baths were studied for the position and position-squared autocorrelation functions.

A. Potentials and system parameters

The potentials studied in this work are a quartic potential, a double well potential, and a quartic potential with various harmonic baths.

The quartic potential was taken as

$$
V_{\mathrm{quartic}}(x) = \frac{m^2\omega^3}{4\hbar}x^4, \quad (14)
$$

where ω is a unit of angular frequency.

The double well potential was taken as

$$
V_{\mathrm{double\ well}}(x) = \frac{m^2\omega^3}{10\hbar}x^4 - \frac{1}{2}m\omega^2 x^2. \quad (15)
$$

The multidimensional systems all use the quartic potential together with the types of baths of Caldeira and Leggett.[28] These systems, thus, have one mostly quartic degree of freedom and several harmonic degrees of freedom that form a bath. The harmonic degrees of freedom in the bath are bilinearly coupled to the quartic degree of freedom. The form of the bath is the one suggested by Craig and Manolopoulos.[29] The bath is a discretized version of a bath with a linear spectral density with an exponential cutoff, and the parameters chosen for the current work are a cutoff frequency of ω and a system–bath coupling strength of $m\omega$. The complete potential is

$$
\begin{aligned}
V_{FD}(x_1, x_2, \ldots, x_{F-1}, x_F) = {} & \frac{m^2\omega^3}{4\hbar}x_1^4 \\
& + \sum_{l=2}^{F} \frac{1}{2}m\omega^2\left(x_l \ln\left(\frac{l-\frac{3}{2}}{F-1}\right) + x_1\sqrt{\frac{2}{(F-1)\pi}}\right)^2, \quad (16)
\end{aligned}
$$

where F is the number of degrees of freedom.

B. Monte Carlo

The maximum stepsize, $\Delta x_{\mathrm{max},l}$, was individually set for all degrees of freedom l, with an initial value of

$$
\Delta x_{\mathrm{max},l} = \sqrt{\frac{2\ln 2}{F\beta\left(\left|\frac{\partial^2 V}{\partial x_l^2}\right|_{x_l=0} + \frac{m_l(N-1)N}{\hbar^2\beta^2}\right)}}. \quad (17)
$$

This choice for stepsize is based on a harmonic approximation of the potential energy, assuming the same average stepsize in x_j and y_j, and aiming for 50% acceptance rate. The change in energy that would give an acceptance likelihood of 50% for a Monte Carlo step

is $N \ln 2/\beta$. $1/F$ of this energy could then be assigned to each degree of freedom. For each degree of freedom, the maximum stepsize is set so that the total energy change resulting from a change in position of $\Delta x_{max,l}$ away from the minimum in the harmonically approximated potential, weighted by N, and the path integral spring potential, weighted by $N-1$, would give this energy. This results in Eq. (17). The above does not work for a situation where $\left|\frac{\partial^2 V}{\partial x_l^2}\right|_{x_l=0} = 0$ and at the same time $N=1$, and in such cases, the maximum stepsize was set to the thermal de Broglie wavelength.

The maximal stepsizes were updated as a group every 50 000th step according to the algorithm of Allen and Tildesley[30] in order to keep the acceptance rate close to 50%.

The momentum, p_N, was sampled from a Maxwell–Boltzmann distribution at the temperature $\frac{N}{k_B\beta}$, where k_B is Boltzmann's constant. The pseudo-random number generator used was ran2 of Press et al.[31] Data were collected, i.e., a molecular dynamics trajectory was run, each 100th Monte Carlo-step.

The Monte Carlo chain begun in a part of phase space that has a low probability of occurring, i.e., far from the equilibrium distribution. It was, however, found that the number of Monte Carlo steps it takes to come close to equilibrium for the various simulated systems is negligible compared to the total length of the Monte Carlo simulation runs and was, therefore, not explicitly accounted for.

C. Molecular dynamics

The molecular dynamics was conducted using the velocity Verlet algorithm.[32,33] The time step was 0.050 ω^{-1} for the quartic and double well one-dimensional systems, and $0.035\omega^{-1}$, $0.025\omega^{-1}$, and $0.020\omega^{-1}$ for the quartic potential with harmonic baths containing 3, 6, and 9 degrees of freedom, respectively. The total time length of each molecular dynamics run was $10\omega^{-1}$.

D. Statistical evaluation of data

The block average method, explained by, e.g., Friedberg and Cameron[34] and Flegal, Haran, and Jones,[35] was used to calculate the standard deviations of the correlation functions. The minimum block size used was 10^6 Monte Carlo-steps. These standard deviations were used as a measure of uncertainty and to determine convergence.

E. Exact correlation functions

In order to have exact classical, quantum mechanical, and classical Wigner results to compare against, numerically exact results were produced for the systems and correlation functions where this was deemed doable.

For the quartic potential and double well potential, the classical mechanics comparison was obtained by setting N = 1, in the same program as was used to find the classical Wigner results, using 10^9 Monte Carlo steps.

The quantum mechanical autocorrelation functions for the quartic potential were calculated with a numerically exact program that uses the lowest 2000 particle in-the-box energy eigenfunctions, with a box length of $40\sqrt{\frac{\hbar}{m\omega}}$, as a basis set to approximate the 40 lowest energy eigenfunctions of the quartic oscillator. These eigenfunctions were then used to evaluate the necessary matrix elements and could be propagated in time analytically. The quantum mechanical autocorrelation functions for the double well potential were calculated in a similar way, but the basis set was the 12 lowest energy eigenfunctions of the harmonic oscillator, $V(x) = \frac{1}{2}m\omega^2x^2$.

For the quartic potential with harmonic bath, just as without the bath, a classical comparison was calculated with one bead, N = 1, in the classical Wigner routine, using 10^9 Monte Carlo steps. The quantum mechanical comparison at $t = 0$ for this case was a path integral Monte Carlo simulation with 80 beads, N = 80, run with the same Monte Carlo parameters as the classical Wigner runs. 64×10^9 Monte Carlo steps were used for 3 degrees of freedom in the bath and 16×10^9 Monte Carlo steps for 6 and 9 degrees of freedom in the bath.

The exact classical Wigner data were generated as follows: First, the matrix elements of the Boltzmann operator were calculated using the numerical matrix multiplication scheme.[36] In this scheme, $N = 50$ and $N = 14$ matrix multiplications of $e^{-\frac{\beta}{N}\hat{H}}$ were used for $\beta\hbar\omega = 8$ and $\beta\hbar\omega = 1$, respectively. Afterward, a numerical Fourier transform of these data was used for computing the Boltzmann Wigner transform. Finally, this Boltzmann Wigner function was represented on a grid for doing classical dynamics.

F. Feynman–Kleinert classical Wigner method

Many of the methods for acquiring an approximate initial distribution for a classical Wigner calculation use a harmonic approximation for the potential.[19,37,38] However, for potentials with negative curvature, these methods all encounter problems when the temperature is too low. For these situations, a modified local Gaussian approximation[39] can be used instead. This is, however, not necessary for the systems and temperatures in this paper.

The Feynman–Kleinert approximation[40] is one of the harmonic approximation methods, and its application to the classical Wigner method is usually called Feynman–Kleinert linearized path integral (FK-LPI).[37] FK-LPI will be used as a comparison for OPCW.

G. Ring polymer molecular dynamics

Ring polymer molecular dynamics (RPMD)[3] is a popular method for calculating approximate quantum dynamics. This method was used as a comparison for the classical Wigner results. The RPMD results were generated by using 32 and 5 beads for $\beta\hbar\omega = 8$ and $\beta\hbar\omega = 1$, respectively, using a time step of $0.009\omega^{-1}$ for the quartic oscillator and a time step of $0.0125\omega^{-1}$ for the double well and quartic oscillator with harmonic baths. The Kubo-transformed results were acquired from the calculations were transformed into the asymmetric placement of the Boltzmann operator through the method by Braams, Miller, and Manolopoulos.[41] The way to calculate momentum-correlation functions with RPMD is through time derivatives of position correlation functions.[29,42] This was considered too complicated for $\langle\hat{p}^2\hat{p}^2(t)\rangle$ so that this function has not been included.

V. RESULTS AND DISCUSSION

In this section, the results from the calculations of a few different autocorrelation functions for a few model systems are presented. Each correlation function is presented by three lines. The middle
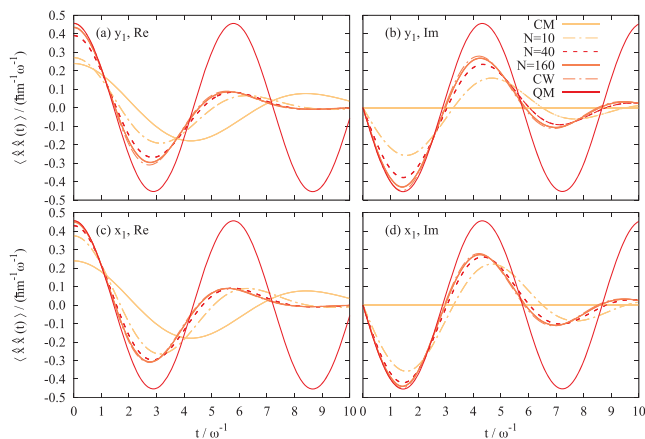
III

FIG. 2. The position autocorrelation function for a quartic potential ($\beta\hbar\omega$ = 8). Comparison between different numbers of beads for the two versions of OPCW and numerically exact solutions for classical mechanics (CM), classical Wigner (CW), and quantum mechanics (QM). The number of Monte Carlo steps used for each number of beads, N, is 1×10^9 for N = 10 and N = 40, and 16×10^9 for N = 160. The outer lines of each type show the standard deviations for the results. If the standard deviation is small enough, the outer lines are not visible. (a) Real part of $\langle \hat{x}\hat{x}(t) \rangle_{y_1}$, (b) imaginary part of $\langle \hat{x}\hat{x}(t) \rangle_{y_1}$, (c) real part of $\langle \hat{x}\hat{x}(t) \rangle_{x_1}$, and (d) imaginary part of $\langle \hat{x}\hat{x}(t) \rangle_{x_1}$.

line is the correlation function itself, and the upper and lower ones show the standard deviation of the result. In most cases presented here, the standard deviations are within the width of the middle line.

A. Quartic potential $\beta\hbar\omega$ = 8

When looking at the correlation functions for the quartic potential calculated with the new method (Figs. 2–4) and numerically exact classical Wigner (Figs. 2 and 3), it can be seen that they flatten out and become constant at long times. This is due

to the fact that the classical Wigner method relies on classical mechanics for propagation forward in time. For all systems with potentials of higher order than harmonic, the classical trajectories do not give the correct coherence, meaning that the individual classical trajectories dephase against each other. Results for a one-dimensional harmonic oscillator, where classical propagation is exact, can be found in Appendix C. Analytic expressions for the harmonic oscillator autocorrelation functions have been placed in Appendix D.

In Fig. 2, it can be seen that at time t = 0, the correlation functions calculated with the new method converge from classical
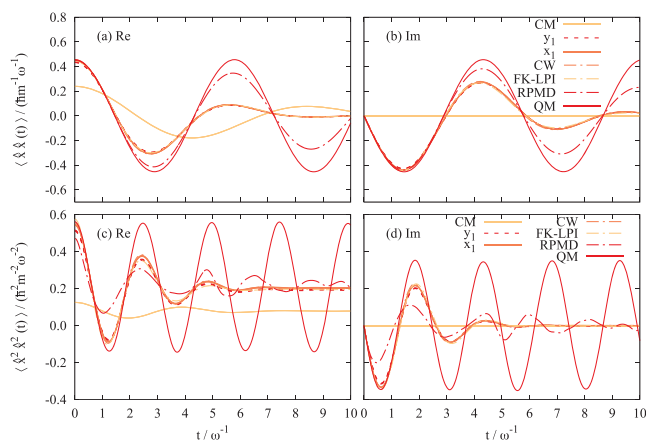

FIG. 3. The position and position-squared autocorrelation functions for a quartic potential ($\beta\hbar\omega$ = 8). Comparison between the two versions of OPCW and numerically exact solutions for classical mechanics (CM), classical Wigner (CW), FK-LPI, RPMD, and quantum mechanics (QM). The number of beads used in the y_1- and x_1-calculations is N = 160, and the number of Monte Carlo steps is 16×10^9. The outer lines of each type show the standard deviations for the results. If the standard deviation is small enough, the outer lines are not visible. (a) Real part of $\langle \hat{x}\hat{x}(t) \rangle$, (b) imaginary part of $\langle \hat{x}\hat{x}(t) \rangle$, (c) real part of $\langle \hat{x}^2\hat{x}^2(t) \rangle$, and (d) imaginary part of $\langle \hat{x}^2\hat{x}^2(t) \rangle$.
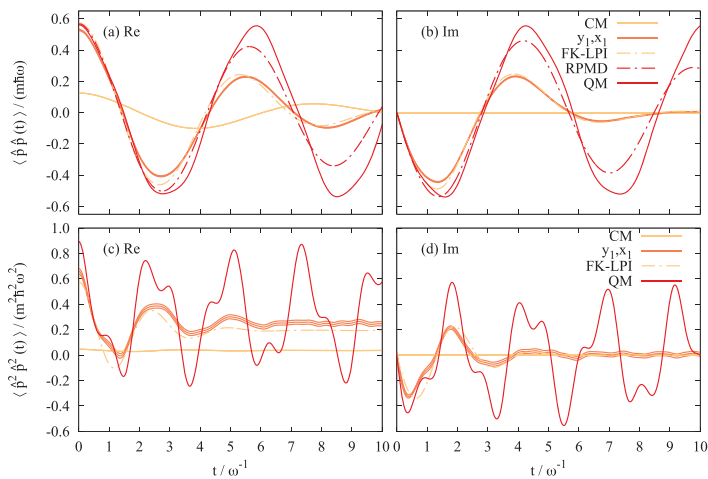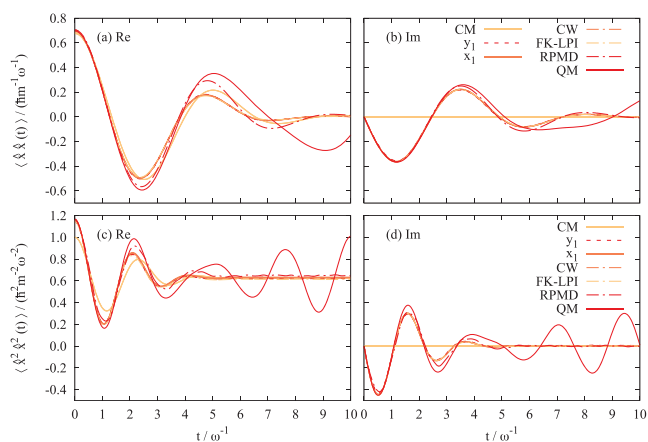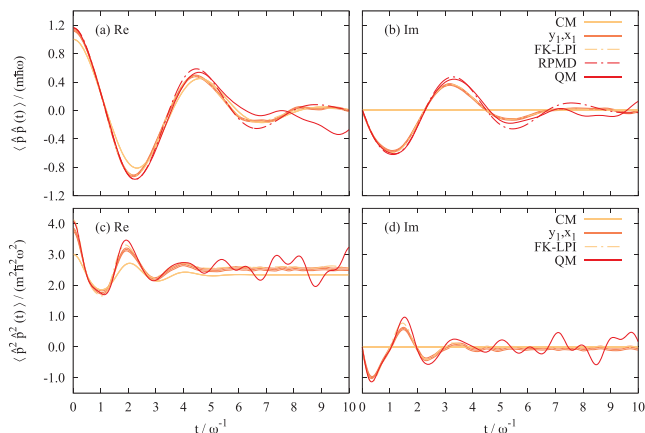
III

FIG. 4. The momentum and momentum-squared autocorrelation functions for a quartic potential ($\beta\hbar\omega = 8$). Comparison between OPCW [with $\langle \hat{p}\hat{p}(t) \rangle_{y_1}$ and $\langle \hat{p}^2\hat{p}^2(t) \rangle_{y_1}$ being identical to $\langle \hat{p}\hat{p}(t) \rangle_{x_1}$ and $\langle \hat{p}^2\hat{p}^2(t) \rangle_{x_1}$, respectively] and numerically exact solutions for classical mechanics (CM), FK-LPI, RPMD, and quantum mechanics (QM). The number of beads used in the calculations of $\langle \hat{p}\hat{p}(t) \rangle_{y_1,x_1}$ is $N = 160$, and the number of Monte Carlo steps is 64×10^9. The number of beads used in the calculations of $\langle \hat{p}^2\hat{p}^2(t) \rangle_{y_1,x_1}$ is $N = 80$, and the number of Monte Carlo steps is 128×10^9. The outer lines of each type show the standard deviations for the results. If the standard deviation is small enough, the outer lines are not visible. (a) Real part of $\langle \hat{p}\hat{p}(t) \rangle$, (b) imaginary part of $\langle \hat{p}\hat{p}(t) \rangle$, (c) real part of $\langle \hat{p}^2\hat{p}^2(t) \rangle$, and (d) imaginary part of $\langle \hat{p}^2\hat{p}^2(t) \rangle$.
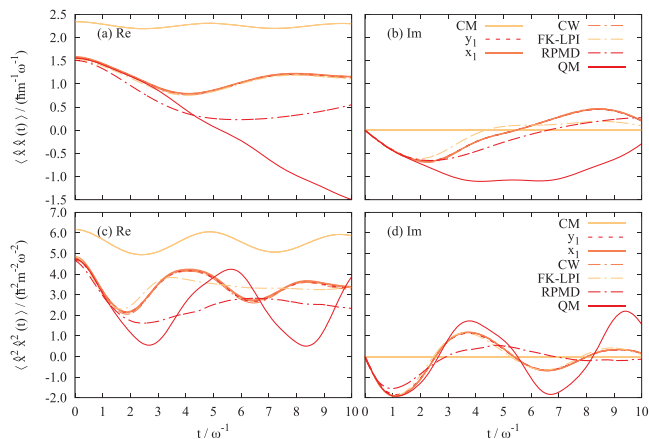

FIG. 5. The position and position-squared autocorrelation functions for a quartic potential ($\beta\hbar\omega = 1$). Comparison between the two versions of OPCW and numerically exact solutions for classical mechanics (CM), classical Wigner (CW), FK-LPI, RPMD, and quantum mechanics (QM). The number of beads used in the y_1- and x_1-calculations of $\langle \hat{x}\hat{x}(t) \rangle$ is $N = 80$, and the number of Monte Carlo steps is 16×10^9. The number of beads used in the y_1- and x_1-calculations of $\langle \hat{x}^2\hat{x}^2(t) \rangle$ is $N = 80$, and the number of Monte Carlo steps is 64×10^9. The outer lines of each type show the standard deviations for the results. If the standard deviation is small enough, the outer lines are not visible. (a) Real part of $\langle \hat{x}\hat{x}(t) \rangle$, (b) imaginary part of $\langle \hat{x}\hat{x}(t) \rangle$, (c) real part of $\langle \hat{x}^2\hat{x}^2(t) \rangle$, and (d) imaginary part of $\langle \hat{x}^2\hat{x}^2(t) \rangle$.

III

FIG. 6. The momentum and momentum-squared autocorrelation functions for a quartic potential ($\beta\hbar\omega = 1$). Comparison between OPCW [with $\langle\hat{p}\hat{p}(t)\rangle_{y_1}$ and $\langle\hat{p}^2\hat{p}^2(t)\rangle_{y_1}$ being identical to $\langle\hat{p}\hat{p}(t)\rangle_{x_1}$ and $\langle\hat{p}^2\hat{p}^2(t)\rangle_{x_1}$, respectively] and numerically exact solutions for classical mechanics (CM), FK-LPI, RPMD, and quantum mechanics (QM). The number of beads used in the calculations of $\langle\hat{p}\hat{p}(t)\rangle_{y_1,x_1}$ is $N = 80$, and the number of Monte Carlo steps is 128×10^9. The number of beads used in the calculations of $\langle\hat{p}^2\hat{p}^2(t)\rangle_{y_1,x_1}$ is $N = 20$, and the number of Monte Carlo steps is 256×10^9. The outer lines of each type show the standard deviations for the results. If the standard deviation is small enough, the outer lines are not visible. (a) Real part of $\langle\hat{p}\hat{p}(t)\rangle_{y_1,x_1}$, (b) imaginary part of $\langle\hat{p}\hat{p}(t)\rangle_{y_1,x_1}$, (c) real part of $\langle\hat{p}^2\hat{p}^2(t)\rangle_{y_1,x_1}$, and (d) imaginary part of $\langle\hat{p}^2\hat{p}^2(t)\rangle_{y_1,x_1}$.

FIG. 7. The position and position-squared autocorrelation functions for a double well potential ($\beta\hbar\omega = 8$). Comparison between the two versions of OPCW and numerically exact solutions for classical mechanics (CM), classical Wigner (CW), FK-LPI, RPMD, and quantum mechanics (QM). The number of beads used in the y_1- and x_1-calculations is $N = 160$, and the number of Monte Carlo steps is 16×10^9. The outer lines of each type show the standard deviations for the results. If the standard deviation is small enough, the outer lines are not visible. (a) Real part of $\langle\hat{x}\hat{x}(t)\rangle$, (b) imaginary part of $\langle\hat{x}\hat{x}(t)\rangle$, (c) real part of $\langle\hat{x}^2\hat{x}^2(t)\rangle$, and (d) imaginary part of $\langle\hat{x}^2\hat{x}^2(t)\rangle$.

mechanics toward quantum mechanics as the number of beads is increased. For all times, the correlation functions calculated with the new method converge toward the exact classical Wigner method. It can also be seen that the x_1-method converges faster than the y_1-method with respect to the number of beads. This is also the case for the harmonic oscillator, see Appendix E, where an explanation for this is also given.

Looking at the individual versions of the new method in Figs. 2 and 3, it can be seen that at least the real parts of $\langle \hat{x}\hat{x}(t)\rangle_{x_1}$ and $\langle \hat{x}^2\hat{x}^2(t)\rangle_{x_1}$ have converged essentially to within the thickness of the line of the exact classical Wigner result for $N = 160$. $\langle \hat{x}\hat{x}(t)\rangle_{y_1}$ and $\langle \hat{x}^2\hat{x}^2(t)\rangle_{y_1}$ converge quite slowly in comparison, and the results for $N = 160$ are not entirely converged to the exact classical Wigner result, even if they are close. $\langle \hat{p}\hat{p}(t)\rangle_{y_1,x_1}$ in Figs. 4(a) and 4(b) has not converged all the way to exact quantum mechanics at $t = 0$ for $N = 160$ but is close.

In Figs. 4(c) and 4(d), it stands out that $\langle \hat{p}^2\hat{p}^2(t)\rangle_{y_1,x_1}$ is far from converged to exact quantum mechanics at $t = 0$, but this is a complicated correlation function. Even though the result for $N = 80$ is not very close to exact quantum mechanics at time $t = 0$, the shapes of the curves have some qualitative agreement.

Correlation functions with $\hat{p}^n$ in the first operator can be expected to be more difficult to converge than correlation functions with $\hat{x}^n$ in the first operator, since $(\hat{p}^n)_W$ will be integrated into an nth-order polynomial of a difference between positions, while $(\hat{x}^n)_W$ will just be a position, or an average of positions, to the power of n (see Appendix A).

In Fig. 3, it can be seen that FK-LPI gives results very close to exact classical Wigner for $\langle \hat{x}\hat{x}(t)\rangle$ and the imaginary part of $\langle \hat{x}^2\hat{x}^2(t)\rangle$, while the real part of $\langle \hat{x}^2\hat{x}^2(t)\rangle$ is a little bit further off. OPCW gives as good, or slightly better, results as FK-LPI, except y_1 for Im$\langle \hat{x}^2\hat{x}^2(t)\rangle$.

In Figs. 4(a) and 4(b), it can be seen that FK-LPI gives a better starting value for $\langle \hat{p}\hat{p}(t)\rangle$ than the calculations with the new method. The oscillations are, however, qualitatively similar. For $\langle \hat{p}^2\hat{p}^2(t)\rangle$ in Figs. 4(c) and 4(d), the results acquired with the new method have a better value at $t = 0$ and has more qualitative agreement with the exact quantum mechanical result than the FK-LPI result.

It is shown in Figs. 3, 4(a), and 4(b) that the classical Wigner method gives worse amplitudes than RPMD for the linear autocorrelation functions, $\langle \hat{x}\hat{x}(t)\rangle$ and $\langle \hat{p}\hat{p}(t)\rangle$. It can, however, also be seen that the classical Wigner method gives better amplitude at short times and better phase overall than RPMD does for the non-linear autocorrelation function $\langle \hat{x}^2\hat{x}^2(t)\rangle$. This is not surprising as it is known that for RPMD to be exact for the harmonic oscillator at least one of the operators in a correlation function has to be linear.[3]

B. Quartic potential $\beta\hbar\omega = 1$

When, for the quartic potential, the temperature is increased so that $\beta\hbar\omega = 1$, instead of $\beta\hbar\omega = 8$, it is shown in Fig. 5 that $\langle \hat{x}\hat{x}(t)\rangle$ and $\langle \hat{x}^2\hat{x}^2(t)\rangle$ for both versions of the new method are almost perfectly converged to the exact classical Wigner result for $N = 80$. This is fewer beads than what seems necessary to achieve a similar convergence at $\beta\hbar\omega = 8$. This is hardly surprising as the classical and quantum mechanical correlation functions are much more similar at $\beta\hbar\omega = 1$ than at $\beta\hbar\omega = 8$.

In Fig. 6, it can be seen that $\langle \hat{p}\hat{p}(t)\rangle_{y_1,x_1}$ is rather well converged toward exact quantum mechanics at $t = 0$. $\langle \hat{p}^2\hat{p}^2(t)\rangle_{y_1,x_1}$ does not reach the limit of the exact quantum mechanics for the $N = 20$ calculation presented here but shows a qualitative agreement with quantum mechanics up to $t = 4\omega^{-1}$
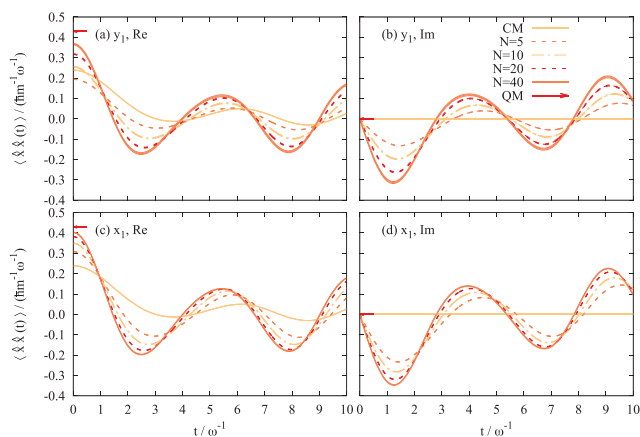

FIG. 8. The position autocorrelation function for a quartic potential with a harmonic bath with 3 degrees of freedom ($\beta\hbar\omega = 8$). Comparison between different numbers of beads for the two versions of OPCW and numerically exact solutions for classical mechanics (CM), at all times and quantum mechanics (QM), at time $t = 0$. The number of Monte Carlo steps used for each number of beads, N, is 1×10^9 for $N = 5$ and $N = 10$, 16×10^9 for $N = 20$, and 64×10^9 for $N = 40$. The outer lines of each type show the standard deviations for the results. If the standard deviation is small enough, the outer lines are not visible. (a) Real part of $\langle \hat{x}\hat{x}(t)\rangle_{y_1}$, (b) imaginary part of $\langle \hat{x}\hat{x}(t)\rangle_{y_1}$, (c) real part of $\langle \hat{x}\hat{x}(t)\rangle_{x_1}$, and (d) imaginary part of $\langle \hat{x}\hat{x}(t)\rangle_{x_1}$.

Generally, even for a lower number of beads the convergence with respect to the number of Monte Carlo steps is worse for $\beta\hbar\omega = 1$ compared to $\beta\hbar\omega = 8$. This is, however, not a problem in practice as fewer beads are required to converge the result to the exact classical Wigner result at the higher temperature.

For $\langle\hat{x}\hat{x}(t)\rangle$ and $\langle\hat{x}^2\hat{x}^2(t)\rangle$, FK-LPI results are essentially the same as the exact classical Wigner results. For $\langle\hat{p}\hat{p}(t)\rangle$, the results from the new method and the FK-LPI results are very similar. However, for $\langle\hat{p}^2\hat{p}^2(t)\rangle$, the FK-LPI results are somewhat closer to the quantum mechanical result than the results produced with OPCW.

For $\langle\hat{x}\hat{x}(t)\rangle$, the classical Wigner method gives worse amplitudes than RPMD. For $\langle\hat{x}^2\hat{x}^2(t)\rangle$, the classical Wigner method possibly gets a somewhat worse amplitude than RPMD. For $\langle\hat{p}\hat{p}(t)\rangle$, it is not obvious if one of the methods performs better than the other.

C. Double well potential $\beta\hbar\omega = 8$

In Fig. 7, it can be seen that all the approximate methods quite early become very different from exact quantum mechanics. This is because dynamical tunneling is important for describing the dynamics of a system like this, which is not taken into account at all in the classical Wigner method and not properly in RPMD. For $\langle\hat{x}\hat{x}(t)\rangle$, the y_1- and x_1-versions of the open polymer method have converged to the exact classical Wigner result by using 160 beads. For $\langle\hat{x}^2\hat{x}^2(t)\rangle$,

the open polymer method has almost converged to the exact classical Wigner result using 160 beads.

The FK-LPI results can be seen to essentially agree with the exact classical Wigner result for the real part of $\langle\hat{x}\hat{x}(t)\rangle$ and to be close to it for the imaginary part of $\langle\hat{x}^2\hat{x}^2(t)\rangle$. For the other cases, FK-LPI is further off. For the real part of $\langle\hat{x}^2\hat{x}^2(t)\rangle$, FK-LPI is substantially off compared to exact classical Wigner. The FK-LPI results do, however, stay almost equal to the exact quantum mechanical results for as long as the exact classical Wigner results do.

The classical Wigner method gives significantly better results than RPMD for the real part of $\langle\hat{x}\hat{x}(t)\rangle$ and the imaginary part of $\langle\hat{x}^2\hat{x}^2(t)\rangle$, and slightly better results for the real part of $\langle\hat{x}^2\hat{x}^2(t)\rangle$. For the imaginary part of $\langle\hat{x}\hat{x}(t)\rangle$, the classical Wigner method and RPMD perform equally well.

D. Quartic potential in harmonic bath $\beta\hbar\omega = 8$

In Figs. 8 and 9, the position and position-squared autocorrelation functions are shown for the quartic oscillator with a harmonic bath of 3 degrees of freedom. The numerically exact quantum mechanical comparison is only available for time $t = 0$ due to the method used for its calculation (see Sec. IV E). It can, in these figures, be seen that the new method converges from classical mechanics toward quantum mechanics at $t = 0$ as the number of beads is increased. The possible exception is for low
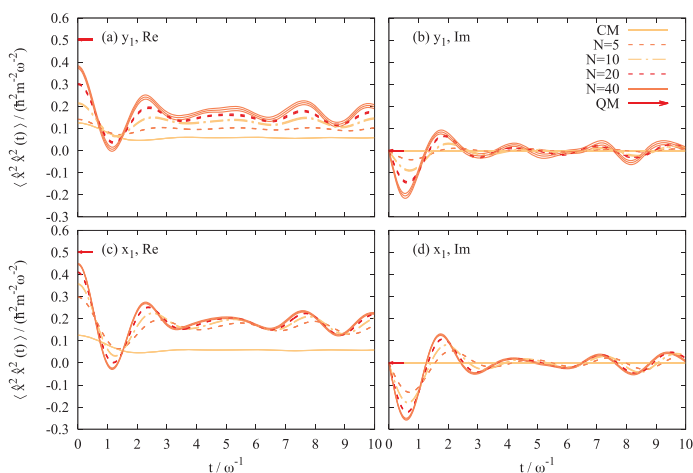

FIG. 9. The position-squared autocorrelation function for a quartic potential with a harmonic bath with 3 degrees of freedom ($\beta\hbar\omega = 8$). Comparison between different numbers of beads for the two versions of OPCW and numerically exact solutions for classical mechanics (CM), at all times and quantum mechanics (QM), at time $t = 0$. The number of Monte Carlo steps used for each number of beads, N, is 1×10^9 for $N = 5$ and $N = 10$, 16×10^9 for $N = 20$, and 64×10^9 for $N = 40$. The outer lines of each type show the standard deviations for the results. If the standard deviation is small enough, the outer lines are not visible. The value in parentheses gives the number of Monte Carlo steps. (a) Real part of $\left\langle\hat{x}^2\hat{x}^2(t)\right\rangle_{y_1}$, (b) imaginary part of $\left\langle\hat{x}^2\hat{x}^2(t)\right\rangle_{y_1}$, (c) real part of $\left\langle\hat{x}^2\hat{x}^2(t)\right\rangle_{x_1}$, and (d) imaginary part of $\left\langle\hat{x}^2\hat{x}^2(t)\right\rangle_{x_1}$.

III

numbers of beads for y_1, as for $N = 5$ $\text{Re}\langle \dot{x}\hat{x}(t)\rangle_{y_1}$ is further from the quantum mechanical result than classical mechanics is.

In Figs. 10–12, the position and position-squared autocorrelation functions are shown for the quartic oscillator with a harmonic bath of 3, 6, and 9 degrees of freedom, respectively.

In Figs. 8, 9, 11, and 12, it can be seen that the x_1-results are significantly closer to quantum mechanics at $t = 0$ than the y_1-results are.

For the case with 3 degrees of freedom in the bath, results are shown that are not entirely converged with respect to the number of Monte Carlo steps used, and it is visible that the x_1-version of the method converges better with respect to the number of Monte Carlo steps than the y_1-version.

Overall, the calculations for the larger numbers of degrees of freedom are fairly computationally intensive and have, therefore, not been numerically converged with respect to the number of beads. However, it is shown in Figs. 10–12 that when the harmonic bath is sampled from a classical distribution, much larger numbers of beads can be used in the quartic oscillator degree of freedom and the number of Monte Carlo steps used is still the same or smaller than used for a one-dimensional quartic potential with a lower number of beads. Making the bath classical, thus, improves the overall convergence drastically. The classical bath calculations are so well converged with regard to both numbers of beads and Monte Carlo steps that the difference between y_1 and x_1 is almost unnoticeable for the correlation functions shown here, and therefore, only the x_1-version is shown. The difference in numerical performance

between the full OPCW calculations and the calculations with classical bath can be seen to increase when the size of the bath is increased.

At time $t = 0$, the calculations employing a classical bath give better values than those using the open polymer for all degrees of freedom. However, even if the quartic oscillator part of a classical bath calculation were to be sampled with an infinite number of beads in the polymer, the classical mechanics of the bath would still mean that the initial value of the correlation functions would not necessarily be the exact quantum mechanical value. The correlation functions for $t > 0$ for the classical bath calculations are qualitatively similar to but have higher amplitudes than the full OPCW calculations. This is the behavior that would be expected from a full OPCW calculation with a larger number of beads.

For the real part of $\langle \hat{x}^2 \hat{x}^2(t)\rangle$, the long time value given by the classical bath calculations is lower than the corresponding result for the full OPCW calculations, except y_1 for 9 degrees of freedom in the bath. From the full OPCW results for the quartic oscillator with a harmonic bath with 3 degrees of freedom (Figs. 8 and 9) and the one-dimensional quartic oscillator (Fig. 2), it can be expected that for the same number of beads in the open polymer, x_1 will be more converged toward exact classical Wigner than y_1 will be. For the quartic oscillator with harmonic baths with 6 and 9 degrees of freedom, Figs. 11 and 12, the results from calculations with classical baths are closer to the y_1-results than to the x_1-results. This indicates that the long time values of $\text{Re}\langle \hat{x}^2 \hat{x}^2(t)\rangle$ may not be very well described
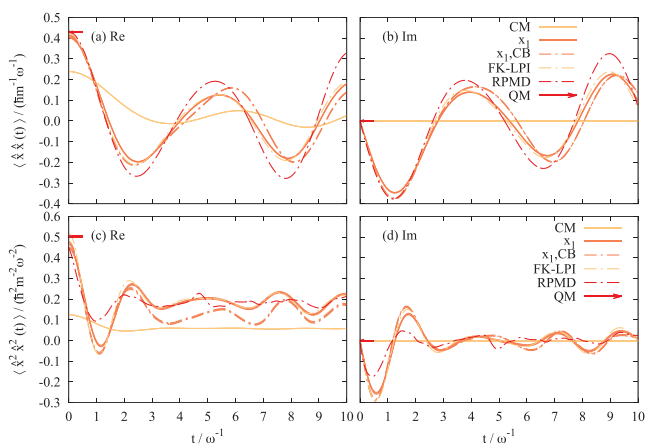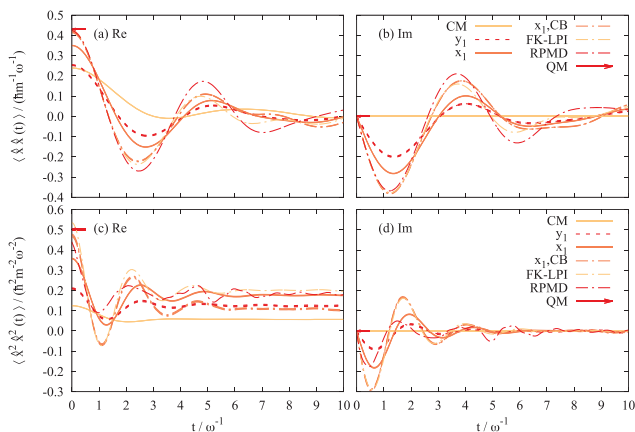

FIG. 10. The position and position-squared autocorrelation functions for a quartic potential with a harmonic bath with 3 degrees of freedom ($\beta\hbar\omega = 8$). Comparison between the x_1-version of OPCW and numerically exact solutions for classical mechanics (CM), FK-LPI, and RPMD, at all times and quantum mechanics (QM), at time $t = 0$. Results for the x_1-version of OPCW with 320 beads in the quartic oscillator and a classical bath, CB, are also shown. The number of beads used in the y_1- and x_1-calculations is $N = 40$, and the number of Monte Carlo steps is 64×10^9. For the calculations with classical bath, the number of Monte Carlo steps used is 16×10^9. The outer lines of each type show the standard deviations for the results. If the standard deviation is small enough, the outer lines are not visible. (a) Real part of $\langle \dot{x}\hat{x}(t)\rangle$, (b) imaginary part of $\langle \dot{x}\hat{x}(t)\rangle$, (c) real part of $\langle \hat{x}^2 \hat{x}^2(t)\rangle$, and (d) imaginary part of $\langle \hat{x}^2 \hat{x}^2(t)\rangle$.

III

FIG. 11. The position and position-squared autocorrelation functions for a quartic potential with a harmonic bath with 6 degrees of freedom ($\beta\hbar\omega = 8$). Comparison between the two versions of OPCW and numerically exact solutions for classical mechanics (CM), FK-LPI, and RPMD, at all times and quantum mechanics (QM), at time $t = 0$. Results for the x_1-version of OPCW with 320 beads in the quartic oscillator and a classical bath, CB, are also shown. The number of beads used in the y_1- and x_1-calculations is $N = 10$, and the number of Monte Carlo steps is 64×10^9. For the calculations with classical bath, the number of Monte Carlo steps used is 16×10^9. The outer lines of each type show the standard deviations for the results. If the standard deviation is small enough, the outer lines are not visible. (a) Real part of $\langle \hat{x}\hat{x}(t) \rangle$, (b) imaginary part of $\langle \hat{x}\hat{x}(t) \rangle$, (c) real part of $\langle \hat{x}^2\hat{x}^2(t) \rangle$, and (d) imaginary part of $\langle \hat{x}^2\hat{x}^2(t) \rangle$.

with the classical bath. This was to be expected as the zero point energy leakage from the system into the bath should be considerable in this type of calculation, and the correlation function, even at long times, is highly dependent on the magnitude of the oscillation in the system degree of freedom.

It can be seen in Figs. 10–12 that the results from the classical bath calculations and the FK-LPI results follow each other closely for the first 2–4 ω^{-1}. At $t = 0$, the classical bath results are as good as or slightly worse than the FK-LPI results.

In Figs. 10(a), 10(b), 11(a), 11(b), 12(a), and 12(b), it can be seen that the classical Wigner method with a classical bath gives slightly worse than or equally good results as RPMD does for $\langle \hat{x}\hat{x}(t) \rangle$ at $t = 0$. Looking at Figs. 10(c), 10(d), 11(c), 11(d), 12(c), and 12(d), it can be seen that the classical Wigner method with a classical bath gives slightly better results than RPMD does for $\langle \hat{x}^2\hat{x}^2(t) \rangle$ at $t = 0$. RPMD, however, goes to higher values at long times for the real part of $\langle \hat{x}^2\hat{x}^2(t) \rangle$, and this may be a better value as it follows $\langle \hat{x}^2\hat{x}^2(t) \rangle_{x_1}$, which should be better converged than $\langle \hat{x}^2\hat{x}^2(t) \rangle_{y_1}$.

E. Summary of results

For all the cases studied here, the results of the new method converge toward exact quantum mechanics at time $t = 0$ as the number of beads increases. Additionally, for all cases where the exact classical Wigner result is available, the new method converges toward this result as the number of beads increases. These convergences are what should be observed according to the derivation of the method.

Some of the results for the one-dimensional quartic oscillator and double well have converged essentially to within the thickness of the line of the exact classical Wigner result.

For the correlation functions where a comparison has been made, the x_1-version of the new method converges faster than the y_1-version with respect to the number of beads used. The x_1-version also converges better than the y_1-version with respect to the number of Monte Carlo steps for these cases. Note also that for almost every graph shown, it can be seen that for a larger number of beads, more Monte Carlo steps have been used to converge the results.

The results for the multidimensional systems using many beads in the polymer for sampling the initial distribution of the quartic oscillator degree of freedom and classical mechanics to sample the initial distribution of the bath show a significant improvement in convergence toward the exact result at $t = 0$ compared to the results of using fewer beads for the full OPCW quartic oscillator with harmonic bath. The long time values of Re$\langle \hat{x}^2\hat{x}^2(t) \rangle$ may, however, be significantly different from the exact classical Wigner result. This is likely to be a result of increased zero point energy leakage when a classical bath is used.

If looking at the one-dimensional and multidimensional potentials, using a classical bath for the multidimensional cases, the results from the open polymer sampled classical Wigner method is about as good as the results from FK-LPI. For the double well potential, the new method clearly reproduces the exact classical Wigner results better than FK-LPI, but the new method does not come closer to
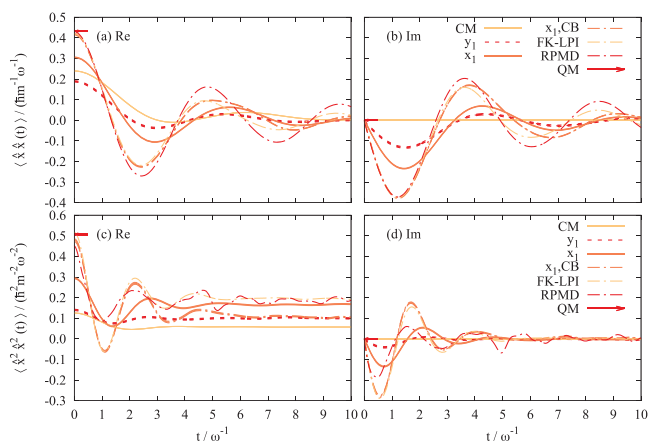
III

FIG. 12. The position and position-squared autocorrelation functions for a quartic potential with a harmonic bath with 9 degrees of freedom ($\beta\hbar\omega = 8$). Comparison between the two versions of OPCW and numerically exact solutions for classical mechanics (CM), FK-LPI, and RPMD, at all times and quantum mechanics (QM), at time $t = 0$. Results for the x_1-version of OPCW with 320 beads in the quartic oscillator and a classical bath, CB, are also shown. The number of beads used in the y_1- and x_1-calculations is $N = 5$, and the number of Monte Carlo steps is 16×10^9. For the calculations with classical bath, the number of Monte Carlo steps used is 16×10^9. The outer lines of each type show the standard deviations for the results. If the standard deviation is small enough, the outer lines are not visible. (a) Real part of $\langle \hat{x}\hat{x}(t) \rangle$, (b) imaginary part of $\langle \hat{x}\hat{x}(t) \rangle$, (c) real part of $\langle \hat{x}^2\hat{x}^2(t) \rangle$, and (d) imaginary part of $\langle \hat{x}^2\hat{x}^2(t) \rangle$.

exact quantum mechanics than FK-LPI. Comparing Figs. 3, 5, and 7, it can be seen that the OPCW method works essentially equally well independent of the potential involved, while in the case of FK-LPI, it works worse for the double well, which contains a region of negative curvature.

In comparison to RPMD, it can be seen that for the one-dimensional quartic oscillator, the classical Wigner method and thereby also the OPCW method perform worse than, or in a single case equally well as, RPMD for autocorrelation functions of linear operators. For the autocorrelation function $\langle \hat{x}^2\hat{x}^2(t) \rangle$, the classical Wigner method gives better results than RPMD at the lower temperature employed here and possibly worse results at the higher temperature. For the one-dimensional double well potential, the classical Wigner method is seen to give better results than RPMD for both $\langle \hat{x}\hat{x}(t) \rangle$ and $\langle \hat{x}^2\hat{x}^2(t) \rangle$. Comparing classical Wigner with a classical bath to RPMD for the multidimensional systems, the classical bath calculations tend to be as good as or better than RPMD, apart from the long time values of $\langle \hat{x}^2\hat{x}^2(t) \rangle$.

VI. CONCLUSION

In this article, two versions of a new way of sampling the initial quantum distribution used in the classical Wigner method for the calculation of correlation functions have been presented and tested for the one-dimensional quartic oscillator and double well

and a quartic oscillator with linearly coupled harmonic baths. The name used for the new method is Open Polymer Classical Wigner (OPCW).

The new method will always converge toward the exact classical Wigner result as the number of beads in the open polymer necklace goes to infinity. For the y_1-version of the new method and the correlation functions and potentials tested here, this convergence is mostly slow. For some cases, the x_1-version of the new method converges considerably faster.

Compared to FK-LPI, the open polymer sampling for the classical Wigner method can give better, worse, or equal results. The double well potential is a case where the two methods give noticeably different results, with the ones from OPCW being closer to exact classical Wigner. Both methods, however, follow exact quantum mechanics equally well for the double well potential. For a well behaved molecular potential, OPCW will always converge toward the exact classical Wigner result as the calculation gets more refined. A harmonic approximation method such as FK-LPI will not necessarily converge toward the exact classical Wigner result for all potential energy surfaces.

The way forward from this study would be to test the method developed here on other potentials and correlation functions. One set of correlation functions that are of chemical interest and that possibly could be calculated by the presented method are the ones of Miller, Schwartz, and Tromp[43,44] that can be used to acquire reaction rate constants. Potential energy surfaces in reaction rate calculations

tend to have barriers, such as the one in the double well tested here, and this is where the new method may be an improvement over methods such as FK-LPI, since OPCW for the double well approximates the exact classical Wigner result noticeably better than FK-LPI does.

Systems with many degrees of freedom are seen to be computationally demanding. Describing the harmonic baths studied with classical mechanics improves the situation considerably. It would thus be of interest to try this out on other multidimensional systems. This should be particularly useful when the coupling between the system and the bath is weak. It would also be of interest to try a less approximate simplification for the less quantum mechanical degrees of freedom in a system, such as an open polymer equivalent to the ring polymer contraction of Markland and Manolopoulos.[45] Another approach of interest for handling the more computationally demanding systems would be to try to enhance convergence using the techniques recently introduced by Bose and Makri.[12]

APPENDIX A: ANALYTIC FORMS OF $A'(y_1, x_2 - x_1)$ FOR $(\hat{A})_W[y_1 p_1]$ BEING A POLYNOMIAL IN p_1

If $(\hat{A})_W[y_1, p_1]$ is a polynomial with respect to p_1, i.e.,

$$(\hat{A})_W[y_1, p_1] = k_n p_1^n + k_{n-1} p_1^{n-1} \ldots k_2 p_1^2 + k_1 p_1 + k_0, \quad \text{(A1)}$$

where $k_n, \ldots, k_0$ are constants, then the solution to Eq. (11) is

$$
\begin{aligned}
A'(y_1, x_2 - x_1) &= \frac{\int_{-\infty}^{\infty} dp_1 \, (\hat{A})_W[y_1, p_1] \, e^{-\frac{\beta}{N}\frac{p_1^2}{2m}} \, e^{-\frac{i}{\hbar} p_1 (x_2 - x_1)}}{\sqrt{\frac{2\pi m N}{\beta}} \, e^{-\frac{\beta}{N}\frac{mN^2(x_2-x_1)^2}{2\hbar^2\beta^2}}} \\
&= k_n(-i)^n \left(\frac{mN}{2\beta}\right)^{\frac{n}{2}} H_n\left(\sqrt{\frac{mN}{2\beta}} \frac{x_2 - x_1}{\hbar}\right) + k_{n-1}(-i)^{n-1}\left(\frac{mN}{2\beta}\right)^{\frac{n-1}{2}} H_{n-1}\left(\sqrt{\frac{mN}{2\beta}} \frac{x_2 - x_1}{\hbar}\right) \ldots \\
&\quad + k_2(-i)^2\left(\frac{mN}{2\beta}\right)^{\frac{2}{2}} H_2\left(\sqrt{\frac{mN}{2\beta}} \frac{x_2 - x_1}{\hbar}\right) + k_1(-i)\left(\frac{mN}{2\beta}\right)^{\frac{1}{2}} H_1\left(\sqrt{\frac{mN}{2\beta}} \frac{x_2 - x_1}{\hbar}\right) + k_0 \\
&= \sum_{j=0}^{n} k_j(-i)^j\left(\frac{mN}{2\beta}\right)^{\frac{j}{2}} H_j\left(\sqrt{\frac{mN}{2\beta}} \frac{x_2 - x_1}{\hbar}\right),
\end{aligned}
\quad \text{(A2)}
$$

where $H_j(\chi)$ is the Hermite polynomial defined by

$$H_j(\chi) = (-1)^j e^{\chi^2} \frac{d^j}{d\chi^j} e^{-\chi^2}, \quad \text{(A3)}$$

where χ is a dummy variable.

APPENDIX B: KUBO TRANSFORM

One possible form of the Kubo transform[24] of the open polymer expression presented in this article is

$$
\begin{aligned}
\langle \hat{A}\hat{B}(t)\rangle_{\text{Kubo}} &= \frac{1}{Z} \text{Tr}\left\{\frac{1}{\beta}\int_0^\beta d\lambda \, e^{-\lambda\hat{H}}\hat{A}\, e^{-(\beta-\lambda)\hat{H}}\hat{B}(t)\right\} \\
&\approx \frac{1}{Z}\left(\frac{mN}{2\pi\beta}\right)^{\frac{N}{2}}\sqrt{\frac{\beta}{2\pi m N}}\hbar^{-N}\left\{\prod_{j=1}^{N}\int_{-\infty}^{\infty} dx_j\right\}\int_{-\infty}^{\infty} dp_N \, e^{-\frac{i}{\hbar}p_N(x_1 - x_N)} \\
&\quad \times e^{-\frac{\beta}{N}\left(\frac{p_N^2}{2m} + \sum_{j=1}^{N} V(y_j) + \frac{mN^2}{2\hbar^2\beta^2}\sum_{j=1}^{N-1}(x_{j+1}-x_j)^2\right)}(\hat{B})_W[x(y_N, p_N, t), p(y_N, p_N, t)] \\
&\quad \times \frac{1}{N}\left(\frac{1}{2}A'(y_1, x_2 - x_1) + \sum_{k=1}^{N-2} A'(y_{k+1}, x_{k+2} - x_{k+1}) + \frac{3}{2}A'(y_{N-1}, x_N - x_{N-1})\right).
\end{aligned}
\quad \text{(B1)}
$$

It can be noted that the double counting of $A'(y_{N-1}, x_N - x_{N-1})$ is due to the approximation $\left(\hat{\Omega}\, e^{-\frac{\beta}{N}\hat{H}}\right)_W[x,p] \approx \left(\hat{\Omega}\right)_W[x,p]\left(e^{-\frac{\beta}{N}\hat{H}}\right)_W[x,p]$
$\approx \left(e^{-\frac{\beta}{N}\hat{H}}\hat{\Omega}\right)_W[x,p]$. This double counting leads to an asymmetry that means that the resulting correlation function may have an imaginary part. If using the Kubo transform, this may be an unwanted property, so the mean of the above expression and its complex conjugate may be used instead,

$$
\begin{aligned}
\langle \hat{A}\hat{B}(t)\rangle_{\text{Kubo}} \approx{}& \frac{1}{Z}\left(\frac{mN}{2\pi\beta}\right)^{\frac{N}{2}}\sqrt{\frac{\beta}{2\pi mN}}\,\hbar^{-N}\left\{\prod_{j=1}^{N}\int_{-\infty}^{\infty}dx_j\right\}\int_{-\infty}^{\infty}dp_N\ e^{-\frac{\beta}{N}\left(\frac{p_N^2}{2m}+\sum_{j=1}^{N}V(y_j)+\frac{mN^2}{2\hbar^2\beta^2}\sum_{j=1}^{N-1}(x_{j+1}-x_j)^2\right)}\left(\hat{B}\right)_W[x(y_N,p_N,t),p(y_N,p_N,t)]\\
&\times\frac{1}{2N}\Bigg(e^{-\frac{i}{\hbar}p_N(x_1-x_N)}\left(\frac{1}{2}A'(y_1,x_2-x_1)+\sum_{k=2}^{N-1}A'(y_k,x_{k+1}-x_k)+\frac{3}{2}A'(y_{N-1},x_N-x_{N-1})\right)\\
&+e^{\frac{i}{\hbar}p_N(x_1-x_N)}\left(\frac{1}{2}A'(y_{N-1},x_{N-1}-x_N)+\sum_{k=1}^{N-2}A'(y_k,x_k-x_{k+1})+\frac{3}{2}A'(y_1,x_1-x_2)\right)\Bigg),
\end{aligned}
\tag{B2}
$$

which should not give an imaginary part. If $A'(y_j, x_{j+1}-x_j)$ is either an even or odd function with regard to $x_{j+1}-x_j$, the expression can be simplified to

$$
\begin{aligned}
\langle\hat{A}\hat{B}(t)\rangle_{\text{Kubo, even}} \approx{}& \frac{1}{Z}\left(\frac{mN}{2\pi\beta}\right)^{\frac{N}{2}}\sqrt{\frac{\beta}{2\pi mN}}\,\hbar^{-N}\left\{\prod_{j=1}^{N}\int_{-\infty}^{\infty}dx_j\right\}\int_{-\infty}^{\infty}dp_N\ e^{-\frac{\beta}{N}\left(\frac{p_N^2}{2m}+\sum_{j=1}^{N}V(y_j)+\frac{mN^2}{2\hbar^2\beta^2}\sum_{j=1}^{N-1}(x_{j+1}-x_j)^2\right)}\left(\hat{B}\right)_W[x(y_N,p_N,t),p(y_N,p_N,t)]\\
&\times\frac{1}{N}\Bigg(\cos\left(\frac{p_N(x_1-x_N)}{\hbar}\right)\left(\frac{1}{2}A'(y_1,x_2-x_1)+\sum_{k=2}^{N-2}A'(y_k,x_{k+1}-x_k)+\frac{1}{2}A'(y_{N-1},x_N-x_{N-1})\right)\\
&+e^{\frac{i}{\hbar}p_N(x_1-x_N)}A'(y_1,x_2-x_1)+e^{-\frac{i}{\hbar}p_N(x_1-x_N)}A'(y_{N-1},x_N-x_{N-1})\Bigg)
\end{aligned}
\tag{B3}
$$

for even A' and

$$
\begin{aligned}
\langle\hat{A}\hat{B}(t)\rangle_{\text{Kubo, odd}} \approx{}& \frac{1}{Z}\left(\frac{mN}{2\pi\beta}\right)^{\frac{N}{2}}\sqrt{\frac{\beta}{2\pi mN}}\,\hbar^{-N}\left\{\prod_{j=1}^{N}\int_{-\infty}^{\infty}dx_j\right\}\int_{-\infty}^{\infty}dp_N\ e^{-\frac{\beta}{N}\left(\frac{p_N^2}{2m}+\sum_{j=1}^{N}V(y_j)+\frac{mN^2}{2\hbar^2\beta^2}\sum_{j=1}^{N-1}(x_{j+1}-x_j)^2\right)}\\
&\times\left(\hat{B}\right)_W[x(y_N,p_N,t),p(y_N,p_N,t)]\\
&\times\frac{1}{N}\Bigg(-i\sin\left(\frac{p_N(x_1-x_N)}{\hbar}\right)\left(\frac{1}{2}A'(y_1,x_2-x_1)+\sum_{k=2}^{N-2}A'(y_k,x_{k+1}-x_k)+\frac{1}{2}A'(y_{N-1},x_N-x_{N-1})\right)\\
&-e^{\frac{i}{\hbar}p_N(x_1-x_N)}A'(y_1,x_2-x_1)+e^{-\frac{i}{\hbar}p_N(x_1-x_N)}A'(y_{N-1},x_N-x_{N-1})\Bigg)
\end{aligned}
\tag{B4}
$$

for odd A'.

APPENDIX C: RESULTS FOR HARMONIC POTENTIAL $\beta\hbar\omega = 8$

Apart from the calculations shown in the main body of this article, the four autocorrelation functions position, position-squared, momentum, and momentum-squared were also calculated for a one-dimensional harmonic oscillator.

The harmonic potential was taken as

$$
V_{\text{harmonic}}(x) = \frac{1}{2}m\omega^2 x^2,
\tag{C1}
$$

where ω is the angular frequency of the harmonic oscillation.

The Monte Carlo procedure and molecular dynamics were conducted as for the other systems. The time step used in the molecular dynamics was $0.050\omega^{-1}$.

In order to have exact values to compare our calculated results against, anaytical classical and quantum mechanical correlation functions were used. These functions are collected in Appendix D.

As shown in Fig. 13 for both versions of the new method, the real and imaginary parts of the position autocorrelation function converge from exact classical mechanics toward exact quantum mechanics as the number of beads increases. $\langle\hat{x}\hat{x}(t)\rangle_{x_1}$ converges toward quantum mechanics, with respect to the number of
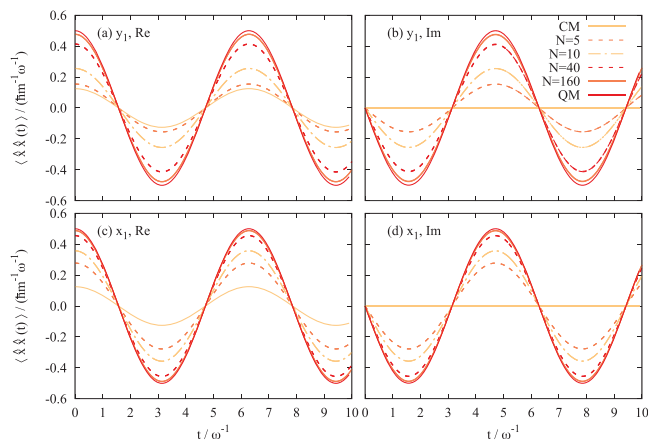
III

FIG. 13. The position autocorrelation function for a harmonic potential ($\beta\hbar\omega$ = 8). Comparison between different numbers of beads for the two versions of OPCW and exact solutions for classical mechanics (CM) and quantum mechanics (QM). The number of Monte Carlo steps used for each number of beads, N, is 1×10^9 for $N = 5$, $N = 10$, and $N = 40$, and 64×10^9 for $N = 160$. The standard deviations are in all cases small enough not to be visible. (a) Real part of $\langle \hat{x}\hat{x}(t) \rangle_{y_1}$, (b) imaginary part of $\langle \hat{x}\hat{x}(t) \rangle_{y_1}$, (c) real part of $\langle \hat{x}\hat{x}(t) \rangle_{x_1}$, and (d) imaginary part of $\langle \hat{x}\hat{x}(t) \rangle_{x_1}$.

beads, noticeably faster than $\langle \hat{x}\hat{x}(t) \rangle_{y_1}$. This ordering of speed of convergence with regard to the number of beads, N, is what could be expected since $\langle \hat{x}\hat{x}(t) \rangle_{x_1}$ requires the positions of neighboring beads to converge to the same value, while $\langle \hat{x}\hat{x}(t) \rangle_{y_1}$ also requires the positions of next neighboring beads to converge to the same value (see Appendix E 1).

In Fig. 14, the position-squared autocorrelation function can be seen for both versions of the method studied. Both versions of the method, just as for the previous correlation function, converge from classical toward quantum mechanics as the number

of beads increases. Similar to the previous correlation function, $\langle \hat{x}^2\hat{x}^2(t) \rangle_{x_1}$ converges faster with respect to the number of beads than $\langle \hat{x}^2\hat{x}^2(t) \rangle_{y_1}$, as could be expected (see Appendix E 2).

In Fig. 15, the position and position-squared autocorrelation functions from the two versions of the open polymer method can be compared to each other, exact classical mechanics, exact quantum mechanics, and RPMD. FK-LPI is always exact for a harmonic potential, so it is equivalent to exact classical mechanics. As RPMD is exact for correlation functions with at least one linear operator in a harmonic potential,[3] the exact RPMD result is also equivalent
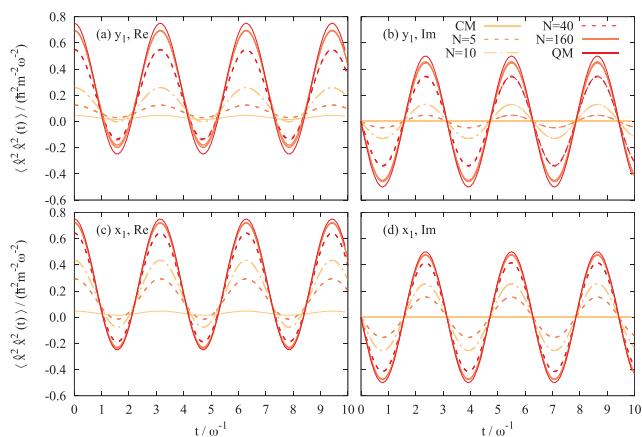

FIG. 14. The position-squared autocorrelation function for a harmonic potential ($\beta\hbar\omega$ = 8). Comparison between different numbers of beads for the two versions of OPCW and exact solutions for classical mechanics (CM) and quantum mechanics (QM). The number of Monte Carlo steps used for each number of beads, N, is 1×10^9 for $N = 5$ and $N = 10$, 4×10^9 for $N = 40$, and 64×10^9 for $N = 160$. The outer lines of each type show the standard deviations for the results. If the standard deviation is small enough, the outer lines are not visible. (a) Real part of $\langle \hat{x}^2\hat{x}^2(t) \rangle_{y_1}$, (b) imaginary part of $\langle \hat{x}^2\hat{x}^2(t) \rangle_{y_1}$, (c) real part of $\langle \hat{x}^2\hat{x}^2(t) \rangle_{x_1}$, and (d) imaginary part of $\langle \hat{x}^2\hat{x}^2(t) \rangle_{x_1}$.
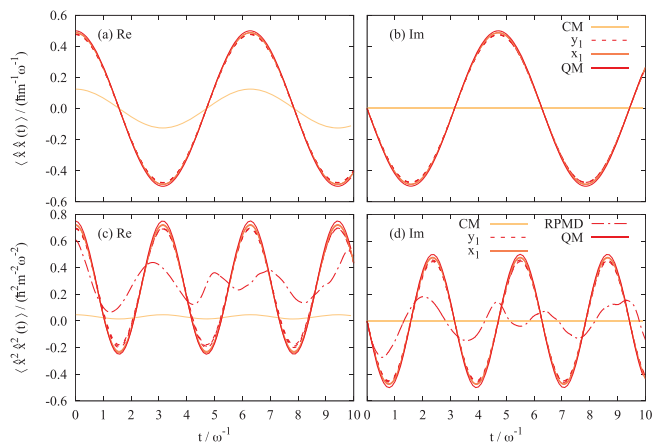
III

FIG. **15**. The position and position-squared autocorrelation functions for a harmonic potential ($\beta\hbar\omega = 8$). Comparison between the two versions of OPCW and numerically exact solutions for classical mechanics (CM), classical Wigner (CW), RPMD, and quantum mechanics (QM). The number of beads used in the y_1- and x_1-calculations is $N = 160$, and the number of Monte Carlo steps is 64×10^9. The outer lines of each type show the standard deviations for the results. If the standard deviation is small enough, the outer lines are not visible. (a) Real part of $\langle \hat{x}\hat{x}(t) \rangle$, (b) imaginary part of $\langle \hat{x}\hat{x}(t) \rangle$, (c) real part of $\langle \hat{x}^2\hat{x}^2(t) \rangle$, and (d) imaginary part of $\langle \hat{x}^2\hat{x}^2(t) \rangle$.

to exact quantum mechanics for $\langle \hat{x}\hat{x}(t) \rangle$. For $\langle \hat{x}^2\hat{x}^2(t) \rangle$, it can be seen that the classical Wigner method gives better results than RPMD. This is to be expected as the classical Wigner method is exact for any correlation function for a harmonic potential, while

RPMD is not exact when both operators in the correlation function are non-linear.

In Fig. 16, the momentum and momentum-squared autocorrelation functions are shown. For these correlation functions, the
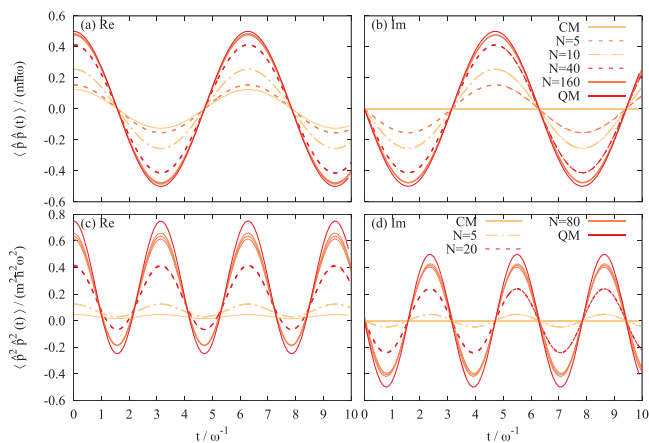

FIG. **16**. The momentum and momentum-squared autocorrelation functions for a harmonic potential ($\beta\hbar\omega = 8$). Comparison between different numbers of beads for OPCW [with $\langle \hat{p}\hat{p}(t) \rangle_{y_1}$ and $\langle \hat{p}^2\hat{p}^2(t) \rangle_{y_1}$ being identical to $\langle \hat{p}\hat{p}(t) \rangle_{x_1}$ and $\langle \hat{p}^2\hat{p}^2(t) \rangle_{x_1}$, respectively] and exact solutions for classical mechanics (CM) and quantum mechanics (QM). The number of Monte Carlo steps used for each number of beads, N, for the calculation of $\langle \hat{p}\hat{p}(t) \rangle_{y_1,x_1}$ is 1×10^9 for $N = 5$ and $N = 10$, 4×10^9 for $N = 40$, and 64×10^9 for $N = 160$. The number of Monte Carlo steps used for each number of beads for the calculation of $\langle \hat{p}^2\hat{p}^2(t) \rangle_{y_1,x_1}$ is 1×10^9 for $N = 5$, 4×10^9 for $N = 20$, and 128×10^9 for $N = 80$. The outer lines of each type show the standard deviations for the results. If the standard deviation is small enough, the outer lines are not visible. (a) Real part of $\langle \hat{p}\hat{p}(t) \rangle_{y_1,x_1}$, (b) imaginary part of $\langle \hat{p}\hat{p}(t) \rangle_{y_1,x_1}$, (c) real part of $\langle \hat{p}^2\hat{p}^2(t) \rangle_{y_1,x_1}$, and (d) imaginary part of $\langle \hat{p}^2\hat{p}^2(t) \rangle_{y_1,x_1}$.

III

two versions of the method are identical. $\langle \hat{p}\hat{p}(t) \rangle_{y_1,x_1}$ converges in a similar way as $\langle \hat{x}\hat{x}(t) \rangle_{y_1}$ does with respect to the number of beads. $\langle \hat{p}^2\hat{p}^2(t) \rangle_{y_1,x_1}$, as all the other correlation functions, converges with respect to the number of beads from classical toward quantum mechanics. In this work, $\langle \hat{p}^2\hat{p}^2(t) \rangle_{y_1,x_1}$ is the most difficult correlation function to converge with respect to the number of Monte Carlo steps. That is why no results from calculations with $N = 160$ are shown, and why the standard deviations are visible in the results for $N = 80$.

APPENDIX D: ANALYTIC CORRELATION FUNCTIONS FOR THE HARMONIC OSCILLATOR

For the harmonic oscillator described in Appendix C, correlation functions can be calculated analytically. $\langle \hat{x}\hat{x}(t) \rangle$ and $\langle \hat{p}\hat{p}(t) \rangle$ are straightforward to derive. $\langle \hat{x}^2\hat{x}^2(t) \rangle$ and $\langle \hat{p}^2\hat{p}^2(t) \rangle$ can be acquired from the simpler correlation functions by using the cumulant expansion of Cao and Voth.[46] The correlation functions are, for classical mechanics,

$$\langle \hat{x}\hat{x}(t) \rangle = \frac{1}{\beta m \omega^2} \cos(\omega t), \tag{D1}$$

$$\langle \hat{x}^2\hat{x}^2(t) \rangle = \frac{1}{\beta^2 m^2 \omega^4}\left(1 + 2\cos^2(\omega t)\right), \tag{D2}$$

$$\langle \hat{p}\hat{p}(t) \rangle = \frac{m}{\beta} \cos(\omega t), \tag{D3}$$

$$\langle \hat{p}^2\hat{p}^2(t) \rangle = \frac{m^2}{\beta^2}\left(1 + 2\cos^2(\omega t)\right), \tag{D4}$$

and, for quantum mechanics,

$$\langle \hat{x}\hat{x}(t) \rangle = \frac{\hbar}{2\,m\omega}\left(\frac{e^{\beta\hbar\omega}}{e^{\beta\hbar\omega}-1}\,e^{-i\omega t} + \frac{1}{e^{\beta\hbar\omega}-1}\,e^{i\omega t}\right), \tag{D5}$$

$$\langle \hat{x}^2\hat{x}^2(t) \rangle = \frac{\hbar^2}{4\,m^2\omega^2}\Bigg(\left(\frac{e^{\beta\hbar\omega}+1}{e^{\beta\hbar\omega}-1}\right)^2$$
$$+ 2\left(\frac{e^{\beta\hbar\omega}}{e^{\beta\hbar\omega}-1}\,e^{-i\omega t} + \frac{1}{e^{\beta\hbar\omega}-1}\,e^{i\omega t}\right)^2\Bigg), \tag{D6}$$

$$\langle \hat{p}\hat{p}(t) \rangle = \frac{m\hbar\omega}{2}\left(\frac{e^{\beta\hbar\omega}}{e^{\beta\hbar\omega}-1}\,e^{-i\omega t} + \frac{1}{e^{\beta\hbar\omega}-1}\,e^{i\omega t}\right), \tag{D7}$$

$$\langle \hat{p}^2\hat{p}^2(t) \rangle = \frac{m^2\hbar^2\omega^2}{4}\Bigg(\left(\frac{e^{\beta\hbar\omega}+1}{e^{\beta\hbar\omega}-1}\right)^2$$
$$+ 2\left(\frac{e^{\beta\hbar\omega}}{e^{\beta\hbar\omega}-1}\,e^{-i\omega t} + \frac{1}{e^{\beta\hbar\omega}-1}\,e^{i\omega t}\right)^2\Bigg). \tag{D8}$$

APPENDIX E: COMPARISON OF THE REAL AND IMAGINARY PARTS OF CORRELATION FUNCTIONS FOR THE HARMONIC POTENTIAL

For the harmonic oscillator, the analytical equations of motion can be put into $\left(\hat{B}\right)_W[x(y_N,p_N,t),p(y_N,p_N,t)]$ and

$\left(\hat{B}\right)_W[x(x_N,p_N,t),p(x_N,p_N,t)]$ in Eqs. (12) and (13). This appendix shows how some autocorrelation functions behave for the two versions of the method presented in this paper.

1. Position autocorrelation function, $\langle \hat{x}\hat{x}(\mathbf{t}) \rangle$

For the case of $\langle \hat{x}\hat{x}(t) \rangle$, entering the analytical equations of motion into Eqs. (12) and (13) leads to

$$\langle \hat{x}\hat{x}(t) \rangle_{y_1} = \frac{1}{Z}\left(\frac{mN}{2\pi\beta}\right)^{\frac{N}{2}}\sqrt{\frac{\beta}{2\pi mN}}\,\hbar^{-N}\left\{\prod_{j=1}^{N}\int_{-\infty}^{\infty}dx_j\right\}$$
$$\times \int_{-\infty}^{\infty}dp_N\;e^{-\frac{i}{\hbar}p_N(x_1-x_N)}$$
$$\times e^{-\frac{\beta}{N}\left(\frac{p_N^2}{2m}+\sum_{j=1}^{N}V(y_j)+\frac{mN^2}{2\hbar^2\beta^2}\sum_{j=1}^{N-1}(x_{j+1}-x_j)^2\right)}$$
$$\times y_1\left(y_N\cos(\omega t) + \frac{p_N}{m\omega}\sin(\omega t)\right), \tag{E1}$$

$$\langle \hat{x}\hat{x}(t) \rangle_{x_1} = \frac{1}{Z}\left(\frac{mN}{2\pi\beta}\right)^{\frac{N}{2}}\sqrt{\frac{\beta}{2\pi mN}}\,\hbar^{-N}\left\{\prod_{j=1}^{N}\int_{-\infty}^{\infty}dx_j\right\}$$
$$\times \int_{-\infty}^{\infty}dp_N\;e^{-\frac{i}{\hbar}p_N(x_1-x_N)}$$
$$\times e^{-\frac{\beta}{N}\left(\frac{p_N^2}{2m}+\sum_{j=1}^{N}V(y_j)+\frac{mN^2}{2\hbar^2\beta^2}\sum_{j=1}^{N-1}(x_{j+1}-x_j)^2\right)}$$
$$\times x_1\left(y_N\cos(\omega t) + \frac{p_N}{m\omega}\sin(\omega t)\right). \tag{E2}$$

To simplify, p_N can be integrated out and all constants that are identical in both cases can be collected into a single constant, C,

$$\langle \hat{x}\hat{x}(t) \rangle_{y_1} = C\left\{\prod_{j=1}^{N}\int_{-\infty}^{\infty}dx_j\right\}e^{-\frac{\beta}{N}\left(\sum_{j=1}^{N}V(y_j)+\frac{mN^2}{2\hbar^2\beta^2}\sum_{j=1}^{N}(x_{j+1}-x_j)^2\right)}$$
$$\times y_1\left(y_N\cos(\omega t) - \frac{iN}{\beta\hbar\omega}(x_1-x_N)\sin(\omega t)\right), \tag{E3}$$

$$\langle \hat{x}\hat{x}(t) \rangle_{x_1} = C\left\{\prod_{j=1}^{N}\int_{-\infty}^{\infty}dx_j\right\}e^{-\frac{\beta}{N}\left(\sum_{j=1}^{N}V(y_j)+\frac{mN^2}{2\hbar^2\beta^2}\sum_{j=1}^{N}(x_{j+1}-x_j)^2\right)}$$
$$\times x_1\left(y_N\cos(\omega t) - \frac{iN}{\beta\hbar\omega}(x_1-x_N)\sin(\omega t)\right). \tag{E4}$$

These correlation functions are Boltzmann-weighted averages, which can be simplified to

$$\langle \hat{x}\hat{x}(t) \rangle_{y_1} = \left\langle y_1\left(y_N\cos(\omega t) - \frac{iN}{\beta\hbar\omega}(x_1-x_N)\sin(\omega t)\right)\right\rangle, \tag{E5}$$

$$\langle \hat{x}\hat{x}(t) \rangle_{x_1} = \left\langle x_1\left(y_N\cos(\omega t) - \frac{iN}{\beta\hbar\omega}(x_1-x_N)\sin(\omega t)\right)\right\rangle. \tag{E6}$$

Now, the correlation functions can be separated into the real parts,

$$\mathrm{Re}\langle \hat{x}\hat{x}(t) \rangle_{y_1} = \cos(\omega t)\langle y_1 y_N \rangle$$
$$= \frac{\cos(\omega t)}{4}\left(\langle x_1^2 \rangle + \langle x_1 x_N \rangle + \langle x_1 x_2 \rangle + \langle x_2 x_N \rangle\right)$$
$$= \frac{\cos(\omega t)}{4}\left(\langle x_1^2 \rangle + 2\langle x_1 x_N \rangle + \langle x_2 x_N \rangle\right), \tag{E7}$$

III

$$\text{Re}\langle \hat{x}\hat{x}(t)\rangle_{x_1} = \cos(\omega t)\langle x_1 y_N\rangle$$
$$= \frac{\cos(\omega t)}{2}\left(\langle x_1^2\rangle + \langle x_1 x_N\rangle\right), \tag{E8}$$

and the imaginary parts,

$$\text{Im}\langle \hat{x}\hat{x}(t)\rangle_{y_1} = -\frac{N}{\beta\hbar\omega}\sin(\omega t)\langle y_1(x_1 - x_N)\rangle$$
$$= -\frac{N}{2\beta\hbar\omega}\sin(\omega t)\left(\langle x_1^2\rangle + \langle x_1 x_2\rangle - \langle x_1 x_N\rangle - \langle x_2 x_N\rangle\right)$$
$$= -\frac{N}{2\beta\hbar\omega}\sin(\omega t)\left(\langle x_1^2\rangle - \langle x_2 x_N\rangle\right), \tag{E9}$$

$$\text{Im}\langle \hat{x}\hat{x}(t)\rangle_{x_1} = -\frac{N}{\beta\hbar\omega}\sin(\omega t)\langle x_1(x_1 - x_N)\rangle$$
$$= -\frac{N}{\beta\hbar\omega}\sin(\omega t)\left(\langle x_1^2\rangle - \langle x_1 x_N\rangle\right), \tag{E10}$$

where it has been used that all beads are equivalent after the last momentum was integrated out, so, e.g., $\langle x_N^2\rangle = \langle x_1^2\rangle$ and $\langle x_1 x_N\rangle = \langle x_1 x_2\rangle$.

For the real part, $\langle x_1^2\rangle\cos(\omega t)$ is the exact quantum mechanics, apart from that the Boltzmann weighting factor in the average is approximate as long as N is finite. $\text{Re}\langle \hat{x}\hat{x}(t)\rangle_{x_1}$ consists to a larger degree of $\langle x_1^2\rangle\cos(\omega t)$ than $\text{Re}\langle \hat{x}\hat{x}(t)\rangle_{y_1}$ does. When $N \to \infty$ and the distance between beads becomes smaller both $\langle x_1 x_N\rangle$ and $\langle x_2 x_N\rangle$ will converge toward $\langle x_1^2\rangle$. $\langle x_2 x_N\rangle$ will most likely converge more slowly than $\langle x_1 x_N\rangle$ as it depends on next neighboring beads instead of immediately neighboring beads. This means that $\text{Re}\langle \hat{x}\hat{x}(t)\rangle_{x_1}$ could be expected to convergence toward exact quantum mechanics faster than $\text{Re}\langle \hat{x}\hat{x}(t)\rangle_{y_1}$ with respect to the number of beads. With the same kind of reasoning, $\text{Im}\langle \hat{x}\hat{x}(t)\rangle_{x_1}$ could be expected to converge faster with respect to the number of beads than $\text{Im}\langle \hat{x}\hat{x}(t)\rangle_{y_1}$, since the former depends on $\langle x_1 x_N\rangle$ and the latter depends on $\langle x_2 x_N\rangle$.

2. Comparison of real and imaginary parts of $\langle \hat{x}^2\hat{x}^2(t)\rangle$ for the harmonic potential

For $\langle \hat{x}^2\hat{x}^2(t)\rangle$, the equivalent of Eqs. (E5) and (E6) is

$$\langle \hat{x}^2\hat{x}^2(t)\rangle_{y_1} = \left\langle y_1^2\left(y_N^2\cos^2(\omega t) - \frac{iN}{\beta\hbar\omega}(x_1 - x_N)y_N\sin(\omega t)\cos(\omega t) - \frac{N^2}{\beta^2\hbar^2\omega^2}(x_1 - x_N)^2\sin^2(\omega t) + \frac{N}{\beta\omega^2 m}\sin^2(\omega t)\right)\right\rangle, \tag{E11}$$

$$\langle \hat{x}^2\hat{x}^2(t)\rangle_{x_1} = \left\langle x_1^2\left(y_N^2\cos^2(\omega t) - \frac{iN}{\beta\hbar\omega}(x_1 - x_N)y_N\sin(\omega t)\cos(\omega t) - \frac{N^2}{\beta^2\hbar^2\omega^2}(x_1 - x_N)^2\sin^2(\omega t) + \frac{N}{\beta\omega^2 m}\sin^2(\omega t)\right)\right\rangle. \tag{E12}$$

Separating into real parts

$$\text{Re}\langle \hat{x}^2\hat{x}^2(t)\rangle_{y_1} = \left\langle y_1^2 y_N^2\cos^2(\omega t) - y_1^2\frac{N^2}{\beta^2\hbar^2\omega^2}(x_1 - x_N)^2\sin^2(\omega t) + y_1^2\frac{N}{\beta\omega^2 m}\sin^2(\omega t)\right\rangle$$

$$= \frac{\cos^2(\omega t)}{16}\langle x_1^4 + 2x_1^3 x_2 + 2x_1^3 x_N + x_1^2 x_2^2 + 4x_1^2 x_2 x_N + x_1^2 x_N^2 + 2x_1 x_2^2 x_N + 2x_1 x_2 x_N^2 + x_2^2 x_N^2\rangle$$

$$- \frac{N^2\sin^2(\omega t)}{4\beta^2\hbar^2\omega^2}\langle x_1^4 + 2x_1^3 x_2 - 2x_1^3 x_N + x_1^2 x_2^2 - 4x_1^2 x_2 x_N + x_1^2 x_N^2 - 2x_1 x_2^2 x_N + 2x_1 x_2 x_N^2 + x_2^2 x_N^2\rangle$$

$$+ \frac{N\sin^2(\omega t)}{4\beta\omega^2 m}\langle x_1^2 + 2x_1 x_2 + x_2^2\rangle$$

$$= \frac{\cos^2(\omega t)}{16}\left(\langle x_1^4\rangle + 4\langle x_1^3 x_N\rangle + 2\langle x_1^2 x_N^2\rangle + 4\langle x_1^2 x_2 x_N\rangle + 4\langle x_1 x_2 x_N^2\rangle + \langle x_2^2 x_N^2\rangle\right)$$

$$- \frac{N^2\sin^2(\omega t)}{4\beta^2\hbar^2\omega^2}\left(\langle x_1^4\rangle + 2\langle x_1^2 x_N^2\rangle - 4\langle x_1^2 x_2 x_N\rangle + \langle x_2^2 x_N^2\rangle\right) + \frac{N\sin^2(\omega t)}{2\beta\omega^2 m}\left(\langle x_1^2\rangle + \langle x_1 x_N\rangle\right), \tag{E13}$$

$$\text{Re}\langle \hat{x}^2\hat{x}^2(t)\rangle_{x_1} = \left\langle x_1^2 y_N^2\cos^2(\omega t) - x_1^2\frac{N^2}{\beta^2\hbar^2\omega^2}(x_1 - x_N)^2\sin^2(\omega t) + x_1^2\frac{N}{\beta\omega^2 m}\sin^2(\omega t)\right\rangle$$

$$= \frac{\cos^2(\omega t)}{4}\left(\langle x_1^4\rangle + 2\langle x_1^3 x_N\rangle + \langle x_1^2 x_N^2\rangle\right) - \frac{N^2\sin^2(\omega t)}{\beta^2\hbar^2\omega^2}\left(\langle x_1^4\rangle - 2\langle x_1^3 x_N\rangle + \langle x_1^2 x_N^2\rangle\right) + \frac{N\sin^2(\omega t)}{\beta\omega^2 m}\langle x_1^2\rangle \tag{E14}$$

and imaginary parts

$$\text{Im}\langle \hat{x}^2 \hat{x}^2(t) \rangle_{y_1} = -\frac{N}{\beta \hbar \omega} \sin(\omega t) \cos(\omega t) \langle y_1^2 (x_1 - x_N) y_N \rangle$$

$$= -\frac{N}{8\beta \hbar \omega} \sin(\omega t) \cos(\omega t) \left(\langle x_1^4 \rangle + 2\langle x_1^3 x_2 \rangle \right.$$

$$+ \langle x_1^2 x_2^2 \rangle - \langle x_1^2 x_N^2 \rangle - 2\langle x_1 x_2 x_N^2 \rangle - \langle x_2^2 x_N^2 \rangle \right)$$

$$= -\frac{N}{8\beta \hbar \omega} \sin(\omega t) \cos(\omega t) \left(\langle x_1^4 \rangle + 2\langle x_1^3 x_2 \rangle \right.$$

$$\left. - 2\langle x_1 x_2 x_N^2 \rangle - \langle x_2^2 x_N^2 \rangle \right), \tag{E15}$$

$$\text{Im}\langle \hat{x}^2 \hat{x}^2(t) \rangle_{x_1} = -\frac{N}{\beta \hbar \omega} \sin(\omega t) \cos(\omega t) \langle x_1^2 (x_1 - x_N) y_N \rangle$$

$$= -\frac{N}{2\beta \hbar \omega} \sin(\omega t) \cos(\omega t) \left(\langle x_1^4 \rangle - \langle x_1^2 x_N^2 \rangle \right). \tag{E16}$$

From these expressions, it can be seen that $\langle \hat{x}^2 \hat{x}^2(t) \rangle_{x_1}$ for both the real and imaginary parts is a combination of fewer and less complex averages than $\langle \hat{x}^2 \hat{x}^2(t) \rangle_{y_1}$. Less complex in this case means averages of fewer different positions and of positions closer to each other. Thus, it can be expected that $\langle \hat{x}^2 \hat{x}^2(t) \rangle_{x_1}$ converges faster with regard to the number of beads than $\langle \hat{x}^2 \hat{x}^2(t) \rangle_{y_1}$ does.

REFERENCES

[1] J. Cao and G. A. Voth, J. Chem. Phys. **99**, 10070 (1993).
[2] S. Jang and G. A. Voth, J. Chem. Phys. **111**, 2357 (1999).
[3] I. R. Craig and D. E. Manolopoulos, J. Chem. Phys. **121**, 3368 (2004).
[4] W. H. Miller, J. Chem. Phys. **53**, 3578 (1970).
[5] W. H. Miller, J. Phys. Chem. A **105**, 2942 (2001).
[6] T. J. H. Hele, M. J. Willatt, A. Muolo, and S. C. Althorpe, J. Chem. Phys. **142**, 134103 (2015).
[7] E. J. Heller, J. Chem. Phys. **65**, 1289 (1976).
[8] H. Wang, X. Sun, and W. H. Miller, J. Chem. Phys. **108**, 9726 (1998).
[9] T. J. H. Hele, M. J. Willatt, A. Muolo, and S. C. Althorpe, J. Chem. Phys. **142**, 191101 (2015).
[10] D. R. Reichman, P.-N. Roy, S. Jang, and G. A. Voth, J. Chem. Phys. **113**, 919 (2000).
[11] X. Sun, H. Wang, and W. H. Miller, J. Chem. Phys. **109**, 4190 (1998).
[12] A. Bose and N. Makri, J. Phys. Chem. A **123**, 4284 (2019).
[13] S. Bonella, M. Monteferrante, C. Pierleoni, and G. Ciccotti, J. Chem. Phys. **133**, 164105 (2010).
[14] S. Bonella and G. Ciccotti, Entropy **16**, 86 (2013).
[15] E. Wigner, Phys. Rev. **40**, 749 (1932).
[16] J. E. Moyal, Math. Proc. Cambridge Philos. Soc. **45**, 99 (1949).
[17] J. Liu, Int. J. Quant. Chem. **115**, 657 (2015).
[18] J. A. Poulsen, J. Scheers, G. Nyman, and P. J. Rossky, Phys. Rev. B **75**, 224505 (2007).
[19] Q. Shi and E. Geva, J. Phys. Chem. A **107**, 9059 (2003).
[20] Q. Shi and E. Geva, J. Phys. Chem. A **107**, 9070 (2003).
[21] S. Habershon and D. E. Manolopoulos, J. Chem. Phys. **131**, 244518 (2009).
[22] N. Marković and J. A. Poulsen, J. Phys. Chem. A **112**, 1701 (2008).
[23] R. P. Feynman and A. R. Hibbs, *Quantum Mechanics and Path Integrals* (McGraw-Hill Companies, Inc., New York, 1965).
[24] R. Kubo, J. Phys. Soc. Jpn. **12**, 570 (1957).
[25] M. Parrinello and A. Rahman, J. Chem. Phys. **80**, 860 (1984).
[26] J. A. Barker, J. Chem. Phys. **70**, 2914 (1979).
[27] J. R. Cendagorta, Z. Bačić, and M. E. Tuckerman, J. Chem. Phys. **148**, 102340 (2018).
[28] A. O. Caldeira and A. J. Leggett, Ann. Phys. **149**, 374 (1983).
[29] I. R. Craig and D. E. Manolopoulos, J. Chem. Phys. **122**, 084106 (2005).
[30] M. P. Allen and D. J. Tildesley, *Computer Simulation of Liquids* (Oxford University Press, Oxford, UK, 1987).
[31] W. H. Press, S. A. Teukolsky, W. T. Vetterling, and B. P. Flannery, *Numerical Recipes in FORTRAN: The Art of Scientific Computing*, 2nd ed. (Cambridge University Press, Cambridge, UK, 1992).
[32] L. Verlet, Phys. Rev. **159**, 98 (1967).
[33] W. C. Swope, H. C. Andersen, P. H. Berens, and K. R. Wilson, J. Chem. Phys. **76**, 637 (1982).
[34] R. Friedberg and J. E. Cameron, J. Chem. Phys. **52**, 6049 (1970).
[35] J. M. Flegal, M. Haran, and G. L. Jones, Stat. Sci. **23**, 250 (2008).
[36] D. Thirumalai, E. J. Bruskin, and B. J. Berne, J. Chem. Phys. **79**, 5063 (1983).
[37] J. A. Poulsen, G. Nyman, and P. J. Rossky, J. Chem. Phys. **119**, 12179 (2003).
[38] J. Liu and W. H. Miller, J. Chem. Phys. **125**, 224104 (2006).
[39] J. Liu and W. H. Miller, J. Chem. Phys. **131**, 074113 (2009).
[40] R. P. Feynman and H. Kleinert, Phys. Rev. A **34**, 5080 (1986).
[41] B. J. Braams, T. F. Miller, and D. E. Manolopoulos, Chem. Phys. Lett. **418**, 179 (2006).
[42] T. F. Miller and D. E. Manolopoulos, J. Chem. Phys. **122**, 184503 (2005).
[43] W. H. Miller, S. D. Schwartz, and J. W. Tromp, J. Chem. Phys. **79**, 4889 (1983).
[44] W. H. Miller, J. Chem. Phys. **61**, 1823 (1974).
[45] T. E. Markland and D. E. Manolopoulos, J. Chem. Phys. **129**, 024105 (2008).
[46] J. Cao and G. A. Voth, J. Chem. Phys. **100**, 5106 (1994).

III

Paper IV

Calculation of Reaction Rate Constants From a Classical Wigner Model Based on a Feynman Path Integral Open Polymer

IV

179

Calculation of Reaction Rate Constants From a Classical Wigner Model Based on a Feynman Path Integral Open Polymer

S. Karl-Mikael Svensson,[1] Jens Aage Poulsen,[1, a)] and Gunnar Nyman[1, b)]

Department of Chemistry and Molecular Biology, University of Gothenburg, SE 405 30 Gothenburg, Sweden

The Open Polymer Classical Wigner (OPCW) method [J. Chem. Phys. 152, 094111 (2020)] is applied to a flux-Heaviside correlation function used to calculate reaction rate constants. The obtained expression is tested on a parabolic barrier and a symmetric Eckart potential. The OPCW method is shown to converge toward the exact classical Wigner result. The OPCW method shows some promise for rate constant calculations and suggestions for future tests are made.

I. INTRODUCTION

Reaction rates are of central importance in chemistry and methods to calculate reaction rate constants are therefore of interest. In many cases classical mechanics is enough to calculate a rate constant, but for light atoms such as hydrogen or cold low density situations quantum mechanics can be essential.

Methods to acquire reaction rate constants from a Wigner distribution include, to some extent, the transition state theory with quantum partition functions of Wigner[1] and Eyring[2], the quantum transition state theory of Pollak and Liao[3], and the classical Wigner method[4,5], with alternatives such as FK-LPI[6] (Feynman-Kleinert Linearized Path Integral) and LGA-LSC-IVR[7] (Local Gaussian Approximation Linearized Semi-Classical Initial Value Representation). Other notable approximate quantum mechanical methods to calculate reaction rate constants are e.g. instanton reaction rate theory[8–10] and Ring Polymer Molecular Dynamics (RPMD)[11].

This article presents one way to calculate reaction rate constants with a recent implementation of the classical Wigner method by the same authors[12]. Section II is an introduction to a general formulation of chemical reaction rates, then section III combines this theory with the OPCW method. Section IV notes some important corrections to factor in when running the calculations. Sections V, VI, and VII respectively declare the details of the computations that have been run, show the results of these computations, and contain the conclusions that have been drawn.

II. REACTION RATE CONSTANTS

Miller and coworkers published[13,14] three quantum mechanical traces that can be used to acquire bimolecular

---

a)Electronic mail: jens72@chem.gu.se
b)Electronic mail: nyman@chem.gu.se

reaction rate constants. These traces are

$$C_{\text{ss}}(t) = \text{Tr}\left\{ e^{-\frac{\beta}{2}\hat{H}}\, h\left(-\hat{x}\right) e^{-\frac{\beta}{2}\hat{H}}\, e^{\frac{i\hat{H}t}{\hbar}}\, h\left(\hat{x}\right) e^{-\frac{i\hat{H}t}{\hbar}} \right\} \quad (1)$$

$$C_{\text{fs}}(t) = \text{Tr}\left\{ e^{-\frac{\beta}{2}\hat{H}}\, \hat{F}\, e^{-\frac{\beta}{2}\hat{H}}\, e^{\frac{i\hat{H}t}{\hbar}}\, h\left(\hat{x}\right) e^{-\frac{i\hat{H}t}{\hbar}} \right\} \quad (2)$$

$$C_{\text{ff}}(t) = \text{Tr}\left\{ e^{-\frac{\beta}{2}\hat{H}}\, \hat{F}\, e^{-\frac{\beta}{2}\hat{H}}\, e^{\frac{i\hat{H}t}{\hbar}}\, \hat{F}\, e^{-\frac{i\hat{H}t}{\hbar}} \right\} \quad (3)$$

where $h(x)$ is the heaviside function, $\hat{x}$ is the position operator, $\beta = (k_{\text{B}}T)^{-1}$, where k_{B} is Boltzmann's constant and T is the absolute temperature, $\hat{H}$ is the Hamiltonian operator of the system, i is the imaginary unit, t is time, $\hbar$ is the reduced Planck constant, and $\hat{F}$ is the probability density flux operator. These functions can be used to obtain reaction rate constants, k_{r}, through the relations

$$k_{\text{r}} Q_{\text{R}} = \lim_{t\to\infty} \frac{\text{d}}{\text{d}t} C_{\text{ss}}(t) \quad (4)$$

$$= \lim_{t\to\infty} C_{\text{fs}}(t) \quad (5)$$

$$= \int_0^\infty \text{d}t\, C_{\text{ff}}(t) = \frac{1}{2} \int_{-\infty}^\infty \text{d}t\, C_{\text{ff}}(t) \quad (6)$$

where Q_{R} is the canonical partition function per unit volume of the reactants.

It can be noted that the traces presented here have a symmetrized Boltzmann operator[15], i.e. $e^{-\frac{\beta}{2}\hat{H}}$ on both sides of the first operator in each trace. The relations 4-6 are just as valid for the real part of the trace with an asymmetrically placed Boltzmann operator[13]. Important to notice is that these relations are defined for potentials where the reactants start infinitely far from each other and the products end up infinitely far from each other. This requires the potential to be unbound. This restriction applies to the potentials employed in this article.

In the computations presented in this article the trace used for the calculation of rate constants is $C_{\text{fs}}(t)$.

III. REACTION RATE CALCULATION WITH THE OPEN POLYMER CLASSICAL WIGNER METHOD

The quantity of interest in this work is the symmetrized trace $C_{\text{fs}}(t)$ in equation 2.

In this section expressions for calculating this quantity with OPCW will be derived. These derivations will follow the ones in the original OPCW article[12] quite closely, but will be using the symmetrized Boltzmann operator and will be specialized for the flux-side trace.

Initially $C_{\mathrm{fs}}(t)$ is written as the integral over position, x_1, of a matrix element.

$$C_{\mathrm{fs}}(t) = \int_{-\infty}^{\infty} \mathrm{d}x_1 \left\langle x_1 \left| \mathrm{e}^{-\frac{\beta}{2}\hat{H}} \hat{F} \, \mathrm{e}^{-\frac{\beta}{2}\hat{H}} \, \mathrm{e}^{\frac{i\hat{H}t}{\hbar}} \, h\left(\hat{x}\right) \mathrm{e}^{-\frac{i\hat{H}t}{\hbar}} \right| x_1 \right\rangle \tag{7}$$

The Boltzmann operators are each divided into $\frac{N}{2}$ factors of $\mathrm{e}^{-\frac{\beta}{N}\hat{H}}$, where N must be an even number. $N-1$ identity operators are inserted between these operators.

$$C_{\mathrm{fs}}(t) = \left\{ \prod_{j=1}^{N} \int_{-\infty}^{\infty} \mathrm{d}x_j \right\} \left\langle x_1 \left| \mathrm{e}^{-\frac{\beta}{N}\hat{H}} \right| x_2 \right\rangle \left\langle x_2 \left| \mathrm{e}^{-\frac{\beta}{N}\hat{H}} \right| x_3 \right\rangle \dots \left\langle x_{\frac{N}{2}} \left| \mathrm{e}^{-\frac{\beta}{N}\hat{H}} \hat{F} \right| x_{\frac{N}{2}+1} \right\rangle$$
$$\dots \left\langle x_{N-1} \left| \mathrm{e}^{-\frac{\beta}{N}\hat{H}} \right| x_N \right\rangle \left\langle x_N \left| \mathrm{e}^{-\frac{\beta}{N}\hat{H}} \, \mathrm{e}^{\frac{i\hat{H}t}{\hbar}} \, h(\hat{x}) \, \mathrm{e}^{-\frac{i\hat{H}t}{\hbar}} \right| x_1 \right\rangle \tag{8}$$

This is an imaginary time, $-i\hbar\beta$, Feynman path integral[16], which can be expressed with Wigner transforms instead of matrix elements,

$$C_{\mathrm{fs}}(t) = \left\{ \prod_{j=1}^{N} \iint_{-\infty}^{\infty} \frac{\mathrm{d}x_j \, \mathrm{d}p_j}{2\pi\hbar} \right\} \mathrm{e}^{-\frac{i}{\hbar}\sum_{j=1}^{N} p_j \left(x_{(j \bmod N)+1} - x_j\right)} \left(\mathrm{e}^{-\frac{\beta}{N}\hat{H}}\right)_{\mathrm{W}} \left[\frac{x_1 + x_2}{2}, p_1\right] \left(\mathrm{e}^{-\frac{\beta}{N}\hat{H}}\right)_{\mathrm{W}} \left[\frac{x_2 + x_3}{2}, p_2\right]$$
$$\dots \left(\mathrm{e}^{-\frac{\beta}{N}\hat{H}} \hat{F}\right)_{\mathrm{W}} \left[\frac{x_{\frac{N}{2}} + x_{\frac{N}{2}+1}}{2}, p_{\frac{N}{2}}\right] \dots \left(\mathrm{e}^{-\frac{\beta}{N}\hat{H}}\right)_{\mathrm{W}} \left[\frac{x_{N-1} + x_N}{2}, p_{N-1}\right]$$
$$\times \left(\mathrm{e}^{-\frac{\beta}{N}\hat{H}} \, \mathrm{e}^{\frac{i\hat{H}t}{\hbar}} \, h(\hat{x}) \, \mathrm{e}^{-\frac{i\hat{H}t}{\hbar}}\right)_{\mathrm{W}} \left[\frac{x_N + x_1}{2}, p_N\right]. \tag{9}$$

In the limit of $N \to \infty$ the Wigner transform of the Boltzmann operator simplifies to the classical Boltzmann factor. Also the Boltzmann operators can be separated from the flux and Heaviside operators in this limit.

$$C_{\mathrm{fs}}(t) = \lim_{N \to \infty} \left\{ \prod_{j=1}^{N} \iint_{-\infty}^{\infty} \frac{\mathrm{d}x_j \, \mathrm{d}p_j}{2\pi\hbar} \right\} \mathrm{e}^{-\frac{i}{\hbar}\sum_{j=1}^{N} p_j \left(x_{(j \bmod N)+1} - x_j\right)} \mathrm{e}^{-\frac{\beta}{N}\sum_{j=1}^{N} H(y_j, p_j)} \left(\hat{F}\right)_{\mathrm{W}} \left[y_{\frac{N}{2}}, p_{\frac{N}{2}}\right]$$
$$\times \left(\mathrm{e}^{\frac{i\hat{H}t}{\hbar}} h(\hat{x}) \mathrm{e}^{-\frac{i\hat{H}t}{\hbar}}\right)_{\mathrm{W}} [y_N, p_N] \tag{10}$$

where $y_j = \frac{x_j + x_{(j \bmod N)+1}}{2}$ and $H\left(y_j, p_j\right)$ is the classical Hamiltonian. For a $V(y_j)$ that is independent of momentum all momenta except $p_{\frac{N}{2}}$ and p_N can be integrated out analytically as done in the original derivation of OPCW[12].

$$C_{\mathrm{fs}}(t) = \lim_{N \to \infty} \left(\frac{mN}{2\pi\beta}\right)^{\frac{N}{2}} \frac{\beta}{2\pi m N} \hbar^{-2N} \left\{ \prod_{j=1}^{N} \int_{-\infty}^{\infty} \mathrm{d}x_j \right\} \iint_{-\infty}^{\infty} \mathrm{d}p_{\frac{N}{2}} \, \mathrm{d}p_N \; \mathrm{e}^{-\frac{\beta}{N}\sum_{j=1}^{N} V(y_j)}$$
$$\times \mathrm{e}^{-\frac{mN}{2\hbar^2\beta}\left(\sum_{j=1}^{\frac{N}{2}-1}(x_{j+1}-x_j)^2 + \sum_{j=\frac{N}{2}+1}^{N-1}(x_{j+1}-x_j)^2\right)} \mathrm{e}^{-\frac{i}{\hbar}p_{\frac{N}{2}}\left(x_{\frac{N}{2}+1}-x_{\frac{N}{2}}\right)} \mathrm{e}^{-\frac{\beta}{N}\frac{p_{\frac{N}{2}}^2}{2m}} \left(\hat{F}\right)_{\mathrm{W}} \left[y_{\frac{N}{2}}, p_{\frac{N}{2}}\right]$$
$$\times \mathrm{e}^{-\frac{i}{\hbar}p_N(x_1-x_N)} \mathrm{e}^{-\frac{\beta}{N}\frac{p_N^2}{2m}} \left(\mathrm{e}^{\frac{i\hat{H}t}{\hbar}} \hat{B} \, \mathrm{e}^{-\frac{i\hat{H}t}{\hbar}}\right)_{\mathrm{W}} [y_N, p_N] \tag{11}$$

For the flux operator $\hat{F} = \frac{1}{2m}\left(\delta(\hat{x})\hat{p} + \hat{p}\delta(\hat{x})\right)$ the Wigner transform is

$$\left(\hat{F}\right)_{\mathrm{W}} [x, p] = \frac{p}{m}\delta(x). \tag{12}$$

Using the momentum integrals of appendix A in our previous article[12] a quantity $F'\left(y_{\frac{N}{2}}, x_{\frac{N}{2}+1} - x_{\frac{N}{2}}\right)$ can be defined as

$$
\begin{aligned}
F'\left(y_{\frac{N}{2}}, x_{\frac{N}{2}+1} - x_{\frac{N}{2}}\right) &= \frac{\int_{-\infty}^{\infty} \mathrm{d}p_{\frac{N}{2}}\, \left(\hat{F}\right)_{\mathrm{W}}\left[y_{\frac{N}{2}}, p_{\frac{N}{2}}\right] \mathrm{e}^{-\frac{\beta}{N}\frac{p_{\frac{N}{2}}^2}{2m}}\, \mathrm{e}^{-\frac{i}{\hbar}p_{\frac{N}{2}}\left(x_{\frac{N}{2}+1} - x_{\frac{N}{2}}\right)}}{\int_{-\infty}^{\infty} \mathrm{d}p_{\frac{N}{2}}\, \mathrm{e}^{-\frac{\beta}{N}\frac{p_{\frac{N}{2}}^2}{2m}}\, \mathrm{e}^{-\frac{i}{\hbar}p_{\frac{N}{2}}\left(x_{\frac{N}{2}+1} - x_{\frac{N}{2}}\right)}} \\
&= \frac{\int_{-\infty}^{\infty} \mathrm{d}p_{\frac{N}{2}}\, \frac{p_{\frac{N}{2}}}{m}\delta\left(y_{\frac{N}{2}}\right) \mathrm{e}^{-\frac{\beta}{N}\frac{p_{\frac{N}{2}}^2}{2m}}\, \mathrm{e}^{-\frac{i}{\hbar}p_{\frac{N}{2}}\left(x_{\frac{N}{2}+1} - x_{\frac{N}{2}}\right)}}{\sqrt{\frac{2\pi mN}{\beta}}\, \mathrm{e}^{-\frac{\beta}{N}\frac{mN^2\left(x_{\frac{N}{2}+1} - x_{\frac{N}{2}}\right)^2}{2\hbar^2\beta^2}}} \\
&= -\frac{iN}{\hbar\beta}\left(x_{\frac{N}{2}+1} - x_{\frac{N}{2}}\right)\delta\left(y_{\frac{N}{2}}\right).
\end{aligned} \tag{13}
$$

This can be put into equation 11, giving

$$
\begin{aligned}
C_{\mathrm{fs}}(t) = \lim_{N\to\infty}\left(\frac{mN}{2\pi\beta}\right)^{\frac{N}{2}}\sqrt{\frac{\beta}{2\pi mN}}\hbar^{-N}\left\{\prod_{j=1}^{N}\int_{-\infty}^{\infty}\mathrm{d}x_j\right\}\int_{-\infty}^{\infty}\mathrm{d}p_N\, \mathrm{e}^{-\frac{\beta}{N}\sum_{j=1}^{N}V(y_j)} \\
\times\, \mathrm{e}^{-\frac{mN}{2\hbar^2\beta}\sum_{j=1}^{N-1}(x_{j+1}-x_j)^2}\frac{iN}{\hbar\beta}\left(x_{\frac{N}{2}} - x_{\frac{N}{2}+1}\right)\delta\left(y_{\frac{N}{2}}\right) \\
\times\, \mathrm{e}^{-\frac{i}{\hbar}p_N(x_1-x_N)}\, \mathrm{e}^{-\frac{\beta}{N}\frac{p_N^2}{2m}}\left(\mathrm{e}^{\frac{i\hat{H}t}{\hbar}}h(\hat{x})\mathrm{e}^{-\frac{i\hat{H}t}{\hbar}}\right)_{\mathrm{W}}[y_N, p_N].
\end{aligned} \tag{14}
$$

Applying the classical Wigner approximation,

$$
\left(\mathrm{e}^{\frac{i\hat{H}t}{\hbar}}h(\hat{x})\mathrm{e}^{-\frac{i\hat{H}t}{\hbar}}\right)_{\mathrm{W}}[y_N, p_N] \approx (h(\hat{x}))_{\mathrm{W}}\left[x\left(y_N, p_N, t\right), p\left(y_N, p_N, t\right)\right] = h\left(x\left(y_N, p_N, t\right)\right), \tag{15}
$$

and assuming finite N results in

$$
\begin{aligned}
C_{\mathrm{fs},y}(t) \approx \left(\frac{mN}{2\pi\beta}\right)^{\frac{N}{2}}\sqrt{\frac{\beta}{2\pi mN}}\hbar^{-N}\left\{\prod_{j=1}^{N}\int_{-\infty}^{\infty}\mathrm{d}x_j\right\}\int_{-\infty}^{\infty}\mathrm{d}p_N\, \mathrm{e}^{-\frac{i}{\hbar}p_N(x_1-x_N)} \\
\times\, \mathrm{e}^{-\frac{\beta}{N}\left(\frac{p_N^2}{2m}+\sum_{j=1}^{N}V(y_j)+\frac{mN^2}{2\hbar^2\beta^2}\sum_{j=1}^{N-1}(x_{j+1}-x_j)^2\right)}\frac{iN}{\hbar\beta}\left(x_{\frac{N}{2}} - x_{\frac{N}{2}+1}\right)\delta\left(y_{\frac{N}{2}}\right)h\left(x\left(y_N, p_N, t\right)\right),
\end{aligned} \tag{16}
$$

which is the expression corresponding to the y_1-version of OPCW for the flux-Heaviside trace. Due to the symmetrization of the Boltzmann operator, $y_{\frac{N}{2}}$ rather than y_1 is used. This trace will be called $C_{\mathrm{fs},y}(t)$.

To get an expression corresponding to the x_1-version of OPCW we start over from equation 8. There the $\hat{x}$-dependent parts of $\hat{F}$ has to operate to the right in the matrix element before rewriting as Wigner transforms.

To be able to operate to the right, the flux operator has to be rearranged into a form where all $\hat{x}$-dependence is to the right of all $\hat{p}$-dependence. Using that $\hat{p} = -i\hbar\frac{\mathrm{d}}{\mathrm{d}x}$ this can be achieved as

$$
\begin{aligned}
\hat{F} &= \frac{1}{2m}\left(\delta(\hat{x})\hat{p} + \hat{p}\delta(\hat{x})\right) = \frac{1}{2m}\left([\delta(\hat{x}),\hat{p}] + \hat{p}\delta(\hat{x}) + \hat{p}\delta(\hat{x})\right) \\
&= \frac{1}{2m}\left(-i\hbar\left(\delta(\hat{x})\frac{\mathrm{d}}{\mathrm{d}x} - \frac{\mathrm{d}}{\mathrm{d}x}\delta(\hat{x})\right) + 2\hat{p}\delta(\hat{x})\right) \\
&= \frac{1}{2m}\left(-i\hbar\left(\delta(\hat{x})\frac{\mathrm{d}}{\mathrm{d}x} - \frac{\mathrm{d}\delta(\hat{x})}{\mathrm{d}x} - \delta(\hat{x})\frac{\mathrm{d}}{\mathrm{d}x}\right) + 2\hat{p}\delta(\hat{x})\right) \\
&= \frac{1}{2m}\left(i\hbar\frac{\mathrm{d}\delta(\hat{x})}{\mathrm{d}x} + 2\hat{p}\delta(\hat{x})\right),
\end{aligned} \tag{17}
$$

where the square brackets denote a commutator. Using this new form of the flux operator and operating $\hat{x}$ to the right we acquire

$$C_{\text{fs}}(t) = \left\{ \prod_{j=1}^{N} \int_{-\infty}^{\infty} \mathrm{d}x_j \right\} \left\langle x_1 \left| \mathrm{e}^{-\frac{\beta}{N}\hat{H}} \right| x_2 \right\rangle \left\langle x_2 \left| \mathrm{e}^{-\frac{\beta}{N}\hat{H}} \right| x_3 \right\rangle \dots \left(\left\langle x_{\frac{N}{2}} \left| \mathrm{e}^{-\frac{\beta}{N}\hat{H}} \hat{p} \right| x_{\frac{N}{2}+1} \right\rangle \frac{1}{m} \delta \left(x_{\frac{N}{2}+1} \right) \right.$$

$$+ \left\langle x_{\frac{N}{2}} \left| \mathrm{e}^{-\frac{\beta}{N}\hat{H}} \right| x_{\frac{N}{2}+1} \right\rangle \frac{i\hbar}{2m} \frac{\mathrm{d}\delta \left(x_{\frac{N}{2}+1} \right)}{\mathrm{d}x_{\frac{N}{2}+1}} \right)$$

$$\dots \left\langle x_{N-1} \left| \mathrm{e}^{-\frac{\beta}{N}\hat{H}} \right| x_N \right\rangle \left\langle x_N \left| \mathrm{e}^{-\frac{\beta}{N}\hat{H}} \mathrm{e}^{\frac{i\hat{H}t}{\hbar}} h(\hat{x}) \mathrm{e}^{-\frac{i\hat{H}t}{\hbar}} \right| x_1 \right\rangle. \tag{18}$$

Rewriting as Wigner transforms, taking the limit where the Wigner transform of the Boltzmann operator is the classical Boltzmann factor, and assuming that $V(y_j)$ is independent of momentum, a new way to write equation 11 can be obtained:

$$C_{\text{fs}}(t) = \lim_{N\to\infty} \left(\frac{mN}{2\pi\beta} \right)^{\frac{N}{2}} \frac{\beta}{2\pi mN} \hbar^{-2N} \left\{ \prod_{j=1}^{N} \int_{-\infty}^{\infty} \mathrm{d}x_j \right\} \iint_{-\infty}^{\infty} \mathrm{d}p_{\frac{N}{2}} \, \mathrm{d}p_N \, \mathrm{e}^{-\frac{\beta}{N}\sum_{j=1}^{N} V(y_j)}$$

$$\times \mathrm{e}^{-\frac{mN}{2\hbar^2\beta}\left(\sum_{j=1}^{\frac{N}{2}-1}(x_{j+1}-x_j)^2 + \sum_{j=\frac{N}{2}+1}^{N-1}(x_{j+1}-x_j)^2 \right)} \mathrm{e}^{-\frac{i}{\hbar}p_{\frac{N}{2}}\left(x_{\frac{N}{2}+1}-x_{\frac{N}{2}} \right)} \mathrm{e}^{-\frac{\beta}{N}\frac{p_{\frac{N}{2}}^2}{2m}}$$

$$\times \left((\hat{p})_{\text{W}} \left[y_{\frac{N}{2}}, p_{\frac{N}{2}} \right] \frac{1}{m} \delta \left(x_{\frac{N}{2}+1} \right) + \frac{i\hbar}{2m} \frac{\mathrm{d}\delta \left(x_{\frac{N}{2}+1} \right)}{\mathrm{d}x_{\frac{N}{2}+1}} \right)$$

$$\times \mathrm{e}^{-\frac{i}{\hbar}p_N(x_1-x_N)} \mathrm{e}^{-\frac{\beta}{N}\frac{p_N^2}{2m}} \left(\mathrm{e}^{\frac{i\hat{H}t}{\hbar}} h(\hat{x}) \mathrm{e}^{-\frac{i\hat{H}t}{\hbar}} \right)_{\text{W}} [y_N, p_N]. \tag{19}$$

Knowing that $(\hat{p})_{\text{W}}[x,p] = p$, $p_{\frac{N}{2}}$ can be integrated out.

$$\frac{\int_{-\infty}^{\infty} \mathrm{d}p_{\frac{N}{2}} \, (\hat{p})_{\text{W}} \left[y_{\frac{N}{2}}, p_{\frac{N}{2}} \right] \mathrm{e}^{-\frac{\beta}{N}\frac{p_{\frac{N}{2}}^2}{2m}} \mathrm{e}^{-\frac{i}{\hbar}p_{\frac{N}{2}}\left(x_{\frac{N}{2}+1}-x_{\frac{N}{2}} \right)}}{\int_{-\infty}^{\infty} \mathrm{d}p_{\frac{N}{2}} \, \mathrm{e}^{-\frac{\beta}{N}\frac{p_{\frac{N}{2}}^2}{2m}} \mathrm{e}^{-\frac{i}{\hbar}p_{\frac{N}{2}}\left(x_{\frac{N}{2}+1}-x_{\frac{N}{2}} \right)}}$$

$$= \frac{\int_{-\infty}^{\infty} \mathrm{d}p_{\frac{N}{2}} \, p_{\frac{N}{2}} \, \mathrm{e}^{-\frac{\beta}{N}\frac{p_{\frac{N}{2}}^2}{2m}} \mathrm{e}^{-\frac{i}{\hbar}p_{\frac{N}{2}}\left(x_{\frac{N}{2}+1}-x_{\frac{N}{2}} \right)}}{\sqrt{\frac{2\pi mN}{\beta}} \, \mathrm{e}^{-\frac{\beta}{N}\frac{mN^2\left(x_{\frac{N}{2}+1}-x_{\frac{N}{2}} \right)^2}{2\hbar^2\beta^2}}}$$

$$= -\frac{iNm}{\hbar\beta} \left(x_{\frac{N}{2}+1} - x_{\frac{N}{2}} \right) \tag{20}$$

$$C_{\text{fs}}(t) = \lim_{N\to\infty} \left(\frac{mN}{2\pi\beta} \right)^{\frac{N}{2}} \sqrt{\frac{\beta}{2\pi mN}} \hbar^{-N} \left\{ \prod_{j=1}^{N} \int_{-\infty}^{\infty} \mathrm{d}x_j \right\} \int_{-\infty}^{\infty} \mathrm{d}p_N \, \mathrm{e}^{-\frac{\beta}{N}\sum_{j=1}^{N} V(y_j)}$$

$$\times \mathrm{e}^{-\frac{mN}{2\hbar^2\beta}\sum_{j=1}^{N-1}(x_{j+1}-x_j)^2} \left(-\frac{iN}{\hbar\beta} \left(x_{\frac{N}{2}+1} - x_{\frac{N}{2}} \right) \delta \left(x_{\frac{N}{2}+1} \right) + \frac{i\hbar}{2m} \frac{\mathrm{d}\delta \left(x_{\frac{N}{2}+1} \right)}{\mathrm{d}x_{\frac{N}{2}+1}} \right)$$

$$\times \mathrm{e}^{-\frac{i}{\hbar}p_N(x_1-x_N)} \mathrm{e}^{-\frac{\beta}{N}\frac{p_N^2}{2m}} \left(\mathrm{e}^{\frac{i\hat{H}t}{\hbar}} h(\hat{x}) \mathrm{e}^{-\frac{i\hat{H}t}{\hbar}} \right)_{\text{W}} [y_N, p_N] \tag{21}$$

If $f(x)$ is a function of x then $\int_{-\infty}^{\infty} \mathrm{d}x \, f(x) \frac{\mathrm{d}\delta(x)}{\mathrm{d}x} = \int_{-\infty}^{\infty} \mathrm{d}x \left(-\frac{\mathrm{d}f(x)}{\mathrm{d}x} \right) \delta(x)$. This can be used to eliminate the

derivative of the delta function through

$$
\int_{-\infty}^{\infty} dx_{\frac{N}{2}} \, e^{-\frac{\beta}{N}\left(V\left(y_{\frac{N}{2}}\right)+V\left(y_{\frac{N}{2}+1}\right)\right)} e^{-\frac{mN}{2\hbar^2\beta}\left(\left(x_{\frac{N}{2}+1}-x_{\frac{N}{2}}\right)^2+\left(x_{\frac{N}{2}+2}-x_{\frac{N}{2}+1}\right)^2\right)} \frac{i\hbar}{2m} \frac{d\delta\left(x_{\frac{N}{2}+1}\right)}{dx_{\frac{N}{2}+1}}
$$

$$
= \int_{-\infty}^{\infty} dx_{\frac{N}{2}} (-1) \left(-\frac{\beta}{N}\left(\frac{1}{2}\frac{dV\left(y_{\frac{N}{2}}\right)}{dy_{\frac{N}{2}}}+\frac{1}{2}\frac{dV\left(y_{\frac{N}{2}+1}\right)}{dy_{\frac{N}{2}+1}}\right) - \frac{mN}{2\hbar^2\beta}\left(2\left(x_{\frac{N}{2}+1}-x_{\frac{N}{2}}\right)-2\left(x_{\frac{N}{2}+2}-x_{\frac{N}{2}+1}\right)\right)\right)
$$

$$
\times e^{-\frac{\beta}{N}\left(V\left(y_{\frac{N}{2}}\right)+V\left(y_{\frac{N}{2}+1}\right)\right)} e^{-\frac{mN}{2\hbar^2\beta}\left(\left(x_{\frac{N}{2}+1}-x_{\frac{N}{2}}\right)^2+\left(x_{\frac{N}{2}+2}-x_{\frac{N}{2}+1}\right)^2\right)} \frac{i\hbar}{2m} \delta\left(x_{\frac{N}{2}+1}\right)
$$

$$
= \int_{-\infty}^{\infty} dx_{\frac{N}{2}} \, e^{-\frac{\beta}{N}\left(V\left(y_{\frac{N}{2}}\right)+V\left(y_{\frac{N}{2}+1}\right)\right)} e^{-\frac{mN}{2\hbar^2\beta}\left(\left(x_{\frac{N}{2}+1}-x_{\frac{N}{2}}\right)^2+\left(x_{\frac{N}{2}+2}-x_{\frac{N}{2}+1}\right)^2\right)}
$$

$$
\times \left(\frac{i\hbar\beta}{4Nm}\left(\frac{dV\left(y_{\frac{N}{2}}\right)}{dy_{\frac{N}{2}}}+\frac{dV\left(y_{\frac{N}{2}+1}\right)}{dy_{\frac{N}{2}+1}}\right)+\frac{iN}{2\hbar\beta}\left(2x_{\frac{N}{2}+1}-x_{\frac{N}{2}}-x_{\frac{N}{2}+2}\right)\right) \delta\left(x_{\frac{N}{2}+1}\right) \tag{22}
$$

leading to

$$
C_{\text{fs}}(t) = \lim_{N\to\infty} \left(\frac{mN}{2\pi\beta}\right)^{\frac{N}{2}} \sqrt{\frac{\beta}{2\pi mN}} \hbar^{-N} \left\{\prod_{j=1}^{N}\int_{-\infty}^{\infty} dx_j\right\} \int_{-\infty}^{\infty} dp_N \, e^{-\frac{\beta}{N}\sum_{j=1}^{N}V(y_j)} e^{-\frac{mN}{2\hbar^2\beta}\sum_{j=1}^{N-1}(x_{j+1}-x_j)^2}
$$

$$
\times \left(-\frac{iN}{\hbar\beta}\left(x_{\frac{N}{2}+1}-x_{\frac{N}{2}}\right)\delta\left(x_{\frac{N}{2}+1}\right)\right.
$$

$$
+ \left.\left(\frac{i\hbar\beta}{4Nm}\left(\frac{dV\left(y_{\frac{N}{2}}\right)}{dy_{\frac{N}{2}}}+\frac{dV\left(y_{\frac{N}{2}+1}\right)}{dy_{\frac{N}{2}+1}}\right)+\frac{iN}{2\hbar\beta}\left(2x_{\frac{N}{2}+1}-x_{\frac{N}{2}}-x_{\frac{N}{2}+2}\right)\right)\delta\left(x_{\frac{N}{2}+1}\right)\right)
$$

$$
\times e^{-\frac{i}{\hbar}p_N(x_1-x_N)} e^{-\frac{\beta}{N}\frac{p_N^2}{2m}} \left(e^{\frac{i\hat{H}t}{\hbar}} h(\hat{x}) e^{-\frac{i\hat{H}t}{\hbar}}\right)_{\text{W}} [y_N, p_N]
$$

$$
= \lim_{N\to\infty} \left(\frac{mN}{2\pi\beta}\right)^{\frac{N}{2}} \sqrt{\frac{\beta}{2\pi mN}} \hbar^{-N} \left\{\prod_{j=1}^{N}\int_{-\infty}^{\infty} dx_j\right\} \int_{-\infty}^{\infty} dp_N \, e^{-\frac{\beta}{N}\sum_{j=1}^{N}V(y_j)} e^{-\frac{mN}{2\hbar^2\beta}\sum_{j=1}^{N-1}(x_{j+1}-x_j)^2}
$$

$$
\times \left(\frac{i\hbar\beta}{4Nm}\left(\frac{dV\left(y_{\frac{N}{2}}\right)}{dy_{\frac{N}{2}}}+\frac{dV\left(y_{\frac{N}{2}+1}\right)}{dy_{\frac{N}{2}+1}}\right)+\frac{iN}{2\hbar\beta}\left(2x_{\frac{N}{2}+1}-x_{\frac{N}{2}}-x_{\frac{N}{2}+2}-2x_{\frac{N}{2}+1}+2x_{\frac{N}{2}}\right)\right)\delta\left(x_{\frac{N}{2}+1}\right)
$$

$$
\times e^{-\frac{i}{\hbar}p_N(x_1-x_N)} e^{-\frac{\beta}{N}\frac{p_N^2}{2m}} \left(e^{\frac{i\hat{H}t}{\hbar}} h(\hat{x}) e^{-\frac{i\hat{H}t}{\hbar}}\right)_{\text{W}} [y_N, p_N]
$$

$$
= \lim_{N\to\infty} \left(\frac{mN}{2\pi\beta}\right)^{\frac{N}{2}} \sqrt{\frac{\beta}{2\pi mN}} \hbar^{-N} \left\{\prod_{j=1}^{N}\int_{-\infty}^{\infty} dx_j\right\} \int_{-\infty}^{\infty} dp_N \, e^{-\frac{\beta}{N}\sum_{j=1}^{N}V(y_j)} e^{-\frac{mN}{2\hbar^2\beta}\sum_{j=1}^{N-1}(x_{j+1}-x_j)^2}
$$

$$
\times \left(\frac{i\hbar\beta}{4Nm}\left(\frac{dV\left(y_{\frac{N}{2}}\right)}{dy_{\frac{N}{2}}}+\frac{dV\left(y_{\frac{N}{2}+1}\right)}{dy_{\frac{N}{2}+1}}\right)+\frac{iN}{2\hbar\beta}\left(x_{\frac{N}{2}}-x_{\frac{N}{2}+2}\right)\right)\delta\left(x_{\frac{N}{2}+1}\right)
$$

$$
\times e^{-\frac{i}{\hbar}p_N(x_1-x_N)} e^{-\frac{\beta}{N}\frac{p_N^2}{2m}} \left(e^{\frac{i\hat{H}t}{\hbar}} h(\hat{x}) e^{-\frac{i\hat{H}t}{\hbar}}\right)_{\text{W}} [y_N, p_N]. \tag{23}
$$

Up to this point the new derivation is equivalent to what was previously done up to equation 14. However, once

the expression is approximated through classical Wigner and the assumption of finite N, giving

$$
C_{\text{fs},x}(t) \approx \left(\frac{mN}{2\pi\beta}\right)^{\frac{N}{2}} \sqrt{\frac{\beta}{2\pi mN}} \hbar^{-N} \left\{\prod_{j=1}^{N} \int_{-\infty}^{\infty} \mathrm{d}x_j\right\} \int_{-\infty}^{\infty} \mathrm{d}p_N \, \mathrm{e}^{-\frac{i}{\hbar}p_N(x_1-x_N)}
$$

$$
\times \mathrm{e}^{-\frac{\beta}{N}\left(\frac{p_N^2}{2m}+\sum_{j=1}^{N} V(y_j)+\frac{mN^2}{2\hbar^2\beta^2}\sum_{j=1}^{N-1}(x_{j+1}-x_j)^2\right)}
$$

$$
\times \left(\frac{i\hbar\beta}{4Nm}\left(\frac{\mathrm{d}V\left(y_{\frac{N}{2}}\right)}{\mathrm{d}y_{\frac{N}{2}}}+\frac{\mathrm{d}V\left(y_{\frac{N}{2}+1}\right)}{\mathrm{d}y_{\frac{N}{2}+1}}\right)+\frac{iN}{2\hbar\beta}\left(x_{\frac{N}{2}}-x_{\frac{N}{2}+2}\right)\right)\delta\left(x_{\frac{N}{2}+1}\right)
$$

$$
\times h\left(x\left(y_N,p_N,t\right)\right), \tag{24}
$$

this is not the case anymore. Equation 24 is the expression corresponding to the x_1-version of OPCW for the flux-Heaviside trace. Due to the symmetrization of the correlation function $x_{\frac{N}{2}+1}$ rather than x_1 is used. This trace will be called $C_{\text{fs},x}(t)$.

IV. CORRECTION FACTORS FOR EVALUATION OF TRACES WITH MONTE CARLO

In this work the position integrals in equations 16 and 24 were evaluated with Metropolis Monte Carlo[17].

Compared to calculating a correlation function, calculating a trace with Monte Carlo can be a bit more complicated. The flux-Heaviside correlation function is

$$
\left\langle \hat{F}\,\mathrm{e}^{\frac{i\hat{H}t}{\hbar}}\,h(\hat{x})\,\mathrm{e}^{-\frac{i\hat{H}t}{\hbar}}\right\rangle = \frac{1}{Z}\,\mathrm{Tr}\left\{\hat{F}\,\mathrm{e}^{-\beta\hat{H}}\,\mathrm{e}^{\frac{i\hat{H}t}{\hbar}}\,h(\hat{x})\,\mathrm{e}^{-\frac{i\hat{H}t}{\hbar}}\right\}, \tag{25}
$$

where the angular brackets denote a thermal average and Z is the canonical partition function

$$
Z = \mathrm{Tr}\left\{\mathrm{e}^{-\beta\hat{H}}\right\}. \tag{26}
$$

In Monte Carlo sampling a weight function is needed. The delta functions in equation 16 and 24 complicate things somewhat, since it is impossible to integrate them numerically. The weight function used is

$$
\left(\frac{mN}{2\pi\beta}\right)^{\frac{N}{2}} \sqrt{\frac{\beta}{2\pi mN}} \hbar^{-N}
$$

$$
\times \mathrm{e}^{-\frac{\beta}{N}\left(\frac{p_N^2}{2m}+\sum_{j=1}^{N} V(y_j)+\frac{mN^2}{2\hbar^2\beta^2}\sum_{j=1}^{N-1}(x_{j+1}-x_j)^2\right)}\delta\left(y_{y,x}\right), \tag{27}
$$

where $y_{y,x}$ is either $y_{\frac{N}{2}}$ or $x_{\frac{N}{2}+1}$. The integrand is thus

$$
\mathrm{e}^{-\frac{i}{\hbar}p_N(x_1-x_N)}\frac{iN}{\hbar\beta}\left(x_{\frac{N}{2}}-x_{\frac{N}{2}+1}\right)h\left(x\left(y_N,p_N,t\right)\right) \tag{28}
$$

for the y-version of OPCW and

$$
\mathrm{e}^{-\frac{i}{\hbar}p_N(x_1-x_N)}
$$

$$
\times \left(\frac{i\hbar\beta}{4Nm}\left(\frac{\mathrm{d}V\left(y_{\frac{N}{2}}\right)}{\mathrm{d}y_{\frac{N}{2}}}+\frac{\mathrm{d}V\left(y_{\frac{N}{2}+1}\right)}{\mathrm{d}y_{\frac{N}{2}+1}}\right)+\frac{iN}{2\hbar\beta}\left(x_{\frac{N}{2}}-x_{\frac{N}{2}+}\right.\right.
$$

$$
\times h\left(x\left(y_N,p_N,t\right)\right) \tag{29}
$$

for the x-version of OPCW. This means that the quantity actually calculated is $\frac{C_{\text{fs}}(t)}{Z'_\delta}$, where Z'_δ is

$$
Z'_\delta = \left(\frac{mN}{2\pi\beta}\right)^{\frac{N}{2}} \sqrt{\frac{\beta}{2\pi mN}} \hbar^{-N} \left\{\prod_{j=1}^{N} \int_{-\infty}^{\infty} \mathrm{d}x_j\right\} \int_{-\infty}^{\infty} \mathrm{d}p_N
$$

$$
\times \mathrm{e}^{-\frac{\beta}{N}\left(\frac{p_N^2}{2m}+\sum_{j=1}^{N} V(y_j)+\frac{mN^2}{2\hbar^2\beta^2}\sum_{j=1}^{N-1}(x_{j+1}-x_j)^2\right)}
$$

$$
\times \delta\left(y_{y,x}\right), \tag{30}
$$

and is something similar to a partition function, but the integrand includes a delta function and lacks a factor of $\mathrm{e}^{-\frac{i}{\hbar}p_N(x_1-x_N)}$. By sampling the integrand $\mathrm{e}^{-\frac{i}{\hbar}p_N(x_1-x_N)}$ in the same Monte Carlo run as $\frac{C_{\text{fs}}(t)}{Z'_\delta}$ a correction factor $\frac{Z_\delta}{Z'_\delta}$ can be acquired, where

$$
Z_\delta = \left(\frac{mN}{2\pi\beta}\right)^{\frac{N}{2}} \sqrt{\frac{\beta}{2\pi mN}} \hbar^{-N} \left\{\prod_{j=1}^{N} \int_{-\infty}^{\infty} \mathrm{d}x_j\right\} \int_{-\infty}^{\infty} \mathrm{d}p_N
$$

$$
\times \mathrm{e}^{-\frac{\beta}{N}\left(\frac{p_N^2}{2m}+\sum_{j=1}^{N} V(y_j)+\frac{mN^2}{2\hbar^2\beta^2}\sum_{j=1}^{N-1}(x_{j+1}-x_j)^2\right)}
$$

$$
\times \mathrm{e}^{-\frac{i}{\hbar}p_N(x_1-x_N)}\delta\left(y_{y,x}\right). \tag{31}
$$

Z_δ is very similar to Z'_δ, but it has $\mathrm{e}^{-\frac{i}{\hbar}p_N(x_1-x_N)}$ in the integrand, and is thus a partition function with a delta function in it. For a parabolic barrier Z_δ can be calculated analytically for the exact quantum mechanical case, $N \to \infty$. It is

$$
Z_\delta = \sqrt{\frac{m\omega}{2\pi\hbar\sin(\beta\hbar\omega)}}. \tag{32}
$$

For the classical case it is

$$
Z_\delta = \sqrt{\frac{m}{2\pi\beta}}\hbar^{-1}. \tag{33}
$$

For the Eckart potential and other potentials without an analytic solution, the correction factor has to be calculated numerically.

The quantity obtained from the Monte Carlo integration is thus $\frac{C_{\text{fs}}(t)}{Z'_\delta}$. A correction factor of $\frac{Z_\delta}{Z'_\delta}$ can likewise be obtained from the Monte Carlo run, but an additional correction factor Z_δ has to be computed.

$$C_{\text{fs}}(t) = \frac{C_{\text{fs}}(t)}{Z'_\delta} \times \frac{Z'_\delta}{Z_\delta} \times Z_\delta \qquad (34)$$

V. COMPUTATIONAL DETAILS

In this work, the integrals in Eqs. 16 and 24 were evaluated by Monte Carlo and the time propagation was conducted with molecular dynamics.

A. Potentials and system parameters

Two different potentials are studied in this work: a parabolic barrier and a symmetric Eckart barrier.

The parabolic barrier has the potential

$$V_{\text{parabolic}}(x) = -\frac{1}{2}m\omega^2 x^2, \qquad (35)$$

where ω is the absolute value of the angular frequency of the system.

The symmetric Eckart barrier used is of the form

$$V_{\text{Eckart}}(x) = \frac{6\hbar\omega}{\pi} \operatorname{sech}^2\left(\sqrt{\frac{\pi m\omega}{12\hbar}}x\right), \qquad (36)$$

where ω is the absolute value of the angular frequency at the top of the barrier, i.e. at the transition state.

B. Traces

The Monte Carlo integration was conducted through the Metropolis Monte Carlo method[17]. The maximum stepsize for the Monte Carlo was choosen and updated according to the procedure in the original OPCW work[12]. A Maxwell–Boltzmann distribution of the inverse temperature β/N was used to sample the momentum, p_N. For the sampling, the ran2 pseudo-random number generator of Press et al.[18] was used.

A molecular dynamics trajectory was run for each 10th Monte Carlo step. The dynamics were run with the velocity Verlet algorithm[19,20], with a timestep of $0.05\ \omega^{-1}$ and a total time of $10\ \omega^{-1}$.

The standard deviations of the results where calculated with the block average method, as explained in e.g.[21,22], using a minimum block size of 10^6 Monte Carlo steps.

To get the correction factor Z_δ for the Eckart potential the numerical matrix multiplication scheme[23] was used to calculate the matrix elements of the Boltzmann operator.

C. Exact comparisons

The exact classical (CM) and quantum mechanical[13] (QM) flux-Heaviside traces for the parabolic barrier can be acquired as analytic functions,

$$C_{\text{fs,CM}}(t) = \frac{1}{2\pi\hbar\beta} \qquad (37)$$

$$C_{\text{fs,QM}}(t) = \frac{1}{2\pi\hbar\beta} \frac{\frac{\beta\hbar\omega}{2}}{\sin\left(\frac{\beta\hbar\omega}{2}\right)} \frac{\sinh(\omega t)}{\sqrt{\sinh^2(\omega t) + \sin^2\left(\frac{\beta\hbar\omega}{2}\right)}}. \qquad (38)$$

For the Eckart barrier the classical result is the same analytic function as for the parabolic barrier, apart from a Boltzmann factor that accounts for the height of the barrier compared to the reactant energy,

$$k_{\text{r,CM}}Q_{\text{R}} = \frac{1}{2\pi\hbar\beta}\,e^{-\beta V(0)}. \qquad (39)$$

The corresponding quantum mechanical result can be calculated from an analytic transmission coefficient[24],

$$\varkappa_{\text{Eckart}}(E) = \frac{\cosh\left(24\sqrt{\frac{\pi E}{6\hbar\omega}}\right) - 1}{\cosh\left(24\sqrt{\frac{\pi E}{6\hbar\omega}}\right) + \cosh\left(\sqrt{576 - \pi^2}\right)}, \qquad (40)$$

but has to be numerically integrated,

$$k_{\text{r,QM}}Q_{\text{R}} = \frac{1}{2\pi\hbar}\int_0^\infty dE\,e^{-\beta E}\,\varkappa_{\text{Eckart}}(E) \qquad (41)$$

$$. \qquad (42)$$

In this work the integral is performed by Romberg integration[25], using an integration interval from 0 to 100 $\hbar\omega$ and a convergence criterion of 10^{-10}.

In the case of the Eckart potential, the reactants are represented as a free particle, which has the partition function per unit of length

$$Q_{\text{R}} = \sqrt{\frac{m}{2\pi\beta}}\hbar^{-1}. \qquad (43)$$

This partition function is the same in the classical and quantum mechanical cases. The parabolic barrier is infinitely high and the partition function for the reactants is therefore infinite, and can not be calculated. The quantity $k_{\text{r}}Q_{\text{R}}$ is, however, a finite calculable quantity, as the rate constant is infinitely small and compensates for the infinite reactant partition function.

To obtain exact classical Wigner flux-Heaviside traces for the Eckart potential the numerical matrix multiplication scheme[23] was used to calculate the matrix elements of the Boltzmann operator.

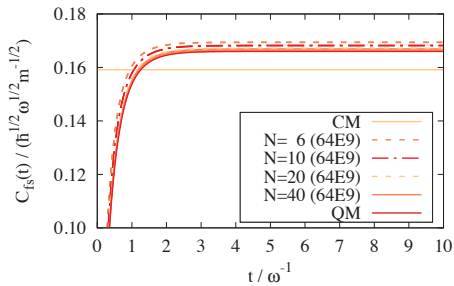An RPMD comparison was calculated for the Eckart barrier, using the formulation of Craig and Manolopoulos[26].

FIG. 1. $C_{fs}(t)$ for a parabolic barrier with $\beta\hbar\omega = 1$. The traces are calculated with the y-version of OPCW for different N, exact Classical Mechanics (CM), and exact Quantum Mechanics (QM). The numbers in parenthesis are the number of Monte Carlo steps used. The top and bottom lines of each type show the standard deviation of the results.
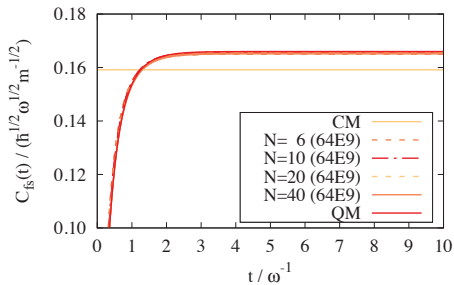

FIG. 3. $C_{fs}(t)$ for a parabolic barrier with $\beta\hbar\omega = 0.5$. The traces are calculated with the y-version of OPCW for different N, exact Classical Mechanics (CM), and exact Quantum Mechanics (QM). The numbers in parenthesis are the number of Monte Carlo steps used. The top and bottom lines of each type show the standard deviation of the results.

FIG. 2. $C_{fs}(t)$ for a parabolic barrier with $\beta\hbar\omega = 1$. The traces are calculated with the x-version of OPCW for different N, exact Classical Mechanics (CM), and exact Quantum Mechanics (QM). The numbers in parenthesis are the number of Monte Carlo steps used. The top and bottom lines of each type show the standard deviation of the results.

FIG. 4. $C_{fs}(t)$ for a parabolic barrier with $\beta\hbar\omega = 0.5$. The traces are calculated with the x-version of OPCW for different N, exact Classical Mechanics (CM), and exact Quantum Mechanics (QM). The numbers in parenthesis are the number of Monte Carlo steps used. The top and bottom lines of each type show the standard deviation of the results.

VI. RESULTS AND DISCUSSION

For the parabolic barrier the results of the case $\beta\hbar\omega = 1$ can be seen in Figs. 1 and 2. The classical Wigner method is exact for harmonic potentials[4], so the OPCW results converge toward the exact quantum mechanical result as N is increased. It can be seen that the y-version of OPCW needs more beads than the x-version to converge to the exact quantum mechanical result. The x-version of OPCW has excellent convergence with respect to the number of beads. It almost gives the exact result for $N = 6$.

For the parabolic barrier the results of the case $\beta\hbar\omega = 0.5$ can be seen in Figs. 3 and 4. The standard deviations are visible around the OPCW-results for this temper-
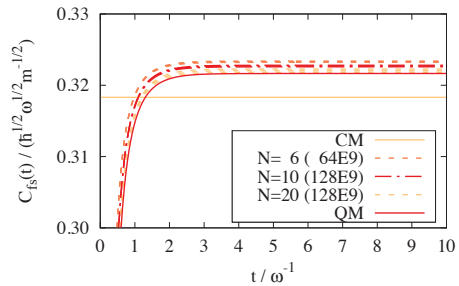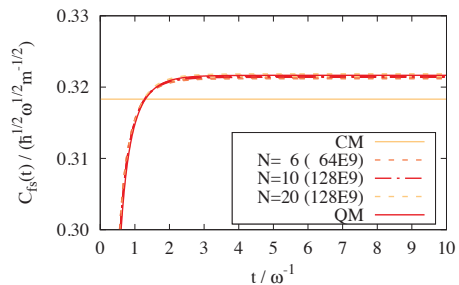
ature. Thus these higher temperature calculations are visibly more difficult than those with $\beta\hbar\omega = 1$. The sampling of the initial conditions in OPCW is known to become more difficult when raising the temperature but keeping the same N[12]. Generally, however, fewer beads are needed for a calculation at higher temperature. The x-version of OPCW converges toward the exact quantum mechanical result significantly faster than the y-version also at $\beta\hbar\omega = 0.5$, when the number of beads is increased.

Particularly for $\beta\hbar\omega = 0.5$ it can be seen that $C_{fs,y}(t)$ converges toward exact quantum mechanics from above and $C_{fs,x}(t)$ converges toward exact quantum mechanics from below.

In Figs. 5-10 $C_{fs}(t)$ for the Eckart barrier at $\beta\hbar\omega = 1$, 3, and 6 are shown. The rate constants and tunneling
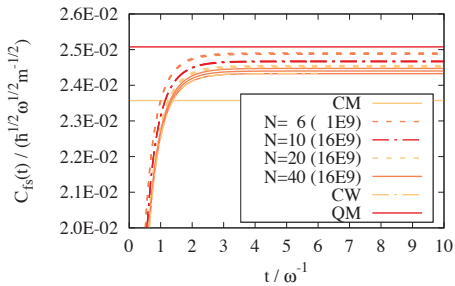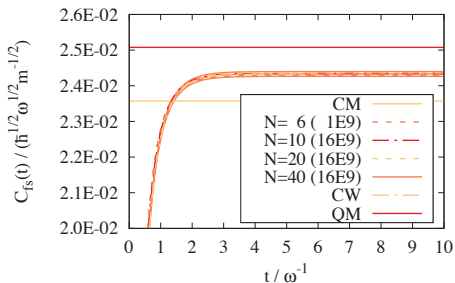
FIG. 5. $C_{\text{fs}}(t)$ for an Eckart potential with $\beta\hbar\omega = 1$. The traces are calculated with the y-version of OPCW for different N, exact Classical Mechanics (CM), exact Classical Wigner (CW), and exact Quantum Mechanics (QM). The QM-line shows the long time result, not the time dependent function. The numbers in parenthesis are the number of Monte Carlo steps used. The top and bottom lines of each type show the standard deviation of the results.

FIG. 7. $C_{\text{fs}}(t)$ for an Eckart potential with $\beta\hbar\omega = 3$. The traces are calculated with the y-version of OPCW for different N, exact Classical Mechanics (CM), exact Classical Wigner (CW), and exact Quantum Mechanics (QM). The QM-line shows the long time result, not the time dependent function. The numbers in parenthesis are the number of Monte Carlo steps used. The top and bottom lines of each type show the standard deviation of the results.

FIG. 6. $C_{\text{fs}}(t)$ for an Eckart potential with $\beta\hbar\omega = 1$. The traces are calculated with the x-version of OPCW for different N, exact Classical Mechanics (CM), exact Classical Wigner (CW), and exact Quantum Mechanics (QM). The QM-line shows the long time result, not the time dependent function. The numbers in parenthesis are the number of Monte Carlo steps used. The top and bottom lines of each type show the standard deviation of the results.

FIG. 8. $C_{\text{fs}}(t)$ for an Eckart potential with $\beta\hbar\omega = 3$. The traces are calculated with the x-version of OPCW for different N, exact Classical Mechanics (CM), exact Classical Wigner (CW), and exact Quantum Mechanics (QM). The QM-line shows the long time result, not the time dependent function. The numbers in parenthesis are the number of Monte Carlo steps used. The top and bottom lines of each type show the standard deviation of the results.

factors, $\Gamma = k_{\text{r,QM}}/k_{\text{r,CM}}$, are presented in Tabs. I and II. For the Eckart potential at $\beta\hbar\omega = 1$ there is only $\sim 6\%$ difference between the quantum mechanical and classical results. For the lower temperatures the difference is significantly bigger, i.e. $\sim 50\%$ for $\beta\hbar\omega = 3$ and a factor ~ 5 for $\beta\hbar\omega = 6$.

The classical Wigner method, as could be expected, gives results that are intermediate between classical mechanics and quantum mechanics.

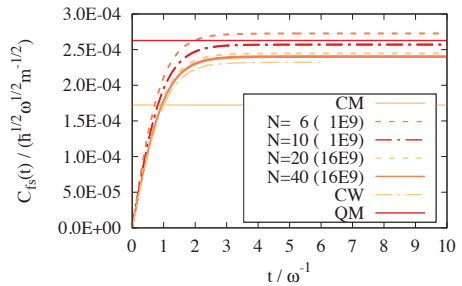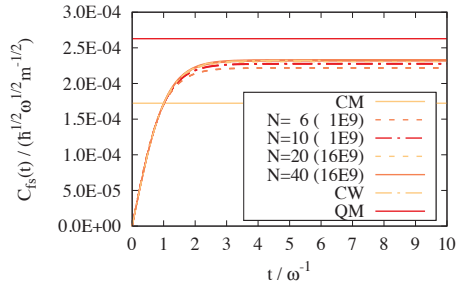The OPCW results, for the Eckart potential, converge to the exact classical Wigner result as the number of

TABLE I. Rate constants (k_{r}) for different inverse temperatures (β) for the Eckart barrier described in Eq. 36. Comparision of OPCW[a], Ring Polymer Molecular Dynamics (RPMD), classical mechanics (CM), exact Classical Wigner (CW), and quantum mechanics (QM).

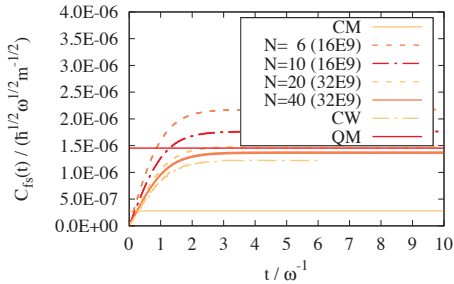|	$k_{\text{r}}/(\hbar^{\frac{1}{2}}\omega^{\frac{1}{2}}m^{-\frac{1}{2}})$				
$\beta\hbar\omega$	OPCW	RPMD	CM	CW	QM
1	6.10E-2	6.17E-2	5.9084E-2	6.0986E-2	6.2856E-2
3	1.009E-3	1.07E-3	7.4821E-4	1.0087E-3	1.1409E-3
6	7.391E-6	7.55E-6	1.7186E-6	7.5092E-6	8.9347E-6

[a] x-version, $N = 40$

IV

FIG. 9. $C_{\mathrm{fs}}(t)$ for an Eckart potential with $\beta\hbar\omega = 6$. The traces are calculated with the y-version of OPCW for different N, exact Classical Mechanics (CM), exact Classical Wigner (CW), and exact Quantum Mechanics (QM). The QM-line shows the long time result, not the time dependent function. The numbers in parenthesis are the number of Monte Carlo steps used. The top and bottom lines of each type show the standard deviation of the results.
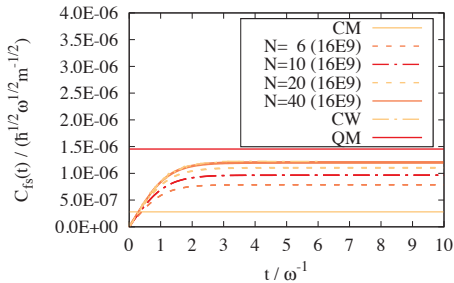

FIG. 10. $C_{\mathrm{fs}}(t)$ for an Eckart potential with $\beta\hbar\omega = 6$. The traces are calculated with the x-version of OPCW for different N, exact Classical Mechanics (CM), exact Classical Wigner (CW), and exact Quantum Mechanics (QM). The QM-line shows the long time result, not the time dependent function. The numbers in parenthesis are the number of Monte Carlo steps used. The top and bottom lines of each type show the standard deviation of the results.

TABLE II. Tunneling factors (Γ) for different inverse temperatures (β) for the Eckart barrier described in Eq. 36. Comparision of OPCW[a], Ring Polymer Molecular Dynamics (RPMD), exact Classical Wigner (CW), and exact results.

$\beta\hbar\omega$	Γ_{OPCW}	Γ_{RPMD}	Γ_{CW}	Γ_{Exact}
1	1.03	1.04	1.0322	1.0638
3	1.349	1.43	1.3481	1.5249
6	4.300	4.39	4.3693	5.1987

[a] x-version, $N = 40$

beads is increased. The x-version converges faster than the y-version. As for the parabolic barrier, $C_{\mathrm{fs},y}(t)$ converge from above and $C_{\mathrm{fs},x}(t)$ converge from below. This is an interesting occurrence, but too few potentials have been studied here to draw conclusions from it.

For both potentials and all temperatures the x-version of OPCW gives results that are very close to the exact classical Wigner result. Particularly for the Eckart potential at $\beta\hbar\omega = 3$ and 6 the classical Wigner method can be seen to be a significant improvement over classical mechanics.

Compared to RPMD the classical Wigner method gives slightly worse results. However, in the perspective of trying to approximate the quantum mechanical reaction rates, the differences between the rate constants calculated by the classical Wigner method and RPMD, at the lowest temperatures, is insignificant compared to the difference between those rate constants from the exact quantum mechanical result. Results from a single symmetric one-dimensional potential is, however, not enough to draw general conclusions.

VII. CONCLUSION

In this work the recently developed Open Polymer Classical Wigner (OPCW) method[12] is extended to the flux-Heaviside correlation function of Miller[14] and applied to a parabolic barrier and a symmetric Eckart potential, for a few different temperatures. The OPCW method is shown to converge to the exact classical Wigner result as the number of beads in the path integral polymer is increased. Particularly the x-version of OPCW shows promise for further tests.

In the future, it would be of interest to apply the OPCW reaction rate constant calculations to multidimesional systems, such as the double well potential of Topaler and Makri[27] coupled to the harmonic bath of Caldeira and Leggett[28]. For such a system modifying OPCW by making the bath classical, as introduced in the preceding article[12], would be of interest. It would also be of interest to try the method on asymmetric potentials, as both potentials tried thus far have been symmetric.

For systems where the reactants are bound it could be of interest to use the Heaviside-Heaviside correlation function of Miller et al.[13] instead of the flux-Heaviside correlation function.

IV

[1] E. Wigner, Zeitschrift für physikalische Chemie B (Leipzig) **19**, 203 (1932).

[2] H. Eyring, The Journal of Chemical Physics **3**, 107 (1935).

[3] E. Pollak and J.-L. Liao, The Journal of Chemical Physics **108**, 2733 (1998).

[4] E. J. Heller, The Journal of Chemical Physics **65**, 1289 (1976).

[5] H. Wang, X. Sun, and W. H. Miller, The Journal of Chemical Physics **108**, 9726 (1998).

[6] J. A. Poulsen, G. Nyman, and P. J. Rossky, The Journal of Chemical Physics **119**, 12179 (2003).

[7] J. Liu and W. H. Miller, The Journal of Chemical Physics **131**, 074113 (2009).

[8] J. Langer, Annals of Physics **41**, 108 (1966).

[9] J. Langer, Annals of Physics **54**, 258 (1969).

[10] W. H. Miller, The Journal of Chemical Physics **62**, 1899 (1975).

[11] I. R. Craig and D. E. Manolopoulos, The Journal of Chemical Physics **122**, 084106 (2005).

[12] S. K.-M. Svensson, J. A. Poulsen, and G. Nyman, The Journal of Chemical Physics **152**, 094111 (2020).

[13] W. H. Miller, S. D. Schwartz, and J. W. Tromp, The Journal of Chemical Physics **79**, 4889 (1983).

[14] W. H. Miller, The Journal of Chemical Physics **61**, 1823 (1974).

[15] P. Schofield, Physical Review Letters **4**, 239 (1960).

[16] R. P. Feynman, Reviews of Modern Physics **20**, 367 (1948).

[17] N. Metropolis, A. W. Rosenbluth, M. N. Rosenbluth, A. H. Teller, and E. Teller, The Journal of Chemical Physics **21**, 1087 (1953).

[18] W. H. Press, S. A. Teukolsky, W. T. Vetterling, and B. P. Flannery, *Numerical Recipes in FORTRAN: The Art of Scientific Computing*, 2nd ed. (Cambridge University Press, The Pitt Building, Trumpington Street, Cambridge CB2 1RP, United Kingdom, 1992).

[19] L. Verlet, Physical Review **159**, 98 (1967).

[20] W. C. Swope, H. C. Andersen, P. H. Berens, and K. R. Wilson, The Journal of Chemical Physics **76**, 637 (1982).

[21] R. Friedberg and J. E. Cameron, The Journal of Chemical Physics **52**, 6049 (1970).

[22] J. M. Flegal, M. Haran, and G. L. Jones, Statistical Science **23**, 250 (2008).

[23] D. Thirumalai, E. J. Bruskin, and B. J. Berne, The Journal of Chemical Physics **79**, 5063 (1983).

[24] H. S. Johnston and D. Rapp, Journal of the American Chemical Society **83**, 1 (1961).

[25] W. Romberg, Det Kongelige Norske Videnskabers Selskab Forhandlinger **28**, 30 (1955).

[26] I. R. Craig and D. E. Manolopoulos, The Journal of Chemical Physics **123**, 034102 (2005).

[27] M. Topaler and N. Makri, The Journal of Chemical Physics **101**, 7500 (1994).

[28] A. O. Caldeira and A. J. Leggett, Annals of Physics **149**, 374 (1983).